Doctoral Thesis

Study on Material Texture Control of Composite Materials by Self-assembly Process -Applications to Piezoelectric Biosensor and High Thermal Conductive Materials-

自己組織化プロセスを用いたコンポジット材料の材料組織制御に関する研究 -圧電体バイオセンサ及び高熱伝導材料への適用-

Mariko Takeda
武田　真理子

Electrical Engineering and Chemistry
Graduate School of Integrative Science and Engineering
Tokyo City University

March 2021

ABSTRACT

The targets applications of the ceramics / polymer and ceramics / stainless steel composite materials were the piezoelectric biosensor and the high thermal conductivity components in this study. Tuberculosis (TB) has become prevalent mainly in developing countries. In this study, the TB diagnostic method that combines the LAMP (Loop-mediated Isothermal Amplification) method and polymer piezoelectric material was proposed to solve the safety and cost problems. In order to achieve the final goal of TB diagnosis by combining the LAMP method and the polymer piezoelectric biosensor, it is necessary to improve the sensitivity and responsivity of the biosensor. Therefore, in this study, the ceramics / polymer composite materials were applied to biosensors to improve the dielectric properties related to the sensitivity and responsivity.

In high thermal conductivity components, the friction and abrasions of the engine generated cause energetic and material losses and decrease the efficiency of mechanical systems. The materials with high thermal conductivity are required. However, the thermal conductivity of general iron alloys is low. Therefore, in order to improve the thermal conductivity, ceramics / stainless steel composites were applied as high thermal conductivity components in this study.

Generally, the dielectric constant of a polymer is low. The thermal conductivity of stainless steel is low. In the general studies of composite materials, ceramic fillers are dispersed. However, the volume fraction of the filler is 50 vol.%, and it is not suitable for the applications. Therefore, the purpose of this study was to design composite materials in order to improve dielectric properties and thermal conductivity with a small amount of ceramic filler addition (0-20 vol.%). The dielectric properties and the thermal conductivity are affected by the material texture. In the material design approach of this

study, it was proposed that the dielectric properties were able to improve by forming self-assembled ceramic aggregates having a ceramics / polymer / ceramics heterointerface. In the thermal conductivity, it was proposed that the thermal conductivity would be improved by forming ceramic particle groups for the thermal conductivity networks. Therefore, in this study, the material texture of the composite was controlled by the self-assembly process involving solids in order to improve the dielectric properties and thermal conductivity. There are few studies on material texture controlled with self-assembly processes involving the solid. In addition, the relationship between the self-assembled material texture and the dielectric properties and the thermal conductivity has not been clarified. Therefore, in this thesis, the relationship between the dispersion states of self-assembled ceramics secondary particle groups under the different manufacturing processes and the dielectric properties and the thermal conductivity of the ceramics / polymer and ceramics / stainless steel composites were investigated. And then, the relationship between the self-assembled material texture and the dielectric constant and the thermal conductivity was discussed, and the material design was proposed. In particular, the multifractal analysis was performed to quantify the morphology, entropy of the configuration, dispersibility of the self-assembled ceramic secondary particle groups and the interface state in the ceramic secondary particle groups.

In this thesis, a polymer piezoelectric biosensor was prepared with polyvinylidene fluoride (β-PVDF) to present the problems of the piezoelectric biosensor. (1) The weight sensing property by loading polymer films and (2) the sensor sensing properties by adsorption of fluorescently labeled avidin and biotin were investigated. It was possible to detect biopolymers using the immobilization characteristics associated with

the host-guest reaction at 100 kHz to 6 MHz by using the relaxation process of the complex permittivity. According to the results of the investigation of the sensor detection characteristics, it was found that (1) the shear vibration of β-PVDF is affected by the viscosity of the solution due to the low elastic modulus of β-PVDF, and (2) the sensitivity of the sensor is 5 μg/ml and the response time is 60 minutes, so the improvement of the sensitivity and response time is necessary for practical use. To solve these problems, ceramics/polymer composites were applied to piezoelectric biosensors. Barium titanate (BT) was used as a ceramic filler, and polylactic acid (PLLA) and PVDF were used as polymer matrices. In order to control the material texture, BT/polymer composites were fabricated by changing (1) the kneading conditions and (2) the viscosity of the dispersant. According to the investigation of the material texture control by the self-assembly process, BT agglomerate with the BT / BT interface was formed under high-speed kneading conditions (30 rpm) and high viscosity of PEG. On the other hand, the BT aggregates with the BT / polymer / BT heterointerface were formed under the low kneading conditions (10 rpm) and low viscosity of PEG. From the results of the material texture and the dielectric properties of the BT / PLLA composites, the dielectric constant of the self-assembled BT aggregates with the BT/ PLLA / BT heterointerface depending on the secondary particle group improved by 24.5 times compared to the BT / PLLA composite with BT / BT interface. This is that the electric dipole of a BT / polymer / BT heterointerface induced to improve the dielectric constant. Similarly, the dielectric constant of the self-assembled BT aggregates depending on the secondary particle group improved by 1.16 times compared to the BT / PVDF composite with BT agglomerates. The fractal analysis was used for the evaluation of the material texture with SEM images. It was suggested that it is possible that multifractal

analyses were applied to evaluate the morphology, configuration entropy, and dispersibility of the self-assembled BT secondary particle groups and the formation of the BT / polymer / BT heterointerfaces in self-assembled BT aggregates. It was expected to improve the sensitivity by 2.1 times and responsivity by 7 times compared to the conventional PVDF by using the BT / PVDF composites.

The material was designed to improve the thermal conductivity (λ_e) of silicon nitride (SN)/stainless steel (SUS316L) composites. To discuss the relationship of the self-assembled material texture and thermal conductivity, SUS316L powders with an average particle size of 3 μm and 8 μm were used. According to the results of the secondary particle area of SN filler and λ_e, it was clarified that the λ_e was efficiently improved by increasing the SN/SN interface and the formation of thermal conductive network with the formation of SN particle groups. The thermal conductivity was improved by 1.22 times at 10 vol.% compared to the volume fraction of 0 vol.% for SN. Based on the results of the multifractal analysis, the morphology, configuration entropy, and dispersibility of the self-assembled SN particle groups due to the difference in packing with the self-assembly process were analyzed to determine the characteristics of the thermal conductive network.

Hence, it was clarified that the fabrication conditions affected the self-assembly process of the reaction-diffusion system and were able to control the morphology, configuration entropy, and dispersibility of the BT and SN particle groups and the interface state in the BT and SN particle groups. From the results of the material texture control, the material designs that solve the problems of conventional PVDF or stainless steel were proposed. The actual application to biosensors is expected to enable more sensitive and rapid TB diagnosis. In the future, it is also expected to contribute to the

electronic substrate materials that are required low loss and high thermal conductivity by combining the material design of the dielectric properties and thermal conductivity of the composite materials of this study. The material design in this study can be applied to electrical, thermal conductivity, strength, optical, and sonic materials and the results of this study can contribute to the development of new materials.

Contents

Chapter 1 Introduction

1.1 Composite material and applications

1.1.1 Composite material

Composite materials are mixed with a matrix material and a filler material. The composite materials have properties that do not appear as a single material by controlling the structure and the interface between materials. This is, two inherently different materials that when combined together produce a material with properties that exceed the constituent materials [1]. Therefore, the composite materials can be designed to have excellent structure, mechanical properties, and chemical conditions depending on the purpose. The composite materials have inorganic / inorganic, inorganic / organic, and organic / organic combinations. Applications of these composite materials have the construction of buildings and bridges, automobile bodies, automobile industry, and biomedical fields [2]. The following factors affect the performance of composite materials.

(1) Properties of matrix and filler

(2) Volume fraction of filler in the composite material

(3) Shape and size of the filler

(4) Distribution of temperature, the electric field between fillers

(5) Dispersion state of fillers

(6) Interface state between matrix and filler

(7) Orientation of fillers

(8) Interface state between fillers

1.1.2 Physical properties and model equations of composite materials

The coefficients which reflect the potential gradient and the flow velocity relate to dielectric constant, magnetic susceptibility, electrical conductivity, and thermal conductivity. These properties are used with the same composite rule. In this study, dielectric composites and thermally conductive composites were focused on.

Many models of conductivity, dielectric constant, magnetic susceptibility, and thermal conductivity have been reported. The volume-fraction average is a simple (but inaccurate) method to estimate the effective dielectric constant of a polymer composite material [3]:

$$\lambda_e = v_c\lambda_c + v_d\lambda_d \tag{1-1}$$

λ_e is the dielectric constant and thermal conductivity of the composites. λ_c is the dielectric constant and thermal conductivity of the matrix material. λ_d is the dielectric constant and thermal conductivity of the filler. v_c and v_d is the volume fraction of matrix and filler, respectively.

Clausius and Mossotti derived independently a mean-field theory for a disordered system of polarizable spheres [4]. The effective medium theory has been proposed since their work. The theory is shown as [5]:

$$\lambda_e = \lambda_c + v_d/[1/(\lambda_d - \lambda_c) + (1 - v_d)/3\lambda_c] \tag{1-2}$$

Maxwell proposed a model in which a single sphere presents in a sufficiently large solid when the distance of spheres is large [6]. The model is considered the temperature

distribution and around the sphere, the following equation is shown [6]:

$$\frac{\lambda_e}{\lambda_c} = \frac{2\lambda_c+\lambda_d-2(\lambda_c-\lambda_d)v}{2\lambda_c+\lambda_d+(\lambda_c-\lambda_d)v} \tag{1-3}$$

where v_d is the volume fraction of particles. In this Maxwell model, it is assumed that the matrix and filler material is isotropy and homogeneous. The shape of the filler affects the physical properties of the composite material. Therefore, a model was proposed that considers the interaction in that the distribution of the shape and the temperature around one particle is disturbed by other particles focusing on one particle.

Fricke proposed an equation for the elliptical model which the theory of the shape effect of the dispersed particle in a two-phase mixture [7], [8]. Hamilton et al. [9] proposed an equation for irregularly shaped fillers dispersed without orientation.

$$\frac{\lambda_e}{\lambda_c} = \frac{x\,\lambda_c+\lambda_d-x(\lambda_c-\lambda_d)v}{x\lambda_c+\lambda_d+(\lambda_c-\lambda_d)v} \tag{1-4}$$

where x is a parameter related to the shape of the filler, thermal conductivity, dielectric constant.

Bruggeman proposed an equation that can be applied to high volume fractions [10]. In this equation, the non-uniform phase around the sphere is regarded as a uniform phase with average thermal conductivity and dielectric constant and the average thermal conductivity and dielectric constant are obtained [10].

$$1 - v = \frac{\lambda_e-\lambda_d}{\lambda_c-\lambda_d}\left(\frac{\lambda_c}{\lambda_e}\right)^{1/3} \tag{1-5}$$

Various studies have indicated that the effective dielectric constant predicted by the Bruggeman model increases sharply for filler volume fractions above 20% and can be very high for ceramic particle loadings higher than 50% by volume [11]. Fig. 1-1 shows the dielectric constant predicted by models of Volume fraction average, Bruggeman spheres, and Maxwell for a blend of inorganic spheres ($\lambda_d = \varepsilon_{filler}$ = 1,000) dispersed in a polymer matrix ($\lambda_e = \varepsilon_{matrix}$ = 2.3).

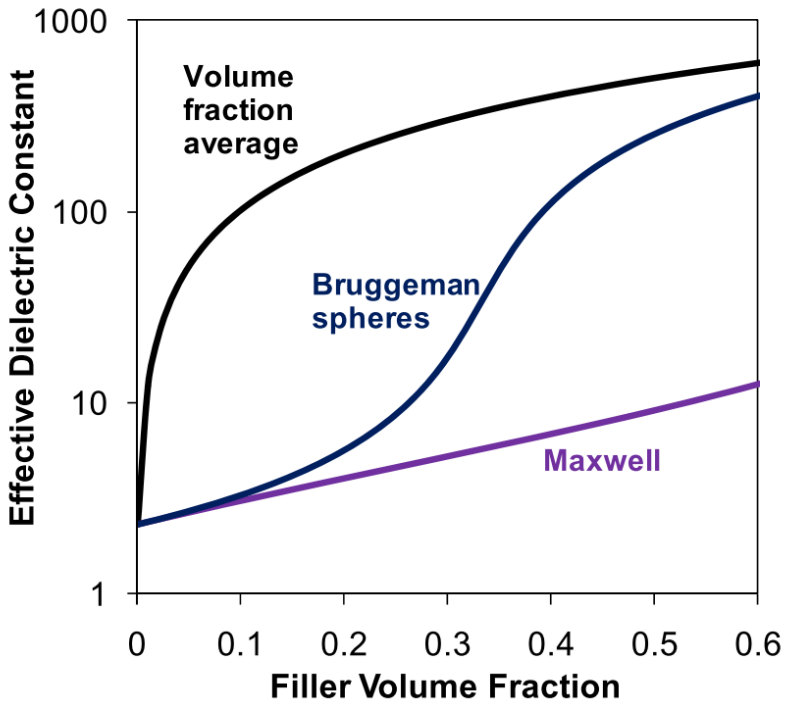

Fig.1-1 The dielectric constant predicted by various models for a blend of inorganic spheres ($\lambda_d = \varepsilon_{filler}$ = 1,000) dispersed in a polymer matrix ($\lambda_e = \varepsilon_{matrix}$ = 2.3) [12].

Meridith expanded Fricke's equation for the case which the ellipsoids are dispersed without orientation [8].

$$1 - v = \frac{\lambda_e - \lambda_d}{\lambda_c - \lambda_d}\left(\frac{\lambda_e + \alpha\lambda_d}{\lambda_c + \alpha\lambda_d}\right)^{\gamma} \cdot \left(\frac{\lambda_c}{\lambda_e}\right)^{\beta} \quad (1\text{-}6)$$

where α, β, and γ are parameters determined only by the shape of the ellipsoid. Kanari's equation was proposed by solving it assuming that x does not depend on the thermal conductivity of the composite [13], [14].

$$1 - v = \frac{\lambda_e - \lambda_d}{\lambda_c - \lambda_d}\left(\frac{\lambda_c}{\lambda_e}\right)^{1/(x+1)} \quad (1\text{-}7)$$

In the behavior of conductivity, Percolation theory describes the connectivity of objects within a network structure and the effects of this connectivity on the macroscale properties of the system (see Fig.1-2) [15]. The theory is shown as [16]:

$$\lambda_e = \lambda_c(v_d - v_p)^t, for\ v_d > v_c \quad (1\text{-}8)$$

where v_p is the percolation threshold and t is the critical exponent based on theoretical prediction.

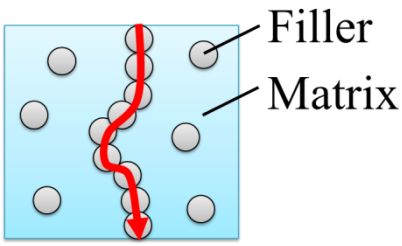

Fig.1-2 Schematic view of Percolation.

1.1.3 Dielectric and Piezoelectric Materials

Dielectrics and piezoelectric materials are used in capacitors, sensors, and energy storage [11]. Table 1-1 and Table 1-2 show the general dielectrics and piezoelectric ceramic and polymer [11]. A part of the ceramic filler and polymer matrix is described below.

1.1.3.1 Barium Titanate ($BaTiO_3$) [11]

Barium titanate (BT) has a crystal with a perovskite structure and is ferroelectric ceramics. BT exists in the paraelectric cubic phase above its Curie point of about 130 °C, while in the temperature range of 0 °C to 130 °C, the ferroelectric tetragonal phase is stable. BT's dielectric properties arise from a structural change where the center Ba^{2+} and Ti^{4+} cations are displaced relative to the O^{2-} ions, leading to the formation of electric dipoles. This spontaneous polarization is the net dipole moment produced per unit volume for the dipoles pointing in a given direction.

1.1.3.2 $Pb(Zr \cdot Ti)O_3$ (PZT) [17]

PLZ is used for a wide range of piezoelectric applications. However, PZT is rigidity, brittleness, toxicity, high density, lower voltage coefficient, and lack of design flexibility limit their energy‐related application to some extent.

Table 1-1 Dielectric permittivity values of commonly used ceramics for capacitors [11] .

Composition	Dielectric permittivity
$BaTiO_3$	1,700
PMN-PT (65/35)	3,640
$PbNb_2O_6$	225
PLZT (7/60/40)	2,590
SiO_2	3.9
Al_2O_3	9
Ta_2O_5	22
TiO_2	80
$SrTiO_3$	2,000
ZrO_2	25
HfO_2	25
$HfSiO_4$	11
La_2O_3	30
Y_2O_3	15
α-$LaAlO_3$	30
$CaCu_3Ti_4O_{12}$	~60,000
$La_{1.8}Sr_{0.2}NiO_4$	~100,000

Table 1-2 List of dielectric permittivities of commonly used polymers in capacitors [11]

Polymer	Dielectric permittivity
Nonfluorinated aromatic polyimides	3.2-3.6
Fluorinated polyimide	2.6-2.8
Poly(phenyl quinoxaline)	2.8
Poly(arylene ether oxazole)	2.6-2.8
Poly(arylene ether)	2.9

1.1.3.3 Polyvinylidene fluoride (PVDF)

The dielectric properties of PVDF based polymers originate from the presence of the highly electronegative fluorine on the polymer chains and from the spontaneous alignment of the C-F dipoles in the crystalline phases [18]. PVDF has four different crystalline phases, including α, β, γ, and δ phases (see Fig.1-3). The α phase is nonpolar, and the β, γ, and δ phases are ferroelectric. The β phase has the largest spontaneous polarization due to its large dipole moment. The β phase is formed by poling the α phase sample under an electric field of 100-200 MV/m. The dielectric constants of the α, β, and γ phases depending on the frequency are different (see Fig.1-4) [19].

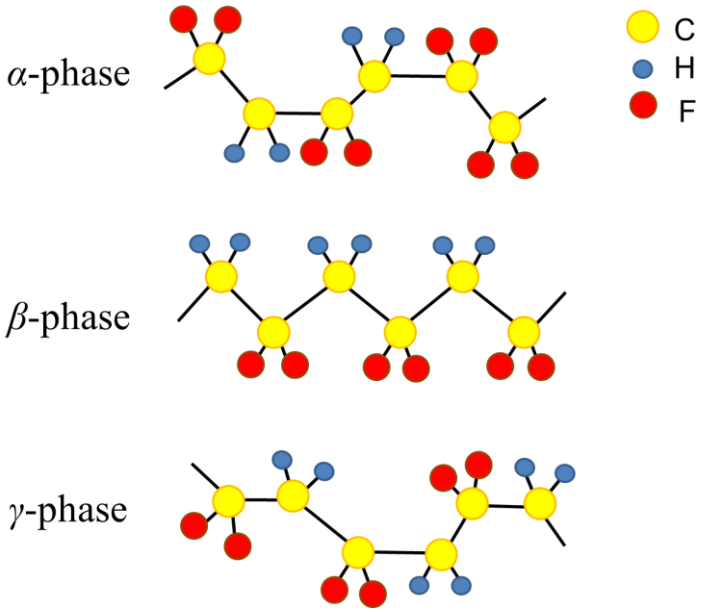

Fig.1-3 The crystalline phases (α, β, and γ) of PVDF.

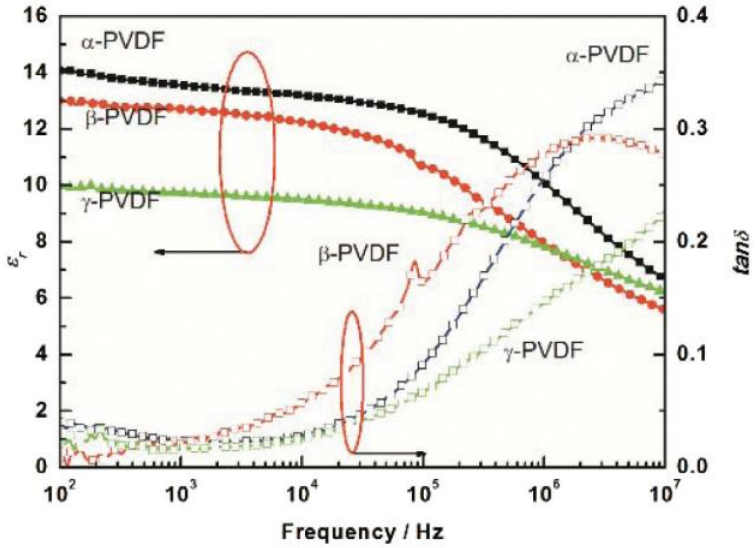

Fig.1-4 Dielectric constant and loss of PVDF with α, β, and γ phase. [19]

1.1.3.4 Poly Lactic Acid (PLA) [20]

PLA is biocompatible and is developed natural piezoelectricity after mechanical stretching. The stretching creates a non-chiral film poly-L-lactic acid (PLLA).

Piezoelectric materials are used in energy harvesting [21], [22], sensors [23]–[25] and actuators. In this study, BT is used for filler, and PVDF and PLLA are used for matrix materials.

1.1.4 Biosensor – Application of ceramics / polymer composites -

Biosensors are used in the food industry, fermentation industry, and medicine including detection of pathogens, where quality and safety are required [26].

Biosensors consist of a biocatalyst that can detect a biological element and a transducer that can convert the combination event of the biocatalyst and the biological element into a detectable parameter [26], [27]. The biocatalyst can be biomolecules such as enzymes, DNA, RNA, metabolites, cells, and oligonucleotides, and the transducers can be electrochemical, optical, piezoelectric, acoustics, calorimetric [26], [27]. The types of biosensors are shown in Fig.1-5 [28].

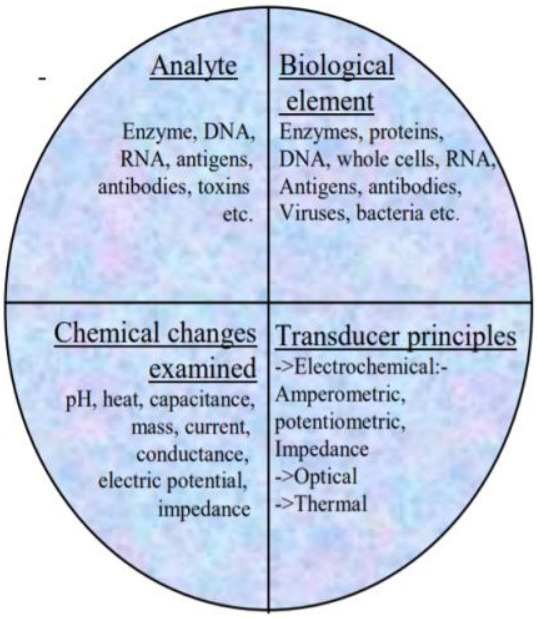

Fig.1-5 Examples of biosensors unit [28].

Examples of biosensors are shown below [26].

- Enzyme-based sensors

  Immobilization methods of the sensor are adsorption of enzymes by van der Waals forces, ionic bonding, or covalent bonding.

- Microbe-based or cell-based sensors

  The tissues for tissue-based sensors are used with plant and animal sources. The

analyte of interest is an inhibitor or a substrate of these processes.

- Immunosensors

  The sensors have anti-bodies that have a high affinity towards their respective antigens.

- DNA biosensors

  The sensors detect a single-strand nucleic acid molecule with a property that can recognize and bind to its complementary strand.

- Magnetic biosensors

  The sensors detect magnetic micro- and nanoparticles in microfluidic channels using the magnetoresistance effect.

- Thermal biosensors or calorimetric biosensors

  The sensors are developed by assimilating biosensor materials into a physical transducer.

- Piezoelectric biosensors

The sensors detect the changes in the resonance frequency of a piezoelectric crystal due to mass changes.

- Optical biosensors

  The sensors have a light source and optical components which generate a light beam with specific characteristics and beeline.

In this study, the ceramics / polymer composite materials are applied to piezoelectric biosensors.

In general, a quartz oscillator is used as a piezoelectric biosensor for weight detection. This piezoelectric biosensor is composed of a bioreceptor which is able to absorb

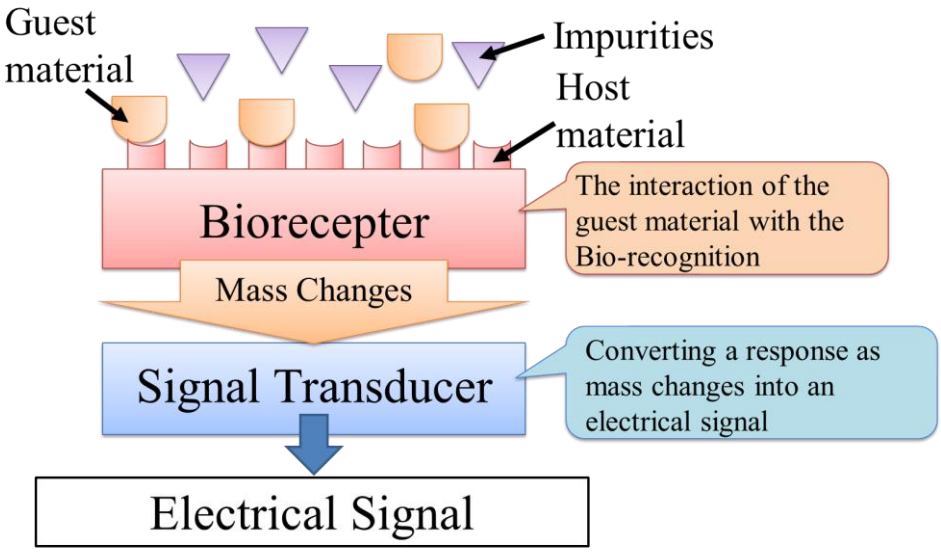

Fig.1-6 The components of the poezoelectric biosensor.

selectively an object to be detected, and a piezoelectric signal transducer sensor which is able to convert a weight change due to adsorption into an electric signal. The components of this biosensor are shown in Fig.1-6. The detection method is that applies an electric field to the quartz oscillator and the shear vibration is driven [23]. The change in weight of the target substance adsorbed on the quartz is detected as a frequency change with the shear vibration (see Fig.1-7) [23].

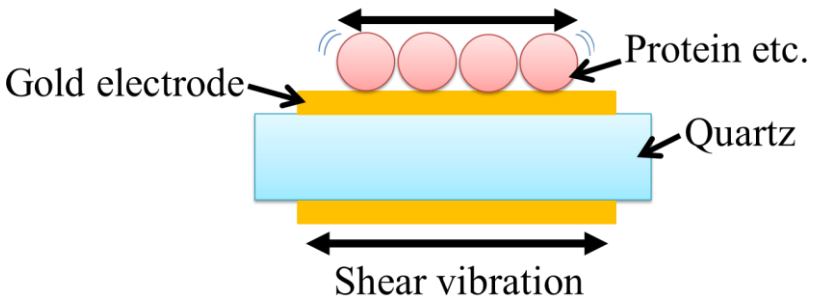

Fig.1-7 Illustration of the detectaion with the shear vibration.

Previously, Sauerbrey [29] has proposed Sauerbrey's equation for the relationship between weight change and frequency change, and it is possible to quantitatively measure weight change. The general mass sensor using quartz are explained with Sauerbrey's equations as shown below [29]:

$$\Delta F = -\frac{2F_0^2}{\sqrt{\mu_q \rho_q}} \frac{\Delta m}{A} \tag{1-9}$$

where F_0 is the fundamental frequency of the sensor, A is the electrode area, μ_q is the elastic constant of the piezoelectric sensor, ρ_q is the density of the piezoelectric sensor, Δm is the weight change, and ΔF is the measured frequency change.

1.1.5 Highly thermally conductive components

–Application of thermal conductive materials-

Thermal conductivity is an important role in a physical property because it determines the reliability and performance of industrial components in many industrial applications. In particular, the development of high thermal conductivity solid materials and the improvement of thermal conductivity are important for manufacturing high-performance and highly reliable insulations. In the case of automotive engines, low thermal conductivity is required for heat insulation components to reduce fuel consumption. Therefore, ceramics / stainless steel composites have been studied. A part of the ceramic filler is described below.

1.1.5.1 Aluminum nitride

Aluminum nitride (AlN) has high thermal conductivity, low thermal expansion

coefficient, and high electrical resistivity [26] .

1.1.5.2 Boron nitride [30]

Boron nitride (BN) has high thermal conductivity and electrical resistance, and has excellent heat resistance and low density. BN has amorphous (*a*-BN) and crystalline (hexagonal and cubic) structures. Hexagonal crystals (*h*-BN) have a layered structure similar to graphite.

1.1.5.3 Silicon nitride

Silicon nitride (Si_3N_4) has a highly thermally conductive compound with excellent mechanical strength, fracture toughness, wear resistance, corrosion resistance, fire resistance, and lightweight. The silicon nitride has two crystal structures, α- and β-. In particular, it was reported that the thermal conductivity of β-Si_3N_4 material with the ceramic crystal nuclei was about 100 $Wm^{-1}K^{-1}$ [33]. The β-Si_3N_4 ceramics is applied as a high-strength material to gas turbine engines and bearings of the components for the aircraft and automobile engines [34].

In general, high thermal conductivity can be achieved by forming thermally conductive pathways (a network of the conductive particles in the matrix material [35] and a percolating network [36]). To form the network and the percolating networks, the fillers are adding with a high volume fraction, which could deteriorate the mechanical and other properties of the composites. Therefore, it is necessary to develop composites with low particle loading. The thermal conductivity is affected by interfacial thermal resistance [37] , filler size [38], filler distribution.

1.2 Self-assembly process

The process of structure and order formation includes self-assembly and self-organization, which involve pattern formation. The self-organization is the pattern-forming system that is driven by an input of energy [39]. The self-assembly is a part of self-organization, and it is the system for equilibrium situations that assemble components to create a new level of the organization without external input [39], [40]. On the other hand, there have been reports of both occurring at the same time (see Fig.1-8).

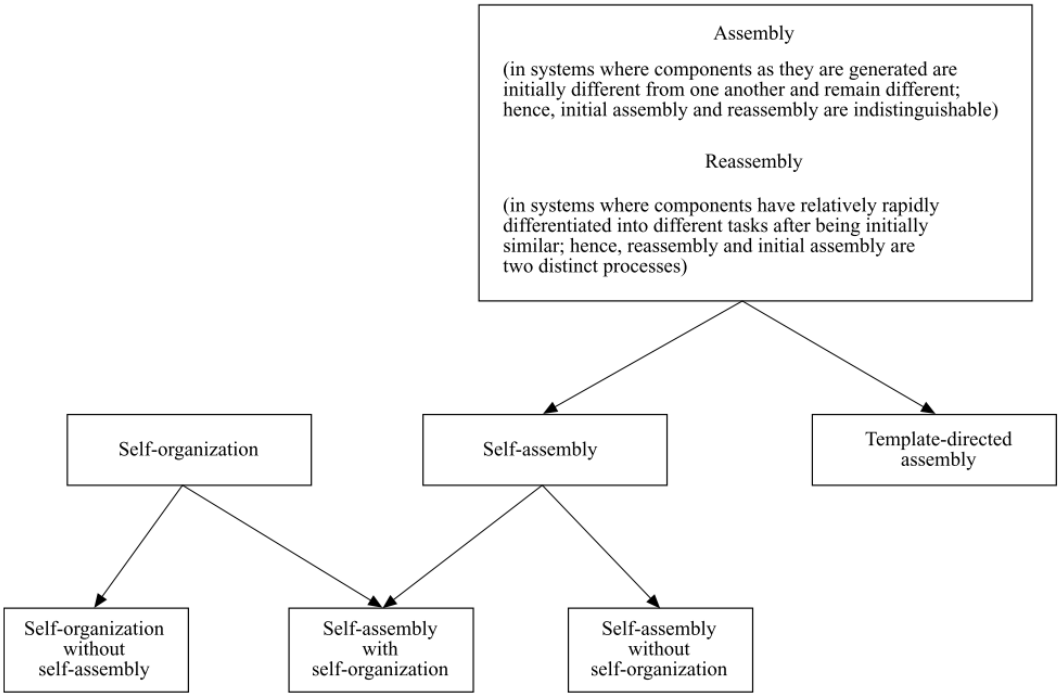

Fig.1-8 The distinction between self-assembly and self-organization [41].

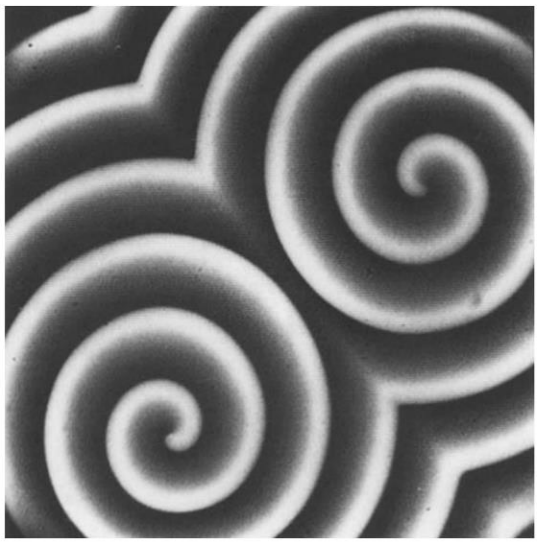

Fig.1-9 One example of BZ reaction [42].

Belousov - Zhabotinsky (BZ) reaction is known as the self-organization processes in a non-equilibrium chemical system in a solution system [43] and the patterns are formed by the BZ reaction. Fig.1-9 shows one example of BZ reaction. The self-organization process is seen in the reaction-diffusion system, which is assumed to occur due to a competitive reaction between an inhibitor and a promoter within a diffusion process. The reaction is shown in the following equation (1-10),

$$\partial v/\partial t = u - v + D_v \nabla^2 v \qquad (1\text{-}10)$$

Where *u* is the active term; *v* is the inhibitive term; *Dv* is the diffusion coefficient. In this study, the composites were prepared with the self-assembly process involving a solid. In general, self-assembly is the spontaneous organization of materials through noncovalent interactions (hydrogen bonding, Van der Waals forces, electrostatic forces, π-π interactions) with no external intervention [44]. In this study, the self-assembly

process involving solid particles is assumed to be driven by both condensing and dispersing forces. Fig.1-10 shows the self-assembly process of a solid based on equation (1-10).

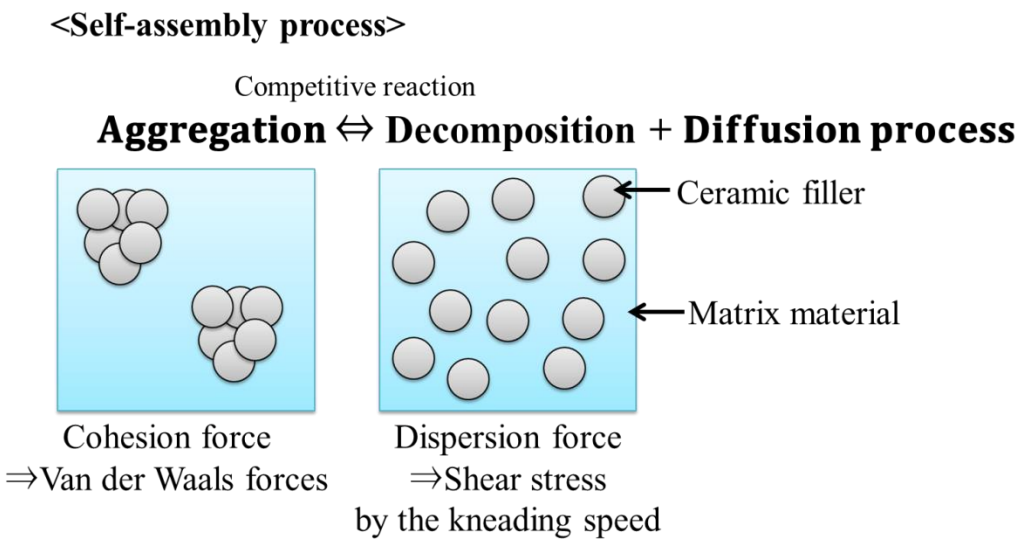

Fig.1-10 Schematic diagram showing the self-assembly process in this study.

In this study, this reaction corresponds to a process of aggregation and decomposition. Van der Waals force acts as a cohesion force. The shear stress by the kneading speed acts for decomposition. The kneading process can indicate the diffusion process in the reaction-diffusion system.

1.3 Aggregates and agglomerates

As shown in Fig.1-11, secondary particle groups are formed by the binding of ceramic fillers. There are two types of secondary particle groups (aggregates and agglomerates), and their definitions are shown in Table 1-3.

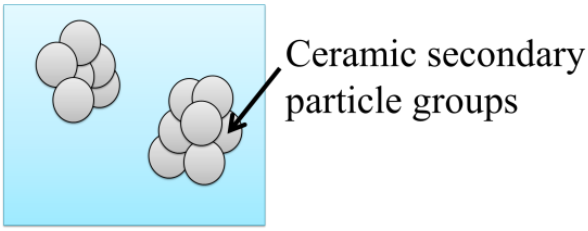

Fig.1-11 Schematic diagram of the ceramic secondary particle groups

Table 1-3 The definitions of aggregates and agglomerates [40], [45], [46].

Term	Definitions
Aggregates	・ A heterogeneous particle in which the various components are held together by relatively strong forces, and thus not easily broken apart ・ A particle comprising strongly bonded or fused particles where the resulting external surface area may be significantly smaller than the sum of calculated surface areas of the individual components ・ The forces holding an aggregate together: strong forces (for example covalent bonds) or those resulting from sintering or complex physical entanglement
Agglomerates	・A group of nanoparticles held together by relatively weak forces, including van der Waals forces, electrostatic forces, and surface tension, that may be broken apart into smaller particles upon processing ・A collection of loosely bound particles or aggregates or mixtures of the two where the resulting external surface area is similar to the sum of the surface areas of the individual components ・Simple physical entanglement

Based on Table 1-3, Fig.1-12 shows a schematic diagram of aggregates and agglomerates in this study. Aggregates are assumed that matrix materials, such as polymer, are included in the ceramic secondary particle group. On the other hand, agglomerates are assumed that the ceramic fillers are bonded in the ceramic secondary

particle group.

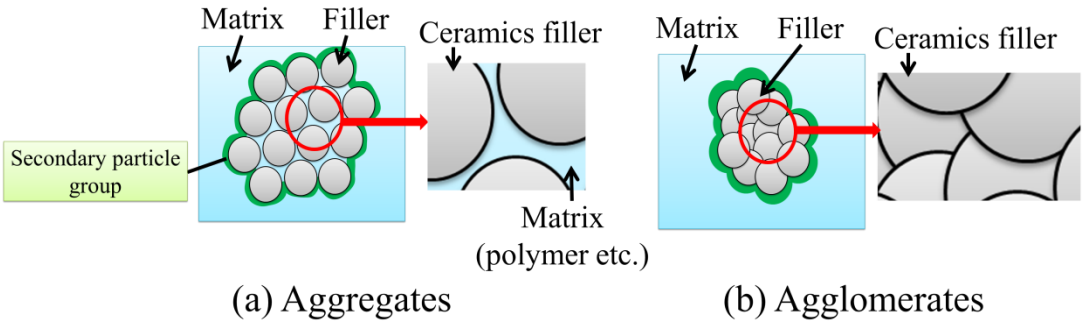

Fig.1-12 The aggregates and agglomerates assumed in this study.

1.4 Fractal analysis

The characteristics of materials such as the physical properties, strength, and toughness are determined by the material texture which is decided by the manufacturing process. It is essential to connect processes, structures, and characteristics to understand their interrelationships [47]. In this study, the structure of the composite material formed by the self-assembly process was quantified by the fractal and multifractal analysis that were able to analyze the pattern, and the relationship between the dielectric properties and thermal conductivity and the material texture was investigated.

1.4.1 Box-counting method

Fractal analysis is used to analyze spatially complex patterns using images [48]. In fact, the feature definition of structural analysis in pattern recognition has been studied [49]–[51]. Generally, the box counting method is used to derive the fractal dimension. The box-counting method was defined by Russel et al.[52]. By covering a binary

signal with boxes of scale *r*, the fractal dimension is estimated as [48] (see Fig.1-13 [53]):

$$D = -\lim_{r \to 0} \frac{\log(N(r))}{\log(r)} \tag{1-11}$$

where $N(r)$ is the number of boxes needed to completely cover the signal.

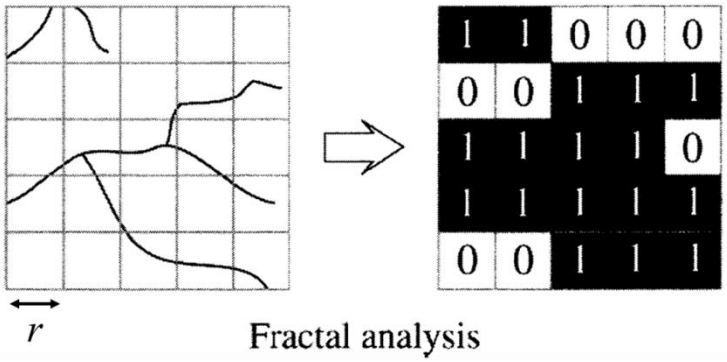

Fig.1-13 Schematic diagram showing the fractal analysis of the crack [53].

1.4.2 Multifractal analysis

The multifractal analysis which is seen as an extension of fractals has been used in medical technology [48]. The generalized dimension, *Dq* was described by the multifractal analysis. The generalized dimensions *Dq* is computed as a function of the order of the probability moment *q*. This is, the multifractal dimension can be characterized on the basis of the generalized dimensions of the *q*th order moment of a distribution, *Dq* [54]:

$$D_q = \lim_{r\to 0}\left(\frac{1}{q-1}\frac{\log \mu(q,r)}{\log(r)}\right) \quad (1\text{-}12)$$

where $\mu(q, r)$ is the partition fraction :

$$\mu(q,r) \;=\; \sum_{i=1}^{N(r)} P_i^q(r) \quad (1\text{-}13)$$

where the probability (P) is a measured quantity varies with scale r (see Fig.1-14). When q takes the values of q=0, 1 or 2, (Eq. 1-10) is reduced to [54]:

$$D_0 = -\lim_{r\to 0}\frac{\log N(r)}{\log r} \quad (1\text{-}13)$$

$$D_1 = \lim_{r\to 0}\frac{\sum_{i=1}^{N(r)} \mu_i(r) log(\mu_i(r))}{log(r)} \quad (1\text{-}14)$$

$$D_2 = \lim_{r\to 0}\frac{log(C(r))}{log(r)} \quad (1\text{-}15)$$

where D_0 is the capacity dimension. $C(r)$ is the correlation function. D_1 and D_2 are the entropy dimension and the correlation dimension, respectively. The relationship between D_0, D_1, and D_2 is,

$$D_2 \le D_1 \le D_0 \quad (1\text{-}16)$$

The equality D_0=D_1=D_2 occurs only if the fractal is statistically or exactly self-similar and homogeneous[54].

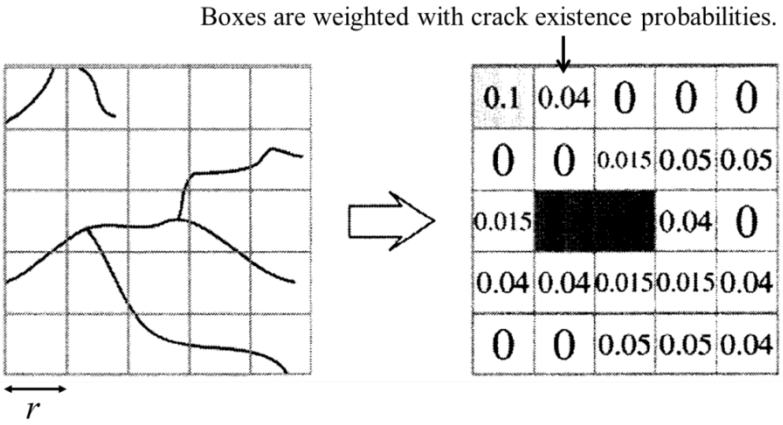

Fig.1-14 Schematic diagram showing the multifractal analysis of the crack [53].

1.5 Problems and concepts for applications and material design of composites

In this study, dielectric composites and thermal conductive composites were focused on because the dielectric constant and thermal conductivity were reflected the potential gradient and the flow velocity and these properties are used with the same composite rule.

1.5.1 Problems and concepts for applications of composites

1.5.1.1 Application of ceramics / polymer composites: piezoelectric biosensor

Tuberculosis (TB) has become prevalent mainly in developing countries. According to the report of World Health Organization (WHO), TB caused an estimated approximately 10 million new cases and 1.6 million deaths per year worldwide [55]. Therefore, it is necessary to detect patients with TB in developing countries. In the diagnostic environment in developing countries, it is essential for a diagnostic method that is portable, can be diagnosed quickly, and can be incinerated after diagnosis. Table

1-4 shows the characteristics of the conventional technology and the concepts of this study for tuberculosis diagnosis.

Table 1-4 Comparison of technologies for TB detection

	<This study> Combination of Loop-mediated Isothermal amplification (LAMP) and piezoelectric biosensors (Polymer)		Combination of LAMP and a piezoelectric biosensor	Polymerase chain reaction (PCR)
	PVDF [56]	Ceramics / polymer composites	(Quartz)	
Sensitivity	5 μg/ml	<Final goal for the application> Less than 1 μg/ml	0.01 μm/ml [57]	1 μg/ml [58]
Response speed	60 minutes	5 minutes	30 minutes [57]	About 200 minutes
Safety	High (Sensors are able to be incinerated after a diagnosis.)		Low (Sensors are reused.)	Medium (Reaction tubes are disposable.)
Total Cost	Low		High	High

Polymerase chain reaction (PCR) is required thermocyclers or equipment for result analysis and experienced staffs, and its applicability is limited in laboratory settings use [59]. In addition, the reaction time is long, and the total cost of the detection is expensive due to the use of the turbidity and fluorescence measuring device. Conversely, the loop-mediated isothermal amplification (LAMP) LAMP amplifies DNA with high efficiency under isothermal conditions with high specificity and sensitivity and detected by visual inspection [59]. Moreover, the results of LAMP are able to be provided faster than those of PCR [60]. As another TB detection method, a method of a combination of a piezoelectric biosensor using quartz which detects the mass change and the LAMP method has been proposed [57]. This method can diagnose TB more quickly. However,

the quartz must be reused after TB diagnosis since it is expensive, and then there is a risk of secondary infection. Therefore, in this study, the diagnostic method of the combination of the piezoelectric polymer biosensor which is disposable and not expensive and the LAMP method was proposed. In the case of a piezoelectric biosensor using PVDF, it is necessary to increase the sensitivity and responsivity in order to achieve the final goal for TB detection (Chapter 2). Thus, this study applied composite materials to the piezoelectric biosensor in order to improve the sensitivity and responsivity of the biosensors.

In the detection of the piezoelectric biosensor, the target materials can be detected by following the vibration of PVDF. A high elastic constant of the transducer of the biosensor is required since the vibration is affected by the viscosity of the liquid. Therefore, the ceramic fillers are added to the polymer matrix to improve the elastic constant. The sensitivity of the biosensor is related to the amount of change in the dielectric constant of the piezoelectric material, and the high dielectric constant is required. In this study, the dielectric constant was improved by controlling the material texture of the ceramics / polymer composite material.

1.5.1.2 Application of ceramics / stainless steel composites: high thermal conductive components

The components of engines are exposed to high loads, high temperatures and move at high speeds [61]. The contact friction of the engine occurs at the places where the engine slips over each other. The friction increases with increasing temperature and load so that the components cause abrasion [61]. The elevated friction and abrasions generated cause essential energetic and material losses and decrease the efficiency of

mechanical systems [62]. However, the thermal conductivity of general iron alloys is low. In order to improve the thermal conductivity, it is necessary to form a thermal conductive network and control the heat as shown in Fig.1-15. Thus, this study applied composite materials to the thermal conductive components to improve thermal conductivity.

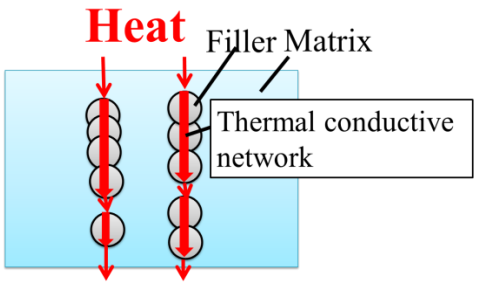

Fig.1-15 Schematic diagram showing the thermal conductive network and heat-control.

1.5.2 Problems and concepts for material design of composites

Dielectric and piezoelectric polymer materials are widely used because they are easily processed into large area films [11].

Thermal conductivity materials are used for industries such as manufacturing and production, chemical plant, building materials, and automobile component including engines.

However, the dielectric and piezoelectric polymer materials and the high thermal conductive components have the following problems.

1.5.2.1 General problems

< Dielectric and piezoelectric material>

Generally, the dielectric constants (ε') of piezoelectric polymers are relatively low at less than 10 [11].

< High thermal conductive components >

1. The thermal conductivity of the iron alloys is relatively low around room temperature.
2. The thermal conductivity of one of the austenitic stainless steel alloys, SUS316L stainless steel, is about 15 W $m^{-1}K^{-1}$, which is lower than carbon steel. Therefore, the sliding component of the engine that operates at high load pressure is limited for the application.

1.5.2.2 Target of material development

1. To increase the ε' for the polymers, ceramic powder fillers with a high ε' are added to the polymer matrix [11]. (Ceramics / polymer composites)
2. It is considered to combine SUS316L stainless steel and excellent ceramics to increase the thermal conductivity of SUS316L stainless steel with maintaining excellent characteristics. (Ceramics / SUS316L stainless steel composite)

1.5.2.3 Material development problems

A 50 vol.% or more of ceramics with a high dielectric constant and thermal conductivity are applied to the polymer or stainless steel matrix to achieve a high dielectric constant or thermal conductivity. Thus, the mechanical properties of these

composites are extremely poor and are not suitable for use in dielectric and piezoelectric materials and thermal conductivity materials, such as capacitors, piezoelectric materials, or automotive engines.

1.5.3 Previous reports and problems for the researches of the composites

In ceramics / polymer composites, it was proposed that the size, shape, and aggregation of $BaTiO_3$ (BT) particles influence the effective bulk ε' of BT fillers or polymer composites with a high ε' [63]. Meanwhile, it was reported that the particle shape and size of the granules in the related ceramics play an important role in the network formation [64]. It was shown that the average secondary particle area of BT filler aggregates of BT filler/poly-L-lactic acid (PLLA) composites is related to the dielectric constant [65]. Hence, it was suggested that the formation of ceramic secondary particle groups improves function. In addition, the electrical properties are controlled by a microstructure with grain boundaries such as ceramics / intergranular material. Therefore, it is important to control the microstructure to increase the dielectric properties.

In order to improve the automobile engine components, it is important to form a thermal conductivity network using ceramic fillers. In addition, it is important to reduce the effect of thermal resistance at the interface between filler and matrix material to improve the thermal conductivity of the composites [37]. Therefore, it is necessary to control the microstructure of the thermally conductive composite material.

Thus, in this thesis, the purpose was to improve the dielectric properties and the thermal conductivity with a small amount of filler (0 vol.% -20 vol.%) for the application, the piezoelectric biosensor and high thermal conductivity component. In

conventional composite research, fillers are dispersed in a matrix material. On the other hand, in this thesis, the ceramics aggregate and the thermal conductivity network using ceramic secondary particle groups were formed by the self-assembly process to improve the dielectric properties and the thermal conductivity. The ceramics / polymer composite relates to the self-assembly process of solids in a liquid. The ceramics / SUS316L stainless steel composite relates to the self-assembly process of solids in solid. The problems of the research are as follows:

(1) The self-assembly process of solids in liquid and solids in solids have not clarified.
(2) There are few research examples of quantitative evaluation of self-assembled material texture.
(3) There are few studies on the ceramics / polymer heterointerface in the ceramics aggregate in the ceramics / polymer composite material and dielectric properties.
(4) There are few studies on the ceramics / stainless steel interface and thermal conductivity with forming the self-assembled ceramic secondary particle group.

1.5.4 Concepts and approach of material design in this study

In this study, the material is designed to improve the dielectric properties and thermal conductivity by adding a small amount of filler (0 to 20 vol.%). In particular, targets of the design materials are piezoelectric biosensor and high thermal conductive components. The material design concepts of this thesis are shown in Fig.1-16. In the material design approach of this study, it was proposed that the dielectric properties would improve by forming self-assembled ceramic aggregates having a ceramics / polymer / ceramics heterointerface. In the thermal conductivity, it was proposed that the

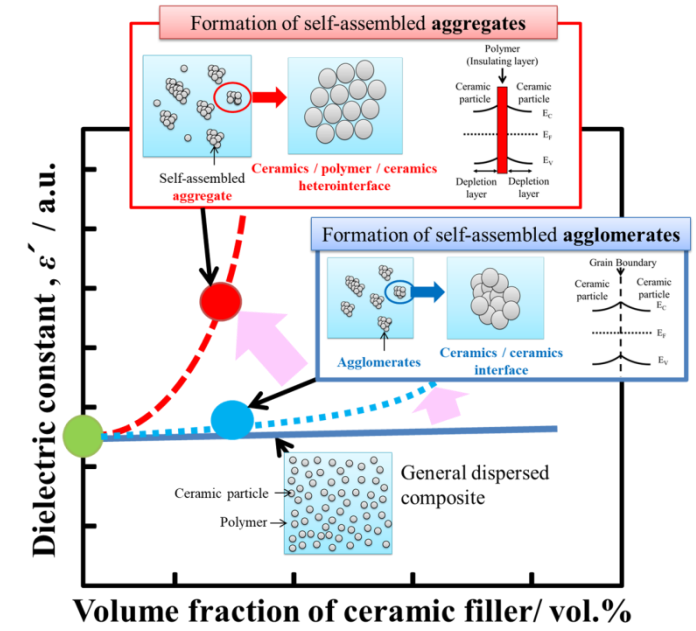

(a) Concept of the dielectric materials

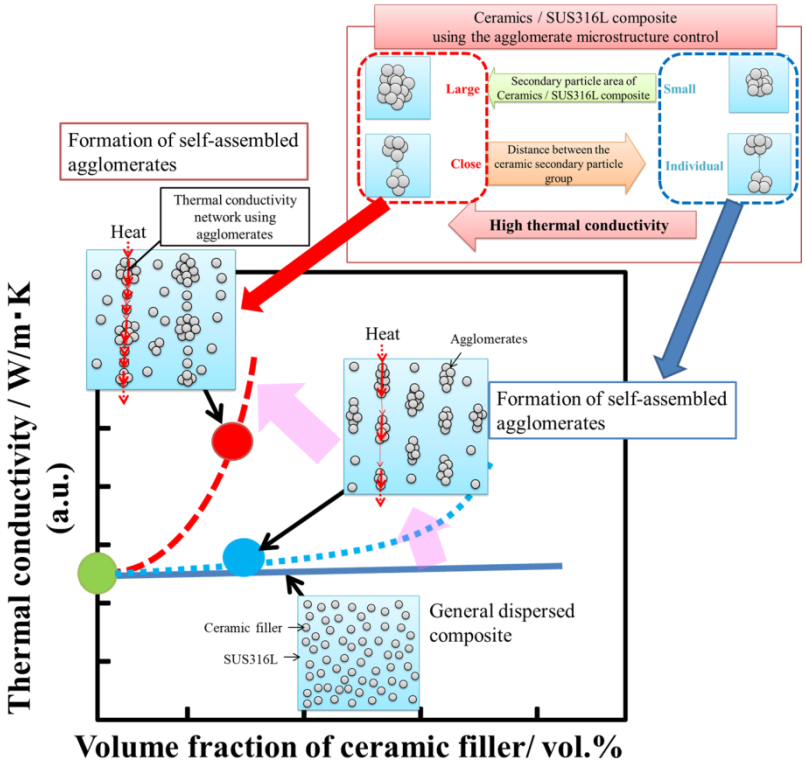

(b) Concept of the thermal conductive materials

Fig.1-16 Concepts of the composites material design to improve the dielectric properties and thermal conductivity.

thermal conductivity was possible to be improved by forming ceramic particle groups for the thermal conductivity networks. In this study, the formation of ceramic secondary particle groups was controlled by the self-assembly process as shown in Fig.1-10. The self-assembly processes in this thesis are as follows:

<Ceramics / polymer composite (solids in liquid)>

The self-assembly process of the ceramics / polymer composites was assumed as shown in Fig.1-17.

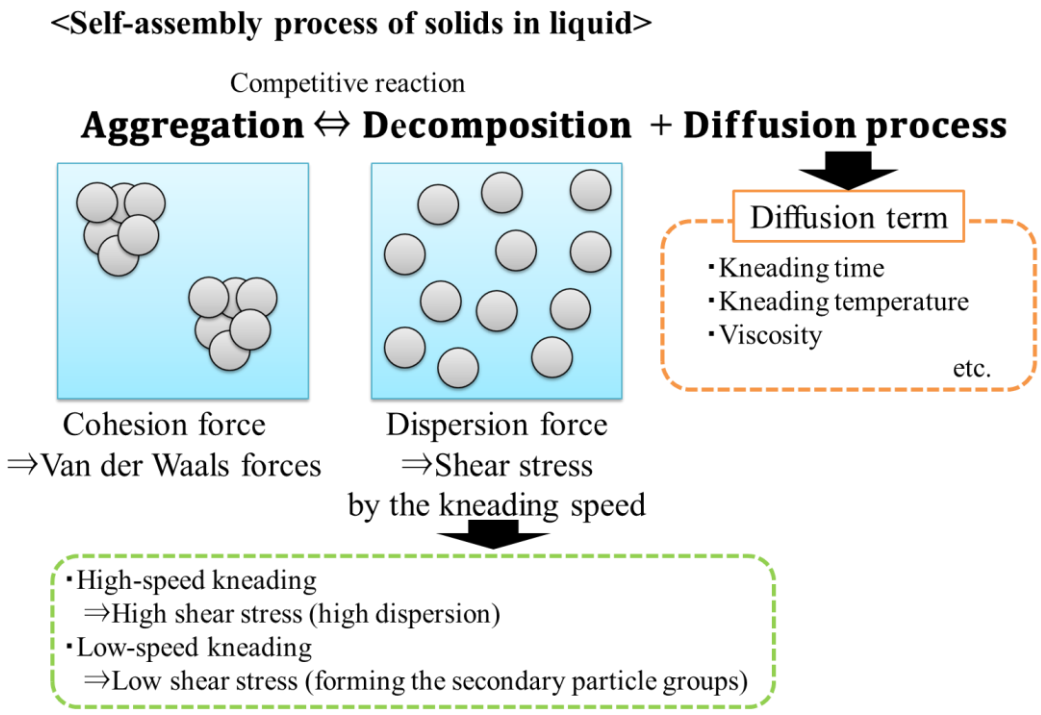

Fig.1-17 Self-assembly process of solids in liquid in this study.

- Van der Waals force acts as a cohesion force.
- The shear stress by the kneading speed acts for decomposition.

- The kneading process can indicate the diffusion process in the reaction-diffusion system, and the temperature, kneading time, and viscosity relate to the diffusion process.

Therefore, (1) the kneading speed and (2) viscosity of the dispersant were controlled to prepare the ceramics / polymer composite materials in this study.

<Ceramics / SUS316L stainless steel composite (solids in solid)>

Fig.1-18 shows the self-assembly process of ceramics / SUS316L stainless steel composites. In the case of ceramics / SUS316L stainless steel composites, it is considered that the diffusion dissipation process and sintering process relate to the diffusion process. In this study, spark plasma sintering (SPS) can exclude the diffusion process due to grain growth.

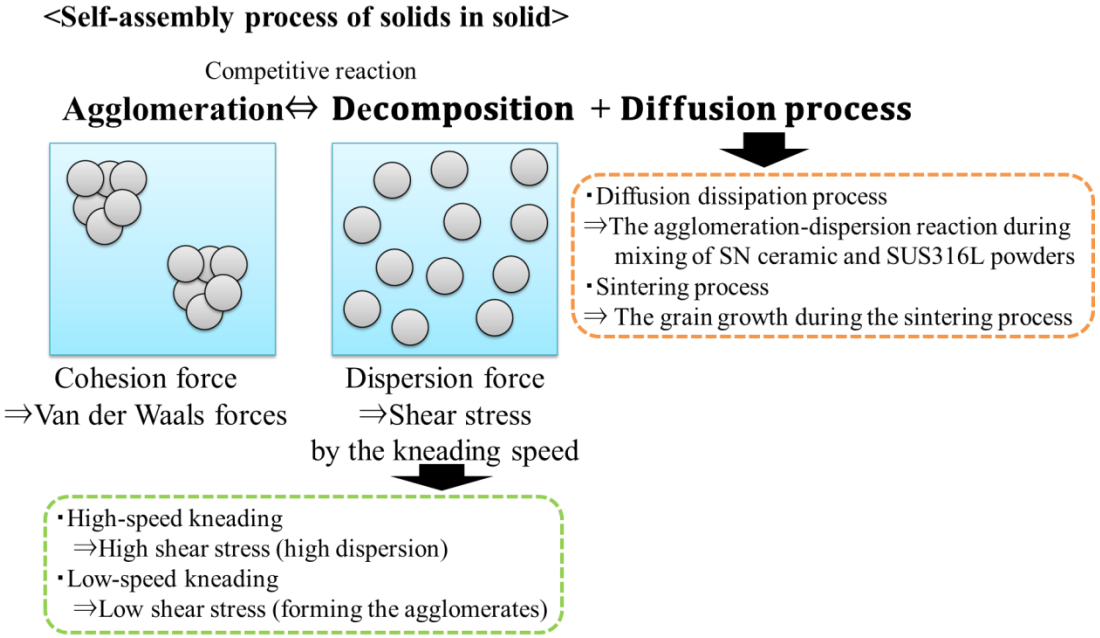

Fig.1-18 Self-assembly process of solids in solid in this study.

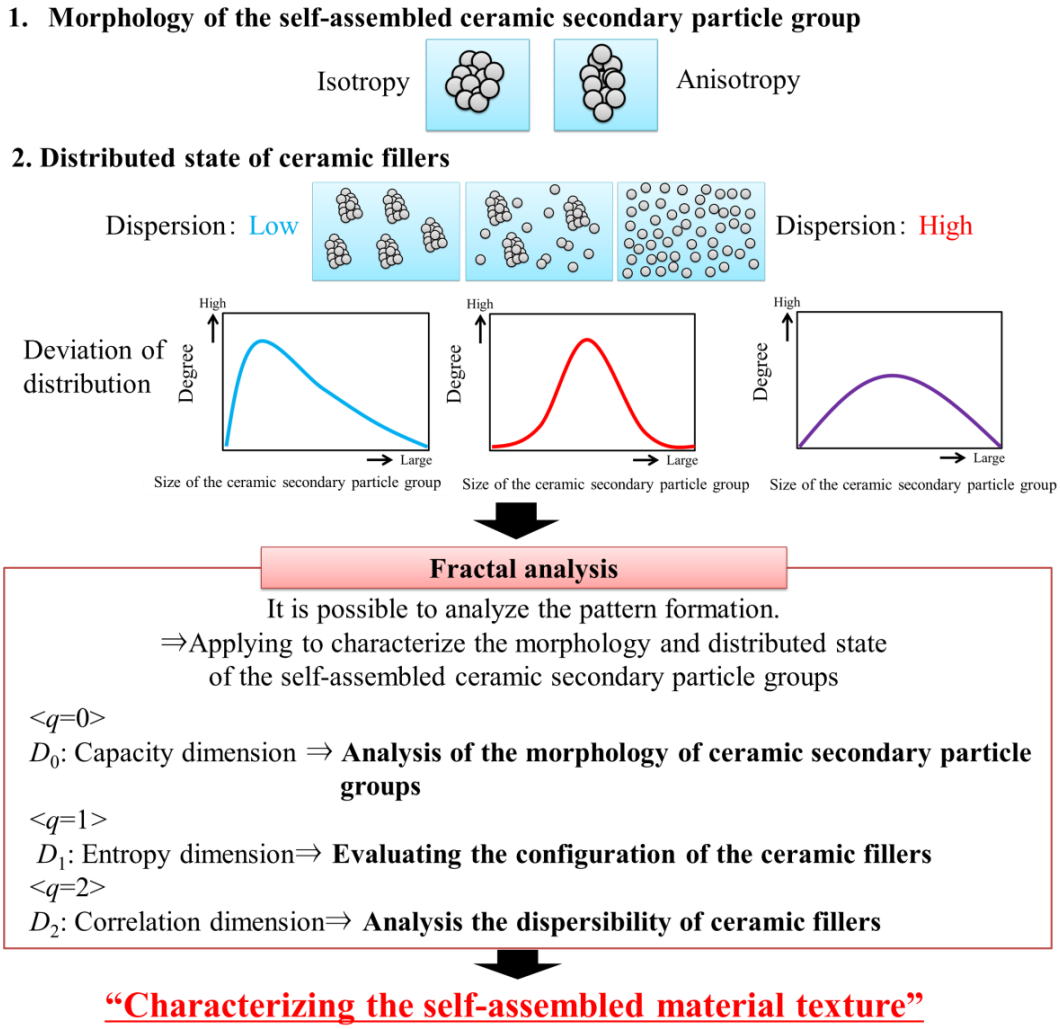

Fig.1-19 Characters of the self-assembled material texture by the fractal analysis.

The pattern is formed within the self-assembly process. In this study, the fractal analysis (the box-counting and multifractal analysis) which evaluates quantitatively the pattern was applied to characterize (1) the morphology of the self-assembled ceramic secondary particle group and (2) the distributed state of ceramic fillers (see Fig.1-19)

The material design approaches of this thesis are as follows (see Fig.1-20):

(1) The morphology of the ceramic secondary particle group, dispersion state (the entropy of configuration and dispersibility of the ceramic secondary particle groups), and formation of the interface of ceramic secondary particle groups by the self-assembly process of solids in solids and solids in liquid were investigated.

(2) The relationship between the self-assembled material texture prepared under the different manufacturing processes and the dielectric properties and thermal conductivity was discussed.

(3) Quantitative evaluation of this self-assembled material texture was performed using the multifractal analysis that analyzes patterns.

1.6 Purpose of this study

In this study, the material is designed to improve the dielectric properties and thermal conductivity by adding a small amount of filler (0 to 20 vol.%). In particular, the targets of the design materials were piezoelectric biosensors and high thermal conductive components. The material texture was controlled by the self-assembly process involving the solid to improve dielectric properties and thermal conductivity. In this study, the morphology, dispersion state, and the formation of the filler / matrix interface formation of fractal ceramic secondary particle groups prepared under the different manufacturing processes were discussed. The morphology, the entropy of configuration and dispersibility of the self-assembled ceramic secondary particle groups were performed by the multifractal analysis. Hence, self-assembled secondary particle groups were formed, and the relationship between the morphology, the dispersion state, and the interface state of the self-assembled ceramic secondary particle groups and the dielectric

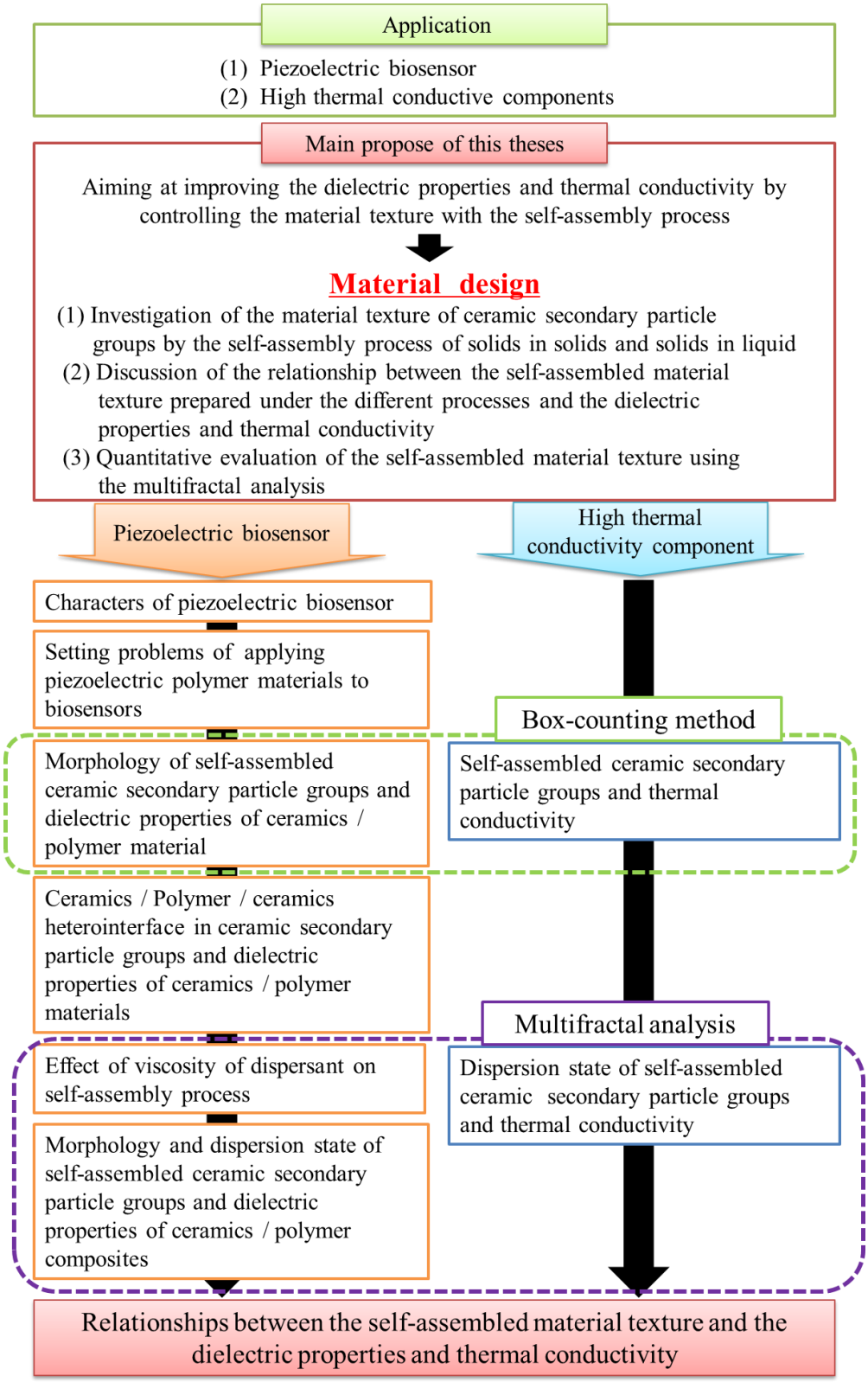

Fig.1-20 The approach of material design in this study.

properties and thermal conductivity was investigated toward the application.

1.7 Thesis organization

The thesis consists of the following 4 Chapters.

Chapter 1 shows the research background, problems, concepts and approach, and purpose.

In Chapter 2, ceramics / polymer composite materials were produced for the application, a piezoelectric biosensor. First, a biosensor with a piezoelectric polymer was prepared and the problems of the polymer piezoelectric biosensor were set. Next, in order to improve the dielectric properties by adding a small amount of filler, the self-assembled ceramics / polymer composites were manufacturing under the different processes, and the multifractal analysis was performed as a quantitative evaluation of the self-assembled material texture. In addition, the dispersion state under different production conditions was investigated. In particular, the ceramics / polymer / ceramics heterointerface in the ceramic particle group and dielectric properties of the ceramics / polymer composites with the manufacturing process were discussed. Finally, the material texture of the self-assembled ceramics / polymer composites and dielectric properties by changing the viscosity of the dispersant were investigated. Furthermore, the morphology, the entropy of configuration, and dispersibility of the ceramic secondary particle groups were characterized by the multifractal. In this study, the piezoelectric materials PLLA and PVDF were used as a matrix, and BT was used as ceramic filler.

In Chapter 3, a silicon nitride (SN) / stainless steel (SUS316L) composite material was prepared. And then, the relationship between the self-assembled material texture

and the thermal conductivity was investigated. In particular, fractal analysis and multifractal analysis were attempted to quantitatively evaluate the thermal conductivity network using the self-assembled SN secondary particle groups.

Chapter 4 shows the conclusions of this thesis and future works.

References

[1] M. K. S. Sai, “Review of Composite Materials and Applications,” vol. 7.

[2] M. K. Egbo, “A fundamental review on composite materials and some of their applications in biomedical engineering,” *Journal of King Saud University - Engineering Sciences*, 2020, doi: 10.1016/j.jksues.2020.07.007.

[3] D. H. Yoon, J. Zhang, and B. I. Lee, “Dielectric constant and mixing model of BaTiO3 composite thick films,” *Materials Research Bulletin*, vol. 38, no. 5, pp. 765–772, 2003, doi: 10.1016/S0025-5408(03)00075-8.

[4] B. Sareni, L. Krähenbühl, A. Beroual, and C. Brosseau, “Effective dielectric constant of periodic composite materials,” *Journal of Applied Physics*, vol. 80, no. 3, pp. 1688–1696, 1996, doi: 10.1063/1.362969.

[5] K. Monden, Y. Okajima, and K. Yashima, “Application of percolation theory and development of high conducting material in a compound thermal component,” *Journal of Japan Institute of Electronics Packaging*, vol. 14, no. 6, pp. 485–491, 2011, doi: 10.5104/jiep.14.485.

[6] C. J. Maxwell, *A Treatise on Electricity and Magnetism*, vol. 1. 1904.

[7] H. Fricke, “A Mathematical Treatment of the Electrical conductivity and Capacity of Disperse Systems,” *Physics Review*, vol. 24, pp. 575–587, 1924, doi: 10.1103/PhysRev.24.575.

[8] E. R. Meredith, *STUDIES ON THE CONDUCTIVITIES OF DISPERSIONS*. Lawrence Berkeley National Laboratory, 1959.

[9] R. L. Hamilton and O. K. Crosser, “Thermal conductivity of heterogeneous two-component systems,” *Industrial and Engineering Chemistry Fundamentals*, vol. 1, no. 3, pp. 187–191, 1962, doi: 10.1021/i160003a005.

[10] V. D. A. G. Bruggeman, “Berechnung verschiedener physikalischer Konstanten von heterogenen Substanzen,” vol. 24, pp. 665–676, 1935.

[11] P. Barber *et al.*, “Polymer composite and nanocomposite dielectric materials for pulse power energy storage,” *Materials*, vol. 2, no. 4, pp. 1697–1733, 2009, doi: 10.3390/ma2041697.

[12] P. Barber *et al.*, *Polymer composite and nanocomposite dielectric materials for pulse power energy storage*, vol. 2, no. 4. 2009.

[13] K. Kanari and T. Ozawa, “充てん材配合エポキシ樹脂の熱伝導率,” 熱物性, vol. 3, no. 2, pp. 106–111, 1989.

[14] K. Kanari, “Thermal Cnnrluctivitv of Composite Matprials,” *Kobunshi*, vol. 26, no. 8, pp. 557–561, 1977.

[15] R. M. Mutiso and K. I. Winey, *Reference Module in Materials Sicence and Materials Englineering -Polymer Science: A Comprehensive Reference-*, vol. 7. Elsevier B.V., 2012.

[16] M. R. Mansor, S. H. S. M. Fadzullah, N. A. B. Masripan, G. Omar, and M. Z. Akop, *Functionalized Graphene Nanocomposites and their Derivatives*. Elsevier Inc., 2018.

[17] S. Mishra, L. Unnikrishnan, S. K. Nayak, and S. Mohanty, “Advances in Piezoelectric Polymer Composites for Energy Harvesting Applications: A

Systematic Review," *Macromolecular Materials and Engineering*, vol. 304, no. 1, pp. 1–25, 2019, doi: 10.1002/mame.201800463.

[18] A. J. Lovinger, "Ferroelectric Polymers," *SCIENCE*, vol. 220, no. 4602, pp. 1115–1121, 1983, [Online]. Available: http://www.sciencemag.org/content/220/4602/1115.short.

[19] W. Xia and Z. Zhang, "PVDF-based dielectric polymers and their applications in electronic materials," *IET Nanodielectrics*, vol. 1, no. 1, pp. 17–31, 2018, doi: 10.1049/iet-nde.2018.0001.

[20] F. Bernard, L. Gimeno, B. Viala, B. Gusarov, and O. Cugat, "Direct Piezoelectric Coefficient Measurements of PVDF and PLLA under Controlled Strain and Stress," *Proceedings*, vol. 1, no. 10, p. 335, 2017, doi: 10.3390/proceedings1040335.

[21] R. Mishra, S. Jain, and C. D. Prasad, "A review on piezoelectric material as a source of generating electricity and its possibility to fabricate devices for daily uses of army personnel," *International Journal of Systems, Control and Communications*, vol. 6, no. 3, pp. 212–221, 2015, doi: 10.1504/IJSCC.2015.068908.

[22] C. Covaci and A. Gontean, "Piezoelectric energy harvesting solutions: A review," *Sensors (Switzerland)*, vol. 20, no. 12, pp. 1–37, 2020, doi: 10.3390/s20123512.

[23] V. M. Mecea, "Is quartz crystal microbalance really a mass sensor?," *Sensors and Actuators, A: Physical*, vol. 128, no. 2, pp. 270–277, 2006, doi: 10.1016/j.sna.2006.01.023.

[24] Y. Okahata and H. Furusawa, "Biosensor Using a Quartz-crystal Microbalance," *IEEJ Transactions on Sensors and Micromachines*, vol. 123, no. 11, pp. 459–464,

2003, doi: 10.1541/ieejsmas.123.459.

[25] J. F. Tressler, S. Alkoy, and R. E. Newnham, “Piezoelectric sensors and sensor materials,” *Journal of Electroceramics*, vol. 2, no. 4, pp. 257–272, 1998, doi: 10.1023/A:1009926623551.

[26] P. Mehrotra, “Biosensors and their applications - A review,” *Journal of Oral Biology and Craniofacial Research*, vol. 6, no. 2, pp. 153–159, 2016, doi: 10.1016/j.jobcr.2015.12.002.

[27] S. K. Metkar and K. Girigoswami, “Diagnostic biosensors in medicine – A review,” *Biocatalysis and Agricultural Biotechnology*, vol. 17, no. October 2018, pp. 271–283, 2019, doi: 10.1016/j.bcab.2018.11.029.

[28] T. Bhardwaj, “A Review on Immobilization Techniques of Biosensors,” *International Journal of Engineering Research & Technology (IJERT)*, vol. 3, no. 5, pp. 294–298, 2014, [Online]. Available: www.ijert.org.

[29] G. Sauerbrey, “Verwendung von Schwingquarzen zur Wägung dünner Schichten und zur Mikrowägung,” *Zeitschrift für Physik*, vol. 155, no. 2, pp. 206–222, 1959, doi: 10.1007/BF01337937.

[30] X. Huang, P. Jiang, and T. Tanaka, “A review of dielectric polymer composites with high thermal conductivity,” *IEEE Electrical Insulation Magazine*, vol. 27, no. 4, pp. 8–16, 2011, doi: 10.1109/MEI.2011.5954064.

[31] G. Long and L. M. Foster, “Aluminum Nitride, a Refractory for Alumium to 2000℃,” vol. 42, no. 2, pp. 53–59, 1959.

[32] G. A. Slack, “Nonmetallic crystals with high thermal conductivity,” vol. 34, pp. 321–335, 1973.

[33] K. Furuya, F. Munakata, K. Matsuo, Y. Akimune, J. Ye, and A. Okada,

"Microstructural control of β-silicon nitride ceramics to improve thermal conductivity," *Journal of Thermal Analysis and Calorimetry*, vol. 69, no. 3, pp. 873–879, 2002, doi: 10.1023/A:1020660006988.

[34] K. Komeya and F. Noda, "Aluminum nitride and silicon nitride for high temperature gas turbine engines," *SAE Paper*, no. 40237, pp. 1030–1035, 1974.

[35] X. Cui, P. Ding, N. Zhuang, L. Shi, N. Song, and S. Tang, "Thermal conductive and mechanical properties of polymeric composites based on solution-exfoliated boron nitride and graphene nanosheets: A Morphology-Promoted Synergistic Effect," *ACS Applied Materials and Interfaces*, vol. 7, no. 34, pp. 19068–19075, 2015, doi: 10.1021/acsami.5b04444.

[36] A. Shimamura, Y. Hotta, H. Hyuga, N. Kondo, and K. Hirao, "Effect of amounts and types of silicon nitride on thermal conductivity of Si_3N_4/epoxy resin composite," *Journal of the Ceramic Society of Japan*, vol. 123, no. 1441, pp. 908–912, 2015, doi: 10.2109/jcersj2.123.908.

[37] H. He, R. Fu, Y. Shen, Y. Han, and X. Song, "Preparation and properties of Si_3N_4/PS composites used for electronic packaging," *Composites Science and Technology*, vol. 67, no. 11–12, pp. 2493–2499, 2007, doi: 10.1016/j.compscitech.2006.12.014.

[38] F. Wang, L. T. Drzal, Y. Qin, and Z. Huang, "Mechanical properties and thermal conductivity of graphene nanoplatelet/epoxy composites," *Journal of Materials Science*, vol. 50, no. 3, pp. 1082–1093, 2015, doi: 10.1007/s10853-014-8665-6.

[39] B. Bensaude-Vincent, "Self-Assembly, self-organization: Nanotechnology and vitalism," *NanoEthics*, vol. 3, no. 1, pp. 31–42, 2009, doi: 10.1007/s11569-009-0056-0.

[40] British Standards Institution, *Terminology for nanomaterials. PAS 136:2007*, vol. PAS 136:20. 2007.

[41] A. B. Sendova-franks and N. R. Franks, “Self-assembly, self-organization and division of labour,” vol. 354, no. 1388, pp. 1395–1405, 1999.

[42] Stefan C. Müller, T. Plesser, and Benno Hess, “Two-dimensional sperctraphotometory and pseudo-color representation of chemical reaction patterns,” vol. 73, pp. 165–179, 1986.

[43] I. R. Epstein, J. A. Pojman, and O. Steinbock, “Introduction:self-organization in nonequilibrium chemical systems,” *Chaos*, vol. 16, no. 3, 2006, doi: 10.1063/1.2354477.

[44] C. J. Brinker, “Evaporation-induced self-assembly: functional nanostructures made easy,” *MRS Bulletin*, vol. 29, no. 9, pp. 631–640, 2004, doi: 10.1557/mrs2004.183.

[45] National Institute for Occupational Safety and Health, *Approaches and safe nanotechnology -Managing the health and safety concerns associated with engineered nanomaterials-*, vol. 2009–125. 2009.

[46] ASTM International, *Standard terminology relating to textiles*, vol. 06, no. ASTM E2456. 2012.

[47] N. Sato, S. Sadamatsu, and Y. Adachi, “A change and prospect of quantitative evaluation of microstructure morphology,” *Tetsu-Hagane*, vol. 100, no. 10, pp. 1182–1190, 2014.

[48] R. Lopes and N. Betrouni, “Fractal and multifractal analysis: A review,” *Medical Image Analysis*, vol. 13, no. 4, pp. 634–649, 2009, doi: 10.1016/j.media.2009.05.003.

[49] M. R. Haralick, K. Shanmugam, and I. Dinstein, “Textural features for image Classifiaction,” *IEEE Transactions on Systems*, vol. SMC-3, no. 6, pp. 610–621, 1973.

[50] W. K. Pratt and S. Member, “Visual discrimination of stochastic texture fields,” vol. SMC-8, no. 11, pp. 796–804, 1978.

[51] S. Kobayashi, R. Kobayashi, and T. Watanabe, “Control of grain boundary connectivity based on fractal analysis for improvement of intergranular corrosion resistance in SUS316L austenitic stainless steel,” *Acta Materialia*, vol. 102, pp. 397–405, 2016, doi: 10.1016/j.actamat.2015.08.075.

[52] D. A. Russell, J. D. Hanson, and E. Ott, “Dimension of strange attractors,” *Physical Review Letters*, vol. 45, no. 14, pp. 1175–1178, 1980, doi: 10.1103/PhysRevLett.45.1175.

[53] 柏谷公希米田哲朗, “岩石の風化過程で生じる亀裂パターン変化とマルチフラクタル解析による評価,” vol. 45, no. 2, pp. 90–100, 2004.

[54] A. Posadas, R. Quiroz, A. Tannús, S. Crestana, and C. M. Vaz, “Characterizing water fingering phenomena in soils using magnetic resonance imaging and multifractal theory,” *Nonlinear Processes in Geophysics*, vol. 16, no. 1, pp. 159–168, 2009, doi: 10.5194/npg-16-159-2009.

[55] WHO, *WHO TB burden report 2018*, vol. 63, no. 10. 2018.

[56] M. Takeda *et al.*, “Properties of biopolymers detection with piezoelectric polymer biosensor in relaxation behavior process,” vol. 140, no. 2, pp. 43–49, 2020, doi: 10.1541/ieejsmas.140.43.

[57] P. Prakrankamanant *et al.*, “The development of DNA-based quartz crystal microbalance integrated with isothermal DNA amplification system for human

papillomavirus type 58 detection," *Biosensors and Bioelectronics*, vol. 40, no. 1, pp. 252–257, 2013, doi: 10.1016/j.bios.2012.07.033.

[58] V. Lorente-Leal *et al.*, "Validation of a real-time PCR for the detection of mycobacterium tuberculosis complex members in Bovine tissue samples," *Frontiers in Veterinary Science*, vol. 6, no. MAR, pp. 1–9, 2019, doi: 10.3389/fvets.2019.00061.

[59] B. Phetsuksiri *et al.*, "Comparison of loop-mediated isothermal amplification, microscopy, culture, and PCR for diagnosis of pulmonary tuberculosis," *Japanese Journal of Infectious Diseases*, vol. 73, no. 4, pp. 272–277, 2020, doi: 10.7883/yoken.JJID.2019.335.

[60] N. Tomita, Y. Mori, H. Kanda, and T. Notomi, "Loop-mediated isothermal amplification (LAMP) of gene sequences and simple visual detection of products," *Nature Protocols*, vol. 3, no. 5, pp. 877–882, 2008, doi: 10.1038/nprot.2008.57.

[61] A. E. Letters, "TRIBOLOGICAL PROPERTIES OF PISTON-CYLINDER SET IN INTERNAL COMBUSTION ENGINES," vol. 1, no. 1, pp. 29–33, 2016.

[62] K. V Chauhan and S. K. Rawal, "A review paper on tribological and mechanical properties of ternary nitride based coatings," *Procedia Technology*, vol. 14, pp. 430–437, 2014, doi: 10.1016/j.protcy.2014.08.055.

[63] J. Robertson and B. R. Varlow, "Non-linear ferroelectric composite dielectric materials," *IEEE Transactions on Dielectrics and Electrical Insulation*, vol. 12, no. 4, pp. 779–790, 2005, doi: 10.1109/TDEI.2005.1511103.

[64] Y. Akimune, F. Munakata, M. Ando, Y. Okamoto, and N. Hirosaki, "Optimization of mechanical and electrical properties of TiN/Si_3N_4 material by agglomerates-microstructure-control," *Journal of the Ceramic Society of Japan*,

vol. 105, no. 2, pp. 122–125, 1997, doi: 10.2109/jcersj.105.122.

[65] F. Munakata, K. Yoshino, K. Nemoto, S. Abe, and A. Ito, “Effect of self-assembly material texture and dielectric properties of $BaTiO_3$/poly-L-lactic-acid composites,” *Materials Letters*, vol. 221, pp. 147–149, 2018, doi: 10.1016/j.matlet.2018.03.008.

Chapter 2 Self-assembled barium titanate (BT) / polymer composite material texture and dielectric properties -application to a piezoelectric biosensor-

The piezoelectric biosensor has a bioreceptor that is able to absorb selectively an object to be detected and a piezoelectric signal transducer sensor which is able to convert a weight change due to adsorption into an electric signal. In this study, the ceramics / polymer composites were prepared to apply to the signal transducer of the biosensor instead of the general material, quartz (see Fig.2-1). First of all, the polymer biosensor was manufactured to present problems for the application. And then, the relationship between the dielectric properties of self-assembled BT / polymer composites and the morphology, entropy of configuration, and dispersibility of the self-assembled BT secondary particle groups under the different manufacturing processes were investigated to improve the dielectric properties of the BT / polymer composites.

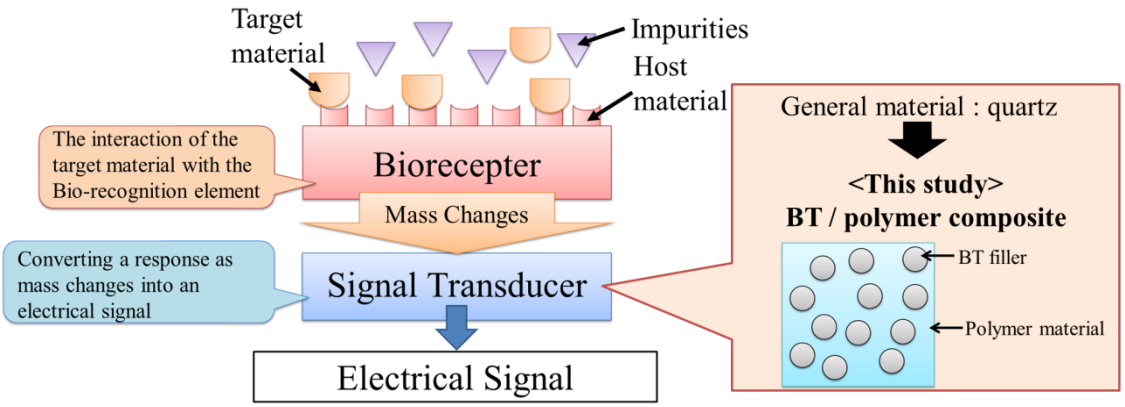

Fig. 2-1 Illustration of the application of the ceramics / polymer composites (the piezoelectric biosensor).

2.1 Properties of biopolymers detection with piezoelectric polymer biosensor in relaxation behavior process

2.1.1 Introduction

Tuberculosis (TB) has become prevalent mainly in developing countries. Therefore, it is essential to detect patients with TB using the diagnose method that is portable, can be diagnosed quickly, and can be incinerated after diagnosis in developing countries. Recently, the method of the dictation of TB in developing countries is the loop-mediated isothermal amplification (LAMP) [1]. In the diagnosis by the LAMP method, TB can be diagnosed by detecting the by-product pyrophosphate generated by the DNA amplification reaction [2], [3]. On the other hand, a quartz oscillator is generally used as a piezoelectric biosensor for weight detection. This quartz oscillator is composed of a quartz oscillator and a feedback amplification type oscillator circuit, and the frequency changes with loading the weight change by the adsorption of the target substance. The detection method is that the shear vibration of the quartz is driven by applying an AC electric field to the quartz oscillator [4]. The change in weight of the target substance adsorbed on the quartz oscillator is detected as a frequency change with the shear vibration [5]. The detection method that combines the LAMP method and the piezoelectric biosensor with quartz has been proposed [6]. In this study, in the future, it will be possible to detect biopolymers such as DNA and RNA in the amplification process of the LAMP method by combining the LAMP method and the piezoelectric biosensor with polymer material, and the development of the sensor is aimed to detect TB quickly in developing countries. The advantage of the piezoelectric polymer biosensor is cheaper than quartz. Therefore, the polymer piezoelectric material is used instead of quartz and will be able to be incinerated after TB diagnosis. This piezoelectric

biosensor is composed of a bioreceptor which is able to absorb selectively an object to be detected, and a piezoelectric signal transducer sensor which is able to convert a weight change due to adsorption into an electric signal (see Fig.2-1). Previously, Sauerbrey [7] proposed Sauerbrey's equation for the relationship between weight change and frequency change, and it is possible to quantitatively measure the weight change. The vibration modes of the polymer piezoelectric material have been reported to be expansion and contraction in the length direction, expansion and contraction in the width direction, and expansion and contraction in the thickness direction [8]. This vibration is used to detect the target substance adsorbed in this study. In the detection, the target materials are adsorbed on the polymer piezoelectric vibrating in the AC electric field, which affects the vibration mode of the polymer piezoelectric polymer, and the frequency at which polarization can follow the AC electric field is shifted on the low frequency. Therefore, in this study, the detection characteristics of the polymer piezoelectric signal transducer sensor for biopolymer detection were proposed. The polymer piezoelectric material used in this experiment was β type polyvinylidene fluoride (β-PVDF), and the sensor detection mechanism with relaxation characteristics instead of the resonance characteristics used in conventional quartz oscillators was investigated. The problems of piezoelectric biosensors using polymer piezoelectric materials were presented with the results.

2.1.2 Experimental procedures

2.1.2.1 Preparation of signal transducer sensor with piezoelectric polymer

β-PVDF films (KF piezo film, thick of the film: 40μm, electrodes: aluminum deposition, Kureha Corporation) were cut out to a size of 20 mm × 3 mm. Leads were

attached to the aluminum electrodes on both sides of the β-PVDF films using a conductive epoxy adhesive (Chemtronics CW2400: Circuit Works) as shown in Fig.2-2. As shown in Fig.2-2, polyimide tape (Kapton tape: Nitto Denko Co., Ltd.) was attached to the β-PVDF films and lead wire to the aluminum electrode in order to prevent solution leakage and electrical isolation.

2.1.2.2 Chemical modification of signal transducer sensor

In order to immobilize the host molecule on the surface of the polyimide tape of the coating material of the signal transducer sensor, a COOH group of a functional group was produced on the surface of the signal transducer sensor by the following procedure using a plasma ion irradiation method (plasma activation). The signal transducer sensor prepared in 2.1.2.1 was attached to a glass plate using double-sided tape (carbon tape). After that, it was set in the chamber of a magnetron type plasma generator (JEC-1100E, JEOL Ltd., [frequency: 50Hz, voltage: 1kV, power: 5W]) (see Fig.2-3). The pressure in the chamber was set to about 10 Pa, and the functional groups (-COOH) on the surface of the signal transducer sensor were prepared by the plasma ion irradiation treatment for 40 minutes in atmospheric air (mainly N_2: 78.08%, O_2: 20.95%). The signal transducer sensors which were not irradiated with plasma ions were also manufactured.

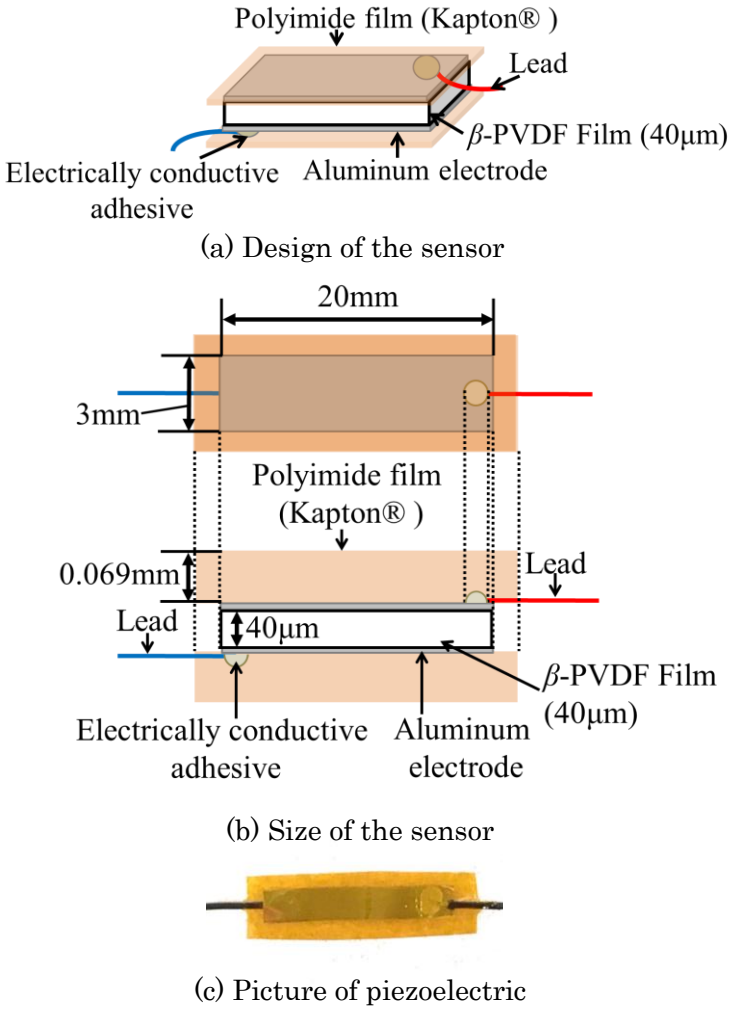

Fig. 2-2 Schematic drawing of the signal transducer sensor with piezoelectric polymer.

2.1.2.3 Attached sensor supporter of signal transducer sensor

Fig.2-4 presents a schematic diagram of the method of attaching the signal transducer sensor. The polymer piezoelectric signal transducer sensor was attached to the sensor supporter as shown in Fig. 2-4 a). As a process of attaching the signal transducer sensors to the sensor supports, the signal transducer sensors that were irradiated by the plasma ion in 2.1.2.2 were bent convexly, and they were attached to the sensor support with the

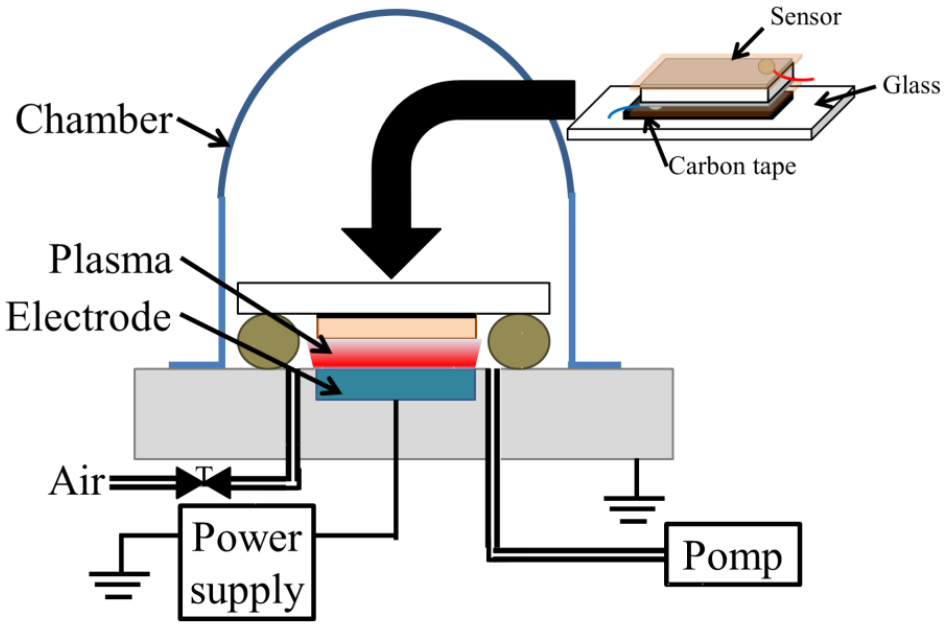

Fig. 2-3 Schematic view of the magnetron type plasma generator

adhesive and O-ring as shown in Fig.2-4 a). The two lead wires were fixed by an O-ring. The side of the polyimide tape adhesive was covered with an adhesive to prevent solution leakage. Similarly, the signal transducer sensors without the irradiation of the plasma ion irradiation were also attached to the sensor support as shown in Fig.2-4.

2.1.2.4 Immobilization of molecular recognition on the surface of the signal transducer sensor

Peptide synthesis condensing agent 1-ethyl-3- (3-dimethylaminopropyl) carbodiimide (WSC, Dojin Chemical Industries, Ltd.) and protein cross-linking agent N-Hydroxysuccinic imide (NHS, Fujifilm Wako Pure Chemical Industries, Ltd. (Wako)) were mixed, and the solution (NHS+WSC) was used for ester reaction with the COOH group on the surface of the signal transducer sensor. And then, the end face of the sensor was cleaned with pure water. After cleaning, 50 μl (100 μg / ml) of an

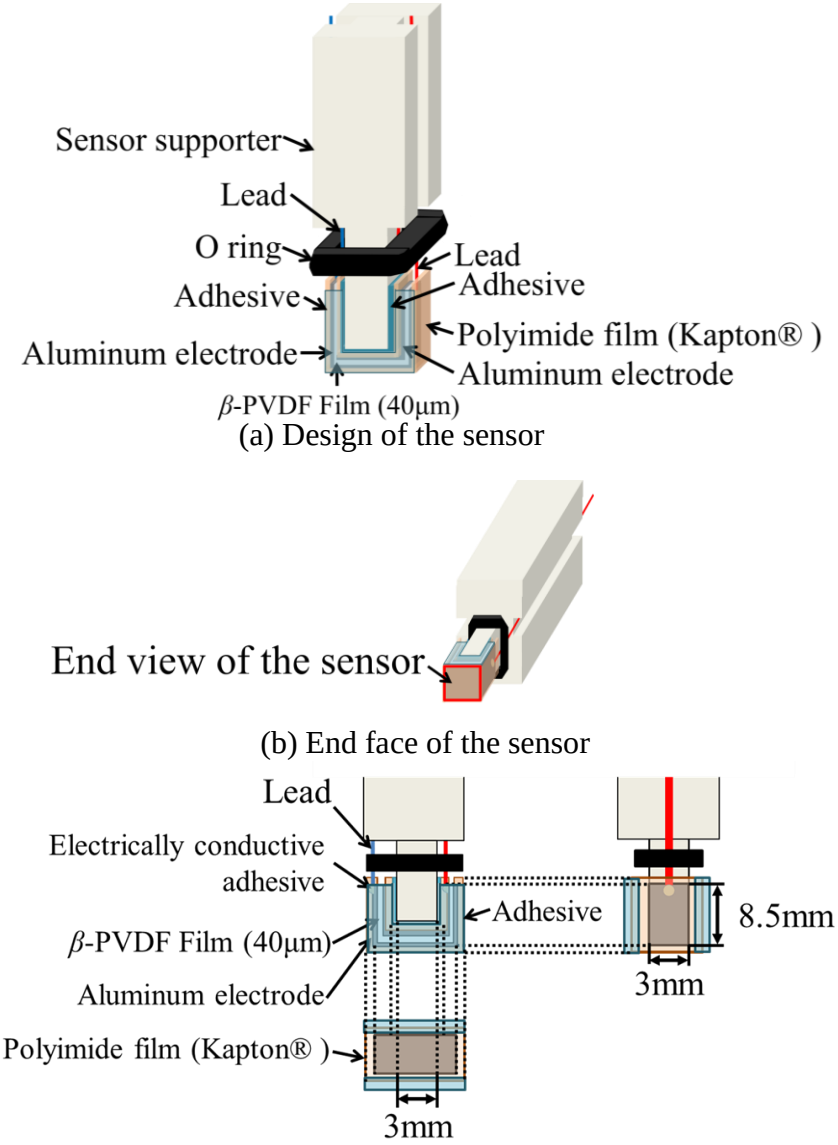

Fig. 2-4 Schematic drawing of the fixed signal transducer sensor on the sensor supporter.

amino-terminal (N-terminal) fluorescently labeled avidin (Avidin D, FITC Conjugate, Vector Laboratorie, Inc.) solution of a host molecule was prepared. The sensor was dipped into the solution for 2 hours, and the fluorescently labeled avidin was immobilized on the surface of the sensor as molecular recognition. The surface of the sensor was cleaned with pure water. A 50 μl (100 μg / ml) of a fluorescently labeled

biotin (ATTO Thio12, ATTO-TEC) solution of a guest molecule was prepared. The sensor was immersed in the solution for 10 minutes and adsorbed on fluorescently labeled avidin. The absorbance of the fluorescently labeled avidin and biotin on the polyimide tape was confirmed by ultraviolet-visible spectroscopy (UV-VIs).

2.1.2.5 Mass detection characters evaluation of signal transducer sensor

To evaluate the mass detection characters of the signal transducer sensor, The complex permittivity (the real part: ε' and the imaginary part: ε'' of the signal transducer sensor were measured

$$\varepsilon^* = \varepsilon' - j\varepsilon'' \tag{2-1}$$

The end face of the sensor without the irradiation of the plasma ions was dipped in pure water and the complex permittivity of the sensors were measured by loading the mass from 1.1 mg to 4.2 mg using an acetate film (mending tape, 3M) of a polymer film (see Fig. 2-5). A frequency range of 40 – 10 MHz was measured using an Agilent 4294A precision impedance analyzer.

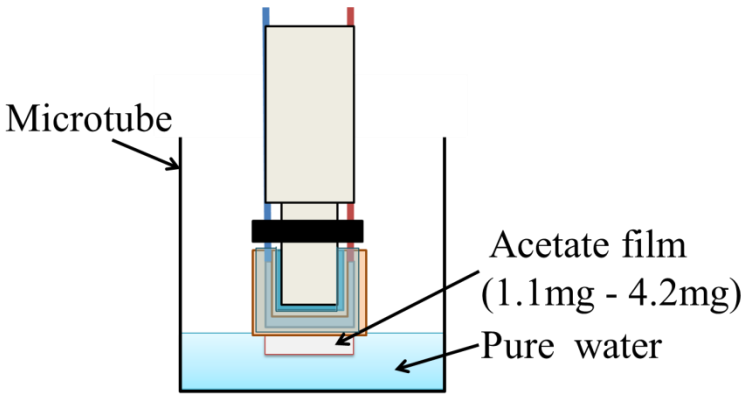

Fig. 2-5 Schematic drawing of the measurement.

2.1.2.6 Evaluation of output characters of signal transducer sensor

The N-terminal fluorescently labeled avidin was immobilized on the end face of the sensor with the irradiation of the plasma ions, and then the output characters of the sensor were evaluated by binding the fluorescently labeled biotin. As the evaluation process of the output characters, the end face of the signal transducer sensor was dipped in 100 μg / ml of an N-terminal fluorescently labeled avidin solution, and the dielectric properties of the signal transducer sensor were measured by immobilizing the fluorescently labeled avidin. The end face of the signal transducer sensor was cleaned with pure water, and then the fluorescently labeled biotin was adsorbed on the

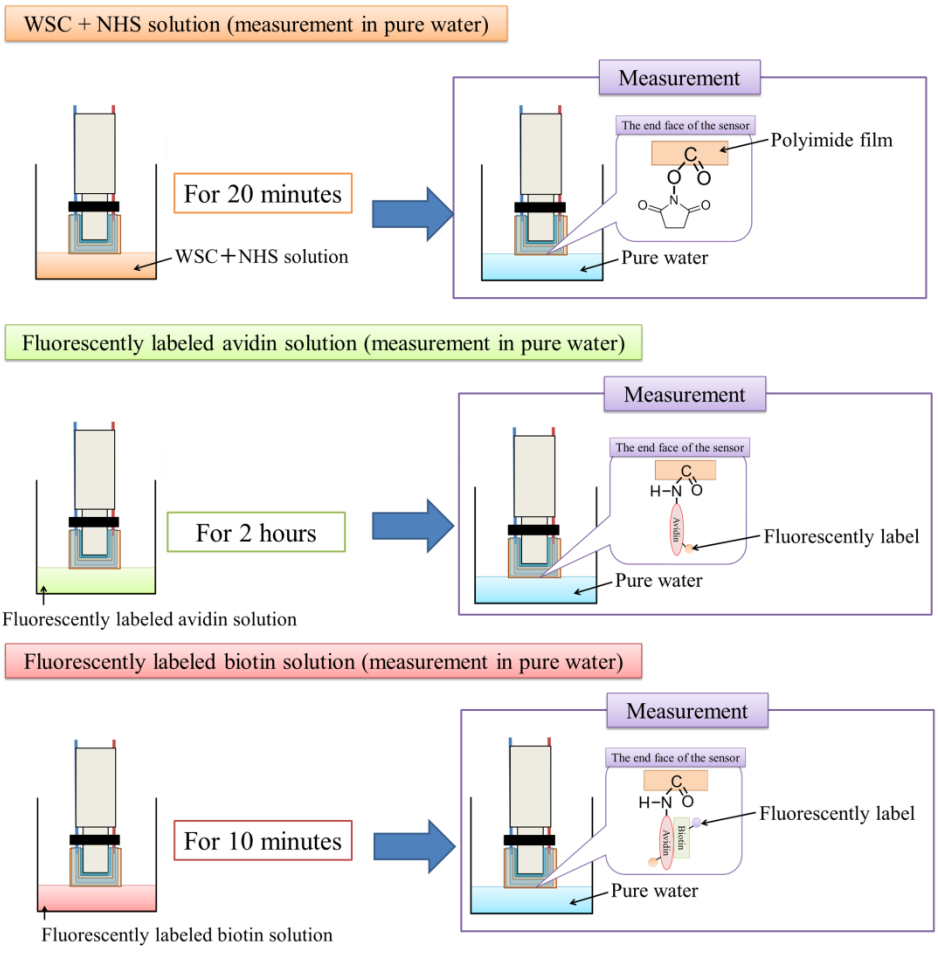

Fig. 2-6 The process of the measurement.

fluorescently labeled avidin on the end face of the signal transducer sensor. After cleaning the end face of the signal transducer sensor with pure water, the complex permittivity of the signal transducer sensor was measured in pure water under the same conditions as in 2.1.2.5. The process of the measurement was shown in Fig. 2-6.

2.1.3 Results and discussion

2.1.3.1 Detection characteristic of the sensor by loading mass of the polymer films

In order to confirm the mass detection characteristics of the signal transducer sensor using β-PVDF film in pure water, the acetate tapes were attached to the end face of the sensor and the complex permittivity of the sensor was measured in pure water. Fig. 2-7 presents the results of the complex permittivity of the signal transducer sensor depending on the frequency by loading the mass of the polymer films. In this experiment, the mass of the polymer film was measured four times each, and the average values were estimated. The behavior of the complex permittivity was confirmed in the frequency range at above10 kHz (see Fig.2-7). Previously, Furukawa et al. [9] reported that the relaxation process of PVDF was measured above 10 kHz. It was considered that the behavior of the complex permittivity above 10 kHz was the relaxation process of β-PVDF. The peak top of ε'' in the relaxation process was near 1.6 MHz as shown in Fig. 2-7. In the dictation characteristics of the piezoelectric polymer sensor in the relaxation process, both ε' and ε'' shifted to the low frequency by loading the mass of the acetate film. The ε' at 1.6 MHz by adding 0.0 mg was 8.77, and the standard deviation of the frequency when ε' was 8.77 was ± 2.5 kHz by adding 0.0 mg, ± 5.9 kHz by adding 1.1 mg,± 3.3kHz by adding 2.2 mg, ± 2.9kHz by adding 3.3mg, and ± 10.1kHz by adding 4.2mg. The sensor was taken out from pure water and the

acetate tape was attached to the end face of the sensor, and then the sensor was dipped into pure water again. Therefore, it was considered that the cause of these errors was the difference in the water content of the acetate tapes. However, the relaxation processes were shifted to the low frequency by changing the mass of the tapes. Hence, it was confirmed that the relaxation process of the signal transducer sensor responded to the change of the mass of the tapes.

The general mass sensor using quartz are explained with Sauerbrey's equation as shown below [7]:

$$\Delta F = -\frac{2F_0^2}{\sqrt{\mu_q \rho_q}} \frac{\Delta m}{A} \tag{2-2}$$

where F_0 is the fundamental frequency of the sensor, A is the electrode area, μ_q is the elastic constant of the piezoelectric sensor, ρ_q is the density of the piezoelectric sensor, Δm is the weight change, and ΔF is the measured frequency change. The frequency change estimated from Eq. (2-2) by loading the mass and the change in the relaxation frequency (f_m) of the real part of the complex permittivity (each frequency: ε', low frequency range: ε'_0, high frequency rage: ε'_∞) [10] were compared.

$$\varepsilon' = \varepsilon'_\infty + \frac{\varepsilon'_0 - \varepsilon'_\infty}{1+(\frac{f}{f_m})^2} \tag{2-3}$$

The ε' of the signal transducer sensor depending on the frequency was estimated base on Fig. 2-7. Fig. 2-8 shows the result of the relaxation frequency change of the signal transducer sensor by loading the mass of the tape and the result of the relaxation

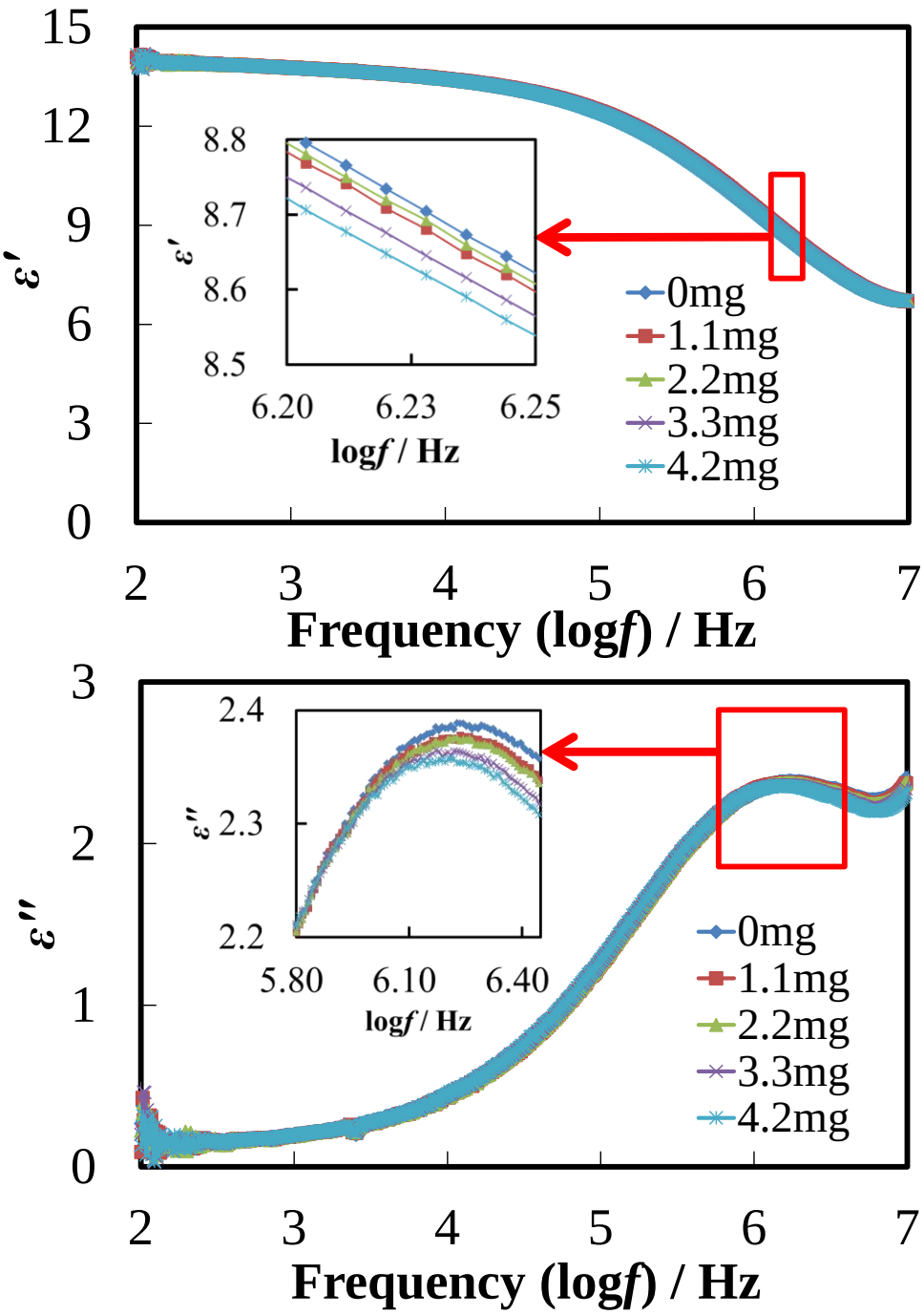

Fig. 2-7 Complex permittivity of the sensor with loading weight of acetate films depending on frequency. The enlarged views of relaxation are shown in ε' and ε" figures.

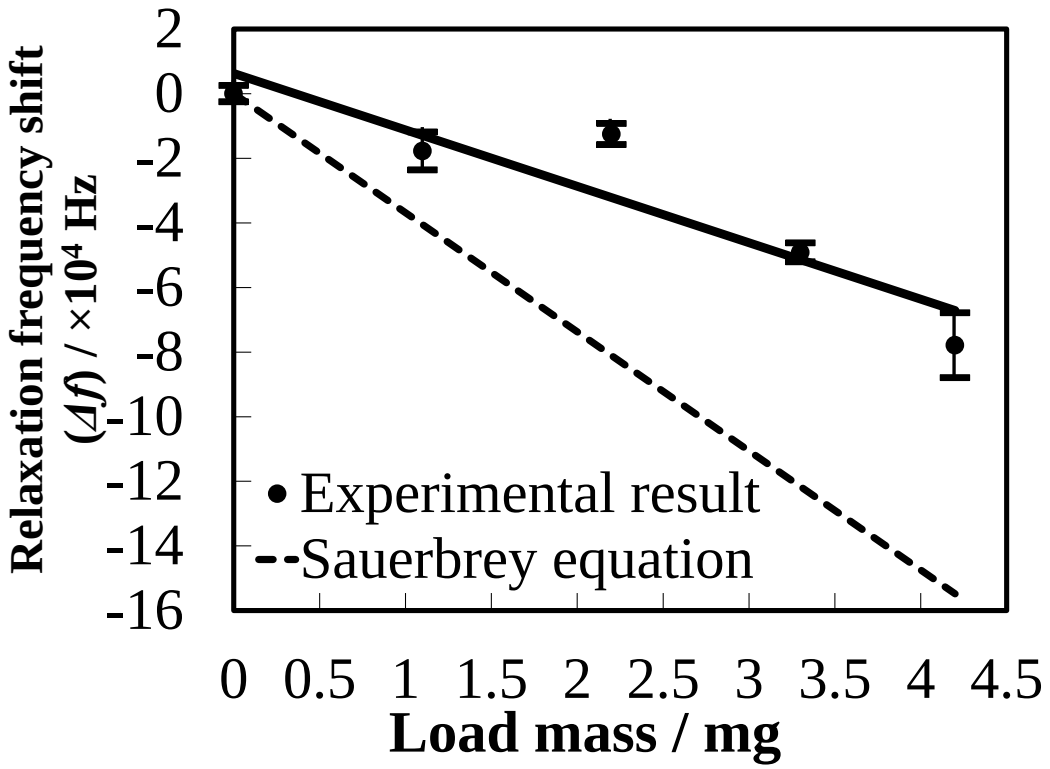

Fig.2-8 Frequency shift of relaxation with loading mass of acetate films.

frequency change based on Eq.(2-2) with the relaxation frequency (F_0=1.6MHz), the aluminum electrode area of the signal transducer sensor (A=6.22×10^{-5}m^2), the elastic constant of β -PVDF (μ_q=3.00×10^{12}gm^{-1}s^{-2}), the density of β-PVDF (ρ_q=1.78×10^6 gm^{-3}), and the mass change with attaching the acetate tape (Δm). In this experiment, it was considered that the error factor was the difference in the water content of the acetate tape.

The relaxation frequency was linearly shifted to the low frequency by loading the mass of the tape (see Fig.2-8). It was suggested that the vibration mode of β-PVDF was affected by loading the mass, the polarization of β-PVDF could not follow the AC electric field and the complex permittivity was changed, and then the relaxation frequency was shifted to the low frequency.

In this experiment, the relaxation frequency linearly changed to the low frequency by

loading the mass of the tape, similar to the general mass sensor shown by Sauerbrey's equation [7]. The frequency change of the result in this experiment was lower than the result of the frequency change estimated from Sauerbrey's equation (see Fig.2-8). It was considered that the polymer tape was viscoelastic and the film tape was thicker by loading the mass of the tape, so the polymer tape did not follow the vibration of the sensor, and the mass detection of the polymer tape was affected [4].

2.1.3.2 Sensor detection characteristics by immobilizing the biopolymer

The host molecule fluorescently labeled avidin and the guest molecule fluorescently labeled biotin were immobilized on the sensor by the host-guest reaction. The fixation of the fluorescently labeled avidin and the fluorescently labeled biotin on the end face of the sensor was confirmed by the ultraviolet-visible absorbance measurement. Fig. 2-9 presents the result of the absorbance of the fluorescently labeled avidin and biotin. The fluorescent dyes of fluorescently labeled avidin and fluorescently labeled biotin were confirmed on the sensor. Previously, Hirata et al. reported that the sensor surface was irradiated with plasma ions and detected by immobilizing a N-terminal material on the sensor surface using a WSC + NHS solution [11]. In another report, they proposed the detection of the avidin and biotin [11].

As an evaluation of the output characteristics of the signal transducer sensor with immobilizing the fluorescently labeled avidin and the fluorescently labeled biotin, Fig. 2-10 shows the complex permittivity of the signal transducer sensor depending on the frequency of the (1) the surface modification condensing agent (WSC + NHS) fixed on the end face of the sensor, (2) the fluorescently labeled avidin adsorption, and (3) the fluorescently labeled biotin adsorption on fluorescently labeled avidin. The

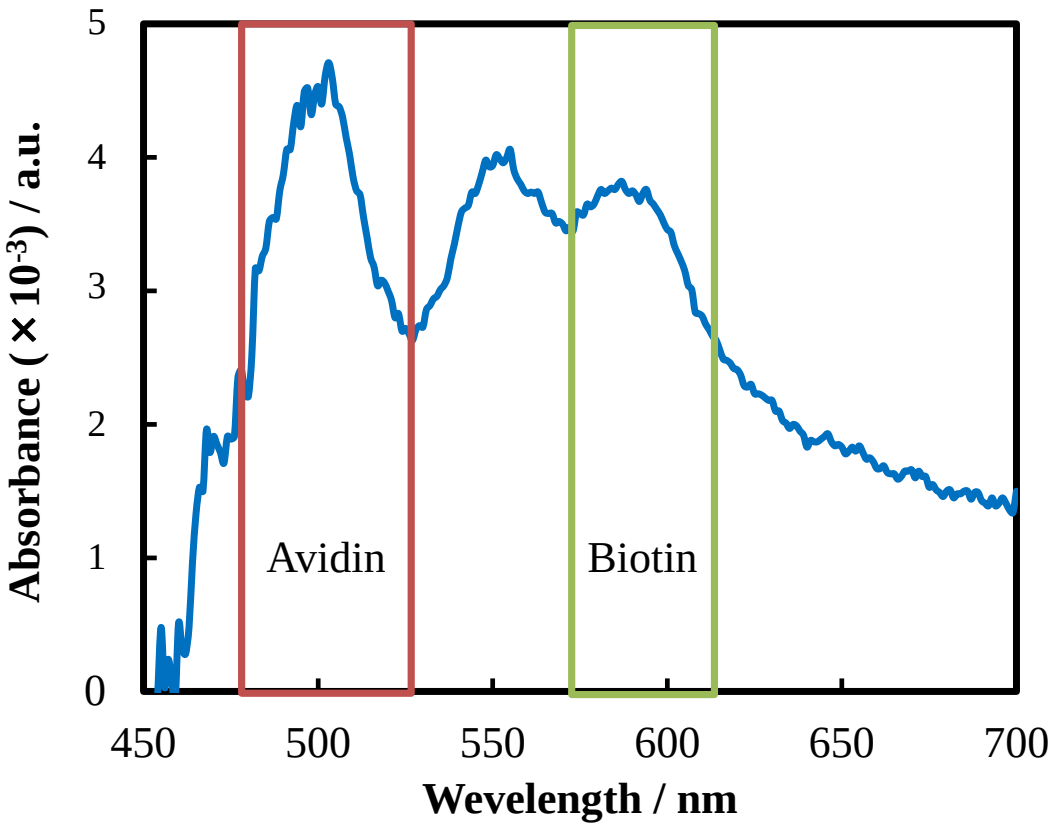

Fig. 2-9 Absorbance of the fluorescently labeled avidin and biotin depending on the wavelength. (Avidin :495nm, Biotin: 582nm)

immobilization of biopolymers was measured three times each, and the average values were estimated. According to the result of the complex permittivity depending on the frequency in Fig. 2-10, the relaxation process from near 100 kHz to 6 MHz was shifted to the low frequency with immobilizing the biopolymer on the sensor. The relaxation frequency shifted to the low frequency with about 93.6 kHz by fixing the N-terminal fluorescently labeled avidin on the sensor. The relaxation frequency changed to the low frequency of about 9.8 kHz by immobilizing the fluorescently labeled biotin. It was suggested that the molecular weights of the N-terminal fluorescently labeled avidin and fluorescently labeled biotin were significantly different and the output of the sensor with

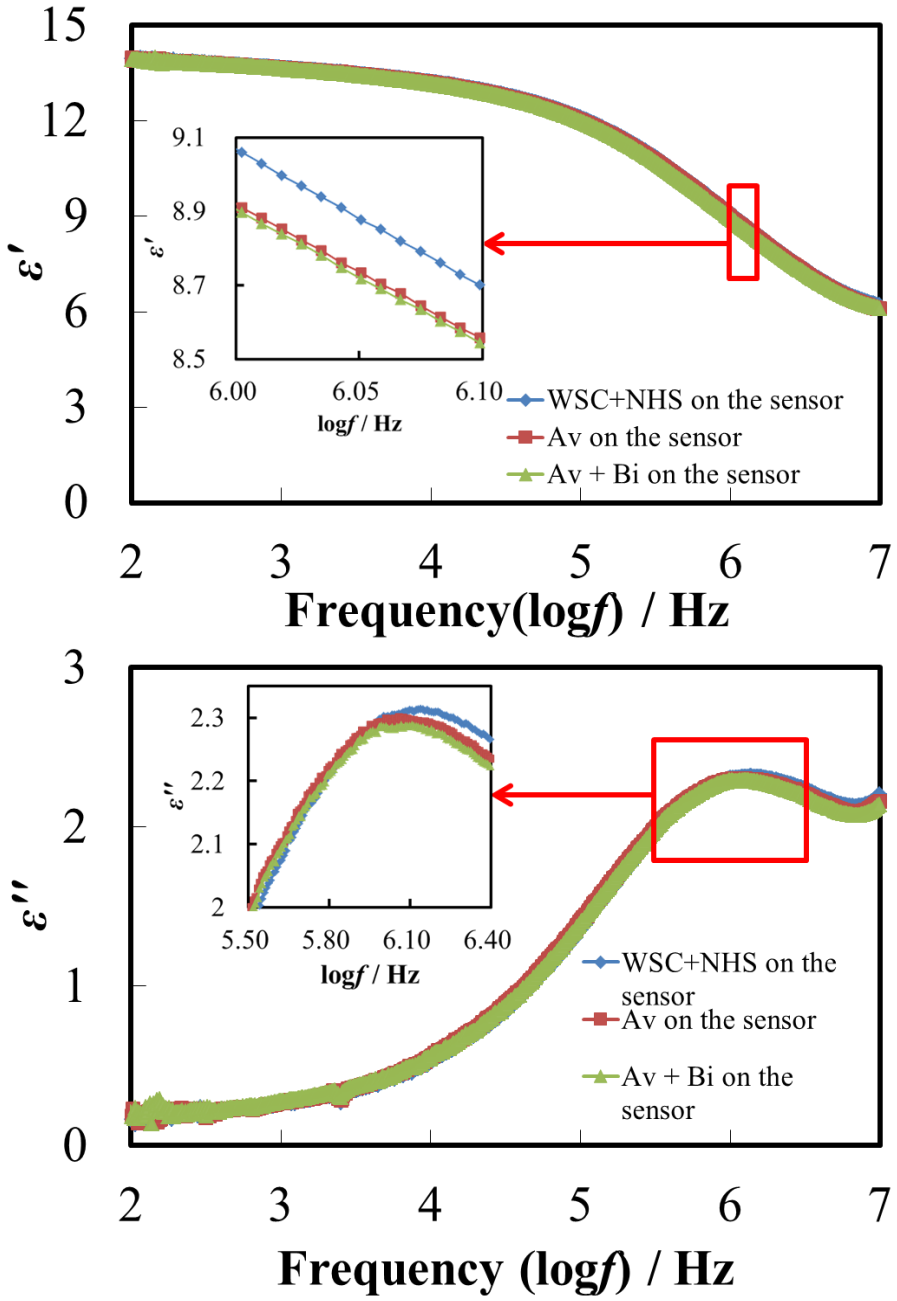

Fig. 2-10 Complex permittivity of the sensor with bonding fluorescence labeling biotin and fluorescence labeling avidin on the sensor depending on frequency. The enlarged views of relaxation are shown in ε' and ε'' figures. Av is the fluorescence labeling avidin on the sensor. Bi is the fluorescence labeling biotin on the sensor.

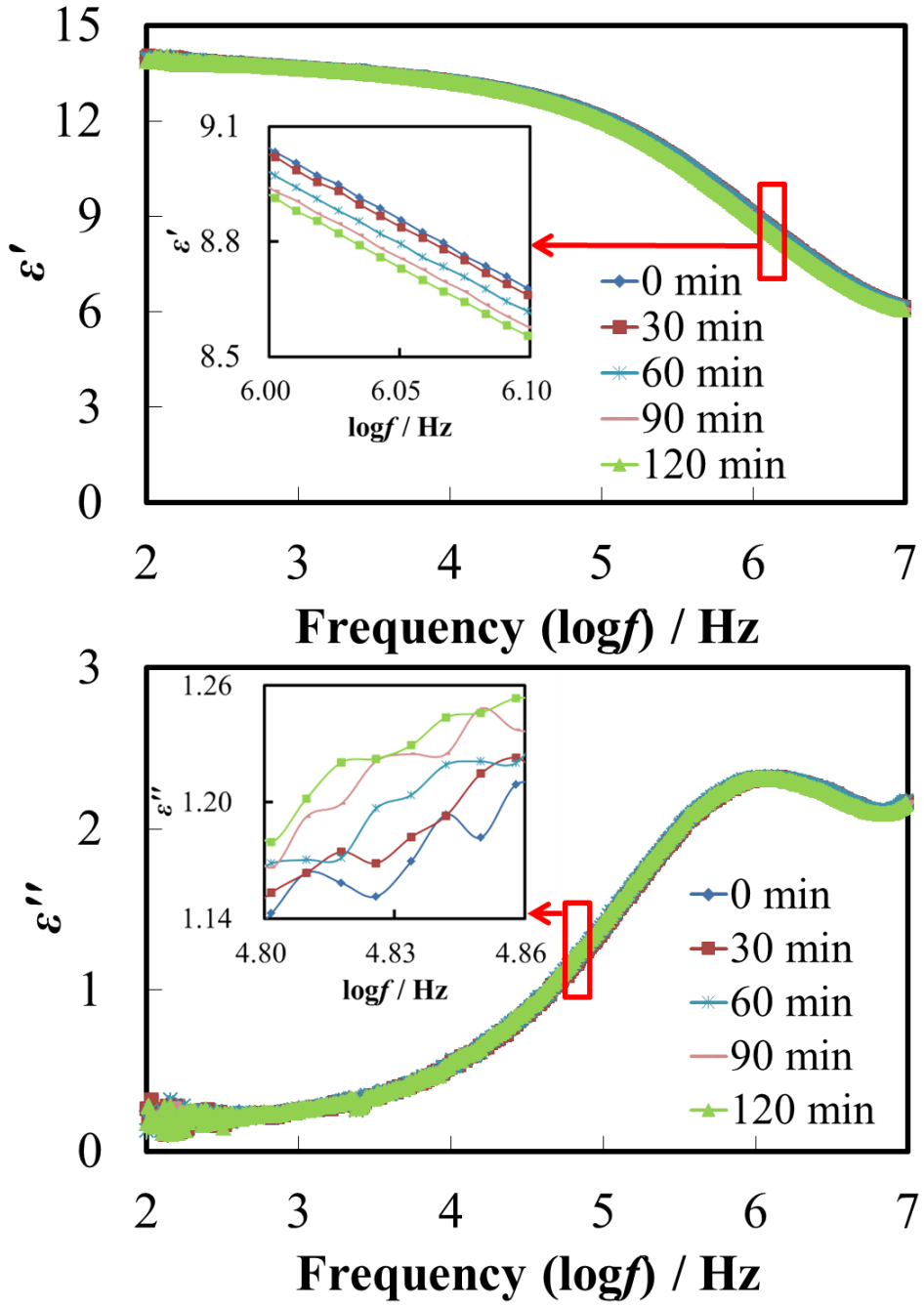

Fig. 2-11 Complex permittivity of the sensor depending on frequency during the immobilization of fluorescence labeling avidin. The enlarged views of relaxation are shown in ε' and ε'' figures. (Each color is shown each immobilization time of fluorescence labeling avidin.)

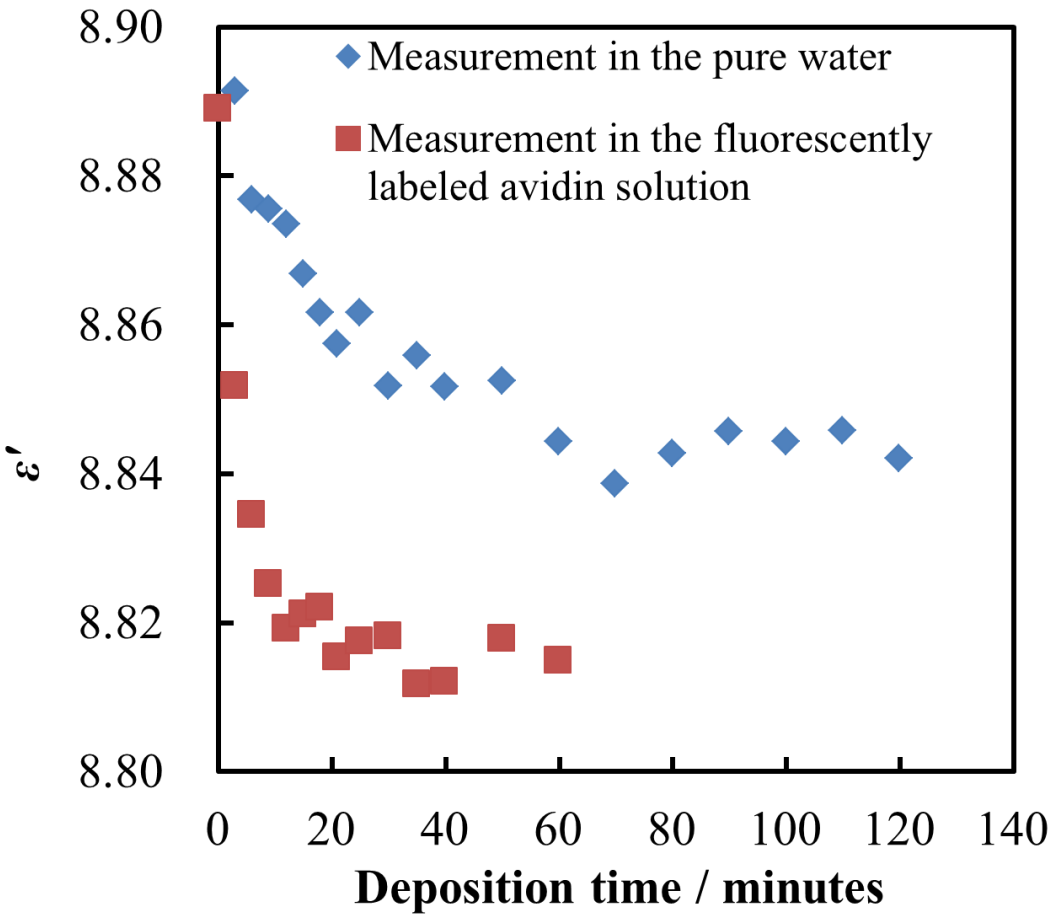

Fig. 2-12 Relationship the deposition time and the ε' in water and in avidin solution.

immobilizing the fluorescently labeled biotin was less than that of N-terminal fluorescently labeled avidin. However, it was proposed that it was possible to detect the fluorescently labeled avidin and biotin. In order to confirm the fixation of the fluorescently labeled avidin immobilized on the sensor, Fig. 2-11 presences the complex permittivity of the signal transducer sensor depending on the frequency during the deposition time of the fluorescently labeled avidin. Fig. 2-12 shows the result of the ε' change of the signal transducer sensor by the deposition time in pure water and

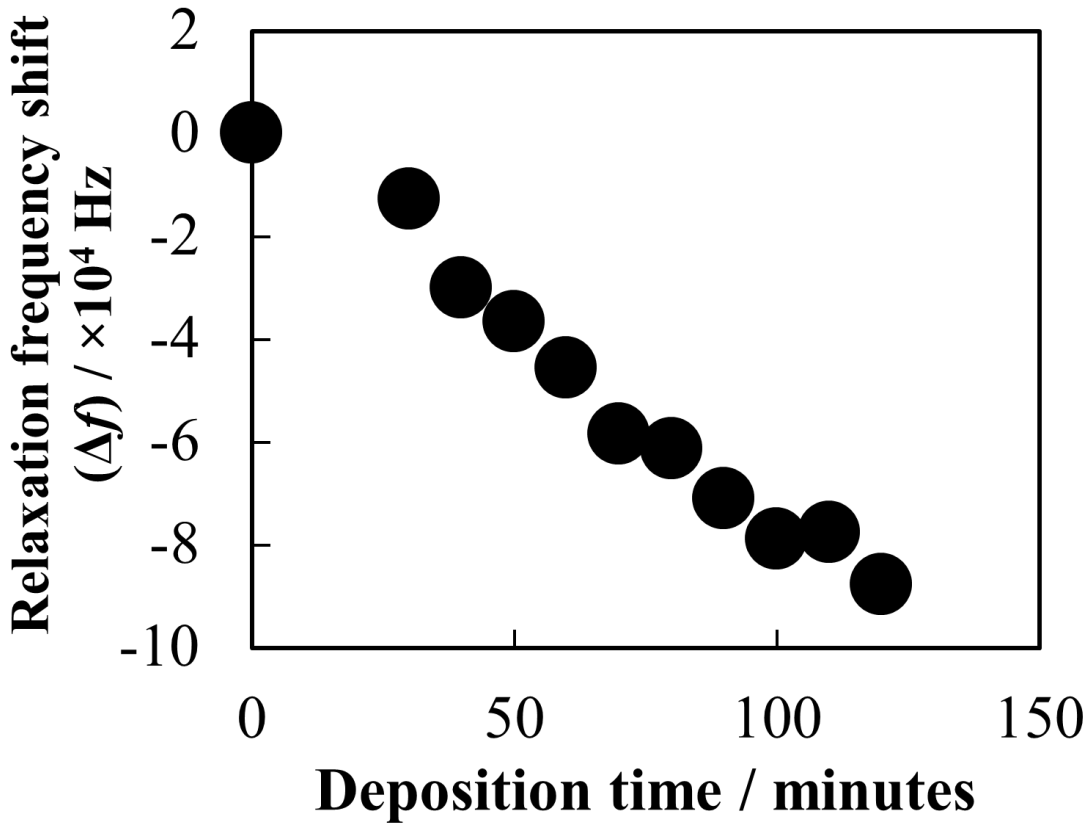

Fig. 2-13 Frequency shift of relaxation with immobilizing fluorescence labeling avidin on the sensor.

N-terminal fluorescently labeled avidin solution without the irradiation of the plasma ion and the treatment of WSC+NHS solution. According to the result of the complex permittivity depending on the frequency in Fig. 2-12, the relaxation process was shifted to the low frequency with the deposition time of the fluorescently labeled avidin solution. The signal transducer sensor without the irradiation of the plasma ions and the treatment of WSC+NHS solution was deposited in pure water for 60 minutes, and the ε' was not changed (see Fig. 2-12). Similarly, the sensor of the same conditions was deposited in N-terminal fluorescently labeled avidin solution for 40 minutes, and the ε' was not changed. On the other hand, the relaxation process of the sensor irradiated with

plasma ions continuously was shifted to the low frequency above 40 minutes (see Fig.2-11). Therefore, it was suggested that the low frequency shift of the relaxation process by depositing the fluorescence labeled avidin solution was because the fluorescence labeled avidin was fixed on the sensor.

Fig. 2-13 presences the results of the frequency change with the fluorescence labeled avidin with the deposition time based on the results in Fig.2-11. The relaxation frequency systematically changed to the low frequency with the deposition time of the fluorescently labeled avidin solution. The mass change of the immobilization of the fluorescently labeled avidin was slight. However, the frequency change with the fixation of the fluorescently labeled avidin in Fig. 2-13 was larger than that in Fig. 2-8. Kanazawa and Gordon [12] proposed that a simple relationship is derived which expresses the change in the oscillation frequency of a quartz crystal in contact with a fluid in terms of material parameters of the fluid and the quartz, and the equation is shown :

$$\Delta f = -f_0^{3/2}\left(\frac{\eta_L \rho_L}{\pi \mu \rho}\right)^{1/2} \tag{2-4}$$

where f_0 is the fundamental frequency of the sensor, η_L is the viscosity of the liquid, ρ_L is the density of the liquid, μ is the elastic constant of the piezoelectric sensor, ρ is the density of the piezoelectric sensor, and Δf is the measured frequency change. This is, it was considered that the solution significantly affected the shear vibration expected by the Kanazawa-Gordon equation [12] since β-PVDF used in this study has a significantly smaller elastic constant than quartz. Hence, it was suggested that it was possible to detect a small amount of biopolymer by using the relaxation process of the β-PVDF

piezoelectric of the signal transducer sensor instead of quartz.

2.1.4 Conclusions

A polymer piezoelectric sensor was produced to set problems for the application of the biosensor using PVDF film. As the signal transducer sensor, it was confirmed the response of the sensor to the mass of the polymer film. And then, the sensor detection characteristics were evaluated from the change in the complex permittivity accompanying the fixation of biopolymers. The conclusions of this study are as follows:

(1) It was confirmed that the signal transducer sensor using β-PVDF detected with loading the weight of the polymer film by using the relaxation process of the complex permittivity.
(2) It was possible to detect biopolymers using the immobilization characteristics associated with the host-guest reaction in the region of the relaxation process of β-PVDF piezoelectric materials at 100 kHz to 6 MHz.

For the diagnosis of TB, it was proposed that this result shows that the detection by the relaxation process of the signal transducer sensor was effective for the detection of biopolymers. Therefore, the detection of biopolymers such as DNA and RNA by the relaxation process of the signal transducer sensor was expected.

2.1.5 Setting of problems for the polymer piezoelectric biosensor

The change in mass of the target materials adsorbed on the sensor is detected as a frequency change with the shear vibration of the piezoelectric polymer sensor. The

measurement is performed in solution. In addition, in order to diagnose rapidly TB, it is expected to measure with a small amount of mycobacterial DNA. Therefore, the influence of the viscosity of the solution is small, and high sensitivity is required.

According to the results, it is possible to detect biopolymers using the adsorption characteristics of the host-guest reaction on the sensor by using the relaxation behavior of the β-PVDF piezoelectric material. However, the problems of the piezoelectric biosensor with polymer are shown as:

(1) β-PVDF has a significantly lower elastic constant than quartz, which is a signal transducer sensor of a general biosensor for mass detection. Therefore, the shear vibration of β-PVDF was affected by the liquid viscosity, which affected the change of the dielectric constant of β-PVDF.

(2) According to the results of this study, the sensitivity of the polymer piezoelectric biosensor is 5 μg / ml based on the amount of fluorescently labeled avidin liquid, and the response speed is 60 minutes based on Fig.1-12 and Fig.1-13. The final goal of TB diagnosis is the sensitivity of less than 1 μg / ml and the response speed of 5 minutes. Therefore, it is necessary to improve the sensitivity and responsivity of the polymer piezoelectric biosensor.

In order to solve the problems, the ceramics / polymer composite materials were proposed in this study. It is expected that the elastic constant will be improved by adding the ceramic filler. It is necessary to increase the dielectric properties since the amount of change in dielectric constant depending on the frequency affects the sensitivity of the polymer piezoelectric biosensor. Hence, the ceramics / polymer

composite materials were applied to improve the sensitivity and responsivity of piezoelectric biosensors.

2.2 Fractal characters and dielectric constant of material texture of self-assembled $BaTiO_3$/Poly-L-Lactic-Acid composites

2.2.1 Introduction

In Session 2.1, it was presented the problems for applying polymer piezoelectric materials to piezoelectric biosensors. The material textures of the ceramics / polymer composites were controlled with the self-assembly process to improve the dielectric properties related to sensitivity and reactivity. In particular, the relationships between the morphology, entropy of configuration, and dispersibility of the self-assembled BT secondary particle groups under different manufacturing processes and dielectric properties of barium titanate ($BaTiO_3$, BT) / polymer composite materials were investigated.

Generally, the dielectric constant (ε') of a polymer is relatively low at less than 10[13]. To increase the ε' for the energy storage in polymers, ceramic powder fillers with a high ε', such as BT with a ε' of 1,000 or more, are added to the polymer matrix [14]. However, a 50vol.% or more of ceramics with a high ε' are applied to the polymer matrix to achieve a high ε'. Thus, the mechanical properties of these composites are extremely poor and are not suitable for use in dielectric materials, such as capacitors, or piezoelectric materials.

Robertson and Varlow [15] demonstrated that the size, shape, and aggregation of BT particles influence the effective bulk ε' of BT fillers or polymer composites with a high ε'. Here the authors suggested the formation of agglomerations, which reduces the

impedance due to the lower ratio of resin to filler across the shortest impedance path [15].Elsewhere, researchers have proposed a more considerable electrical flux for the movement of the agglomerated rather than the non-agglomerated particles, which will result in a higher permittivity for the per unit sample [15]. Meanwhile, Akimune et al.[16] conducted an analysis of the mechanical and electrical properties of TiN / Si_3N_4, in which the particle shape and size of the granules in the related ceramics play an important role in the network formation. Here, the authors highlighted that the formation of agglomerates improves functioning [16]. Phan et al.[17] reported the effect of controlled BT nanoparticle aggregates on the dielectric properties of epoxy nanocomposites in terms of various experimental parameters, including frequency, ceramics content, and temperature. Here, the authors suggested that the nature of an interphase region depends not only on the chemical bonding at the filler interface but also on the network confinement between the nanoparticles[17] .

Recently, researchers have also shown that the average secondary particle area of BT filler aggregates of BT filler/poly-L-lactic acid (PLLA) composites is related to dielectric constant, regulating the microstructure of aggregates [18]. Therefore, it is essential to evaluate the microstructure. A method using fractal analysis has been reported to quantitatively analyze the shape of particles [19]. Suzuki et al. reported that the particle shape of the projected image of powder particles was characterized by the fractal dimension by the box count method [19]. Kobayashi et al. [20] investigated that the grain boundary microstructures in SUS316L stainless steel with the fractal analysis. They highlighted that the maximum random boundary connectivity was found to have a fractal nature for SUS316L stainless steel specimens, and it was suggested that it was possible to characterize the grain boundary microstructures by the fractal analyses. On

the other hand, image is analyzed by multifractal analysis in medical technology in recent years [21]. In a previous report [18], it was proposed that the secondary particle area of BT aggregates was increased by increasing the dielectric constant. Therefore, in this session, the self-assembled BT / PLLA composites were prepared under different conditions. The self-assembly process is assumed as shown in Fig.2-14. According to the process, the kneading speed was changed to control the self-assembled material texture. The multifractal analysis was attempted to apply to the evaluation of the morphology of the filler secondary particle group in the composites. In addition, the purpose was that the morphology of the self-assembled BT secondary particle groups was quantified by the multifractal analysis, and then the aggregated state under the process of the manufacture such as kneading speed which was related to the aggregation and decomposition during the self-assembly process was characterized.

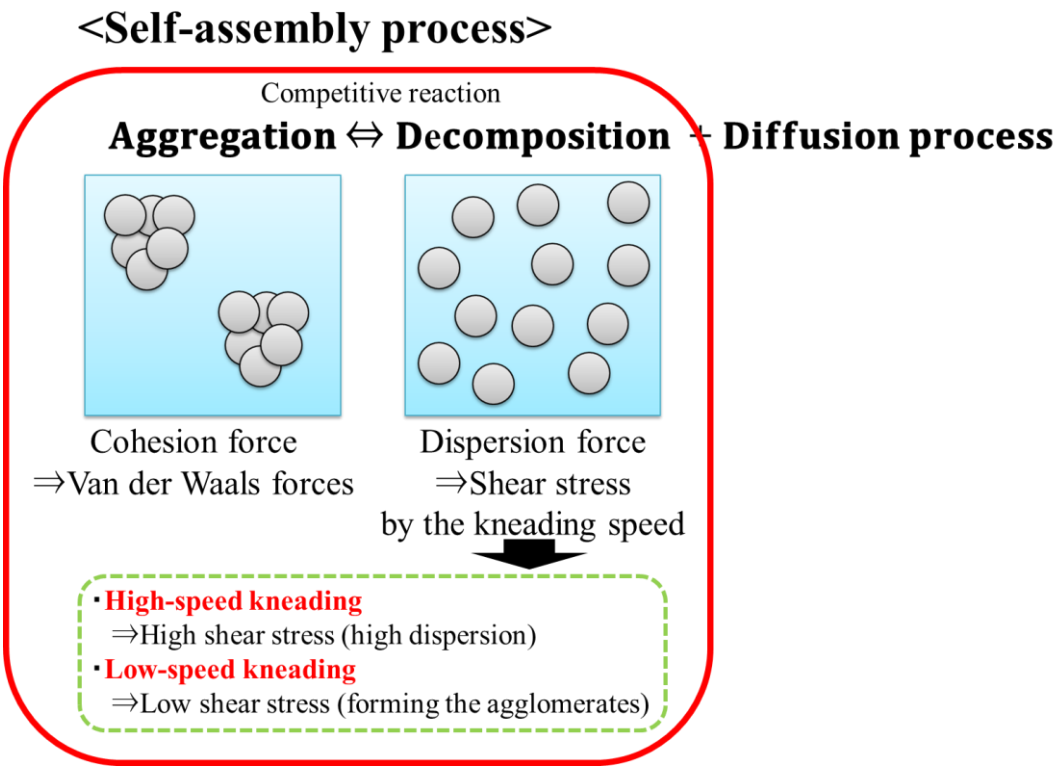

Fig. 2-14 Focused points of the self-assembly process in this session.

2.2.2 Experimental procedures

2.2.2.1 Sample preparation

BT powder was prepared using a conventional solid-state synthesis technique. $BaCO_3$ (99.95%, High Purity Chemical Co., Japan) and TiO_2 (99%, High Purity Chemical Co., Japan) were used as the starting materials. Powders used for the experiments were ground and properly mixed. The powder mixture was fired at 1373 K for 4 h. The sintered BT was ground to get a BT powder. The resultant BT powder had an average particle diameter of approximately 1 μm. The powder exhibited a single phase, which was determined using powder X-ray diffraction. BT / polymer composites were generated from BT powder and granular PLLA (PLLA, Nature Work, Japan). PLLA was melted at a temperature of 473 K, and BT powder was added to PLLA to form mixtures. The volume fractions of BT were 0%, 5%, 10%, and 20%. Two different processes have been adopted during the mixing: (1) slow-speed hand mixing for 30 min with approximately 10 rpm and (2) high-speed mixing via a kneader for 10 min with 30 rpm. After the mixing was over, each sample was cooled in the air. In order to generate BT / PLLA composites with dispersion, both BT powder and Tegomer® P121 (polyolefin type, Evonik, U.S.A.) were mixed and kneaded under the same conditions, as described earlier. The amount of additive Tegomer® P121 in the mixture was approximately 4 wt% in BT powder.

2.2.2.2 Measurement method

The dielectric constants of BT / PLLA composite at the frequency range from 40 Hz to 1M Hz were measured at 298 K using an Agilent 4294 A precision impedance analyzer; lead wires were made of platinum. Each sample was a rectangle with a surface

area of 64 mm^2 and a thickness of 0.3 mm. Gold was deposited on electrodes with square faces. The results of the dielectric constants and the average secondary particle area were based on a previous study [18].

2.2.2.3 Field emission scanning electron microscope (FE-SEM) observation and multi-fractal analysis

The aggregated state of the BT particles in the cross sections of the samples was observed using a field emission scanning electron microscope (FE-SEM S-4100 (Hitachi, Ltd.)). The FE-SEM images were converted to binary images for the multifractal analysis. This analysis was used to estimate the probability ($p_i[r]$) of an image by covering it with boxes of size r and counting the number of boxes. The partition function is as follows:

$$P_r^q = \sum_{i=1}^{N(r)} \left[p_i(r)\right]^q \tag{2-5}$$

where q is the order moment ($-\infty<q<\infty$). The generalized dimensions of the q of a distribution, Dq, can be defined as follows:

$$D_q = \frac{1}{q\text{-}1} \lim_{r\to 0} \frac{\ln P_r^q}{\ln r} = \frac{1}{q\text{-}1} \lim_{r\to 0} \frac{\ln N(q,r)}{\ln r} \tag{2-6}$$

When q takes the values of 0, Eq. 2-6 is reduced to the following:

$$D_0 = -\lim_{r \to 0} \frac{\ln N(r)}{\ln r} \tag{2-7}$$

where D_0 is the capacity dimension. This is the same equation as the box-counting method. In this session, the D_0 was obtained from the multifractal analysis as an initial analysis, and the morphology of the BT secondary particle groups was characterized. Fig. 2-15 shows the box-counting method in this session.

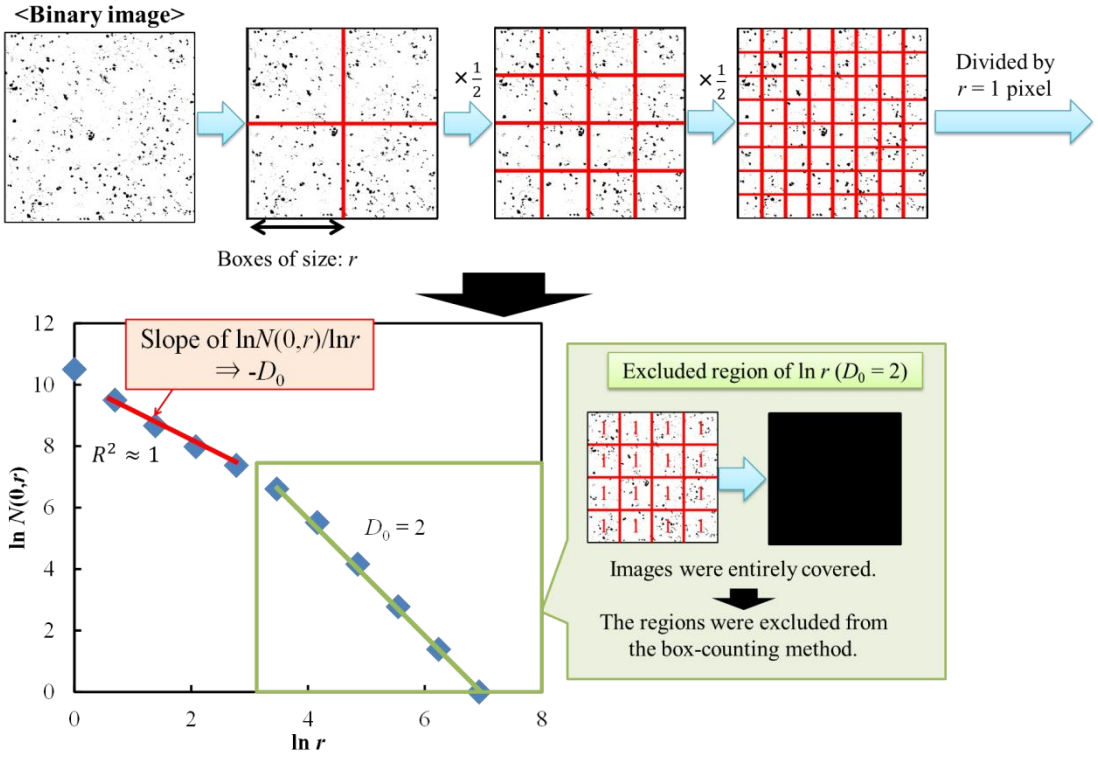

Fig. 2-15 Box-counting method.

Fig. 2-16 shows the process of the manufacturing BT / PLLA composites, measurement and the analysis.

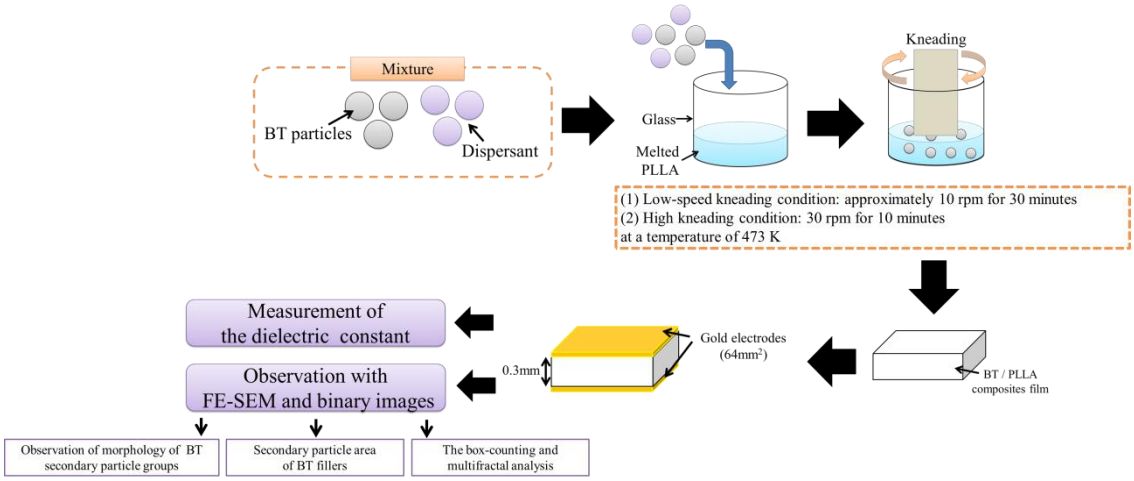

Fig. 2-16 The process of the manufacturing BT / PLLA composites, measurement and the analysis.

2.2.3 Results

Fig. 2-17 presents the FE-SEM micrograph and binary images of the BT / PLLA composites with Tegomer® P121 with a BT volume fraction of 5 vol.% – 20 vol.% under low-speed kneading condition (at 10 rpm for 30 minutes). Fig. 2-18 shows the FE-SEM micrograph and binary images of the BT/PLLA composites without Tegomer® P121 with a BT volume fraction of 5vol.%–20vol.% under low-speed kneading condition (at 10 rpm for 30 minutes). The FE-SEM micrograph and binary images of the BT/PLLA composites with and without Tegomer® P121 with a BT volume fraction of 5 vol.% under high-speed kneading condition (at 30 rpm for 10 minutes) are shown in Fig.2-19. In Fig.2-17 to Fig.2-19, the black part of the binary images shows the BT particle groups, while the white part shows PLLA. As Fig.2-17 and Fig.2-18, the formation of BT secondary particle groups was promoted by increasing the volume fraction BT fillers. Comparing the BT secondary particle groups with and without Tegomer® P121 depending on the volume fractions of BT in Fig.2-17 and Fig.2-18, the formation of BT secondary particle groups with Tegomer® P121 was promoted more

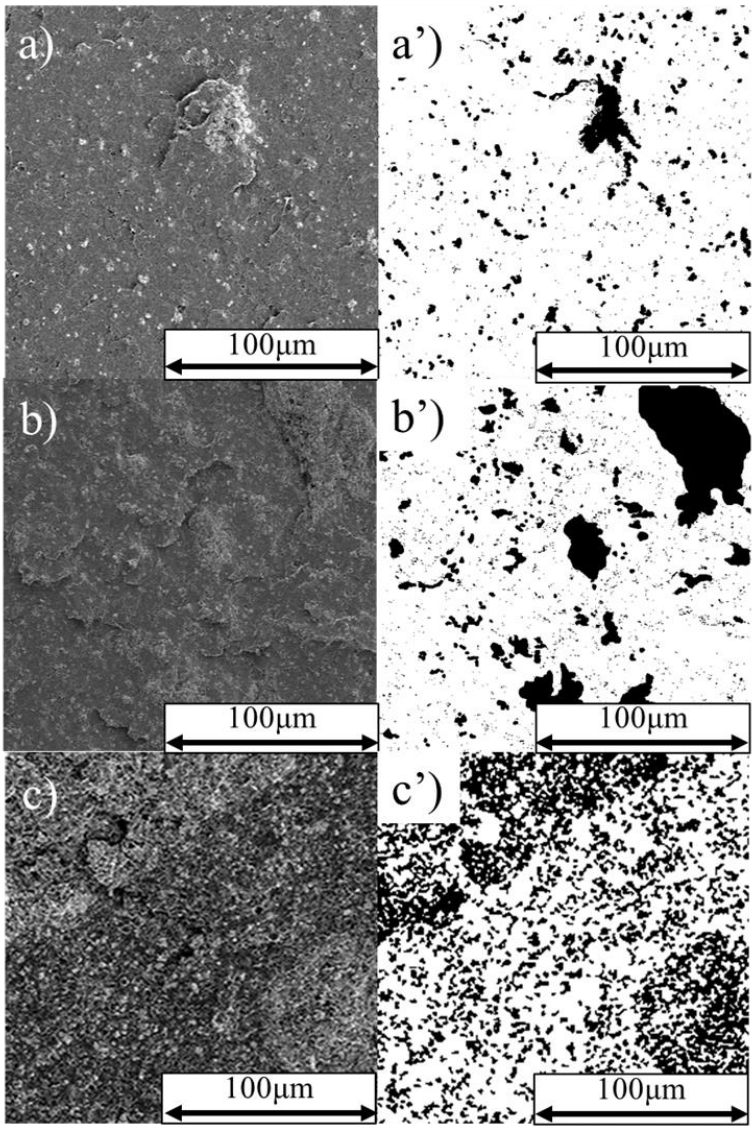

Fig.2-17 Cross sectional FE-SEM images (a, b, and c) and image processing pictures (a', b', and c') of samples with 5 (a, a'), 10 (b, b') , and 20 (c, c') % volume fraction of BT prepared under low kneading conditions with Tegomer® P 121.

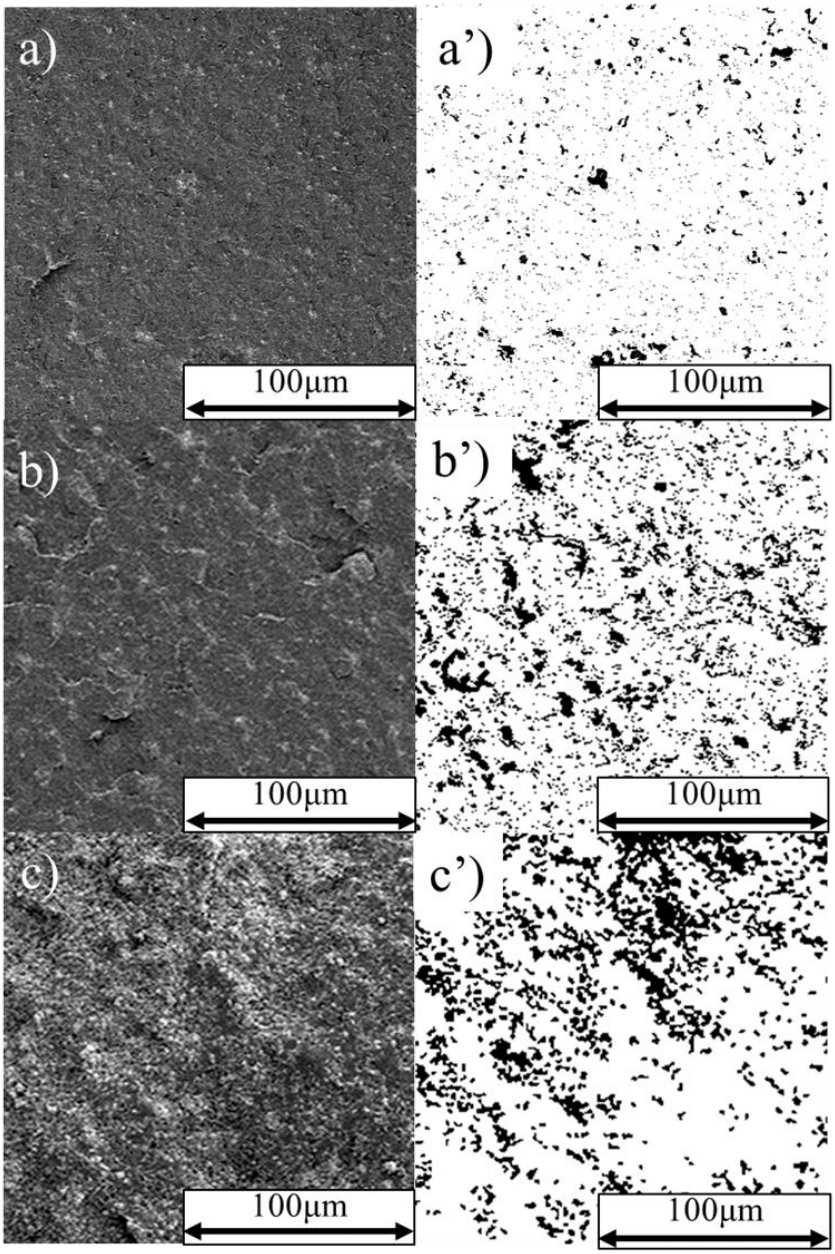

Fig. 2-18 Cross sectional FE-SEM images (a, b, and c) and image processing pictures (a', b', and c') of samples with 5 (a, a'), 10 (b, b') , and 20 (c, c') % volume fraction of BT prepared under low kneading conditions without Tegomer® P 121.

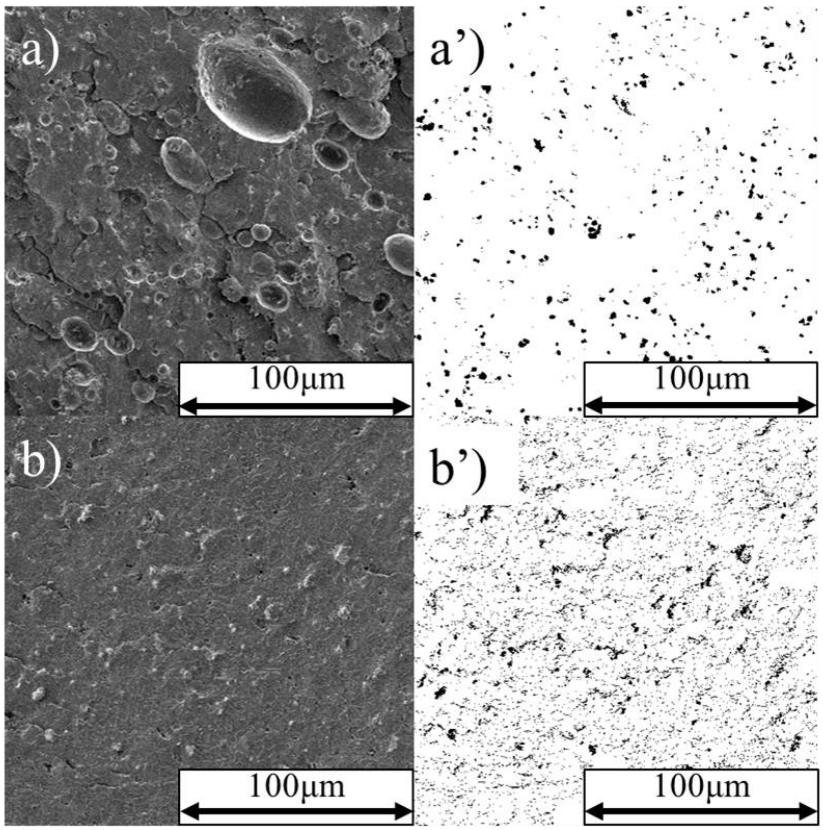

Fig.2-19 Cross sectional FE-SEM images (a, and b) and image processing pictures (a', and b') of samples with 5 % volume fraction of BT prepared under high kneading conditions with Tegomer® P 121 (a, a') without Tegomer® P 121 (b, b').

than the sample without Tegomer® P121. It was suggested that the secondary particle groups were formed because of the cohesive force of the intermolecular force such as the Van der Waals force [18]. It was considered that the size of the BT secondary particle groups was controlled by the dispersion and aggregation in the kneading process.

In the volume fraction 5 % of BT in Fig.2-17 to Fig.2-19, the formation of the BT secondary particle groups were promoted in the order of (1) the sample with Tegomer® P121 under low-speed kneading condition, (2) the sample without Tegomer® P121

Table 2-1 The capacity dimension (D_0) and characteristic [18] of BT / PLLA composites.

Kneading speed	BT Volume fraction		Capacity dimension (D_0)	Dielectric constant (ε')[18]	Average secondly particle area of BT fillers (S)[18] /μm^2
High kneading (30rpm, 10 min)	5	Without Tegomer P121	1.02	3.62	23.62
		With Tegomer P121	1.02	3.36	16.06
Low kneading (10rpm, 30 min)	5	Without Tegomer P121	1.00	3.65	28.52
		With Tegomer P121	1.19	4.10	47.75
	10	Without Tegomer P121	1.26	4.34	39.83
		With Tegomer P121	1.42	5.18	74.22
	20	Without Tegomer P121	1.38	6.99	115.58
		With Tegomer P121	1.60	10.16	183.06

under low-speed kneading condition, (3) the sample without Tegomer® P121 under high-speed kneading condition, and (4) the sample with Tegomer® P121 under high-speed kneading condition.

A method using the box-counting of the fractal analysis has been reported to quantitatively analyze the shape of particles and the packing structure of the particle group [22]. The capacity dimension (D_0) was obtained from the multifractal analysis as an initial analysis, and the BT secondary particle groups were characterized. In order to obtain D_0 from the multifractal analysis, the D_0 was obtained from the multifractal analysis and compared with the D_0 obtained from the fractal analysis to confirm whether both D_0 was the same. The multifractal analysis and the box-counting method were performed using the binary images shown in Fig.2-17 to Fig. 2-19. Table 2-1 shows the D_0 estimated by the multifractal analysis, the average secondary particle area (S) [18], and the average dielectric constant (ε') [18]. This multifractal analysis and the box-counting method were performed under the same conditions. In the box-counting method, the box-counting method was performed in the region where the box size ln r

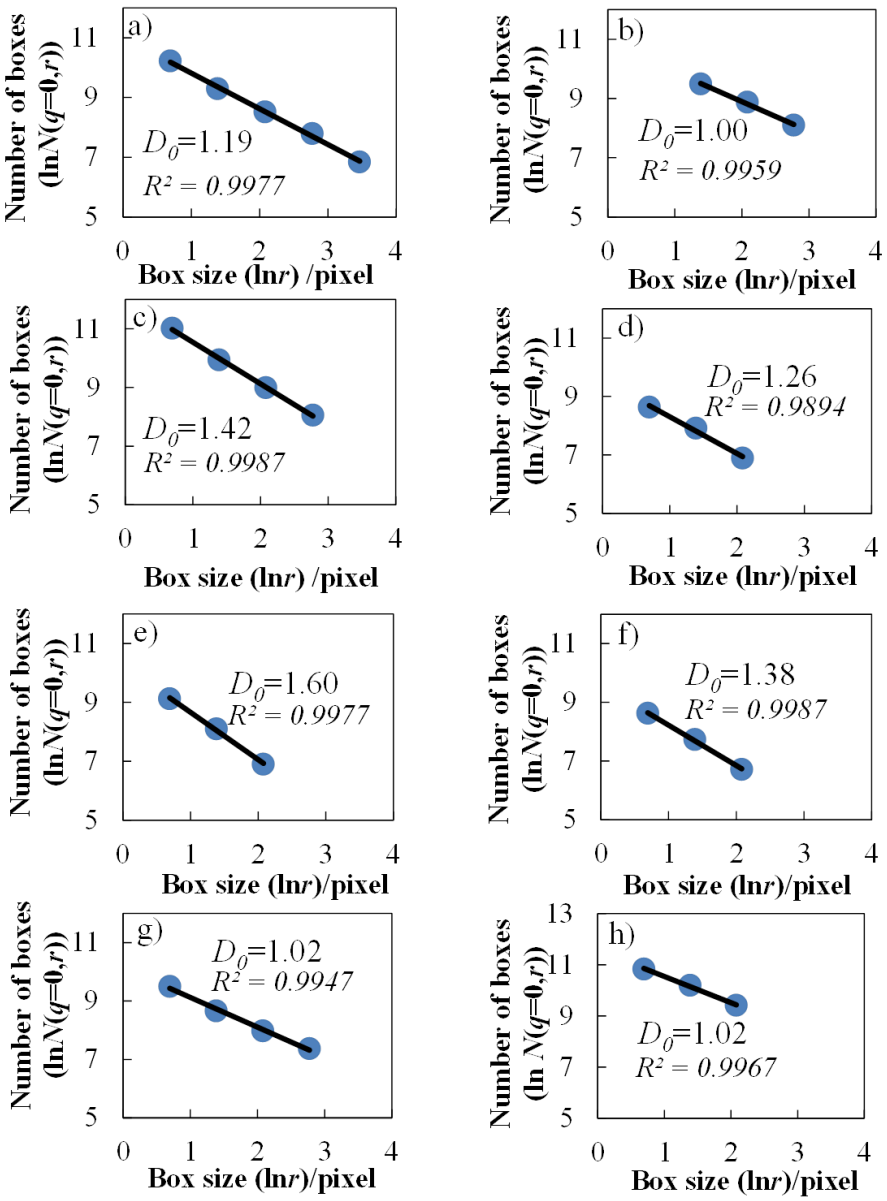

Fig.2-20 Relationship between the number of boxes ln$N(q$=0,$r)$ for BT/PLLA composites and the box size (ln$r$) ; a) and b) 5% volume fraction of BT under low kneading with and without Tegomer® P 121, c) and d) 10% volume fraction of BT under low kneading with and without Tegomer® P 121, e) and f) 20% volume fraction of BT under low kneading with and without Tegomer® P 121, g) and h) 5% volume fraction of BT under high kneading with and without Tegomer® P 121. R^2 indicates the correlation coefficient of ln$N(q$=0,$r)$-ln$r$ plot. D_0 is the capacity dimension for BT secondary particle groups.

was 0 to 6.93 pixels, and D_0 was calculated from the slope derived by the least-squares method. At ln$r$ = 0, the size of the box and the size of the pixels were the same, and ln r (= 0) was excluded from the box-counting method. In addition, the region of ln r (D_0 = 2) was excluded from the box-counting method since it meant that the image was entirely covered. In the sample without Tegomer® P121 under low-speed kneading condition with a volume fraction of 5 vol.%, three slops in the regions of 0 pixel $\leq$ ln $r \leq$ 0.69 pixel, 1.39 pixel $\leq$ ln $r \leq$ 2.77 pixel and 3.47 pixel $\leq$ ln $r \leq$ 6.93 pixel was obtained. 3.47 pixel $\leq$ ln $r \leq$6.93 pixel regions where ln r=0 and D_0=2 were excluded from the fractal analysis for the above reasons. D_0<1 was at ln r=0.69 pixel. This means that the shape of the secondary particle groups was a dashed line, and ln r=0.69 pixel was excluded since the morphology of the BT particle group was not confirmed. Fig. 2-20 shows the results of the fractal analysis with the optimum region. The correlation coefficient of the least-squares method of ln N(q=0, r)-ln r plot as shown in Fig.2-20 was above 0.98, and the slop linear has fractal properties [23], it was determined that the morphology of BT secondary particle groups had fractal properties. The value of D_0 estimated by the multifractal analysis in Table 2-1 and the value of D_0 estimated by the box-counting method in Fig. 2-20 were the same.

According to the sample under low-speed kneading condition in Table.2-1, the slope of the line increased with increasing the volume fraction of BT, and D_0 was also increased. Comparing the D_0 of the sample with and without the Tegomer® P121 under high-speed kneading condition, D_0 was approximately the same. On the other hand, D_0 of the sample under low-speed kneading condition was increased by adding Tegomer® P121. In addition, in the sample with 5 vol. % of BT, D_0 of the sample with Tegomer® P121 under low-speed kneading condition was the highest as shown in Fig. 2-20.

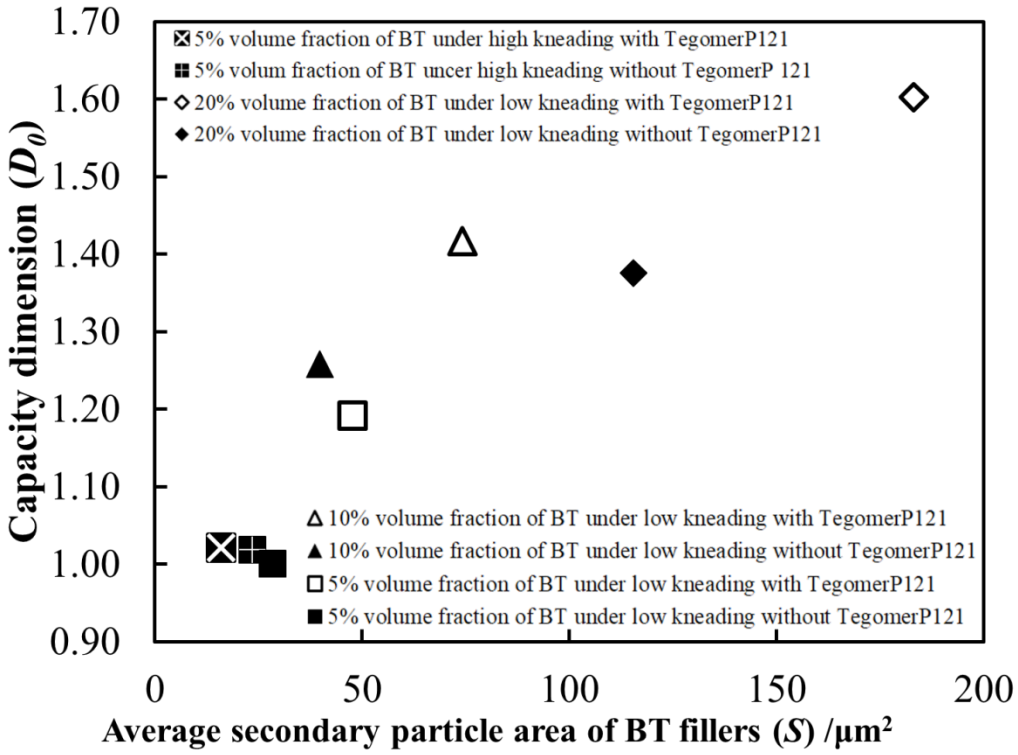

Fig. 2-21 Relationship between the capacity dimension (D_0) and the average secondary particle area of BT fillers with 5, 10, and 20 % BT/PLLA composites.

2.2.4 Discussion

Fig.2-21 presents the results of S and D_0 of the BT / PLLA composites under high and low-speed kneading conditions. Fig.2-22 shows that the relationship between D_0 and ε'. As Fig. 2-21, the D_0 was increased by increasing the S, and the S and D_0 had a correlation. In general, the D_0 has increased with increasing the complexity of the particles. This is, it was considered that the BT / PLLA interface was increased with forming the BT secondary particle groups. It was suggested to contribute to the increase in the ε' in Fig.2-22.

The self-organization processes in a non-equilibrium chemical system have been

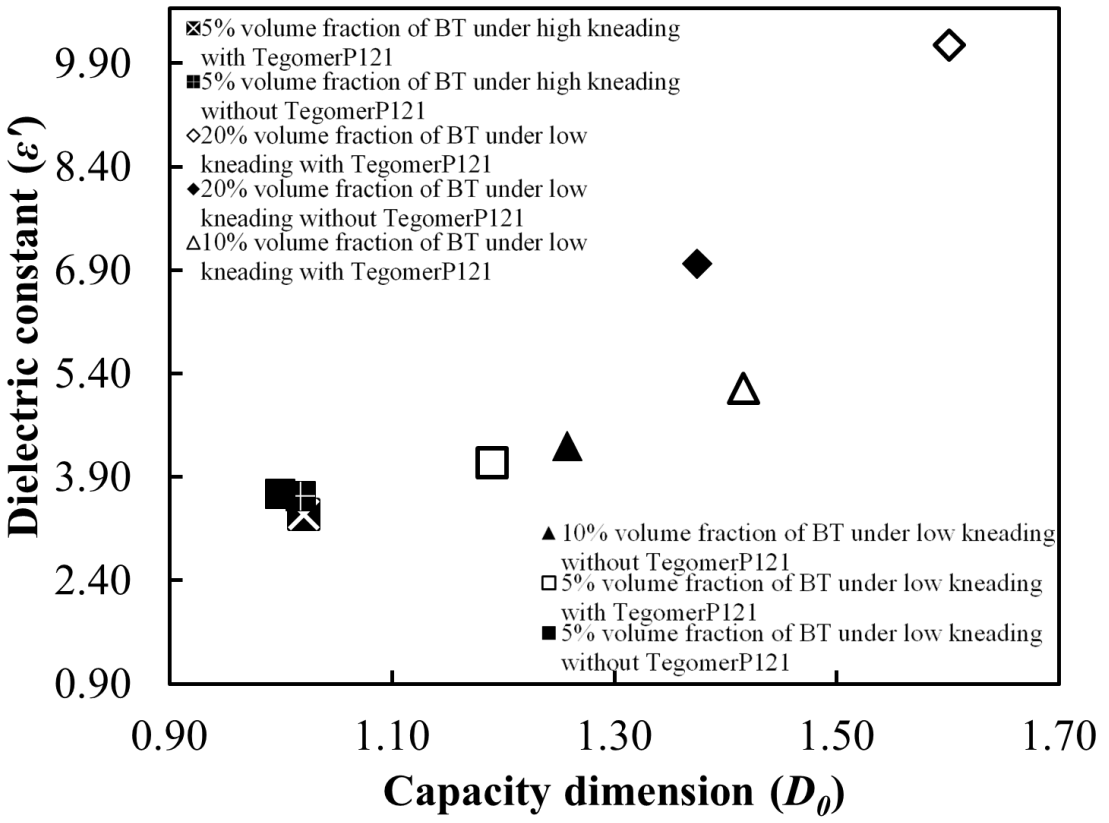

Fig.2-22 Relationship between the capacity dimension (D_0) and the dielectric constant (ε', at 1 kHz) with 5, 10, and 20 % BT/PLLA composites.

studied in a solution system described by the Belousov-Zhabotinsky reaction. The self-assembly process is seen in the reaction-diffusion system, which is assumed to occur due to a competitive reaction between an inhibitor and a promoter within a diffusion process. In the kneading process of solid material, the cohesive force and dispersion force act. The kneading process can indicate the diffusion process in the reaction-diffusion system and the size of the secondary particle groups by the self-assembly process of the cohesive force and dispersion force are discussed.

$$\text{Aggregation} \Leftrightarrow \text{Decomposition} + \text{Diffusion process} \qquad (2\text{-}8)$$

According to the above equation, it was suggested that the formation of BT secondary particle groups was promoted by the reactions of both condensation and dispersion forces.

Generally, organic functional groups are generated on the surface of BT particles with dispersant is added, and it is attempted to improve the dielectric constant by increasing the degree of dispersion in the polymer matrix [24]. In the sample under low-speed kneading condition, the BT particles were dispersed by the effect of the dispersant; however, the shear stress was low, and then it was suggested that the formation of the self-assembled BT secondary particle groups was promoted with the re-aggregation. That is, it was considered that the BT particles were secondary particle groups while forming the BT / PLLA interface with Tegomer® P121 under low-speed kneading condition. On the other hand, it was suggested that the BT secondary particle groups were small with Tegomer® P121 since the shear stress was high and the dispersion effect was high.

According to Fig.2-22, the ε' was increased by increasing the D_0. In a previous report [18], it was proposed that the inorganic / organic interface was important for the dielectric constant. In general, the polymer is p-type and BT is n-type, and it was considered that a heterointerface was formed at the BT / PLLA interface. Therefore, a depletion layer was formed between BT and PLLA, and BT / depletion layer / PLLA was formed, and it was considered that the depletion layer contributed to the improvement of the dielectric constant. According to the result of D_0, it was suggested that the simple BT / BT interface did not sufficiently contribute to the improvement of the dielectric constant since the formation of the BT / PLLA interface was promoted. Comparing the samples with and without Tegomer® P121 in Fig. 2-22, the ε' and D_0 of

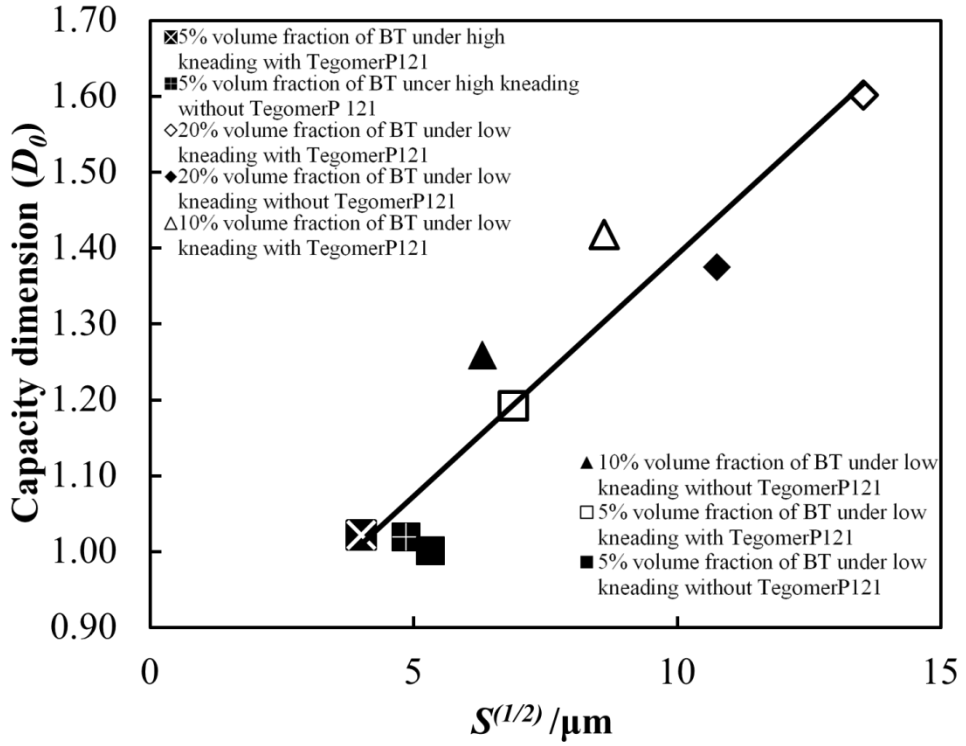

Fig. 2-23 Relationship between the capacity dimension (D_0) and the outer perimeter of BT secondary particle groups with 5, 10, and 20 % BT/PLLA composites.

the samples with Tegomer® P121 were higher than the samples without Tegomer® P121. This is, it was suggested that the ε' of the sample with TegomerP121 was improved since the BT / PLLA interface was formed while forming the self-assembled BT secondary particle groups. According to the correlation between the D_0 and ε', D_0 was reflected in the complexity of the BT / PLLA interface, and it was suggested that the formation of the BT / PLLA heterointerface was promoted, which affected the improvement of the ε'. Thus, it was suggested that the control of the kneading speed and the additive Tegomer® P121 affected the self-assembly process of the BT secondary particle groups, and the morphology of the self-assembled BT secondary particle groups affected the dielectric properties.

Fig. 2-23 shows the relationship between $S^{1/2}$ and D_0. In general, $S^{1/2}$ corresponds to the outer parameter change and correlates with the outer length L of the particle group. The relationship between $S^{1/2}$ and L can be described by the following equation [25]:

$$L \propto S^{1/2} \propto V^{1/3} \tag{2-9}$$

where V is the volume. According to Eq. (2-9), it is shown that the change in the shape (unevenness) of the BT secondary particle group corresponds to the change of the outer circumference length and reflects the change in $S^{1/2}$. As Fig.2-23, $S^{1/2}$ and D_0 had a correlation. The relationship can be described by the following equation:

$$S^{1/2} \propto L \propto D_0 \tag{2-10}$$

Therefore, it was suggested that D_0 reflected to indices of the morphology of the self-assembled BT secondary particle group. It was considered that it was possible to evaluate the effect of the kneading conditions of composites by using the multifractal analysis.

2.2.5 Conclusions

In order to quantitatively analyze the morphology of the self-assembled BT secondary particle group under the different manufacturing conditions, the BT / PLLA composites were prepared with and without the dispersant under two kneading conditions (1) low-speed kneading condition (10 rpm for 30 minutes) and (2) high-speed kneading condition (30 rpm for 10 minutes) with 5 vol.% to 20 vol.%, and

the multifractal analysis was attempted to apply the evaluation for the morphology of BT secondary particle group. The conclusions are as follows:

(1) According to the FE-SEM images of the sample under the low-speed kneading condition, it was shown the formation of BT secondary particle groups was promoted by increasing the volume fraction of BT. In addition, in the sample preparation under low-speed kneading conditions, the D_0 was increased with increasing the volume fraction of BT.

(2) In the sample with the dispersant under low-speed kneading condition, the formation of BT secondary particle groups was promoted more than the sample without the dispersant.

(3) The D_0 was increased linearly with increasing $S^{1/2}$. It was suggested that the morphology of BT secondary particle groups became complex with adding BT fillers since $S^{1/2}$ correlates with the length L of the outer circumference of the BT secondary particle group.

Hence, it was suggested that the BT secondary particle groups were small under high-speed kneading condition since the shear stress is high and the dispersibility is high. On the other hand, it was suggested that the formation of the BT secondary particle groups was promoted since the shear stress was low under the low-speed kneading condition.

According to the results of D_0 by the multifractal analysis, the multifractal analysis was effective as indices for evaluating the morphology of the self-assembled BT secondary particle group under the different processes. In particular, it was clarified that

D_0 was reflected in the degree of complexity of the outer circumference of the secondary particle group.

2.3 Effect of ceramics / polymer heterointerface on dielectric property of self-assembled BT / PLLA composite materials

2.3.1 Introduction

In Session 2.2, the morphology of the self-assembled BT secondary particle group under the different manufacturing processes and the dielectric properties were investigated. In this session, the dispersion state and interface state of BT particle groups in self-assembled BT / PLLA composites prepared under different fabrication conditions was investigated in more detail.

Heterointerface of ZnO with Bi_2O_3 or Pr-Co Oxide has been investigated. The insulating region, such as Bi_2O_3 and Pr-Co, is essential for controlling electrical properties, whereas an insulator zone exists between the grain boundaries. Previously, Yano et al. [26] fabricated multilayered composites with Ni / ZnO / PrCoOxide / Au structure to investigate electrical properties at junctions. They found a depletion region formed in ZnO films near the ZnO / PrCo Oxide interface [26]. Matsuoka [27] reported nonohmic properties of ZnO ceramics with five additives, such as Bi_2O_3, CoO, MnO, Cr_2O_3, and Sb_2O_3, and proposed a microstructure model that surround each of ZnO grains with a segregation layer responsible for the nonohmic property. In their model, the electrical capacitance of ZnO ceramic was primarily attributed to segregation layers [27]. The electrical properties are therefore controlled by a microstructure with grain boundaries such as ceramics / intergranular material.

Munakata et al. [18] reported that the dielectric constant of the BT / PLLA composites was increased with increasing the secondary particle area of self-assembled BT secondary particle groups. In Session 2.2, the morphology of the self-assembled BT secondary particle groups was affected by the kneading speed. Therefore, it was assumed that the BT secondary particle groups under the different processes were different. In this paper, the dispersion state and the interface state of BT secondary particle groups in self-assembled BT / PLLA composites prepared by changing the fabrication conditions was investigated. In particular, the BT / PLLA / BT heterointerface of the BT aggregates by the self-assembly process was analyzed and the effect of the BT / PLLA / BT heterointerface and the BT / BT interface on the dielectric properties of BT / PLLA composites was investigated. Fig.2-24 shows the points of the self-assembly process and the BT secondary particle groups in this session.

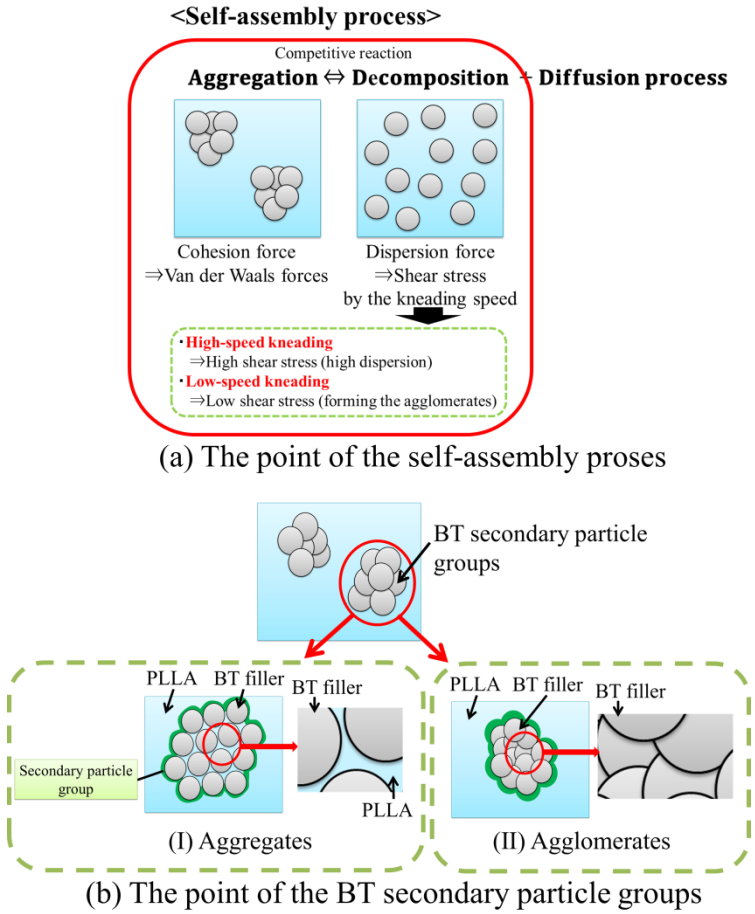

Fig. 2-24 Focused points of (a) the self-assembly process and (b) the BT secondary particle groups in session 2.2.

2.3.2 Experimental procedures

2.3.2.1 Sample preparation

BT powder was prepared using a conventional solid-state synthesis technique. $BaCO_3$ (99.95%, High Purity Chemical Co., Japan) and TiO_2 (99%, High Purity Chemical Co., Japan) were used as the starting materials. Powders used for the experiments were ground and properly mixed. The powder mixture was fired at 1373 K for 4 h. The sintered BT was ground to get a BT powder. The resultant BT powder had an average

particle diameter of approximately 1 μm. The powder exhibited a single phase, which was determined using powder X-ray diffraction. BT granules were made using the same method and had average particle diameters of over 20 μm and 150 μm. BT / polymer composites were generated from BT powder and granular PLLA (PLLA, Nature Work, Japan). PLLA was melted at a temperature of 473 K, and BT powder was added to PLLA to form mixtures. The volume fractions of BT were 0%, 5%, 10%, and 20%. Two different processes have been adopted during the mixing: (1) slow-speed hand mixing for 30 min with approximately 10 rpm and (2) high-speed mixing via a kneader (TOYOSEIKI, Labo Plastomill (4C150)) for 10 min with 30 rpm. After the mixing was over, each sample was cooled in the air. In order to homogenize BT / PLLA composites with dispersion, both BT powder and Tegomer® P121 (polyolefin type, Evonik, U.S.A.) were mixed and kneaded under the same conditions, as described earlier. The amount of additive Tegomer® P121 in the mixture was approximately 4.0 wt% in BT powder. The required dosage level is 2.0 – 4.0 %, and we decided the added amount of Tegomer® P121 by a preliminary experiment. 4.0 wt% of Tegomer® P121 was slight for PLLA. BT powders with two different diameters (average particle diameters: over 20 μm and over 150 μm) and PLLA were mixed under low kneading speed to prepare BT / PLLA composites by adding BT granules, respectively. The volume fraction of the BT granule was 5%.

2.3.2.2 Measurement method

The dielectric constant and loss tangent of BT / PLLA composite at the frequency range from 100 Hz to 100M Hz were measured at 298 K using an Agilent 4294 A precision impedance analyzer; lead wires were made of platinum. Each sample was a

rectangle with a surface area of 64 mm^2 and a thickness of 0.3 mm. Gold was deposited on electrodes with square faces. A part of the results of the dielectric constant was based on a previous study [18].

The cross-sections of samples were analyzed using a field emission scanning electron microscope, FE-SEM (Hitachi Co., Japan: S-4100 and SU-8230, JEOL Ltd.: JSM-7001F). FE-SEM images have been converted to binary images to estimate an average secondary particle area of BT filler for each sample. A part of the FE-SEM images was based on session 2.2. A part of the results of the average secondary particle area of BT filler was based on a previous study [18].

2.3.3 Results

Fig.2-25 presents the images of FE-SEM micrographs of BT / PLLA composites with and without Tegomer® P121 under high-speed kneading, low-speed kneading, and the presence of BT granules (particle size of BT: 20 μm and 150 μm, 5 vol%). Fig.2-25a-b shows samples with 5 vol% fraction of BT prepared under high-speed kneading conditions with and without Tegomer® P 121. Samples with 5, 10, 20 % volume fraction of BT prepared under low-speed kneading conditions with Tegomer® P 121 are shown in Fig. 2-25c-e. Samples with 5, 10, 20 % volume fraction of BT prepared under low-speed kneading conditions without Tegomer® P 121 are presented in Fig. 2-25f-h. Fig.2-25i depicts a sample with 5 % volume fraction of small BT granules prepared under low-speed kneading conditions without Tegomer® P 121, whereas Fig.2-25j shows a sample with 5 % volume fraction of large BT granules prepared under low-speed kneading without Tegomer® P 121.

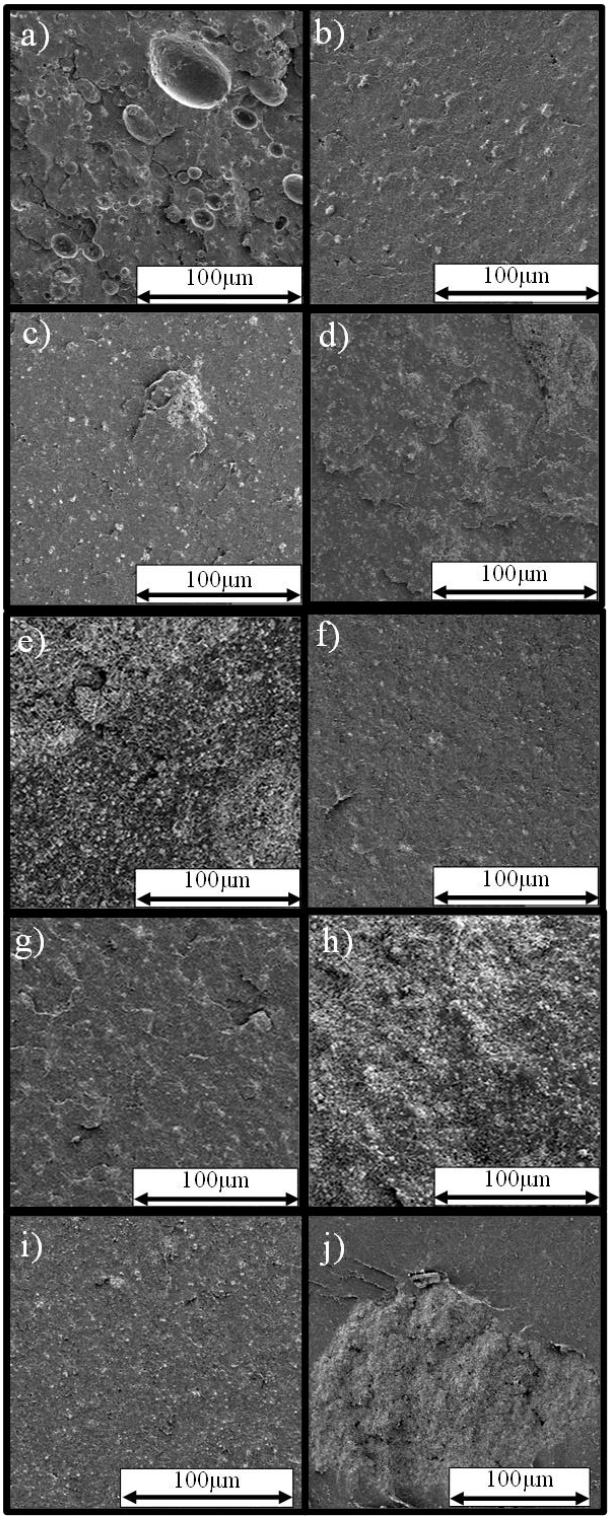

Fig.2-25 Cross-sectional FE-SEM images of the barium titanate (BT) / poly-L-lactic acid(PLLA) composites under low and high-speed kneading conditions with and without Tegomer® P 121. (See the text)

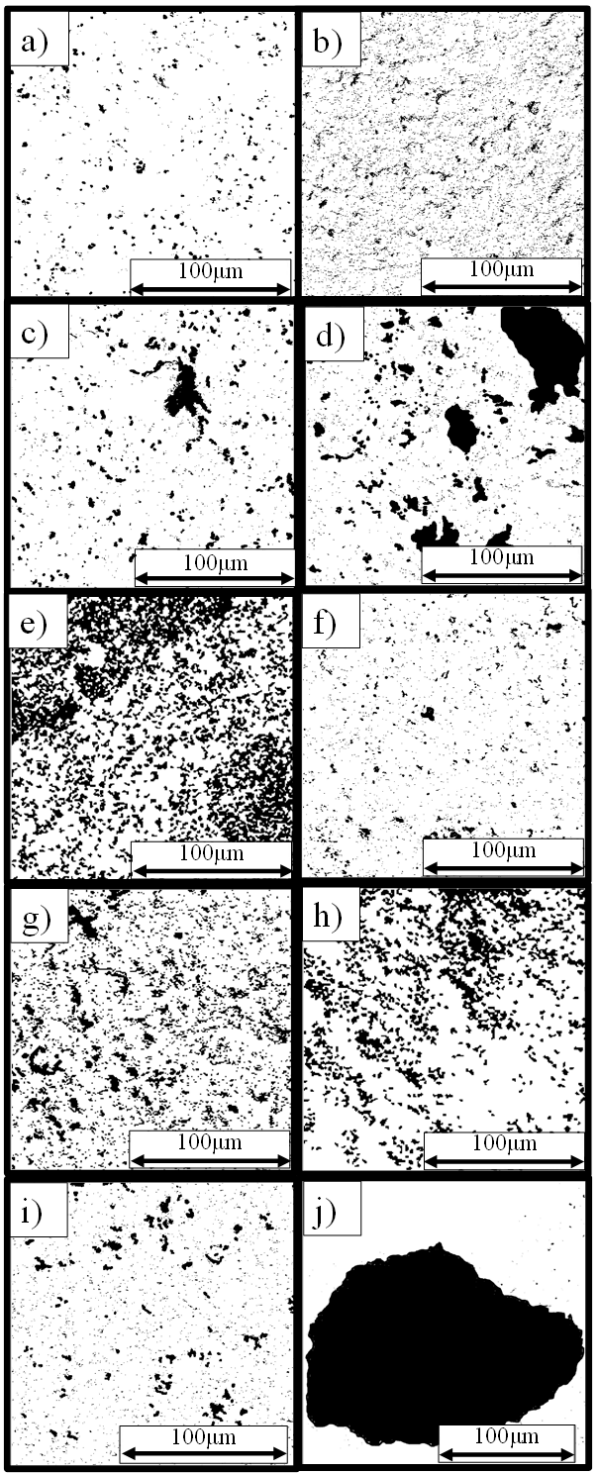

Fig. 2-26 Image processing cross-sectional pictures of the BT / PLLA composites under low and high-speed kneading conditions with and without Tegomer® P 121. (See the text)

The binary images based on Fig.2-25 are shown in Fig.2-26. The result showed that BT fillers were highly dispersible in the presence of Tegomer® P121 under high-speed kneading. BT aggregates produced under low-speed kneading conditions. Comparing samples with and without Tegomer® P 121 under low-speed kneading conditions, it was observed that BT aggregates were better promoted with Tegomer® P 121 than without Tegomer® P 121. The starting material (BT powder) was aggregated by van der Waals [18]. BT aggregates were formed in the presence of BT granules additive, having a particle size of 20 μm (see Fig.2-25 i). However, BT aggregates were not formed by adding BT granules when particle size is close to 150 μm (see Fig.2-25 j).

Fig. 2-27 presents the result of the volume fraction of BT and dielectric constant (ε') at 1 kHz. The addition of Tegomer® P 121 had a negligible effect on the dielectric constant of pure PLLA materials. However, the dielectric constant of BT / PLLA composites increased by the addition of BT powder. In order to evaluate the effects of the filler, the Bruggeman model is used to composite materials wherein the fillers are homogeneously dispersed in the matrix, as shown in Fig. 2-27 [28]. The model shows as follows: [28]

$$1 - V = \frac{\varepsilon'_{composite} - \varepsilon'_{filler}}{\varepsilon'_{matrix} - \varepsilon'_{filler}} \left(\frac{\varepsilon'_{matrix}}{\varepsilon'_{composite}} \right)^{1/3} \quad (2\text{-}11)$$

Where V refers to the volume fraction of BT; $\varepsilon'_{\text{matrix}}$ refers to the dielectric constant of PLLA (ε'_{matrix} = 3.2); ε'_{filler} is the dielectric constant of BT (ε'_{filler} = 1000); $\varepsilon'_{composite}$ is the dielectric constant of BT / PLLA composite. The dielectric constant of BT/PLLA composites with Tegomer® P121 under low-speed kneading was higher than that of the Bruggeman model. Earlier, researchers found a higher dielectric constant in the coarse

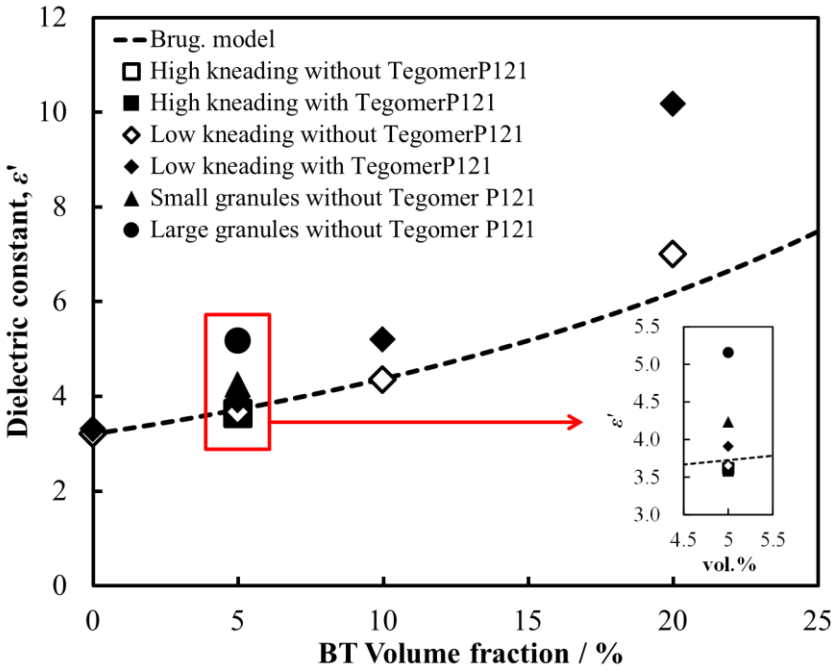

Fig.2-27 Dielectric constants (ε') at 1 kHz of the BT / PLLA composites depending on the volume fraction of BT powders under the high and low-speed kneading conditions with and without the additive Tegomer® P 121.

(agglomeration) particle samples, which could be explained by considering the number of particles along the agglomerated low-impedance path [15]. Comparing composites of 5 vol.%, the dielectric constant of (1) a sample with large granules, (2) a sample with small granules, and (3) a sample prepared under a low-speed kneading condition with Tegomer® P121 was higher than the Bruggeman model. The data related to the average secondary particle area, average dielectric constant, and tanδ are shown in Table 2-2.

In order to investigate the formation of interface for the BT secondary particle groups, the extended FE-SEM images of samples with Tegomer® P121 under high-speed kneading and low-speed kneading are shown in Fig.2-28. Fig. 2-28a-a′ and 4b-b′ show samples with 5 vol.% fraction of BT prepared under high-speed and low-speed

Table 2-2 The characteristic of BT / PLLA composites.

Kneading speed	BT Volume fraction		Dielectric constant, ε'	Loss tangent, $\tan\delta$	Average secondary particle area of BT fillers, S /μm^2
High kneading (30rpm, 10 min)	5	Without Tegomer P121	3.62 [18]	-	23.62 [18]
		With Tegomer P121	3.58	0.0047	16.06 [18]
Low kneading (10rpm, 30 min)	5	Without Tegomer P121	3.65 [18]	-	28.52 [18]
		With Tegomer P121	3.91	0.0030	47.75 [18]
	10	Without Tegomer P121	4.34 [18]	-	39.83 [18]
		With Tegomer P121	5.18 [18]	-	74.22 [18]
	20	Without Tegomer P121	6.99 [18]	-	115.58 [18]
		With Tegomer P121	10.16 [18]	-	183.06 [18]
	5	Small granules Without Tegomer P121	4.23	0.0054	90.43
		Large granules Without Tegomer P121	5.16	0.0472	1541.67

kneading with Tegomer® P 121, respectively. Fig.2-29 depicts magnified FE-SEM images of samples with large granules and small granules under low-speed kneading. Fig.2-29 a and a′ presents of a sample with 5 % volume fraction of BT prepared with small granules under low-speed kneading without Tegomer® P 121, whereas 2-29b and 2-29b′ shows of a sample with 5 % volume fraction of BT prepared with large granules under low-speed kneading without Tegomer® P 121. BT powder indicates a blue arrow and PLLA as a red arrow. The images of a and b in Fig.2-28 and Fig.2-28 present BT secondary particle groups. The images of a′ and b′ in Fig.2-28 and Fig. 2-29 are the magnified images of BT secondary particle groups. BT particles of a sample with Tegomer® P121 prepared under high-speed kneading were dispersed, and BT agglomerates were small. It is observed that a sample with Tegomer® P121 prepared under high-speed kneading has a small BT / BT interface. The effect of BT / polymer / BT interface was decreased due to a large distance between BT particles. It was confirmed that BT and PLLA of the sample with Tegomer® P121 under the high-speed kneading condition were not partially contacted. The dielectric constant of the samples with Tegomer® P121 under the high-speed kneading condition was lower than the

Bruggeman model (see Fig.2-27). The dielectric constant of air is lower than PLLA and BT. Therefore, it was suggested that these voids affected the dielectric properties. BT aggregates having the BT / polymer / BT heterointerfaces of a sample with Tegomer® P121 under low-speed kneading condition were formed are found (see Fig.2-28 b) and b′). Researchers suggested BT aggregates were formed by a repetition of dispersion and aggregation between particles under low-speed kneading [18]. This model explains an outcome of the present experiment. The BT / PLLA / BT heterointerface was formed under the low-speed kneading condition within the self-assembly process. It was confirmed that BT and PLLA were not partially contacted. However, the dielectric constant of the samples with Tegomer® P121 under the low-speed kneading condition was higher than the Bruggeman model (see Fig.2-27). Therefore, it was suggested that the dielectric constants of the BT / PLLA composite with Tegomer® P121 under the low-speed kneading condition were not efficiently affected by the voids. The spherical voids were confirmed in the sample with Tegomer® P121 under the low-speed kneading condition in Fig.2-28 b) and b'). It was suggested that the BT particles were eliminated when the samples were cut to prepare for the cross-sections of the samples. Therefore, the spherical voids in the BT aggregates did not affect by the dielectric constant of the sample. In order to clarify the BT / BT interface and the BT / PLLA / BT heterointerface in the BT secondary particle groups, BT granules with a BT / BT interface were added to PLLA. BT agglomerates of small granules had polymer, suggesting the formation of BT / BT and BT/polymer/BT heterointerfaces (see Fig.2-29 a and a′). The distance between BT particles of the sample with Tegomer® P121 under low-speed kneading was closer than the small granules sample. BT agglomerates with large granules had BT / BT interface and had a coarse (see Fig.2-29 b and b′). Hence, the formation of

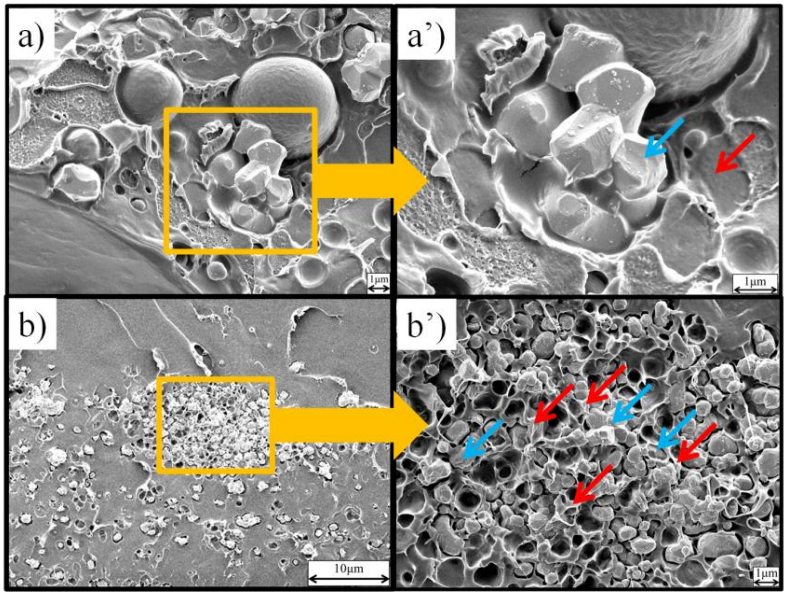

Fig.2-28 Cross-sectional FE-SEM images and magnified images of samples with 5 % volume fraction of BT prepared under a) high and b) low-speed kneading conditions with Tegomer® P 121.

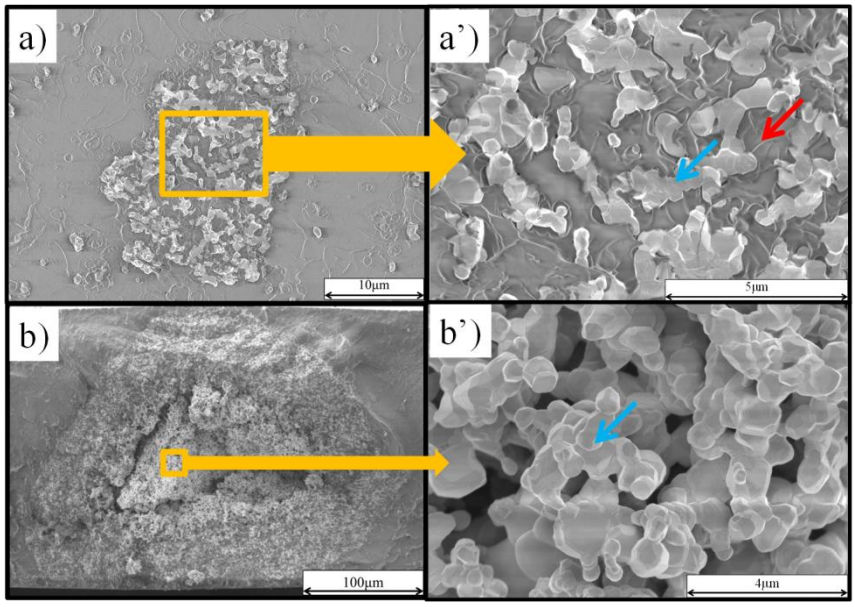

Fig.2-29 Cross-sectional FE-SEM images and magnified images of samples with 5 % volume fraction of BT prepared with a) small and b) large granules under low-speed kneading conditions without Tegomer® P 121.

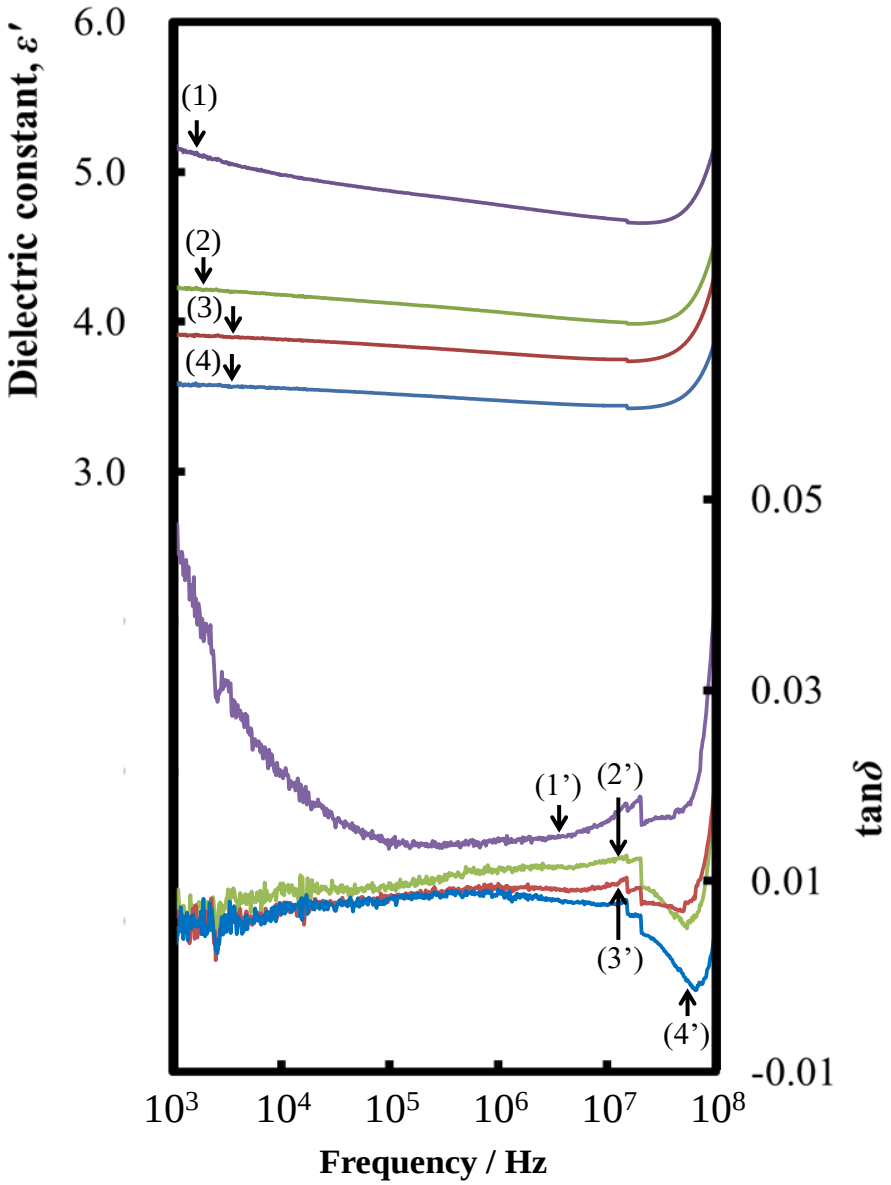

Fig.2-30 Plots of dielectric constant (ε') and loss tangent (tanδ) of the BT / PLLA composites depending on the frequency. (See the text)

BT / polymer / BT heterointerface was different depending on the production of BT / PLLA composites.

Fig. 2-30 presents results of the dielectric constant and tanδ, depending on the frequency used to examine the effects of granules. Fig. 2-30 1 and 1′ shows a sample

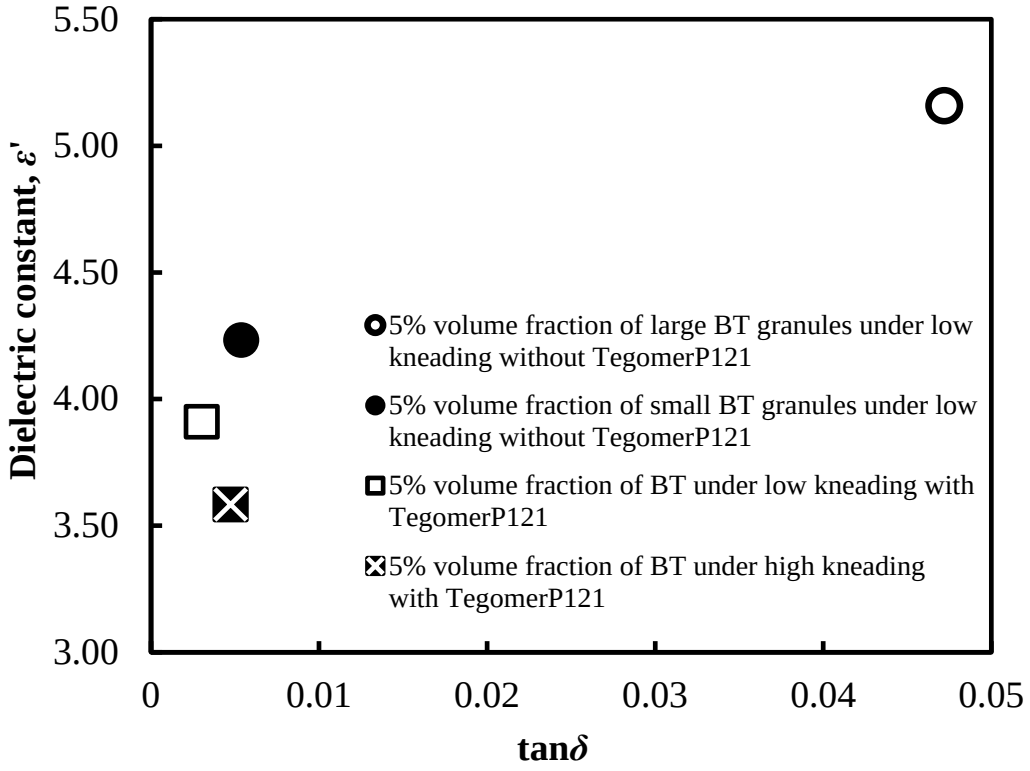

Fig.2-31 A relationship between dielectric constant (ε') and loss tangent (tanδ) of the BT / PLLA composites with 5 % volume fraction of BT prepared with small and large granules and BT powders under low-speed kneading condition with and without Tegomer® P 121.

with 5 % volume fraction of BT prepared by adding large granules under low-speed kneading without Tegomer® P 121, whereas Fig. 2-30 2 and 2-30 2′ shows a sample with a 5 % volume fraction of BT prepared by adding small granules under low-speed kneading without Tegomer® P 121. Furthermore, Fig. 2-30 3 and 2-30 3′ and Fig. 2-30 4 and 2-30 4′ depicts a sample with 5 % volume fraction of BT formed under low-speed and high-speed kneading with Tegomer® P 121, respectively. The relationship between tanδ and ε' is shown in Fig.2-31. Figs 2-30 and Fig. 2-31 present the results of a sample of 5 vol.% of BT particles, which is higher than the Bruggeman model and a sample of 5 vol.% of BT with Tegomer® P121 under high-speed kneading condition. The ε' of these samples with large granules was highest at all frequencies, as shown in Fig.2-30.

In contrast, the ε' of a sample under high-speed kneading was lowest at all frequencies. The value of tanδ of BT / PLLA composites with Tegomer® P121 under low-speed kneading and high-speed kneading is almost similar. The tanδ of the sample by adding BT large granules was the highest, and it was considered that a loss at the interface was large as the BT particles were not bonded; thus, delaying the dielectric response (see Fig.2-30 b and b′). According to Fig. 2-31, the tanδ of the samples with Tegomer® P121 under low-speed kneading condition was lower than the tanδ of the sample by adding BT large granules, which is 1/15.6 that of the sample with the large granules. It was considered that the voids at the BT / PLLA interface of the BT aggregates with Tegomer® P121 under the low-speed kneading condition did not efficiently reflect the dielectric properties. Based on the results of small granules, samples with Tegomer® P121 under low-speed kneading and high-speed kneading condition, ε' were increased without raising the tanδ (see Fig.2-31).

2.3.4 Discussion

Fig. 2-32 shows that a dielectric constant (ε') of the self-assembled BT / PLLA composites is increased with an increase of average secondary particle area of BT fillers. Robertson and Varlow [29] suggested that a low-impedance path formed BT agglomerations, resulting in an improvement of the dielectric constant. In addition, researchers suggested that the dielectric constant of self-assembled BT / PLLA composites was increased with increasing the BT secondary particle groups. In order to clarify the BT / BT interface and the BT / PLLA / BT heterointerface in the BT secondary particle groups, the BT / PLLA composite was prepared by adding BT granules with a BT / BT interface. Comparing the results of BT volume fraction (5%),

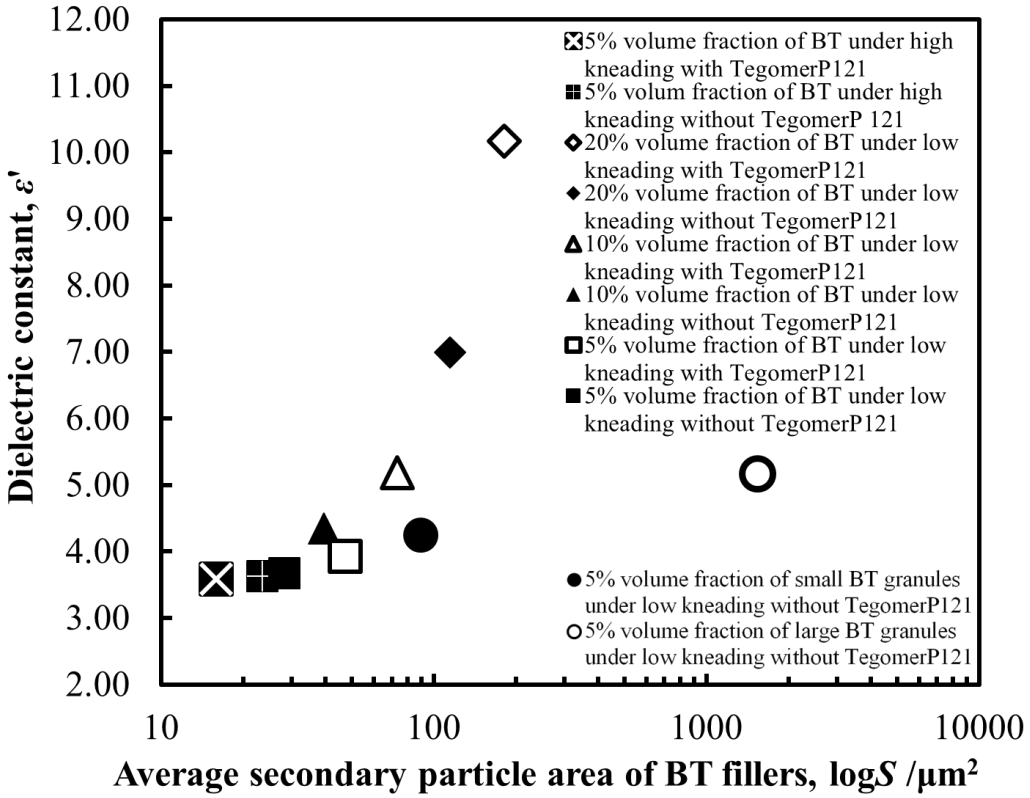

Fig.2-32 A relationship between dielectric constant (ε') and average secondary particle area (S) of BT fillers of the BT / PLLA composites.

the change in ε' was saturated with an increase in the average secondary particle area of BT secondary particle groups. The slopes of the change in the ε' depending on the secondary particle area of BT fillers were different between the sample having the BT / PLLA / BT heterointerface and the sample having the BT / BT interface. In particular, the amount of change in ε' depending on the average secondary particle area of the self-assembled BT / PLLA under the low-speed kneading condition, which had the higher dielectric constant than the Bruggeman model, was 1.8 times higher than that of the sample with the small granules and 24.5 times higher than that of the sample with the large granules. That is, it was suggested that the interface effect was different and

the BT / PLLA / BT heterointerface improved the ε' more efficiently than the BT / BT interface.

The self-organization processes in a non-equilibrium chemical system have been studied in a solution system described by the Belousov-Zhabotinsky reaction [30]. The self-organization process is seen in the reaction-diffusion system, which is assumed to occur due to a competitive reaction between an inhibitor and a promoter within a diffusion process. The reaction is shown in the following equation (2-12),

$$\partial v/\partial t = u - v + D_v \nabla^2 v \qquad (2\text{-}12)$$

Where *u* is the active term; *v* is the inhibitive term; *Dv* is the diffusion coefficient. The self-assembly process of solid particles is assumed to be driven by both condensing and dispersing forces. Equation (2-12) shows the self-assembly process of a solid based on equation (2-13).

$$\text{Aggregation} \Leftrightarrow \text{Decomposition} + \text{Diffusion process} \qquad (2\text{-}13)$$

This reaction corresponds to a process of aggregation and decomposition. That is, BT aggregates are formed by the competitive reaction of dispersion and aggregation. Van der Waals force acts as a cohesion force. The shear stress by the stirring speed acts for decomposition. The kneading process can indicate the diffusion process in the reaction-diffusion system. As a result of self-assembly progress, the secondary particle group of BT particles can be formed by reactions of both condensation and dispersion forces. In order to homogenize BT fillers in PLLA, Tegomer® P121 was added to BT /

PLLA composites. After BT fillers were homogeneity, the shear stress is high in the high-speed kneading condition, and the BT fillers were dispersed. In the low-speed kneading condition, the shear stress is low, and the BT aggregates are formed within the self-assembly process. Therefore, a material texture was dependent on the shear stress. As a consequence, BT aggregates with BT / PLLA / BT heterointerface have been developed within the self-assembly process, wherein grain boundaries play an essential role in electrical properties. From the magnified images in Fig.2-29 b and b′, it is considered that the self-assembled BT aggregates had a BT / polymer / BT heterointerface by adding Tegomer® P121 under low kneading speed. In general, a depletion layer is formed at the interface between the semiconductor and insulator. In this experiment, it was suggested that the BT / PLLA / BT heterointerface in which PLLA acts as an insulating layer of the semiconductor–insulator–semiconductor (n–i–n) model was formed in the BT aggregates. The schematic drawing of the model of the electronic structure was shown in Fig.2-33. E_c is the conduction band, E_f is the Fermi level, and E_v is the valence band. It was considered that the electric structure of the BT / BT interface related to the double Schottky barrier model (see Fig.2-33 a). On the other hand, the BT particles were surrounded by PLLA, and the depletion regions which trap the electrons at grain boundaries of the BT particles were formed (see Fig.2-33 b). That is, in the BT / PLLA / BT heterointerface, it was considered that the electric dipoles were increased. Thus, the electric dipole of a BT / PLLA / BT heterointerface was induced to improve the dielectric constant (see Fig.2-32). In addition to small BT granules, the polymer also contained BT aggregates. In contrast, the composite with large BT granules had developed BT / PLLA /BT heterointerface. However, the BT / BT interface was dominantly formed, as shown in Fig.2-29 b and b′. For the sample with

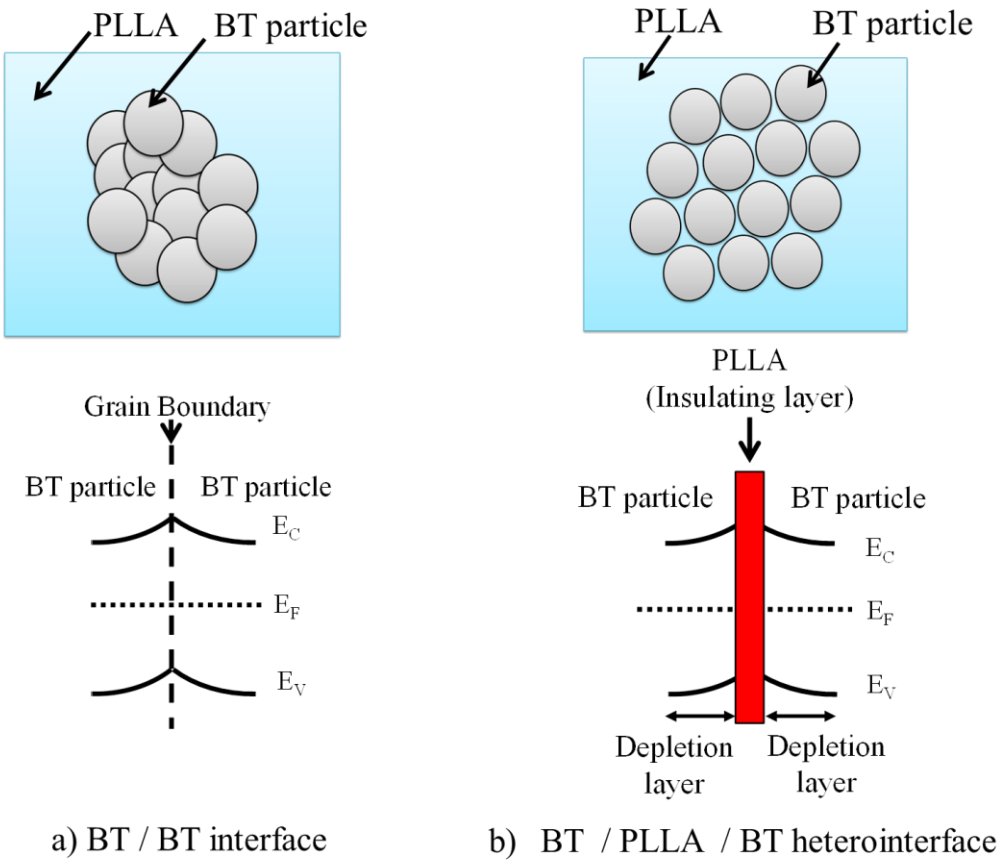

Fig. 2-33 The schematic drawing the model of the electronic structure. a) is the model of the BT / BT interface, and b) is the model of the BT / PLLA/ BT heterointerface.

Tegomer® P121 by high kneading speed, BT / PLLA / BT heterointerface was not formed. Therefore, it is proposed that the dielectric properties significantly improved by the formation of BT / PLLA / BT heterointerface within the self-assembly process.

2.3.5 Conclusions

BT / PLLA composites were prepared under different processes based on three conditions: (1) low-speed kneading, (2) high-speed kneading, and (3) granules (particle

sizes: 20 μm and 150 μm) to investigate the dispersion state and the interface state of BT secondary particle groups. In particular, the BT / PLLA / BT heterointerface in the self-assembled BT aggregates and the effect of the BT / PLLA / BT heterointerface and the BT / BT interface in the BT secondary particle groups on the dielectric properties of the BT / PLLA composites were investigated.

(1) According to FE-SEM images, it was confirmed that the process of preparing composite materials affected the formation of BT aggregates and agglomerates. In particular, BT agglomerates having BT / BT interfaces were formed under the high-speed kneading condition, and BT aggregates having BT / PLLA / BT heterointerfaces were formed under the low-speed kneading condition. It was suggested that BT aggregates having the BT / PLLA / BT interface were formed under the low-speed kneading condition and the self-assembly process was driven.

(2) Comparing BT granules having the BT / BT interface with the self-assembled BT aggregates having the BT / PLLA / BT heterointerface, the tanδ of the self-assembled BT aggregates was lower than that of BT granules having the BT / BT interface, and the amount of the change in the dielectric constant of the self-assembled BT aggregates depending on the secondary particle area was higher than that of the BT granules. In particular, comparing the sample of 10 vol.%, the amount of the change in the ε' of the self-assembled BT / PLLA composites depending on the S was 24.5 times higher than that of the sample with the large granules, and the tanδ of the self-assembled BT / PLLA composites was 1/15.6 that of the sample with the large granules.

Hence, it was suggested that it was an important role in improving the dielectric properties to form ceramics secondary particle groups having the ceramics / polymer / ceramics heterointerface by the self-assembly process. It is expected that the dielectric properties can be improved by controlling the formation of ceramics aggregates with a ceramics / polymer / ceramics heterointerface.

2.4 Material texture of self-assembled BT / polyvinylidene fluoride composites and dielectric properties

2.4.1 Introduction

Polyvinylidene Fluoride (PVDF) was used as the polymer matrix material, and the relationship between the self-assembled material texture of the BT / PVDF composite material and the dielectric constant was discussed. The effect of dispersant viscosity on self-assembled BT / PVDF composites and the dielectric properties was investigated with the multifractal dimension.

A method incorporating fractal analysis was devised to quantitatively analyze the shape of particles [19], with Kobayashi et al.[20] investigating the grain boundary microstructures in SUS316L stainless steel using the fractal analysis method. Here, the authors highlighted how the maximum random boundary connectivity was found to have a fractal nature in the SUS316L specimens and suggested that it was possible to characterize the grain boundary microstructures via fractal analysis [20]. In another of the previous report in session 2.2, the characteristics of the aggregated morphology of the secondary particle group in BT / PLLA polymers using multifractal analysis was investigated [31]. Here it reports that the self-assembled BT aggregate morphology had fractal characteristics and that the self-assembled BT aggregate morphology affected the

dielectric properties [31]. In fact, recently, multifractal analysis, which is seen as an extension of fractal analysis, has been widely used in the medical field.[21] Here, Pérez et al.[32] reported the dispersion of $CaCO_3$ particles in polypropylene (PP) and the fracture morphology of tensile samples using the box-counting method and multifractal analysis (multifractal spectrum (α,$f(\alpha)$). Here, the authors suggested that multifractal theory can be applied to elucidate the relationship between the structure and the mechanical behavior of PP–$CaCO_3$ composite materials [32]. Meanwhile, the report previously estimated the multifractal dimensions of the β-Si_3N_4 (SN) secondary particle network, Dq (q = 0, 1, 2), to investigate the relationship between the thermal conductivity and the connectivity of SN secondary particles in the SN / SUS316L composites related to the propagation path of heat conduction, while it also highlighted the usefulness of the analysis of the multifractal dimensions of material textures in the solid-state reaction [33]. This report also outlined how the capacity dimension D_0 is related to the morphology of β-Si_3N_4 agglomerates, how the information dimension D_1 for these samples was related to the entropy of configuration affected by the dispersion of the β-Si_3N_4 particles, and how the correlation dimension D_2 reflected the connectivity (or dispersibility) among the particles [33].

As shown in Fig. 2-34, it is considered that the viscosity affects the kneading and diffusion process and is able to control the self-assembly material texture. In this study, the multifractal dimensions and the ε' of the self-assembled BT / PVDF composites depending on the material texture are investigated, with a specific focus on the viscosity of the dispersant which was related to the diffusion process of the self-assembly process (see Fig. 2-34). The multifractal analysis was adopted for the evaluation of the morphology, entropy of configuration, and dispersibility of the self-assembled BT

secondary particle groups in BT / PVDF composites.

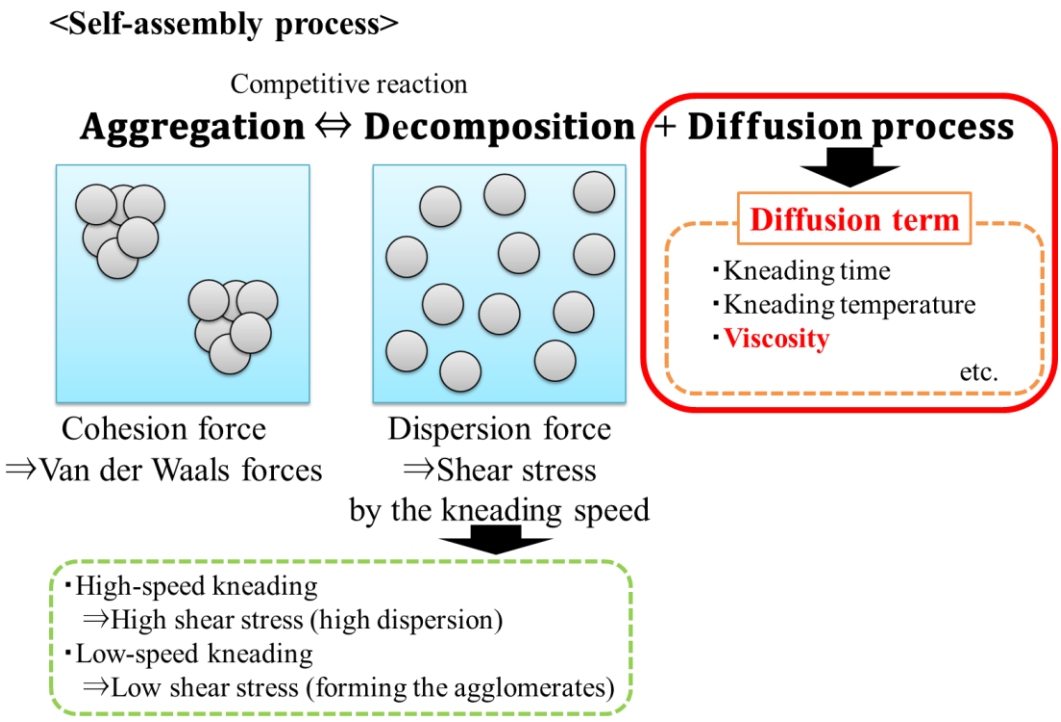

Fig. 2-34 Focused points of the self-assembly process in Session 2.4.

2.4.2. Experimental procedures

2.4.2.1 Sample preparation

The BT powder (Fuji Titanium Industry Co., Ltd., Japan, HPBT-1) used as the starting material had a particle diameter of approximately 0.58–0.75 μm (D50). BT/PVDF composites were generated from the BT powder and PVDF powder (Arkema S.A., KYNAR®711), with the PVDF melted at a temperature of 483 K and the BT powder subsequently added to the PVDF to form a mixture. The volume fractions of the BT were 0%, 5%, 10%, and 20%. The BT/PVDF composites were mixed under 10 rpm

for 30 min, with each sample cooled in air following mixing. To generate BT/PVDF composites with dispersion, both BT powder and polyethylene glycol (FUJIFILM Wako Pure Chemical Corporation, Japan, PEG [PEG1000, average molecular weight = 900–1,100, viscosity = 15–35 mPa・s at 25°C]) were mixed and kneaded under the same conditions as described above. The dispersant was decided by a preliminary experiment. The amount of additive PEG in the mixture was approximately 4wt% of the BT powder. To investigate the effect of the viscosity of the dispersion on the self-assembly process, the BT/PVDF composites were manufactured under the same conditions as PVDF (KYNAR®711) and PEG (1: PEG2000, FUJIFILM Wako Pure Chemical Corporation, Japan, average molecular weight = 1,800–2,200, viscosity = 35–60 mPa・s [at 25°C], and 2: PEG20000, Showa Chemical Co., Ltd., Japan, average molecular weight = 20,000, 10,000–15,000 cst [at 99°C]). The viscosity of the PEG20000 was estimated using the PEG density:

$$\mu = (\nu\rho)/10^{-3} \ / \ \mathrm{mPa \cdot s} \tag{2-14}$$

where μ is the viscosity of PEG20000/mPa・s, ν is the kinematic viscosity (10,000–15,000 cst), and ρ is the density of PEG (1.12).

2.4.2.2 Measurement method

The ε' and the loss tangent (tanδ) of the BT/PVDF composite at a frequency range of 100–110 MHz were measured at 298 K using an Agilent 4294A precision impedance analyzer with lead wires made of platinum. Each sample presented a rectangle with a surface area of 70 mm^2 and a thickness of 0.3 mm. The electrodes were gold with

square faces.

The cross-sections of the samples were analyzed using a scanning electron microscope (SEM, Hitachi High-Tech Co., Japan TM3000) and a field emission scanning electron microscope (FE-SEM, Hitachi Co., Japan: S-4100 and SU-8230, JEOL Ltd.: JSM-7001F) . The SEM images were converted to binary images to estimate the *S* of the BT particles for each sample.

2.4.2.3 Multifractal analysis

The morphology and dispersion state of self-assembled BT/PVDF composites were characterized using multifractal analysis, which was performed using the binary images described in 2.4.2.2. This analysis was used to estimate the probability ($p_i[r]$) of an image by covering it with boxes of size r and counting the number of boxes. The partition function is as follows:

$$P_r^q = \sum_{i=1}^{N(r)} [p_i(r)]^q \tag{2-15}$$

where q is the order moment ($-\infty<q<\infty$). The generalized dimensions of the q of a distribution, Dq, can be defined as follows:

$$D_q = \frac{1}{q\text{-}1} \lim_{r \to 0} \frac{\log P_r^q}{\log r} = \frac{1}{q\text{-}1} \lim_{r \to 0} \frac{\log N(q,r)}{\log r} \tag{2-16}$$

When q takes the values of 0, 1, or 2, Eq. 2-16 is reduced to the following:[34]

$$D_0 = -\lim_{r \to 0} \frac{\log N(r)}{\log r} \tag{2-17}$$

$$D_1 = \lim_{r \to 0} \frac{\sum_{i=1}^{N(r)} \mu_i(r) log(\mu_i(r))}{log(r)} \tag{2-18}$$

$$D_2 = \lim_{r \to 0} \frac{log(C(r))}{log(r)} \tag{2-19}$$

where D_0 is the capacity dimension, $C(r)$ is the correlation function, and D_1 and D_2 are the entropy dimension and the correlation dimension, respectively. The relationship

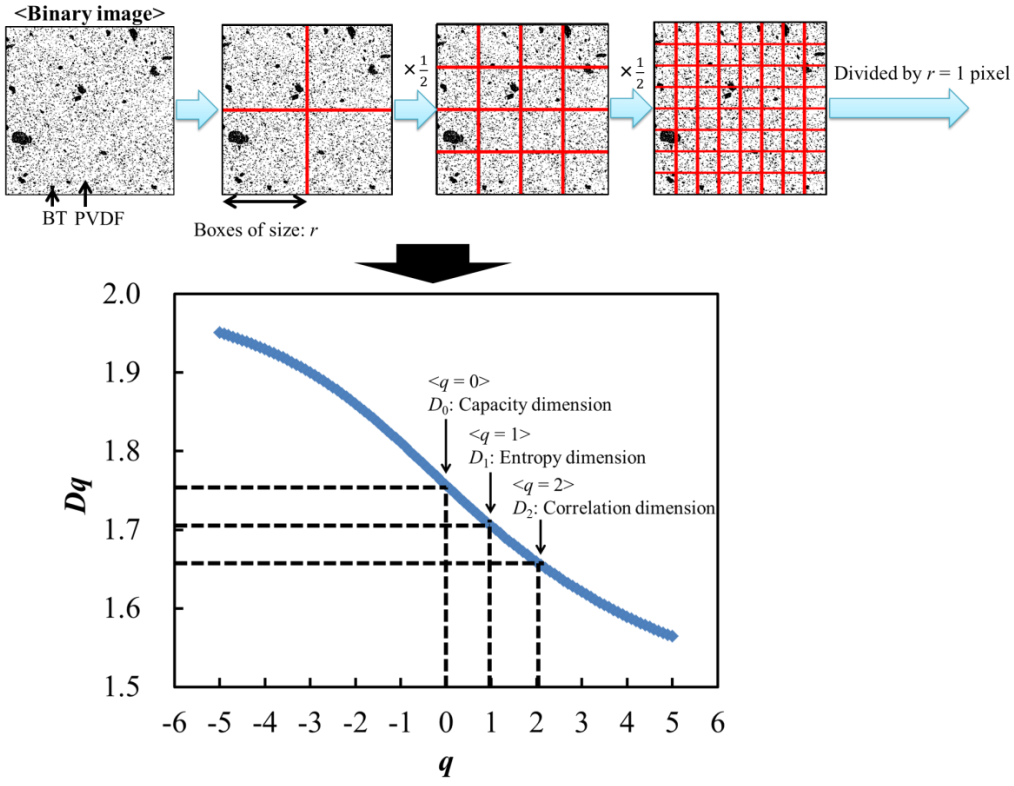

Fig. 2-35 The method of the multifractal analysis.

between D_0, D_1, and D_2 is as follows:

$$D_2 \leq D_1 \leq D_0 \tag{2-20}$$

In this paper, D_0, D_1, and D_2 were estimated to evaluate the morphology (D_0), entropy of configuration (D_1), and dispersibility (D_2) of the self-assembled BT secondary particle groups in the BT / PVDF composite. Fig. 2-35 shows the method of the multifractal analysis.

2.4.3 Results

Fig.2-36 to Fig. 2-38 presents the SEM micrograph and binary images of the BT/PVDF composites without the dispersant under low-speed kneading. In Fig. 2-36 to Fig. 2-38, the black part of the binary images shows the BT particle group, while the white part shows PVDF. As Fig.2-36 shows, the formation of self-assembled BT secondary particle groups was promoted with the addition of BT particles, while as Fig.2-37 shows, the formation of self-assembled BT secondary particle groups was promoted with an increase in PEG viscosity. Meanwhile, as Fig.2-38g and Fig.2-38h show, the formation of self-assembled BT secondary particle groups of the BT / PVDF composites with PEG1000 was promoted with the addition of BT particles with a BT volume fraction of 5 vol.% and 20 vol.%. However, the formation of self-assembled BT secondary particle groups was not promoted from 10vol.% to 20vol.%. Comparing the 10vol.% BT particles, it was confirmed that self-assembled BT secondary particle groups were larger in the order of (1) the sample with additives of PEG20000, (2) the sample with additives of PEG2000, (3) the sample with additives of PEG1000, and (4)

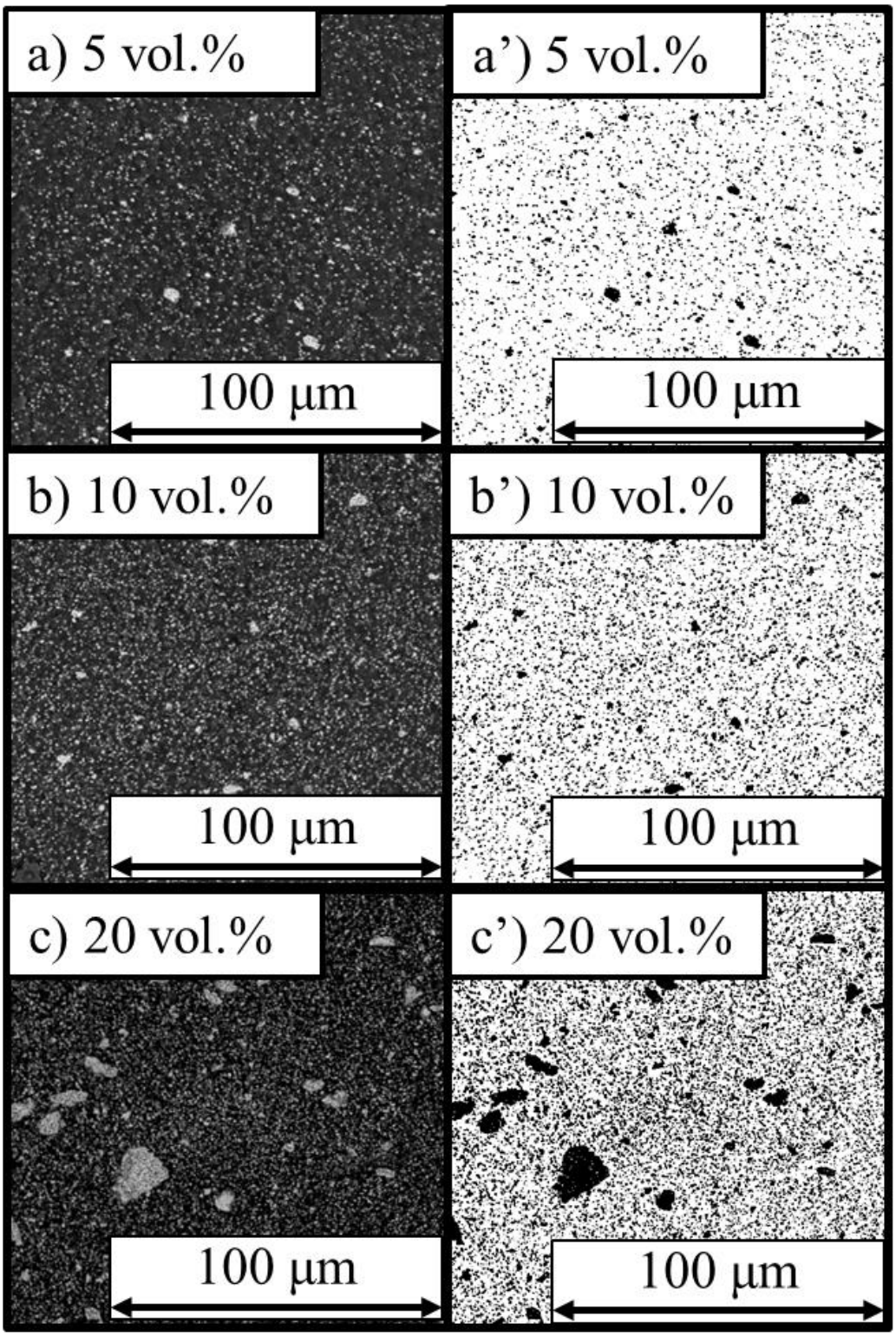

Fig. 2-36 Cross-sectional SEM images of self-assembled BT/PVDF composites under the low-speed kneading condition without the dispersant.

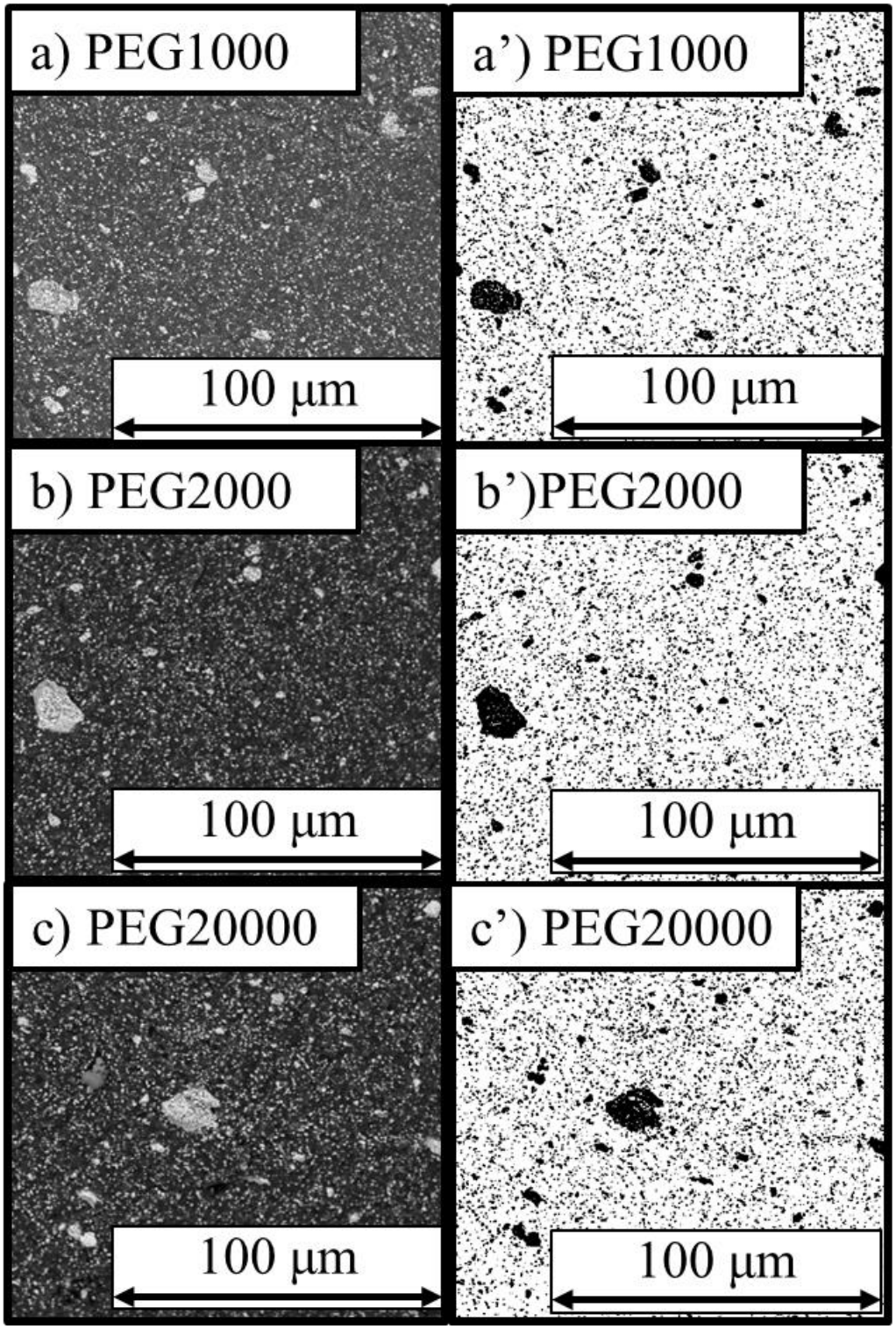

Fig. 2-37 Cross-sectional SEM images of self-assembled BT/PVDF composites under the low-speed kneading condition PEG1000, PEG2000, and PEG20000.

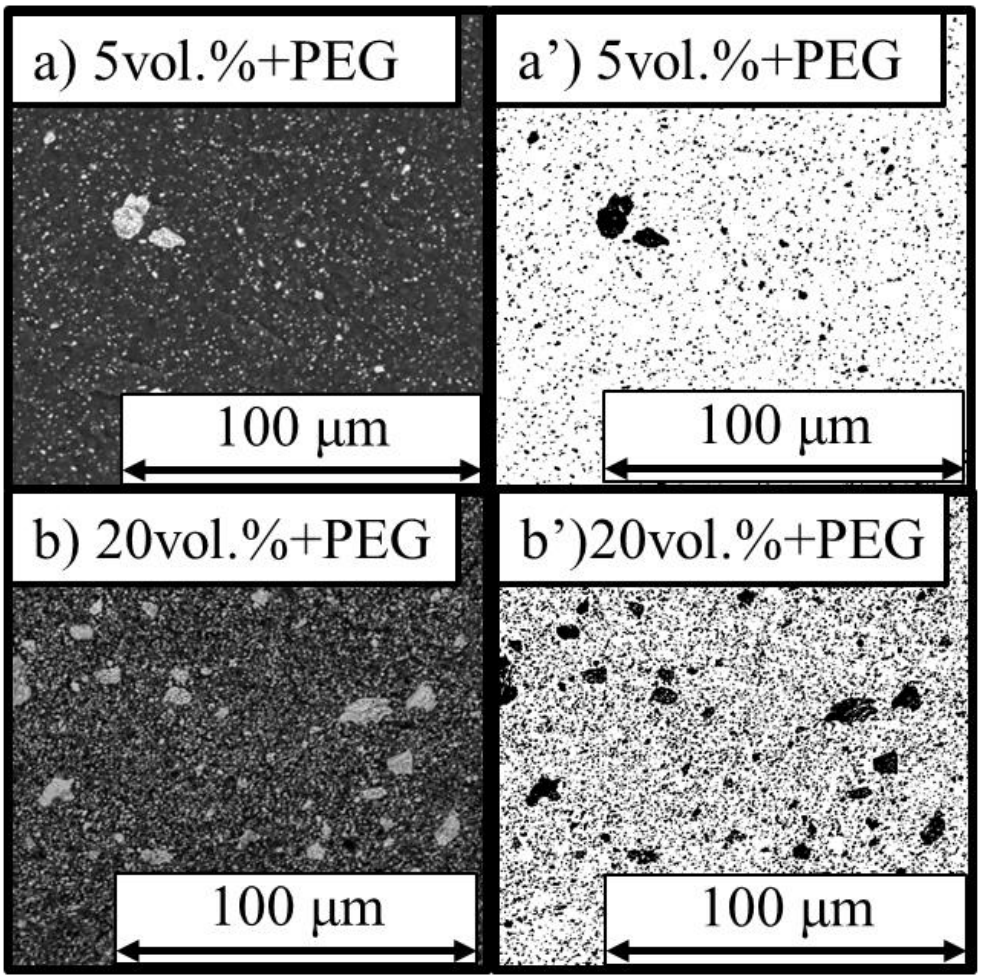

Fig. 2-38 Cross-sectional SEM images of self-assembled BT/PVDF composites with 5 and 20 vol.% under the low-speed kneading condition with PEG1000.

the sample without the dispersant. It was also found that the formation of self-assembled BT secondary particle groups was affected by viscosity due to the diffusion process of the self-assembly process.

Fig.2-39 shows the ε' in relation to the frequency dependence with the addition of BT powder. The ε' of the samples with and without PEG1000 with 20vol.% BT was the highest at all frequencies. Xia et al.[35] proposed the dielectric response of three PVDF phases of α, β, and γ as a function of frequency. Here, the authors reported that the dielectric loss ($\tan\delta$) of α-PVDF and γ-PVDF increased clearly at above 1 MHz due to

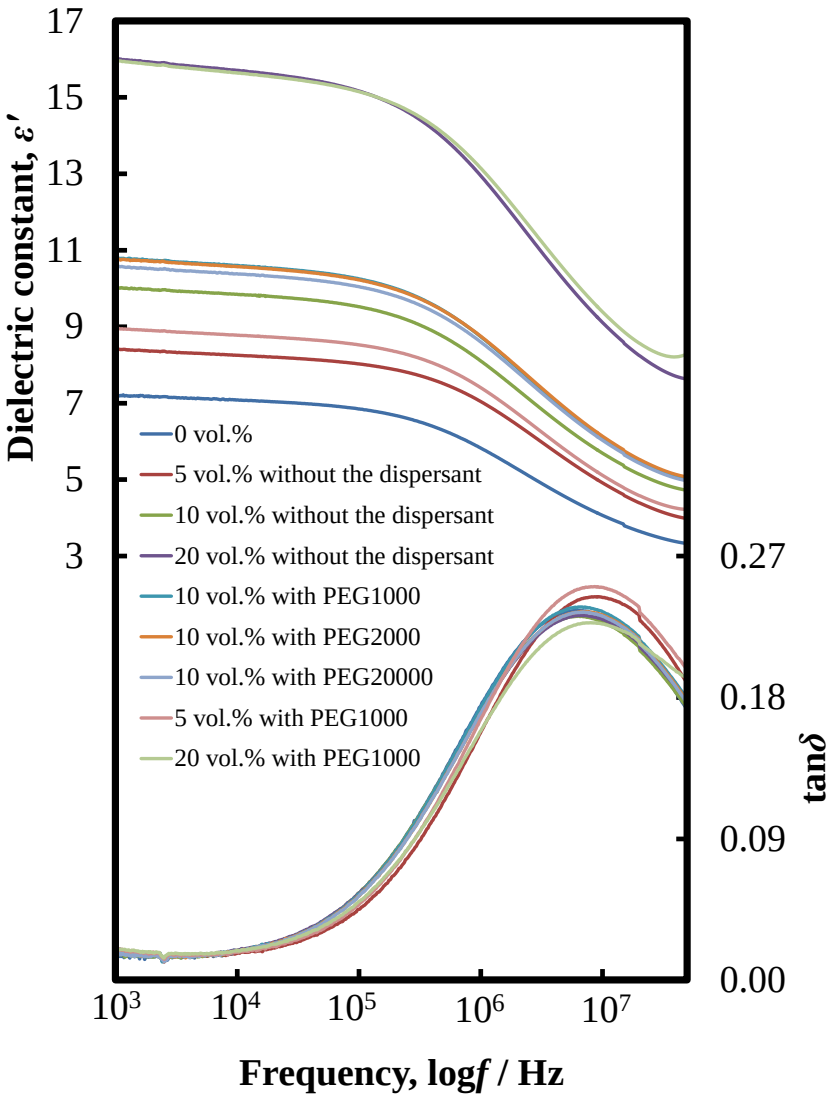

Fig. 2-39 Plots of ε' and tanδ of BT/PVDF composites with and without PEG1000, PEG2000, and PEG 20000 in relation to the frequency.

the dielectric relaxation [35]. As shown in Fig.2-39, the maximum value of tanδ was confirmed at 4 MHz, while it subsequently decreased at values above 4 MHz. Here, it is suggested that β-PVDF was partially formed by adding BT powder.

Fig. 2-40 presents the results of the volume fraction of BT and the ε' at 1 kHz. To evaluate the effects of the filler, the Bruggeman model [36] was used with the composite materials as shown in Fig. 2-40. The model can be described as follows:[28]

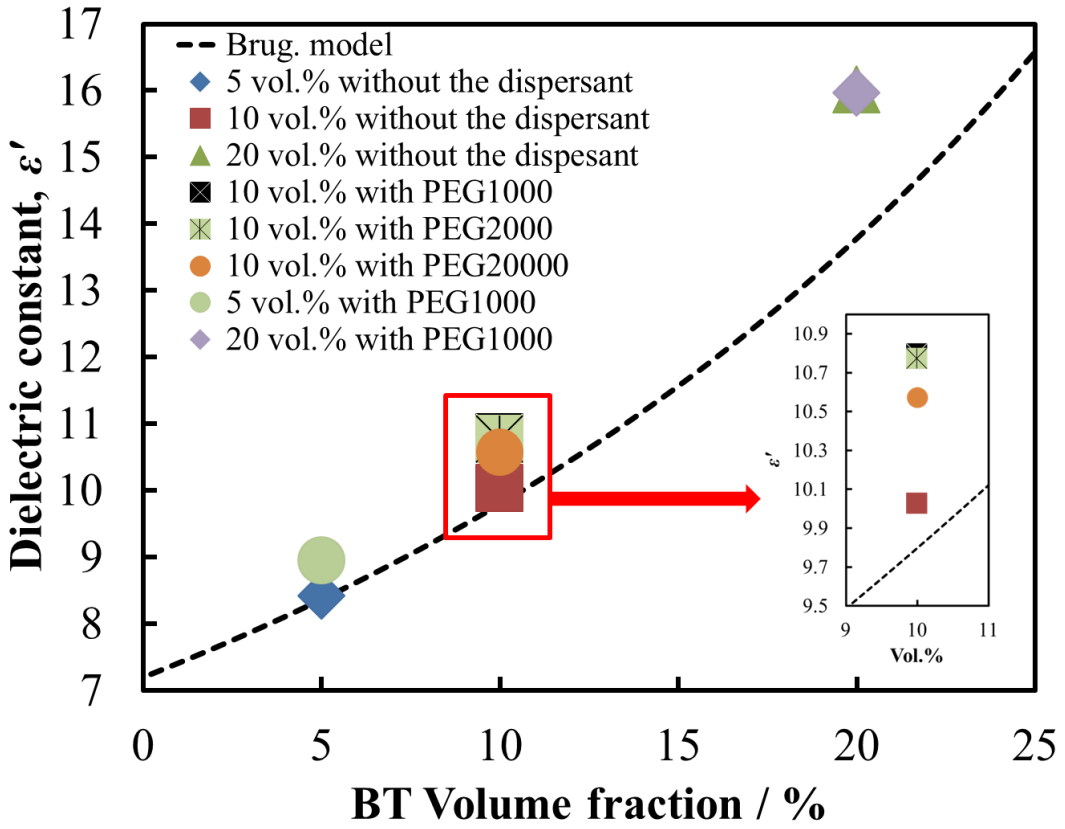

Fig. 2-40 ε' of BT/PVDF composites at 1 kHz in relation to the volume fraction of BT powders.

$$1 - V = \frac{\varepsilon'_{composite} - \varepsilon'_{filler}}{\varepsilon'_{matrix} - \varepsilon'_{filler}} \left(\frac{\varepsilon'_{matrix}}{\varepsilon'_{composite}} \right)^{1/3} \quad (2\text{-}21)$$

where V is the volume fraction of BT, $\varepsilon'_{\text{matrix}}$ is the ε' of PVDF (ε'_{matrix} = 7.2 [0 vol.%]), ε'_{filler} is the ε' of BT (ε'_{filler} = 1,000), and $\varepsilon'_{composite}$ is the ε' of the BT / PVDF composite. The relationship between the viscosity of the dispersant and the ε' was then examined. In the 10vol.% BT particles, the ε' of the BT / PVDF without PEG was slightly higher than that of the Bruggeman model, while the ε' of the BT / PVDF composites with PEG was higher than that of the Bruggeman model. Comparing the ε' of the samples of 10vol.% BT particles with and without PEG, it was confirmed that the ε' were in the

order of (1) the sample with PEG1000, (2) the sample with PEG2000, (3) the sample with PEG20000, and (4) the sample without PEG. The dielectric constant of the BT / PVDF composite with PEG1000 was 1.08 times higher than that of the sample without PEG. In this paper, samples of 5vol.% and 20vol.% were prepared with PEG1000 since the ε' of the sample with PEG1000 was the highest among the samples with the dispersant. In the sample without PEG1000, the ε' of the 10vol.% and 20vol.% samples were higher than that of the Bruggeman model. By adding 20 vol.% of BT filler to PVDF, the dielectric constant of the sample with PEG1000 of 20 vol.% could be improved 2.22 times compared to the sample with 0 vol.%. However, the ε' of the 5vol.% sample was the same as that of the Bruggeman model. This could have been due to the coarse (agglomeration) particle samples that can be explained in terms of the number of particles along the agglomerated low-impedance path [15].

The morphology, entropy of configuration, and dispersibility of the self-assembled BT secondary particle groups in the BT/PVDF composites were investigated using D_0, D_1, and D_2 estimated with the multifractal analysis. Fig. 2-41 shows the results for the generalization dimension of all samples, with D_0, D_1, and D_2 determined based on these results. Generally, the relationship between D_0, D_1, and D_2 is reported to be $D_2 \leq D_1 \leq D_0$ [34]. However, the equality $D_0 = D_1 = D_2$ occurs only if the fractal is statistically or exactly self-similar and homogeneous [34]. The data related to the S, the average ε', and D_0, D_1, and D_2 are shown in Table 2-3.

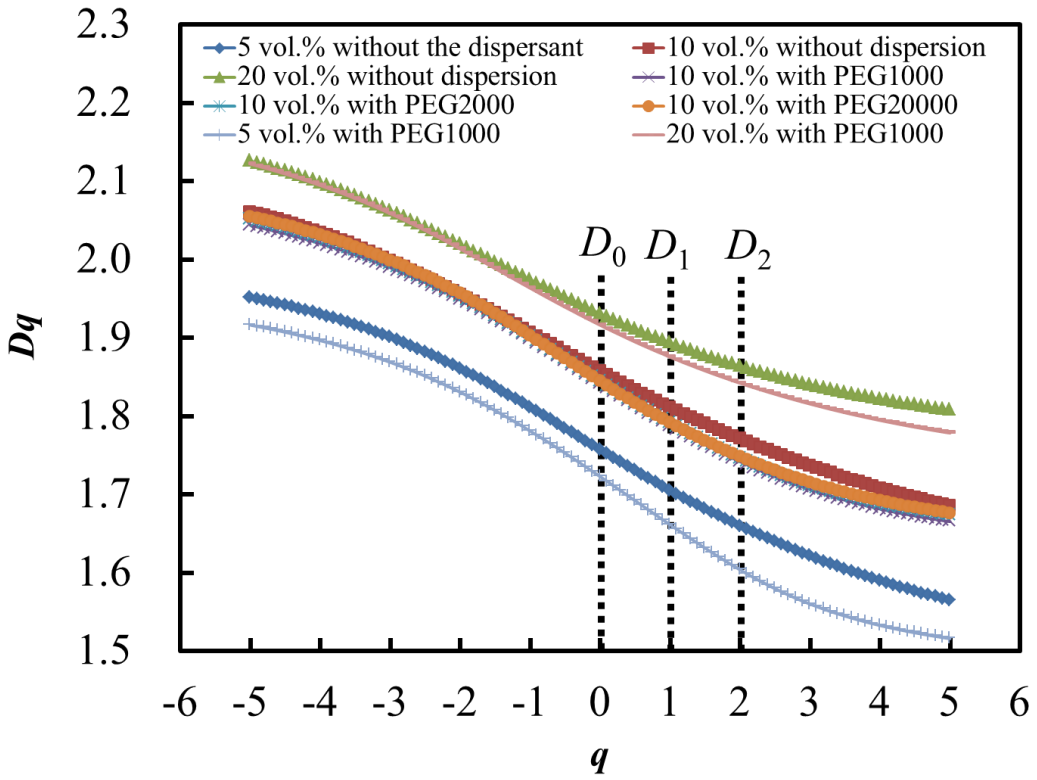

Fig. 2-41 Multifractal spectra curves ($D[q]$-q) for BT/PVDF composites with and without PEG1000, PEG2000, and PEG20000.

Table 2-3 Characteristics of BT/PVDF composites

BT Volume fraction / %		Capacity dimension (D_0)	Entropy dimension (D_1)	Correlation dimension (D_2)	Dielectric constant (ε')	Average secondly particle area of BT particles (S) /μm^2
5	Without PEG1000	1.75(0)	1.69(5)	1.64(5)	8.42	0.98
	With PEG1000	1.72(5)	1.66(6)	1.61(1)	8.95	0.98
10	Without PEG1000	1.85(7)	1.81(1)	1.77(1)	10.03	1.10
	With PEG1000	1.84(3)	1.78(9)	1.74(4)	10.80	1.29
	With PEG2000	1.84(2)	1.79(0)	1.74(6)	10.77	1.36
	With PEG20000	1.83(4)	1.78(2)	1.73(9)	10.57	1.47
20	Without PEG1000	1.93(3)	1.89(9)	1.87(1)	16.01	1.38
	With PEG1000	1.92(0)	1.88(1)	1.84(9)	15.96	1.42

The third decimal place in parenthesis contains an error.

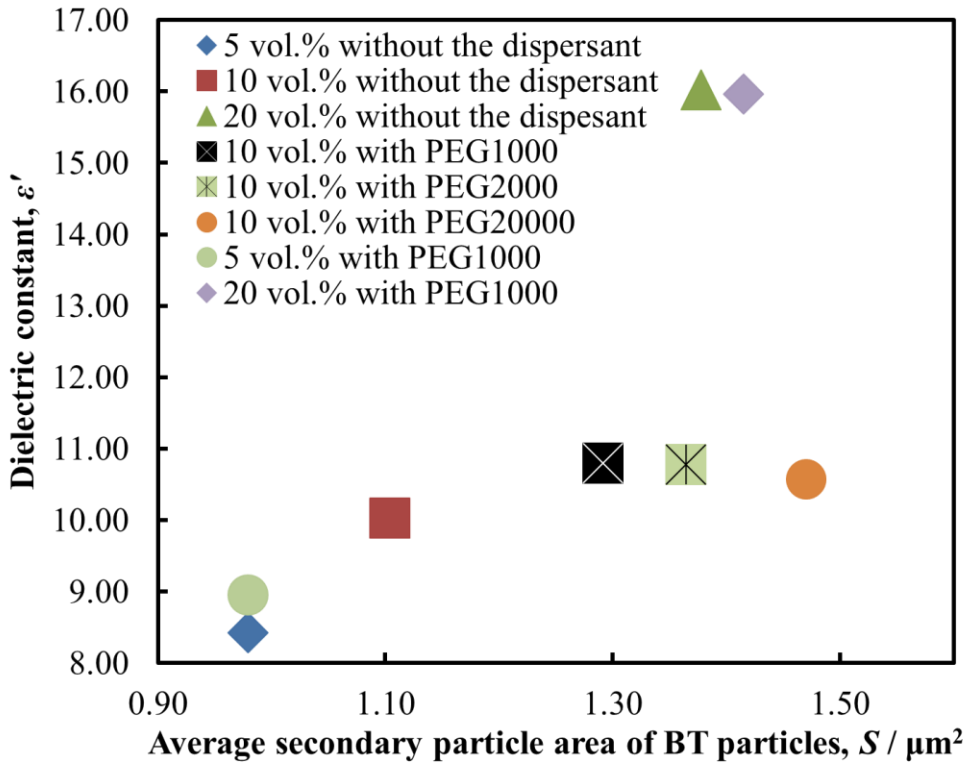

Fig. 2-42 Relationship between ε' and S of BT particles of BT/PVDF composites.

2.4.4 Discussion

Fig. 2-42 shows the results for the S and ε'. It has previously been reported that the ε' of self-assembled BT/PLLA composites increases with an increase in the S of BT particles when BT aggregates are formed via the self-assembling process in BT/PLLA composites [18]. Robertson and Varlow [15] suggested that a low-impedance path forms BT agglomerations, improving the ε'. From the results shown in Fig. 2-42, it is clear that the ε' of the sample with and without PEG1000 increased with the formation of a self-assembled BT secondary particle group. Meanwhile, comparing the 10vol.% BT samples, the S of the BT particles of the samples increased with an increase in PEG

viscosity, while the ε's of the samples with PEG1000 and PEG2000 were close to equal. However, the ε' was decreased by increasing PEG viscosity. The amount of change in the dielectric constant of the sample with PEG1000 depending on the average secondary particle area of BT filler was 1.06 times higher than that of the sample with PEG2000 and 1.16 times higher than that of the sample with PEG20000. This means the ε' was affected by the viscosity of the dispersant. On comparing the volume fractions of BT powder in the samples with and without PEG1000, the *S* of BT particles of the 10vol.% and 20vol.% BT samples were found to be the same, while the number of self-assembled BT secondary particle groups was increased by adding BT powder.

Fig. 2-43 presents the results for PEG viscosity and *S* of the BT particles of the BT / PVDF composites with 10vol.% BT powder. In the sample without PEG1000, the viscosity of the dispersant was set to 0. The formation of BT secondary particle groups was promoted with an increase in PEG viscosity, as shown in Fig. 2-43. Comparing the average secondary particle area of the sample with PEG1000 and PEG20000, the *S* of the sample with PEG20000 was 1.14 times larger than that of the sample with PEG1000. The self-organization processes in a non-equilibrium chemical system have been studied in a solution system described by the Belousov–Zhabotinsky reaction [30]. The self-organization process is observed in the reaction–diffusion system, which is assumed to occur due to a competitive reaction between an inhibitor and a promoter within the diffusion process. The reaction can be described by the following equation:

$$\partial v/\partial t = u - v + D_v \nabla^2 v \qquad (2\text{-}22)$$

where *u* is the active term, *v* is the inhibitive term, and *Dv* is the diffusion coefficient.

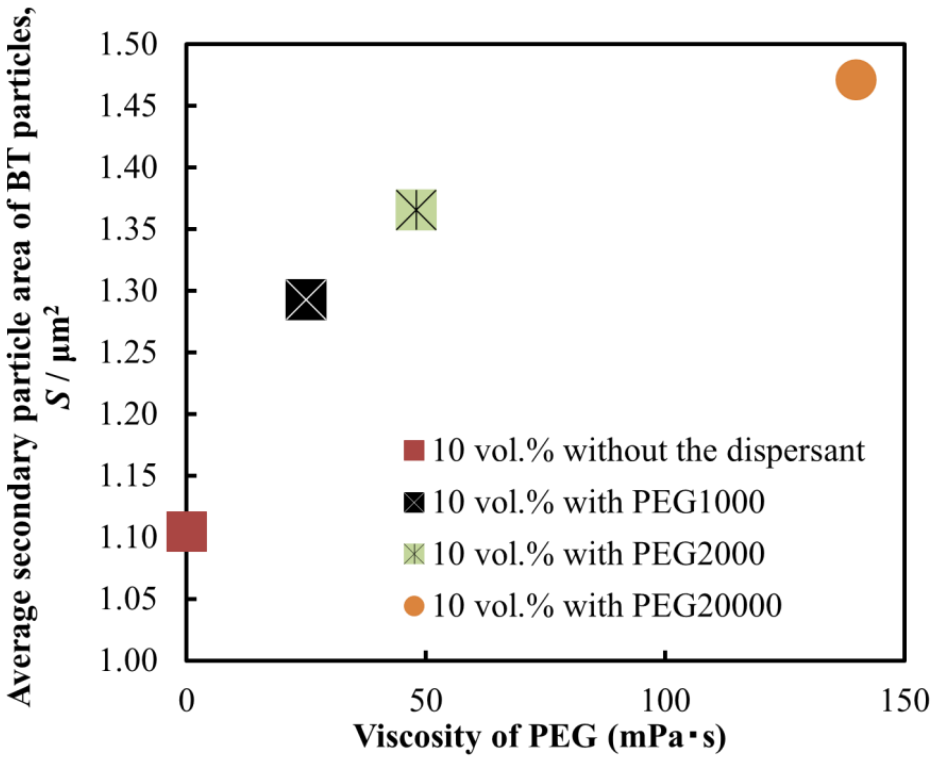

Fig. 2-43 *S* of BT particles of BT / PVDF composites in relation to the PEG viscosity.

Eq. 2-19[37], [38] presents the self-assembly process of a solid based on Eq. 2-19:

$$\text{Aggregation} \Leftrightarrow \text{Decomposition} + \text{Diffusion process} \tag{2-23}$$

This reaction corresponds to a process of aggregation and decomposition, where the van der Waals force acts as a cohesion force, and the shear stress induced by the stirring speed acts in terms of decomposition. The kneading process can indicate the diffusion process in the reaction–diffusion system. Generally, when particles are mixed in a viscous liquid, the diffusivity of the particles is affected by the viscosity of the liquid. As such, it is suggested that the formation of self-assembled BT secondary particle groups was promoted with the increase in PEG viscosity.

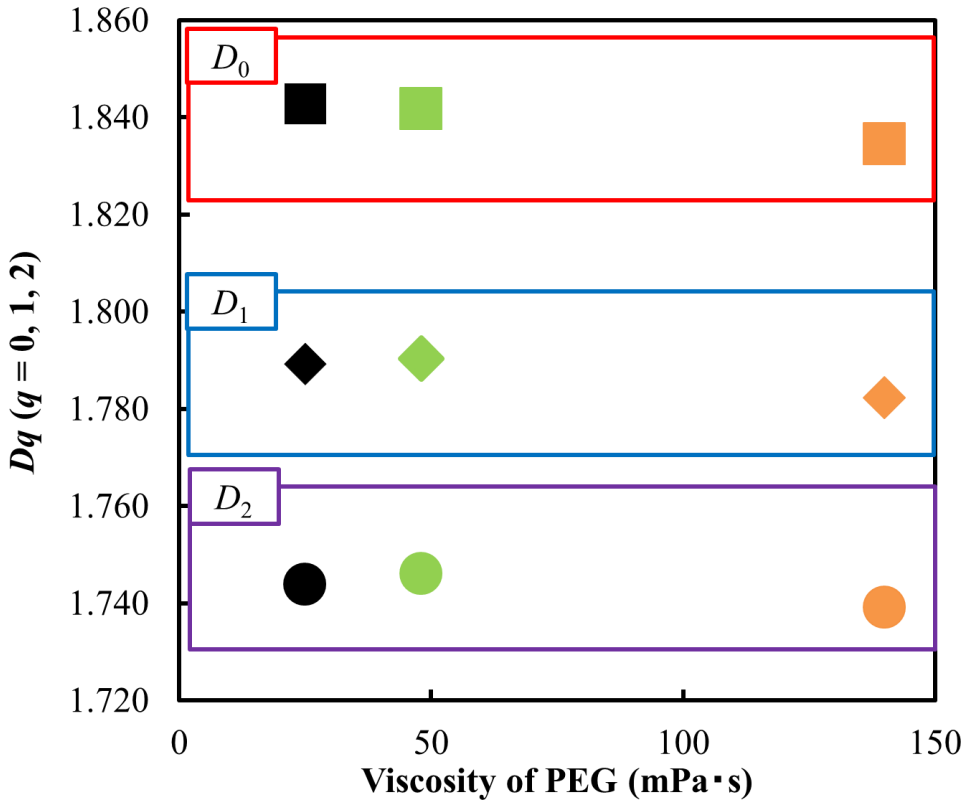

Fig. 2-44 *Dq* of BT/PVDF composites in relation to the PEG viscosity.

To investigate the formation of the self-assembled BT secondary particle groups in relation to the viscosity of the dispersant, the morphology, entropy of configuration, and dispersibility of the self-assembled BT secondary particle groups were characterized via multifractal analysis. In a previous report, D_0 was found to be related to the morphology of ceramics agglomerates, D_1 to the entropy of configuration affected by the dispersion of ceramic particles, and D_2 to the dispersibility (or connectivity) among the particles [33]. Fig. 2-44 shows the D_0, D_1, and D_2 in relation to PEG viscosity. Here, the D_0, D_1, and D_2 of the samples with PEG1000 and PEG2000 were almost the same, while those of the sample with PEG20000 were very close to those of the PEG1000 and PEG2000 samples; however, the D_0, D_1, and D_2 of the sample with PEG20000 were slightly lower than those of the samples with PEG1000 and PEG2000. As such, it is suggested that the

viscosity of the dispersant affected the formation of the secondary particle group.

To investigate the formation of self-assembled BT aggregates with the BT/PVDF/BT heterointerface resulting from the change in the viscosity of the dispersant, FE-SEM was performed for samples with and without PEG1000, PEG2000, and PEG20000 with 10vol.% BT, with the resulting images shown in Fig. 2-45. Fig. 2-45a and Fig. 2-45a' show the sample without PEG, while Fig. 2-45b and b', Fig. 2-45c and c', and Fig. 2-45d and d' present the samples with PEG1000, PEG2000, and PEG20000, respectively. The BT powder is indicated by the blue arrow and the PVDF by the red arrow. In the sample without PEG (Fig. 2-45a and a'), it was confirmed that the self-assembled BT aggregates had a BT/PVDF/BT heterointerface. However, the formation of voids between the BT and PVDF was confirmed. In the sample with PEG1000 (Fig. 2-45b and b'), it was confirmed that the BT particles and the PVDF were aggregated in the secondary particle groups. Furthermore, the self-assembled BT aggregates with a BT / PVDF / BT heterointerface were predominantly formed in the secondary particle groups. In the sample with PEG2000 (Fig. 2-45c and c'), the formation of self-assembled BT aggregates with a BT / PVDF / BT heterointerface was confirmed. However, here, a BT/BT interface was also formed. Finally, in the sample with PEG20000 (Fig. 2-45d and d'), the formation of self-assembled BT aggregates with a BT/PVDF/BT heterointerface was confirmed. However, here, the BT/BT interface was dominantly formed. Therefore, it is suggested that the PEG viscosity affected the formation of the BT/PVDF/BT heterointerface. As such, the sample with PEG1000 had BT aggregates, the sample with PEG20000 had BT agglomerates, and the sample with PEG2000 had a mixture of BT aggregates and agglomerates. In session 2.3, it was suggested that the electric dipole of a BT/polymer/BT heterointerface can be induced by improving the ε'

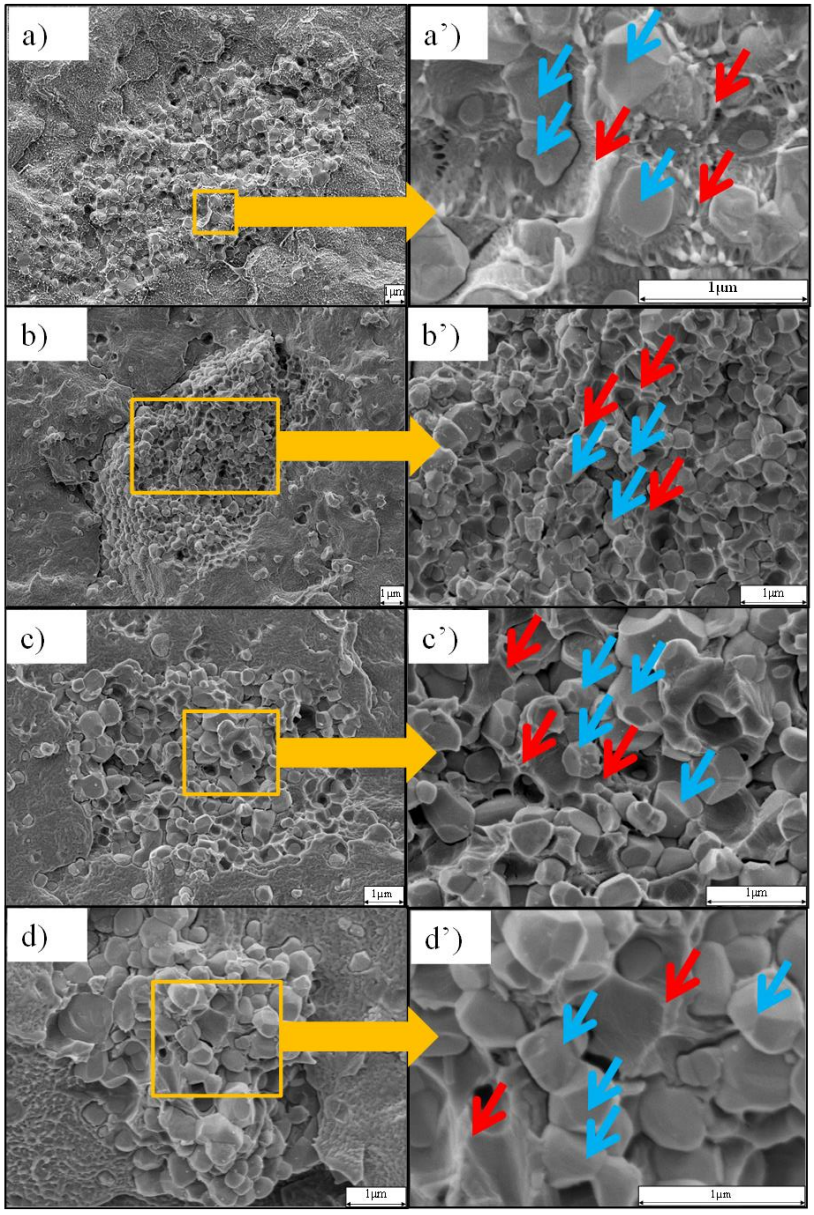

Fig. 2-45 Cross-sectional FE-SEM images and magnified images of BT/PVDF with and without PEG1000, PEG2000, and PEG20000, with 10%vol. fraction of BT.

[37]. In fact, when BT granules with a BT/BT interface were added, the S was found to be large, while the change in the ε' was found to be saturated [37]. In our results for the S and ε' of the samples with PEG2000 and PEG20000 (Fig. 2-42), it was clear that the S increased with the increase in PEG viscosity. However, the ε' decreased, which was likely due to the formation of the BT/BT interface (Fig. 2-45). As such, it is suggested that the viscosity of the dispersant affected the formation of the BT/PVDF/BT heterointerface and that the heterointerface plays an important role in improving the ε'. As Fig. 2-44 and Fig. 2-45 show, the self-assembled BT agglomerates with PEG20000 had a predominant BT/BT interface, while the D_1 and D_2 of the sample were lower than those of the PEG1000 and PEG2000 samples. It is thus suggested that the viscosity of the dispersant affected the self-assembling process and that the multifractal dimension was affected by the viscosity.

To investigate the effect of the BT fillers, the D_0, D_1, and D_2 of the samples with and without PEG1000 were examined, with the results shown in Fig. 2-46. Here, the D_0 of the samples increased with the addition of BT powder. Therefore, it is suggested that the morphology of the self-assembled BT aggregates with and without PEG1000 depended on the volume fraction of the BT powder. On comparing the samples with and without PEG1000, it was confirmed that the D_0 of the samples without PEG1000 was higher than that of the sample with PEG1000. This was likely because the morphology of the self-assembled BT aggregate with the dispersant was more anisotropic than the samples without the dispersant. As Fig. 2-46 shows, the D_1 of the samples with and without PEG1000 was increased by adding the BT powders. On comparing the samples with and without PEG1000, it was confirmed that the D_1 of the samples with PEG1000 was lower than that of the samples without PEG1000, with the configuration entropy likely

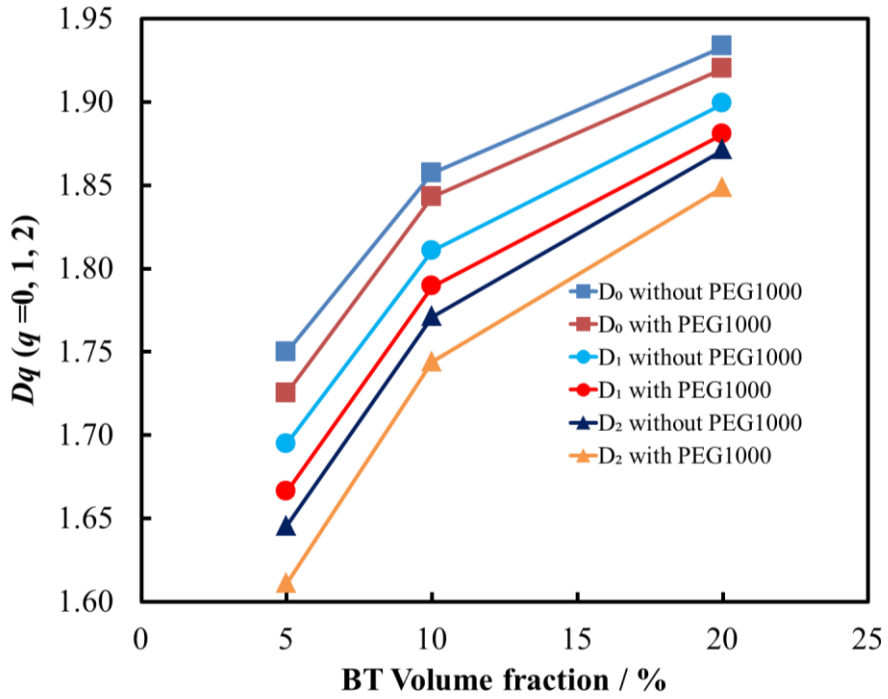

Fig. 2-46 Dq (q = 0, 1, and 2) of BT/PVDF composites in relation to the volume fraction of BT powders.

decreased with the addition of the PEG1000. That is, the formation of BT aggregates was promoted by adding PEG1000. Meanwhile, the D_2 was estimated to investigate the dispersibility of the BT aggregates. The D_2 of the samples with and without PEG1000 was increased by increasing the volume fraction of the BT particles. On comparing the sample with and without PEG1000, it was confirmed that the D_2 of the samples with PEG1000 was lower than that of the samples without PEG1000. As such, it is suggested that the bias was reduced. As Fig. 2-46 shows, the D_1 and D_2 decreased with the addition of PEG1000. This indicated that the distribution was biased by adding the PEG1000 and that the formation of self-assembled BT aggregates was promoted. The D_0, D_1, and D_2 of the samples with PEG1000 approached those of the samples without

PEG1000 with the addition of BT powder. Here, it is suggested that the morphology and distribution of BT aggregates with and without PEG1000 were approached with the addition of the BT powder. Therefore, the ε' and the *S* of the self-assembled BT aggregates of the samples with and without PEG1000 of 20vol% BT were almost the same.

2.4.5 Conclusions

To investigate the formation of BT aggregates in relation to the viscosity of the dispersant, samples without the dispersant, samples with PEG1000, samples with PEG2000, and samples with PEG20000 of 5vol.%–20 vol.% BT were prepared. The conclusions are as follows:

(1) The ε' of the BT / PVDF composites with self-assembled BT secondary particle groups was higher than that of the Bruggeman model. The ε' increased with an increase in the *S* of the BT particles. The *S* of the BT particles increased in accordance with the increase in PEG viscosity. However, the change in ε' was decreased. The amount of change in the ε' of the sample with PEG1000 depending on the *S* was 1.16 times higher than that of the sample with PEG20000.

(2) On comparing the *S* of the BT particles with PEG1000, PEG2000, and PEG20000, the formation of self-assembled BT secondary particle groups was found to have been promoted with the increase in PEG viscosity. The *S* of the sample with PEG20000 was 1.14 times larger than that of the sample with PEG1000. Here, it can be concluded that the viscosity of the dispersant affected the self-assembly process.

(3) On comparing the results of the multifractal analysis for the samples with PEG1000, PEG2000, and PEG20000, the D_0, D_1, and D_2 of the sample with PEG20000 were found to be slightly lower than those of the samples with PEG1000 and PEG2000. Here, it can be concluded that the viscosity of the dispersant affected the self-assembling process and the multifractal dimension was affected by the viscosity.

(4) The FE-SEM results for the samples with PEG1000, PEG2000, and PEG20000 indicated that the formation of a BT / PVDF / BT heterointerface was promoted with the addition of the lowest PEG viscosity. That is, the formation of self-assembled BT aggregates was dependent on the viscosity of the dispersant.

(5) On comparing the samples with and without PEG1000, the morphology and distribution of self-assembled BT aggregates were found to be different. That is, it was indicated that the distribution was biased by adding PEG1000, while the formation of self-assembled BT aggregates was promoted.

Hence, BT aggregates were formed in the sample with PEG1000, BT agglomerates were formed in the sample with PEG20000, and both aggregates and agglomerates were formed in the sample with PEG2000. The viscosity of the dispersant affected the self-assembly process, with the multifractal dimension subsequently reflecting this.

2.5 Conclusions of chapter 2

In this chapter, the problems were presented for the application to a piezoelectric biosensor using a polymer first. The self-assembled material texture (the morphology, entropy of configuration, and dispersibility of the self-assembled BT secondary particle

groups in BT / polymer composites) and dielectric properties of the BT / polymer composite material were investigated from the results. The conclusions are as follows:

In the polymer piezoelectric sensor, β-PVDF was applied to the signal transducer sensor of a polymer piezoelectric biosensor, and the fixation with the host-guest reaction was detected with the relaxation process of the complex permittivity of β-PVDF in 2.1. In Session 2-1, the problems of the polymer piezoelectric biosensor were presented.

(1) It was proposed that the shear vibration was affected by the liquid since the elastic constant of β-PVDF is lower than the quartz of the general material.
(2) It was necessary to improve the sensitivity and responsivity of the sensor for the application.

It is expected that the elastic constant will be improved by adding the ceramic filler. In order to improve the sensitivity, it is necessary to improve the dielectric properties. Therefore, the relationship between self-assembled material texture (the morphology, entropy of configuration, and dispersibility of the self-assembled BT secondary particle groups) and dielectric properties was investigated by adding BT fillers to the polymer in session 2.2, 2.3, and 2.4. The conclusions of this chapter are as follows:

(1) It was suggested that it was possible that the fractal analysis was applied to evaluate the morphology, the entropy of configuration and dispersibility of self-assembled BT secondary particle groups and the formation of BT / polymer / BT heterointerfaces based on the results of the D_0, D_1 and D_2 using the box-counting

method and the multifractal analysis.

(2) According to the results of the dielectric properties and the D_0, D_1, and D_2, it was suggested that the morphology and dispersion states of self-assembled BT secondary particle groups affected the dielectric properties. From the results of the dielectric constant and box-counting method for BT / PLLA composites of 20 vol.% with and without Tegomer® P121, the D_0 was increased by 1.16 times and the ε' was increased by 1.45 times.

(3) From the results of S and ε', it was suggested that the BT / polymer / BT heterointerface is an important role in improving the dielectric properties since it was considered that the electric dipole of a BT / polymer / BT heterointerface induced to improve the dielectric properties. In particular, the amount of change in the ε' of the self-assembled BT / PLLA composites with Tegomper® P121 of 10 vol.% depending on the S was 24.5 times higher than that of the sample with the large granules.

(4) It was suggested that the viscosity and kneading condition affected the self-assembly process involved in the solid. The formation of BT secondary particle groups was promoted under the low-speed kneading condition. The S of the sample with PEG20000 was 1.14 times larger than that of the sample with PEG1000 based on the results of the relationship between the S and the viscosity of PEG.

Hence, it was suggested that the morphology, entropy of configuration, and dispersibility of the self-assembled BT secondary particle groups and the formation of BT / polymer / BT heterointerface in BT aggregates were controlled by using the self-assembly process. Thus, the dielectric constant of the BT/ PVDF could be improved

2.22 times compared to the sample with 0 vol.%

Table 2-4 shows the assumption values of the sensitivity and responsivity of the piezoelectric biosensors with the BT / PVDF composite materials based on the results. The assumption values of the sensitivity and responsivity were determined as follows.

<Sensitivity of the piezoelectric biosensors with BT / PVDF composite materials>

The sensitivity of the sensor detection shows the detectable minimum concentration of the target. The sensitivity depends on the dielectric properties. In this study, the adsorption characteristics of biopolymers are detected by the change in the dielectric constant and the frequency. The sensitivity was determined by the amount of change in the dielectric constant depending on the frequency (see Fig.2-47). For instance, it was assumed that the sensitivity of the BT / PVDF with PEG1000 was higher 1.03 times than the sample with PEG20000. The comparison of the sensitivity in Table 2-4 was decided from the results of the dielectric constant of the BT / PVDF composite materials of 0 vol.% (slope: 0.77)and the sample with PEG1000 of 20 vol.% (slope: 1.62) based on session 2.4.

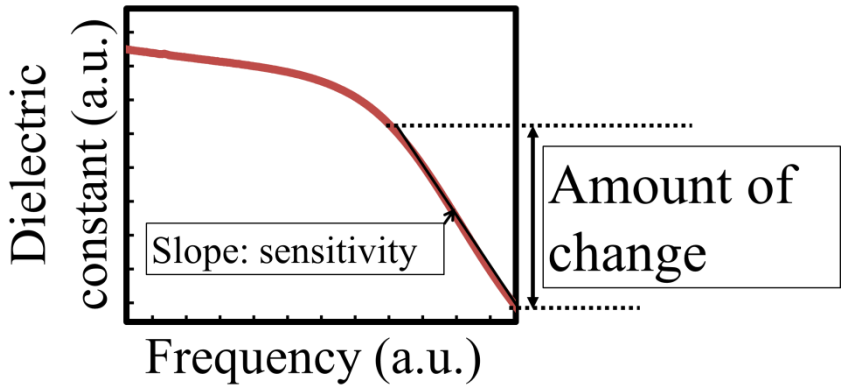

Fig. 2-47 Schematic drawing of the sensitivity of the piezoelectric biosensor with BT / PVDF composite materials.

<Responsivity of the piezoelectric biosensors with BT / PVDF composite materials>

The responsivity of the piezoelectric biosensor was decided from the amount of change in the capacitance of the sensor depending on deposition time in pure water. In this study, the amount of change in the capacitance of the PVDF sensor depending on the deposition time shown in Fig. 2-12 and the amount of change in the capacitance of the prototype biosensor using BT / PVDF composite material of 10 vol.% depending on the deposition time were compared. The deposition time in pure water was between 15 minutes (PVDF sensor: 122.15 pF, the BT / PVDF composite with 10 vol.%: 32.75 pF) and 25 minutes (PVDF sensor: 122.08 pF, the BT / PVDF composite with 10 vol.%: 32.23 pF).

Table 2-4 Comparison of the piezoelectric biosensor of this study and the technologies for TB detection.

	<This study> Combination of Loop-Mediated Isothermal Amplification (LAMP) and piezoelectric biosensors (Polymer)		Combination of LAMP and a piezoelectric biosensor (Quartz)	Polymerase chain reaction (PCR)
	PVDF	Ceramics / polymer composites based on this study		
Sensitivity	5 μg/ml	<Assumption> Approximately 2.4 μm/ml	0.01 μm/ml [6]	1 μg/ml [39]
Response speed	60 minutes	<Assumption> Approximately 8.2 minutes	30 minutes [6]	About 200 minutes
Safety	High (Sensors are able to be incinerated after a diagnosis.)		Low (Sensors are reused.)	Medium (Reaction tubes are disposable.)
Total Cost	Low		High	High

According to Table 2-4, it was expected that the sensitivity could be improved by about 2.1 times and the responsivity by about 7.4 times by applying the BT / PVDF composite materials of this study to the piezoelectric biosensor as compared with the PVDF materials (BT / PVDF of 0 vol.%). From this result, it is expected to be applied the BT / PVDF composite materials to piezoelectric biosensors for TB detection used in developing countries. In order to apply the BT / PVDF composite materials to the piezoelectric biosensor in the future, it is necessary to treat the BT / PVDF composite material with the electrical and mechanical polarization to manufacture the sensor and investigate the relationship between the self-assembled material texture and the dictation characteristics related to the piezoelectricity of the BT / PVDF composites. In addition, it is necessary to investigate the biopolymer fixation control of DNA, RNA, and protein for the bioreceptor.

References

[1] J. Rudeeaneksin *et al.*, "Rapid identification of mycobacterium tuberculosis in BACTEC MGIT960 cultures by in-house loop-medicated isothermal amplification," *Japanese Journal of Infectious Diseases*, vol. 65, no. 4, pp. 306–311, 2012, doi: 10.7883/yoken.65.306.

[2] N. Tomita, Y. Mori, H. Kanda, and T. Notomi, "Loop-mediated isothermal amplification (LAMP) of gene sequences and simple visual detection of products," *Nature Protocols*, vol. 3, no. 5, pp. 877–882, 2008, doi: 10.1038/nprot.2008.57.

[3] B. Phetsuksiri *et al.*, "Loop-mediated isothermal amplification for rapid

identification of mycobacterium tuberculosis in comparison with immunochromatographic sd bioline mpt64 rapid® in a high burden setting," *Japanese Journal of Infectious Diseases*, vol. 72, no. 2, pp. 112–114, 2019, doi: 10.7883/yoken.JJID.2018.128.

[4] Y．Okahata, *バイオセンシングのための水晶発振子マイクロバランス法―原理から応用例まで(Quaetz-crystal microbalance for bio-sensing).* KODANSHA LTD., 2013.

[5] V. M. Mecea, "Is quartz crystal microbalance really a mass sensor?," *Sensors and Actuators, A: Physical*, vol. 128, no. 2, pp. 270–277, 2006, doi: 10.1016/j.sna.2006.01.023.

[6] P. Prakrankamanant *et al.*, "The development of DNA-based quartz crystal microbalance integrated with isothermal DNA amplification system for human papillomavirus type 58 detection," *Biosensors and Bioelectronics*, vol. 40, no. 1, pp. 252–257, 2013, doi: 10.1016/j.bios.2012.07.033.

[7] G. Sauerbrey, "Verwendung von Schwingquarzen zur Wägung dünner Schichten und zur Mikrowägung," *Zeitschrift für Physik*, vol. 155, no. 2, pp. 206–222, 1959, doi: 10.1007/BF01337937.

[8] H. Kodama, T. Osawa, Y. Yasuno, and T. Furukawa, "A series of

electromechanical measurements for determination of piezoelectric, dielectric and elastic tensor components in porous polypropylene electrets," *Proceedings - International Symposium on Electrets*, no. c, pp. 163–164, 2011, doi: 10.1109/ISE.2011.6085033.

[9] T. Furukawa, M. Ohuchi, A. Chiba, and M. Date, "Dielectric relaxations and molecular motions in homopolymers and copolymers of vinylidene fluoride and trifluoroethylene," *Macromolecules*, vol. 17, no. 7, pp. 1384–1390, 1984, doi: 10.1021/ma00137a015.

[10] Y. Inuishi, 電気学会大学講座 誘電体現象論. IEEJ (Ohmsha, Ltd.), 1986.

[11] T. Hirata, S. Amiya, M. Akiya, O. Takei, T. Sakai, and R. Hatakeyama, "Development of a vitamin-protein sensor based on carbon nanotube hybrid materials," *Applied Physics Letters*, vol. 90, no. 23, 2007, doi: 10.1063/1.2746077.

[12] K. Keiji Kanazawa and J. G. Gordon, "The oscillation frequency of a quartz resonator in contact with liquid," *Analytica Chimica Acta*, vol. 175, no. C, pp. 99–105, 1985, doi: 10.1016/S0003-2670(00)82721-X.

[13] P. Barber *et al.*, *Polymer composite and nanocomposite dielectric materials for pulse power energy storage*, vol. 2, no. 4. 2009.

[14] P. Barber *et al.*, “Polymer composite and nanocomposite dielectric materials for pulse power energy storage,” *Materials*, vol. 2, no. 4, pp. 1697–1733, 2009, doi: 10.3390/ma2041697.

[15] J. Robertson and B. R. Varlow, “Non-linear ferroelectric composite dielectric materials,” *IEEE Transactions on Dielectrics and Electrical Insulation*, vol. 12, no. 4, pp. 779–790, 2005, doi: 10.1109/TDEI.2005.1511103.

[16] Y. Akimune, F. Munakata, M. Ando, Y. Okamoto, and N. Hirosaki, “Optimization of mechanical and electrical properties of TiN/Si_3N_4 material by agglomerates-microstructure-control,” *Journal of the Ceramic Society of Japan*, vol. 105, no. 2, pp. 122–125, 1997, doi: 10.2109/jcersj.105.122.

[17] T. T. M. Phan, N. C. Chu, V. B. Luu, H. Nguyen Xuan, I. Martin, and P. Carriere, “The role of epoxy matrix occlusions within $BaTiO_3$ nanoparticles on the dielectric properties of functionalized $BaTiO_3$/epoxy nanocomposites,” *Composites Part A: Applied Science and Manufacturing*, vol. 90, no. January, pp. 528–535, 2016, doi: 10.1016/j.compositesa.2016.08.018.

[18] F. Munakata, K. Yoshino, K. Nemoto, S. Abe, and A. Ito, “Effect of self-assembly material texture and dielectric properties of $BaTiO_3$/poly-L-lactic-acid composites,” *Materials Letters*, vol. 221, pp. 147–149,

2018, doi: 10.1016/j.matlet.2018.03.008.

[19] S. Mihcitaka, M. Yohikane, H. Mitsuaki, and O. Toshino, “Fractal dimensions of particle projected shapes,” vol. 25, pp. 11–15, 1988, doi: https://doi.org/10.1163/156855290X00126.

[20] S. Kobayashi, R. Kobayashi, and T. Watanabe, “Control of grain boundary connectivity based on fractal analysis for improvement of intergranular corrosion resistance in SUS316L austenitic stainless steel,” *Acta Materialia*, vol. 102, pp. 397–405, 2016, doi: 10.1016/j.actamat.2015.08.075.

[21] R. Lopes and N. Betrouni, “Fractal and multifractal analysis: A review,” *Medical Image Analysis*, vol. 13, no. 4, pp. 634–649, 2009, doi: 10.1016/j.media.2009.05.003.

[22] M. Yoshihisa, S. Toshiyuki, T. Keijiro, and K. Miyanami, “Application of fractal dimension for evaluation of dispersion of filler in composite material,” 1992, doi: https://doi.org/10.1002/pc.25482.

[23] M. Matsushita, *フラクタルの物理（I） －基礎編－(Physics of Fractals (I) － An Introduction －)*. Shokabo, 2002.

[24] S. H. Choi, I. D. Kim, J. M. Hong, K. H. Park, and S. G. Oh, “Effect of the dispersibility of $BaTiO_3$ nanoparticles in $BaTiO_3$/polyimide composites on the

dielectric properties," *Materials Letters*, vol. 61, no. 11–12, pp. 2478–2481, 2007, doi: 10.1016/j.matlet.2006.09.040.

[25] H.TAKAYASU, "フラクタル (Fractal)." Asakura Shoten, pp. 18–20, 1990.

[26] Y. Yano, Y. Shirakawa, and H. Morooka, "Electrical properties of ZnO / PrCoOxide multilayered composites," *Jornal of the Ceramic Society of Japan*, vol. 100, pp. 547–550, 1992, doi: https://doi.org/10.2109/jcersj.100.547.

[27] M. Matsuoka, "Nonohmic properties of zinc oxide ceramics," *Japanese Journal of Applied Physics*, vol. 10, no. 6, p. 736, 1971, doi: 10.1143/JJAP.10.736.

[28] H. Looyenga, "Dielectric constants of heterogeneous mixtures," *Physica*, vol. 31, no. 3, pp. 401–406, 1965, doi: 10.1016/0031-8914(65)90045-5.

[29] J. Robertson and B. R. Varlow, "Non-linear ferroelectric composite dielectric materials," *IEEE Transactions on Dielectrics and Electrical Insulation*, vol. 12, no. 4, pp. 779–790, 2005, doi: 10.1109/TDEI.2005.1511103.

[30] I. R. Epstein, J. A. Pojman, and O. Steinbock, "Introduction: self-organization in nonequilibrium chemical systems," *Chaos*, vol. 16, no. 3, 2006, doi: 10.1063/1.2354477.

[31] M. Takeda *et al.*, "Fractal characters of material texture of self-assembled $BaTiO_3$ /poly-l-lactic-acid composites," *Funtai Oyobi Fummatsu Yakin/Journal of the*

Japan Society of Powder and Powder Metallurgy, vol. 66, no. 3, pp. 122–127, 2019, doi: 10.2497/jjspm.66.122.

[32] E. Pérez, C. Bernal, and M. Piacquadio, "Multifractal analysis of tensile toughness and filler dispersion for polypropylene-$CaCO_3$ composites," *Applied Surface Science*, vol. 258, no. 22, pp. 8940–8945, 2012, doi: 10.1016/j.apsusc.2012.05.124.

[33] F. Munakata *et al.*, "Multifractal characteristics of the self-assembly material texture of β-Si_3N_4/SUS316L austenitic stainless steel composites," *Journal of Alloys and Compounds*, vol. 853, p. 156570, 2021, doi: 10.1016/j.jallcom.2020.156570.

[34] A. Posadas, R. Quiroz, A. Tannús, S. Crestana, and C. M. Vaz, "Characterizing water fingering phenomena in soils using magnetic resonance imaging and multifractal theory," *Nonlinear Processes in Geophysics*, vol. 16, no. 1, pp. 159–168, 2009, doi: 10.5194/npg-16-159-2009.

[35] W. Xia and Z. Zhang, "PVDF-based dielectric polymers and their applications in electronic materials," *IET Nanodielectrics*, vol. 1, no. 1, pp. 17–31, 2018, doi: 10.1049/iet-nde.2018.0001.

[36] A. Lakhtakia, B. Michel, and W. S. Weiglhofer, "Bruggeman formalism for two

models of uniaxial composite media: Dielectric properties," *Composites Science and Technology*, vol. 57, no. 2, pp. 185–196, 1997, doi: 10.1016/S0266-3538(96)00122-4.

[37] T. Mariko *et al.*, "Effect of Ceramic / Polymer Heterointerface on Dielectric Property of Self-Assembled $BaTiO_3$ / Poly-L-Lactic Acid Composite Materials," *(accepted to Journal of the Ceramic Society of Japan)*, pp. 1–6.

[38] M. Takeda *et al.*, "Fractal characters and thermal conductive properties of self-assembled material texture of silicon nitride/stainless steel (SUS316L) composites," *Funtai Oyobi Fummatsu Yakin/Journal of the Japan Society of Powder and Powder Metallurgy*, vol. 67, no. 6, pp. 307–312, 2020, doi: 10.2497/jjspm.67.307.

[39] V. Lorente-Leal *et al.*, "Validation of a real-time PCR for the detection of mycobacterium tuberculosis complex members in Bovine tissue samples," *Frontiers in Veterinary Science*, vol. 6, no. MAR, pp. 1–9, 2019, doi: 10.3389/fvets.2019.00061.

Chapter 3 Self-assembled silicon nitride / stainless steel (SUS316L) composites material texture and thermal conductivity

3.1 Fractal characters and thermal conductive properties of self-assembled material texture of silicon nitride / stainless steel (SUS316L) composites

3.1.1 Introduction

Thermal conductivity is an important physical property, as it determines the reliability and performance of industrial components in many industrial applications. In particular, the development of highly thermal conductive solid materials and the improvement of thermal conductivity are important for manufacturing high-performance and highly reliable insulations. In the case of automotive engines, low thermal conductivity is necessary for heat insulation components to reduce fuel consumption. In contrast, high thermal conductivity is required for excellent thermal shock resistance, and iron alloys are often used in engine components. However, the thermal conductivity of iron alloys is relatively low around room temperature.

Silicon nitride (Si_3N_4) has a highly thermally conductive compound with excellent mechanical strength, fracture toughness, wear resistance, corrosion resistance, and fire resistance, and it is lightweight. The silicon nitride has two crystal structures, α- and β-. In particular, it was reported that the thermal conductivity of β-Si_3N_4 material with the ceramic crystal nuclei was about 100 $Wm^{-1}K^{-1}$[1]. It was also reported that the thermal conductivity of β-Si_3N_4 along the a-axis and c-axis decreases due to the crystal defects of the impurities, the empty lattice points, and the dislocations. The β-Si_3N_4 ceramics is applied as a high-strength material to gas turbine engines and bearings of the components for aircraft and automobile engines [2].

Stainless steel (SUS316L) is one of the austenitic stainless steel alloys containing molybdenum. It has excellent corrosion resistance, mechanical strength, toughness, and weldability. However, the thermal conductivity of stainless steel alloys is much lower than that of carbon steel. Therefore, it has limitations for the application in the sliding components of the engine that operates at high load pressure. Thus, it is found to combine SUS316L and β-Si_3N_4 to increase the thermal conductivity of SUS316L while maintaining excellent characteristics. However, few studies have been done on β-Si_3N_4 / SUS316L composites.

In a report on the thermal conductivity of composite materials, Shimamura et al. [3] propose that α- and β-Si_3N_4 additives be added to epoxy to prepare the Si_3N_4 / epoxy composites, and a percolation network of α and β-Si_3N_4 additives can be formed to improve the thermal conductivity. In a similar example, Hong He et al. [4] propose the importance of reducing the effect of thermal resistance at the interface between Si_3N_4 and polystyrene to improve the thermal conductivity of Si_3N_4 / polystyrene composites. Therefore, it is essential to control the microstructure of the thermal conductive composite material and to investigate the dispersed state of the SN particles to improve thermal conductivity.

A method using fractal analysis has been reported to quantitatively analyze the shape of particles[5]. Kobayashi et al. [6] investigate that the grain boundary microstructures in SUS316L stainless steel with fractal analysis. They highlight that the maximum random boundary connectivity was found to have a fractal nature for SUS316L stainless steel specimens, and it was suggested that it was possible to characterize the grain boundary microstructures by fractal analyses [6]. There are few reports that fractal analysis has never been used for the quantitative evaluation of dispersion and

agglomerated particles.

In this session, the β-Si_3N_4 (SN) / SUS316L composites were prepared with SN fillers and SUS316L matrix with different particle sizes. And then, the self-assembled material structure formed was evaluated using the multifractal analysis to investigate the relationship between the material texture and the thermal conductivity. In particular, the purpose of this session was that the morphology of the self-assembly SN secondary particle groups using the multifractal, and the thermal conductivity network with the SN agglomerates in SN / SUS316L stainless steel composites were discussed. The point of the self-assembly process in this session was shown in Fig. 3-1.

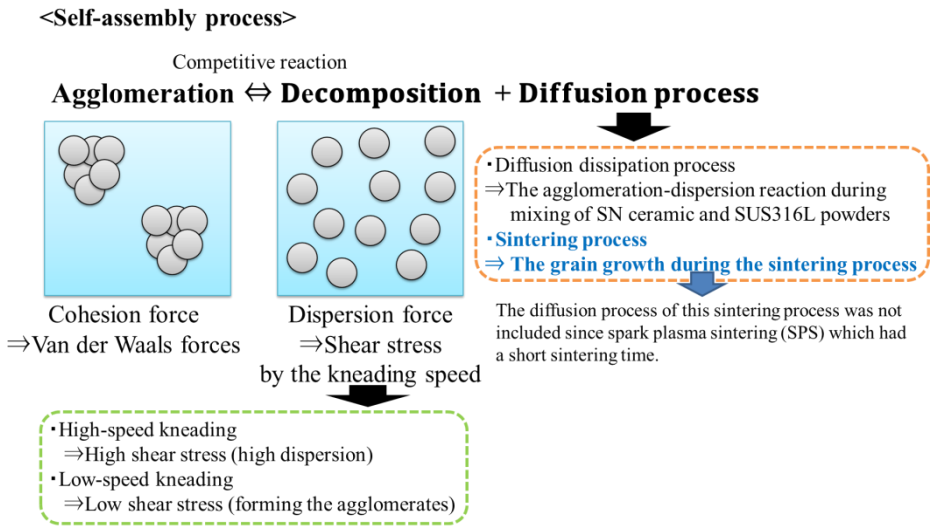

Fig. 3-1 The point of the self-assembly process in this session.

3.1.2 Experimental procedures

3.1.2.1 Sample preparation

The β-Si_3N_4 (SN) powder (Denka Corp., HP-60, average particle size：about 1μm) and SUS316L powder (Epson Atomix Corp., PF-3F, average particle size：3μm) were used as the starting material to manufacture SN / SUS316L stainless steel composites.

The volume fractions of β-Si_3N_4 fillers were 0 vol.% to 10 vol.%. As the composite materials fabrication process, weighted powders (12 g) were put into a poly-ethylene jar (100 ml) with ϕ5 mm Si_3N_4 balls (60 g) and then ball-milled for 24 hours. The rotation speed of the ball-milling for the mixture of SUS316L powder with a particle size of 3 μm was 120 rpm. A mixed powder was also prepared by using SUS316L powder (average particle size: 8 μm). The rotation speed of the ball-milling for the mixture of SUS316L powder with a particle size of 8 μm was 150 rpm. The powder was put into a carbon mold and sintered by a spark plasma sintering (SPS) at 900℃ 50 MPa for 10 minutes in a vacuum (less than 5 Pa). The sintered samples were mirror-polished by using sandpaper and alumina powders.

3.1.2.2 Measurement method

The bulk densities (ρ_{bulk}) of the obtained samples were measured by the Archimedes method using pure water. The relative densities (ρ_{rel}) were calculated from the measured bulk densities and estimated theoretical densities from these of SUS316L (7.98 gcm^{-3}) and β-Si_3N_4 (3.18 g cm^{-3}). The thermal diffusivities α was measured by the laser flash method and the thermal conductivities λ_e of the samples were obtained:

$$\lambda_e = \alpha \cdot \rho_{bulk} \cdot C_p \tag{3-1}$$

where C_p is specific heat capacity estimated from those of SUS316L (0.54 $Jg^{-1}K^{-1}$) and β-Si_3N_4 (0.71 $Jg^{-1}K^{-1}$).

The average secondary particle area (S) of the SN fillers of the SN / SUS316L composite material was estimated. The polished surfaces of the samples were analyzed using a scanning electron microscope (SEM, Hitachi High-Tech Co., Japan TM3000)

and a field emission scanning electron microscope (FE-SEM, Hitachi Co., Japan: SU-8230). The FE-SEM images were converted to binary images to estimate the *S* of the SN fillers for each sample.

3.1.2.3 Multifractal analysis

The morphology and dispersion of self-assembled SN / SUS316L stainless steel composites were characterized using multifractal analysis, which was performed using the binary images described in section 2.2. This analysis was used to estimate the probability ($p_i[r]$) of an image by covering it with boxes of size r and counting the number of boxes. The partition function is as follows:

$$P_r^q = \sum_{i=1}^{N(r)} \left[p_i(r)\right]^q \tag{3-2}$$

where q is the order moment ($-\infty<q<\infty$). The generalized dimensions of the q of a distribution, Dq, can be defined as follows:

$$D_q = \frac{1}{q\text{-}1} \lim_{r\to 0} \frac{\ln P_r^q}{\ln r} = \frac{1}{q\text{-}1} \lim_{r\to 0} \frac{\ln N(q,r)}{\ln r} \tag{3-3}$$

When q takes the values of 0, 1, or 2, Eq. 3-4 is reduced to the following:[7]

$$D_0 = -\lim_{r\to 0} \frac{\log N(r)}{\log r} \tag{3-4}$$

where D_0 is the capacity dimension. In this session, the D_0 was obtained from the multifractal analysis as an initial analysis, and the morphology of the SN secondary particle groups was characterized.

3.1.3 Results and discussion

3.1.3.1 The volume fraction of SN fillers and thermal conductivity

Fig. 3-2 presents the FE-SEM micrograph and the binary images of the SN / SUS316L stainless steel composites of SUS316L powder with a particle size of 3 μm of 5 vol.% and 10 vol.%. Fig. 3-3 shows the FE-SEM micrograph and the binary images of the SN / SUS316L stainless steel composites of SUS316L powder with a particle size of 8 μm of 5 vol.% and 10 vol.% under the different fabrication condition. In Fig. 3-2 and Fig.3-3, the black part of the binary images shows the SN secondary particle group, while the white part shows SUS316L. In Fig.3-2, the formation of self-assembled SN secondary particle groups was promoted by increasing the volume fraction of SN. It was considered that the self-assembled SN secondary particle groups had the same similarity with increasing the volume fraction of SN. In the result of the SN / SUS316L stainless steel composites of SUS316L powder with a particle size of 8 μm at 150 rpm as shown in Fig.3-3, the SN secondary particle groups were anisotropy with increasing the volume fraction of SN fillers, and the formation of the similarity SN secondary particle group was promoted. Comparing the results of Fig. 3-2 and Fig. 3-3, it was considered that the self-assembled SN secondary particle groups were distributed homogenize in the SUS316L matrix with a particle size of 3 μm. On the other hand, it was considered that SN particles of the samples of SUS316L powder with a particle size of 8 μm were introduced to the vacant space because of the difference in particle size of

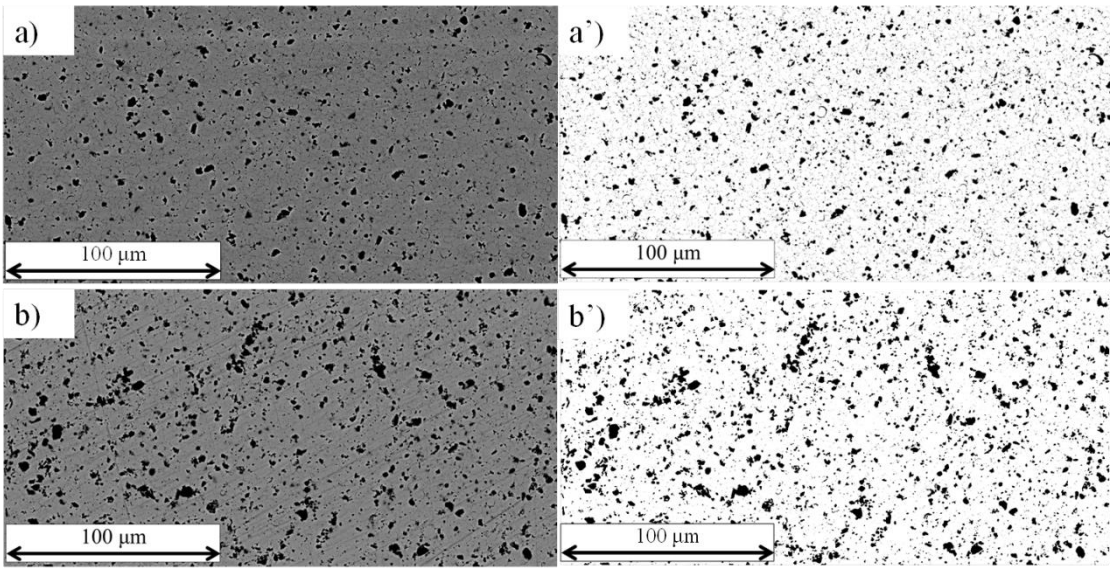

Fig. 3-2 Cross sectional FE-SEM images (a and b) and image processing pictures (a'and b') of samples with 5 (a, a') and 10 (b, b') % volume fraction of SN with SN/SUS316L (average particle diameter: 3μm).

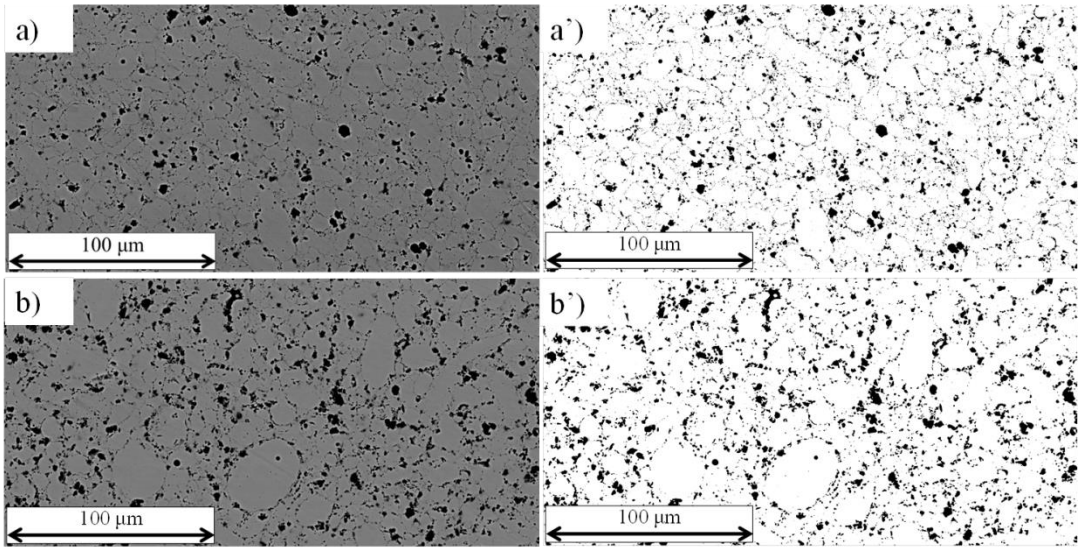

Fig. 3-3 Cross sectional FE-SEM images (a and b) and image processing pictures (a'and b') of samples with 5 (a, a') and 10 (b, b') % volume fraction of SN with SN/SUS316L (average particle diameter: 8μm)

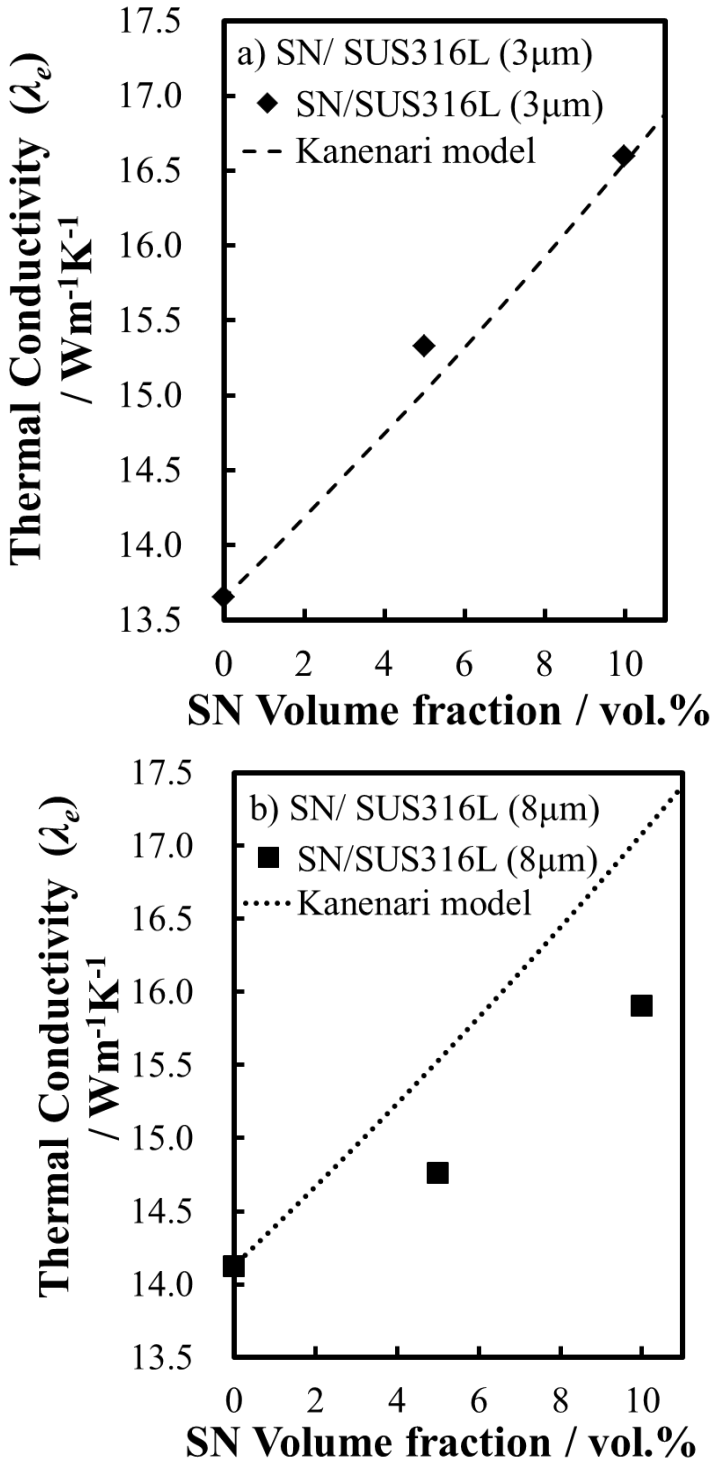

Fig. 3-4 Relationship between the volume fraction of SN and the thermal conductivity (λ_e) with 5% and 10% SN/SUS316L (average particle diameter: a) 3μm and b) 8μm) composites.

SN powder and SUS316L powder. This is, it was suggested that the formation of the SN secondary particle groups of the samples of SUS316L powder with a particle size of 8 μm was limited.

In order to investigate the effect of the SN additive, the thermal conductivity estimated by Kanari's model and the results of this experiment were compared. Kanari's model is an example assuming that a composite material in which particles are uniformly and randomly dispersed is a continuous medium. The model can be described as follows [8][9]:

$$1 - \nu = \frac{\lambda_e - \lambda_d}{\lambda_c - \lambda_d} \cdot \left(\frac{\lambda_c}{\lambda_e}\right)^{1/(x+1)} \quad (3\text{-}5)$$

where v is the volume fraction of the filler. λ_c, λ_d, and λ_e are the thermal conductivities of the matrix material (SUS316L), filler (SN), and composite material, respectively. x is determined by the particle shape of the additive and is 2 for a spherical shape. Fig.3-4 a presents the results of the volume fraction and thermal conductivity (λ_e) of the self-assembled SN / SUS316L stainless steel composites of SUS316L powder with a particle size of 3 μm. Fig.3-4 b shows the results of the volume fraction and thermal conductivity (λ_e) of the self-assembled SN / SUS316L stainless steel composites of SUS316L powder with a particle size of 8 μm. The thermal conductivity of the composite was calculated with λ_d of SN volume fraction 0 vol.% of each SUS316L particle size, assuming that λ_c of SN was 80$Wm^{-1}K^{-1}$. The results of thermal conductivity estimated by Kanari's model were shown in Fig. 3-4 a and b. Table. 3-1 shows the bulk density (ρ_{bulk}) and relative density (ρ_{rel}) of the samples. The relative density was calculated by the density of SN (3.18 gcm^{-3}) and the density of SUS316L (7.98 gcm^{-3}). According to the result of the samples of SUS316L powder with a

particle size of 3 μm in Fig. 3-4 a, λ_e was increased by increasing the volume fraction of SN fillers. Comparing the results of the thermal conductivity of Kanari's model and this study, the behavior of the samples of SUS316L powder with a particle size of 3 μm was slightly different from Kanari's model. The thermal conductivity was improved by 1.22 times at 10 vol.% compared to the volume fraction of 0 vol.% for SN. The λ_e of the samples of SUS316L powder with a particle size of 8 μm was increased with increasing the volume fraction of SN filler as shown in Fig. 3-4 b. However, the λ_e of the samples of SUS316L powder with a particle size of 8 μm was lower than Kanari's model. It was suggested that the SN particles were deviation since the SN particles were selectively introduced to the vacant space and that the thermal conductivity network using the SN secondary particle groups was not effectively formed. In addition, it was considered that there were large and small SN secondary particle groups in the self-assembled SN / SUS316L stainless steel, approaching the effective medium approximation theories [10] that assume homogeneous dispersion and the thermal conductivity was lower than Kanari's model. Therefore, it was suggested that the distributed state of the SN secondary particle groups affected the thermal conductivity.

3.1.3.2 Multifractal analysis of self-assembled material texture

The particle shape and grain boundary shape are evaluated by the box count method for fractal analysis [5], [6]. In chapter 2, it was reported that the multifractal analysis was applied to the morphology of the self-assembled BT aggregate of BT / polymer composite materials. In the self-assembled BT / PLLA composites, the capacity dimension (D_0) obtained from the fractal analysis using the box-counting method and the multifractal analysis using the generalized dimension were the same and

self-assembled BT secondary particle groups were characterized with the D_0 by the different fractal analysis. This is, it was proposed that the characteristics of the ceramics secondary particle groups are able to be evaluated with the D_0. The multifractal analysis was performed based on the binary images as shown in Fig. 3-2 and Fig. 3-3. Table 3-1 presences the D_0 obtained from the multifractal analysis, the average particle swarm area (S), and the result of λ_e shown in Fig. 3-4. Fig. 3-5 shows the result of the SN volume fractions and D_0 of the samples of SUS316L powder with a particle size of 3 μm and 8 μm. According to the results of Table.3-1 and Fig.3-5, the average particle group area of the SN particle group of the samples of SUS316L powder with a particle size of 3 μm was increased by increasing the volume fraction of SN; however, D_0 was not changed. It was considered that the similarity of the self-assembled SN secondary particle group was not changed by forming the self-assembled SN secondary particle groups.

Table 3-1 The capacity dimension (D_0) and characteristic of SN/SUS316L stainless steel composites.

Average particle diameter of SUS316L powder / μm	SN Volume fraction / vol%	Average particle area of SN particles (s) / μm^2	Capacity dimension (D_0)	Bulk density (ρ_{bulk})/ gcm^{-3}	Relative density (ρ_{rel})/ %	Thermal Conductivity (λ) / $Wm^{-1}k^{-1}$
	0	0	-	7.35	92.1	13.65
3	5	1.40	1.72	7.49	96.7	15.33
	10	1.93	1.70	7.25	96.7	16.60
	0	0	-	7.75	97.1	14.13
8	5	1.31	1.68	7.49	96.8	14.76
	10	1.66	1.68	7.29	97.2	15.91

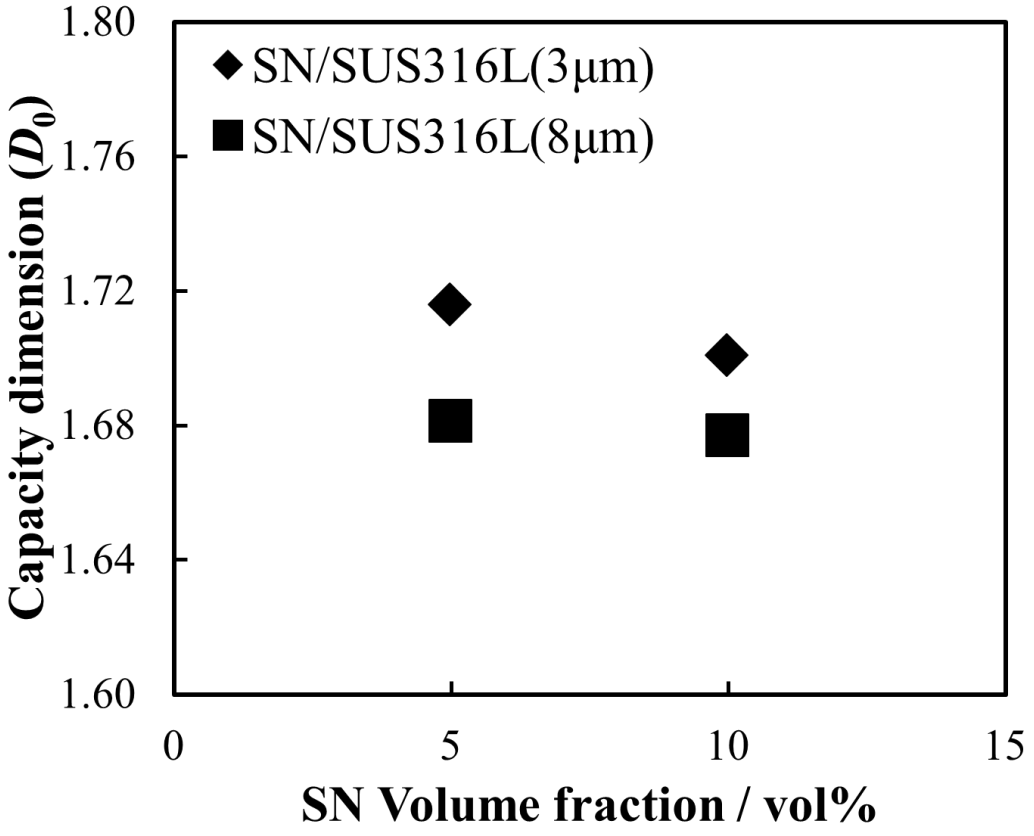

Fig.3-5 Relationship between the volume fraction of SN and the capacity dimension (D_0) with 5% and 10% SN/SUS316L (average particle diameter: 3μm and 8μm) composites.

In general, the self-assembly (self-organization) process is observed in the reaction–diffusion system, which is assumed to occur due to a competitive reaction between an inhibitor and a promoter within the diffusion process. In the kneading process of solid material, the formation of self-assembled SN secondary particle groups is proposed.

$$\text{Agglomeration} \Leftrightarrow \text{Decomposition} + \text{Diffusion process} \tag{3-6}$$

The Van der Waals force acts as a cohesion force. The shear stress caused by the kneading speed acts for decomposition. It is considered that the diffusion processes

include the diffusion dissipation process, which arises in the agglomeration-dispersion reaction during the powder agitation mixing of SN ceramics and SUS and the subsequent sintering process, which is produced by the volume diffusion process that promotes grain growth [11]. The kneading process corresponds to one of the diffusion processes in the reaction-diffusion system. In this study, the subsequent sintering process was not contained in the diffusion process within the self-assembly process. It was reported that SN particles formed the secondary particle groups by the Van der Waals forces [12]. It was suggested that the similarity of self-assembled SN secondary particle groups was formed since the cohesion force of the SN powder within the self-assembly process was not changed. The SN secondary particle area of the SUS316L powder with a particle size of 8 μm was increased with increasing the volume fraction of SN; however, the D_0 was not changed. It was suggested that the packing degree of the SN secondary particle groups aggregated by van der Waals forces was controlled; however, the SN secondary particle group was similar.

Fig. 3-6 presents the relationship between the S and the λ_e. The thermal conductivity of the samples of the SUS316L powder with a particle size of 3 μm was increased with the secondary particle area of SN particles. Similarly, the thermal conductivity of the samples of the SUS316L powder with a particle size of 8 μm was increased with the secondary particle area of SN particles. Therefore, it was suggested that the formation of the SN secondary particle group was an important role in improving the thermal conductivity. It was highlighted that the interface of the two-phase composite acts as a barrier of heat transmission [4]. In this result, it was suggested that the amount of the SN / SUS316L interface was decreased and the SN / SN interface was increased with forming the SN secondary particle group of the SN particle group, and then the thermal

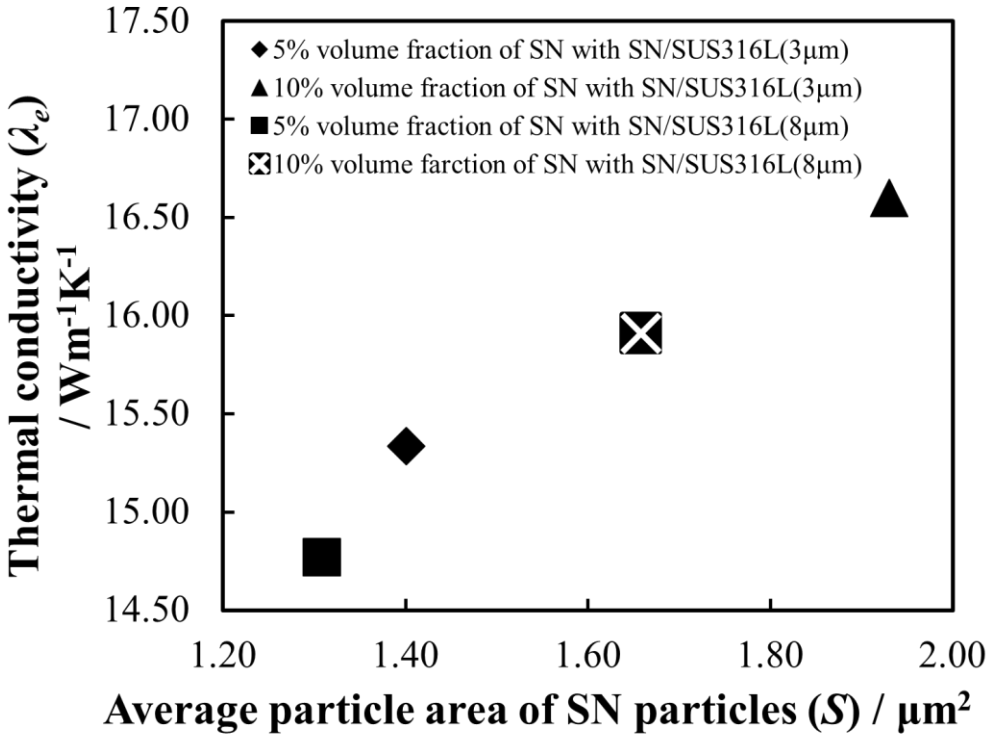

Fig. 3-6 Relationship between the average particle area of SN particles and the thermal conductivity (λ_e) with 5% and 10% SN/SUS316L (average particle diameter: 3μm and 8μm) composites

conductivity networks using the self-assembled SN secondary particle groups were formed effectively.

Shimamura et al. [3] proposed that α- and β-Si_3N_4 additives were added to epoxy to prepare the Si_3N_4 / epoxy composites, and a percolation network of α and β-Si_3N_4 additives was formed to improve the thermal conductivity. In order to discuss the relationship between the material texture and the thermal conductivity, Fig. 3-7 presents the results of the D_0 and λ_e. The D_0 was related to the morphology of the self-assembled SN secondary particle groups, and it was suggested that the SN secondary particle group was formed similarity. According to the result in Fig. 3-7, the

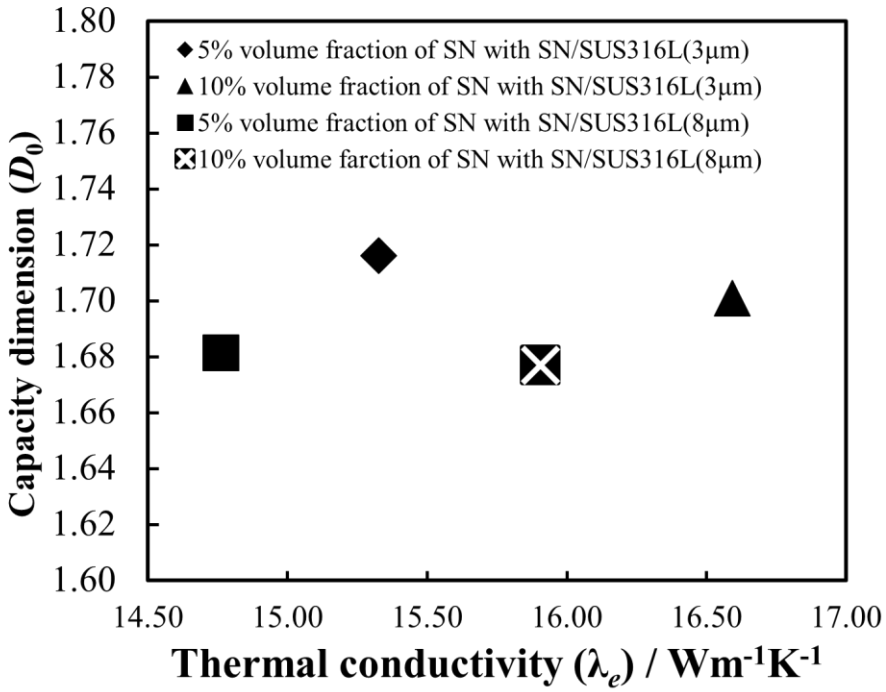

Fig. 3-7 Relationship between the capacity dimension (D_0) and the thermal conductivity (λ_e) with 5% and 10% SN/SUS316L (average particle diameter: 3μm and 8μm) composites.

thermal conductivity of the samples of the SUS316L powder with a particle size of 3 μm that was prepared at 120 rpm was increased; however, D_0 was constant. In addition, the thermal conductivity of the samples of the SUS316L powder with a particle size of 8 μm that was prepared at 150 rpm was increased; however, D_0 was constant. That is, in this manufacturing process, the thermal conductivity was improved without changing the morphology of the self-assembled SN secondary particle groups. It was suggested that the thermal conductivity of the samples of the SUS316L powder with a particle size of 8 μm was lower than Kanari's model since the SN particles were introduced to the vacant space selectively and the thermal conductivity network using the SN secondary particle groups was not formed effectively. Therefore, it was considered that the distribution of SN particle groups was important for the thermal conductivity of

self-assembled SN / SUS316L composites. Sarika Jalan et al. [13] reported that the network was estimated by the generalized dimension of the multifractal analysis. They proposed that the D_0 reflected to the morphology of the SN particle group morphology, the D_1 reflected the information entropy, and the D_2 reflected the correlation dimension can be obtained from the generalized dimension. It is considered that it may be possible to evaluate network properties, that is, the configuration and connectivity of SN particles with the D_1 and the D_2. Therefore, it is expected that it is possible to quantify the network with the D_0, D_1 and D_2. The D_0, D_1, and D_2 were discussed in Session 3.2.

3.1.4 Conclusions

In order to quantitatively analyze the morphology of the self-assembled SN secondary particle group, (1) SN / SUS316L stainless steel composites of the SUS316L powder with a particle size of 3 μm and under the rotation speed of ball-milling at 120 rpm and (2) SN / SUS316L stainless steel composites of the SUS316L powder with a particle size of 8 μm and under the rotation speed of ball-milling at 150 rpm were prepared. In the formation of the self-assembly SN agglomerates with adding SN fillers of the volume fraction 5 % and 10 % of SN, the multifractal analysis was applied to evaluate the morphology of the self-assembled SN secondary particle groups. The conclusions are as follows:

(1) According to the relationship between the volume fraction of SN and λ_e, the λ_e of the SN / SUS316L stainless steel composite of the SUS316L powder with a particle size of 3 μm showed higher than the Kanari's model since it was suggested that the self-assembled SN secondary particle group was formed. The thermal

conductivity was improved by 1.22 times at 10 vol.% compared to the volume fraction of 0 vol.% for SN.

(2) The self-assembled secondary particle area of SN particle was increased by increasing the thermal conductivity since it was considered that the SN secondary particle group was formed and the thermal conductivity network using the SN secondary particle group was formed in the SN / SUS316L stainless steel composite.

(3) According to the multifractal analysis, D_0 was constant; however, the volume fraction of SN was increased. This is, it was considered that the similarity of self-assembled SN secondary particle group was formed with increasing the volume fraction of SN.

Hence, it was suggested that the formation of the thermal conductivity network using the SN secondary particle groups was an important role in improving the thermal conductivity, and it was expected that the thermal conductivity was higher than Kanari's model.

3.2 Grain size effect of material matrix SUS316L in SN / SUS316L stainless steel composites on self-assembled texture and thermal conductivity

3.2.1 Introduction

In Session 3.1, it was considered that the dispersant state of SN secondary particle groups was important for the thermal conductivity of self-assembled SN / SUS316L composites to form the thermal conductivity network using the SN secondary particle group. Therefore, in this session, the morphology, entropy of configuration, and

dispersibility of the self-assembled SN secondary particle groups and the thermal conductivity of the self-assembled SN / SUS316L composites were investigated by the multifractal analysis in detail.

A method using fractal analysis has been reported to quantitatively analyze the shape of particles[5]. Kobayashi et al. [6] investigate that the grain boundary microstructures in SUS316L stainless steel with the fractal analysis. They highlight that the maximum random boundary connectivity was found to have a fractal nature for SUS316L stainless steel specimens, and it was suggested that it was possible to characterize the grain boundary microstructures by fractal analyses [6]. The characters of the morphology of the secondary particle group in the BT / poly-L-lactic-acid (PLLA) polymer were investigated through the multifractal analysis [14] (Chapter 2). The multifractal analysis was applied to evaluate the morphology of the self-assembled SN secondary particle groups of the SN/SUS316L composite material [15]. It was suggested that the similarity of the SN secondary particle group was not changed by adding the SN fillers [15]. In order to improve thermal conductivity, it was proposed that it was necessary to investigate the formation of the thermal conduction network by the SN secondary particle group. Recently, the multifractal analysis, which is seen as an extension of fractals has been used in the image analysis of medical technology [16]. Sarika Jalan et al. [13] report that the network was estimated by the generalized dimension of the multifractal analysis. In another example, E. Pérez et al. [17] report on the dispersion of $CaCO_3$ particles in polypropylene (PP) and the fracture morphology of tensile samples using the box-counting method and multifractal analyses (multifractal spectrum [f ,α]. They suggest that multifractal theory can be applied to elucidate the relationship between the structure and mechanical behavior of PP–$CaCO_3$ composite materials [17].

They reported that the multifractal dimensions of the β-Si_3N_4 secondary particle network, Dq (q=0, 1, 2), were estimated to investigate the relationship between the thermal conductivity and the connectivity of the SN secondary particles in the SN / SUS316L composites related to the propagation path of heat conduction [11]. In addition, the usefulness of the analysis of multifractal dimensions for material texture in a solid-state reaction was proposed [11]. The report highlights that the capacity dimension D_0 related to the morphology of β-Si_3N_4 agglomerates, and the information dimension D_1 for these samples are related to the entropy of configuration affected by the dispersion of β-Si_3N_4 particles, and the correlation dimension D_2 reflected the dispersibility between the particles [11].

In this session, the self-assembled SN / SUS316L composite materials were prepared using the SUS316L particle sizes of 3 μm and 8 μm to investigate the effect of the SUS316L particle size on thermal conductivity. In particular, the morphology, entropy of configuration, and dispersibility of the self-assembled SN secondary particle groups were investigated. The formation of the self-assembled SN secondary particle groups was investigated by changing the dispersant state of the SN secondary particle groups with the different SUS316L particle sizes. The self-assembled SN / SUS316L stainless steel composite with the SUS316L particle size was evaluated by multifractal analysis D_q (q = 0, 1, 2).

3. 2.2Experimental procedures

3. 2.2.1 Sample preparation

The β-Si_3N_4 (SN) powder (Denka Corp., HP-60, average particle size: about 1 μm) and the SUS316L powder (Epson Atomix Corp., PF-3F, average particle size: 3 μm)

were used as the starting material to manufacture SN/SUS316L composites. The starting compositions were 0 vol.% β-Si_3N_4 –100 vol.% SUS316L, 5 vol.% β-Si_3N_4 –95 vol.% SUS316L, and 10 vol.% β-Si_3N_4 –90 vol.% SUS316L. In the composite materials fabrication process, weighted powders (12 g) were put into a polyethylene jar (100 ml) with ϕ5 mm Si_3N_4 balls (60 g) and then ball-milled for 24 hours. A mixed powder was also prepared using the SUS316L powder (average particle size: 8 μm). The powder was put into a carbon mold and sintered by a spark plasma sintering (SPS) at 900°C 50 MPa for 10 minutes in a vacuum (less than 5 Pa). The sintered samples were mirror-polished using sandpaper and alumina powders.

3. 2.2.2 Measurements

The bulk densities (ρ_{bulk}) of the obtained samples were measured by the Archimedes method using water. The relative densities (ρ_{rel}) were calculated from the measured bulk densities, and the estimated theoretical densities were calculated from those of SUS316L (7.98 g cm^{-3}) and β-Si_3N_4 (3.18 g cm^{-3}). The thermal diffusivities, α, were measured by the laser flash method, and the thermal conductivities λ_e of the samples were obtained by:

$$\lambda_e = \alpha \cdot \rho_{bulk} \cdot C_p \tag{3-7}$$

where C_p is the specific heat capacity estimated from those of SUS316L (0.54 $Jg^{-1}K^{-1}$) and β-Si_3N_4 (0.71 $Jg^{-1}K^{-1}$).

The average secondary particle area (S) of the SN fillers of the SN / SUS316L composite material was estimated. The polished surfaces of the samples were analyzed

using a scanning electron microscope (SEM, Hitachi High-Tech Co., Japan TM3000) and a field emission scanning electron microscope (FE-SEM, Hitachi Co., Japan: SU-8230) . The FE-SEM images were converted to binary images to estimate the *S* of the SN fillers for each sample. The ρ_{rel}, λ_e, and *S* were based on session 3.1.

3. 2.2.3 Multifractal analysis

The morphology, entropy of configuration, and dispersibility of self-assembled SN / SUS316L stainless steel composites were characterized using multifractal analysis, which was performed using the binary images described in section 3.2.2.2. This analysis was used to estimate the probability ($p_i[r]$) of an image by covering it with boxes of size *r* and counting the number of boxes. The partition function is as:

$$P_r^q = \sum_{i=1}^{N(r)} [p_i(r)]^q \tag{3-8}$$

where *q* is the order moment ($-\infty<q<\infty$). The generalized dimensions of the *q* of a distribution, *Dq*, can be defined as:

$$D_q = \frac{1}{q\text{-}1} \lim_{r\to 0} \frac{\log P_r^q}{\log r} = \frac{1}{q\text{-}1} \lim_{r\to 0} \frac{\log N(q,r)}{\log r} \tag{3-9}$$

When *q* takes the values of 0, 1, or 2, Eq. 3-9 is reduced to the following:[7]

$$D_0 = -\lim_{r\to 0} \frac{\log N(r)}{\log r} \tag{3-10}$$

$$D_1 = \lim_{r\to 0} \frac{\sum_{i=1}^{N(r)} \mu_i(r) log(\mu_i(r))}{log(r)} \tag{3-11}$$

$$D_2 = \lim_{r\to 0} \frac{log(C(r))}{log(r)} \tag{3-12}$$

where D_0 is the capacity dimension, $C(r)$ is the correlation function, and D_1 and D_2 are the entropy dimension and the correlation dimension, respectively. The relationship between D_0, D_1, and D_2 is as:

$$D_2 \leq D_1 \leq D_0 \tag{3-13}$$

In this paper, D_0, D_1, and D_2 were estimated to evaluate the morphology, entropy of configuration, and dispersibility of the self-assembled SN agglomerates in the SN / SUS316L stainless steel composite.

3.2.3 Results

Fig. 3-8 presents the FE-SEM micrograph, binary images, and magnified images of the SN / SUS316L stainless steel composites of the SUS316L powder with a particle size of 3 μm. Fig.3-9 shows the FE-SEM micrograph, binary images, and magnified images of the SN / SUS316L stainless steel composites of the SUS316L powder with a particle size of 8 μm. In Fig. 3-8 and Fig.3-9, the black portion of the binary images shows the SN particle group, while the white portion shows SUS316L. According to the FE-SEM micrograph of the samples of the SUS316L powder with a particle size of 3 μm as shown in Fig. 3-8, the formation of the self-assembled isotropic SN agglomerates was promoted by increasing the volume fraction of SN. In Fig. 3-9, the formation of the self-assembled anisotropic SN agglomerates of the samples of the SUS316L powder with a particle size of 8 μm was promoted by increasing the volume fraction of SN. In the magnified images of the samples of the SUS316L powder with a particle size of 3

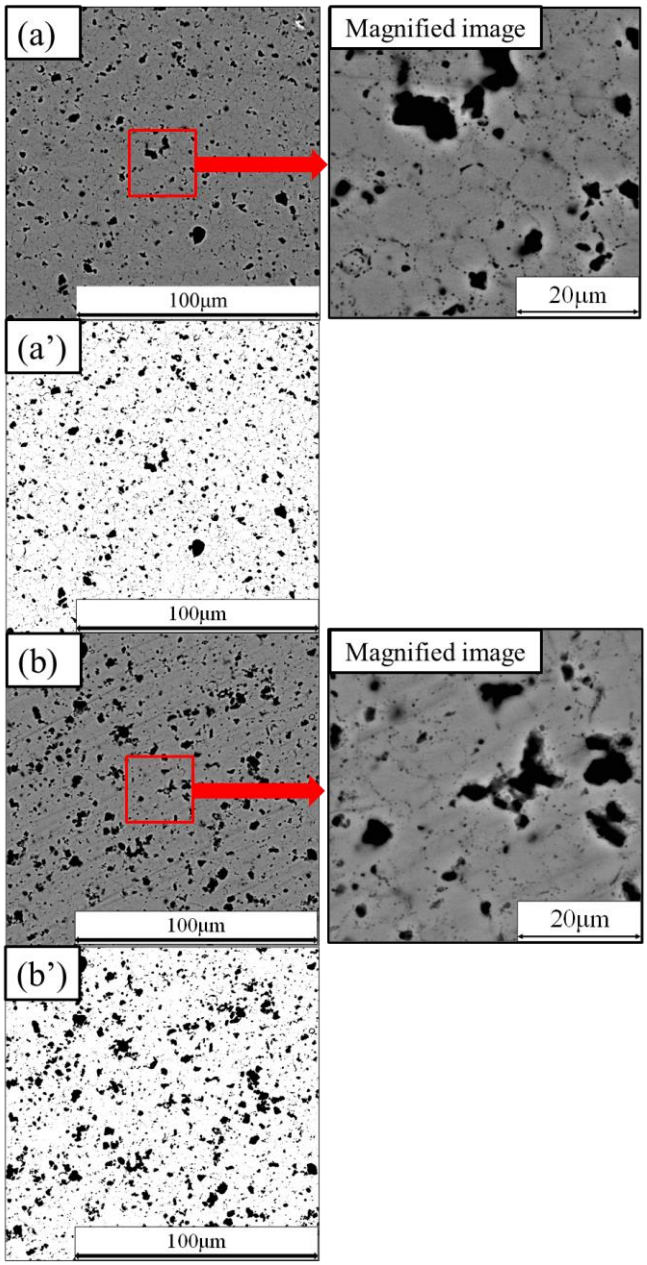

Fig.3-8 Cross-sectional FE-SEM images (a and b) and image processing pictures (a'and b') of samples with 5 (a and a') and 10 (b and b') % volume fraction of SN with SN / SUS316L stainless steel composites (average particle diameter: 3μm).

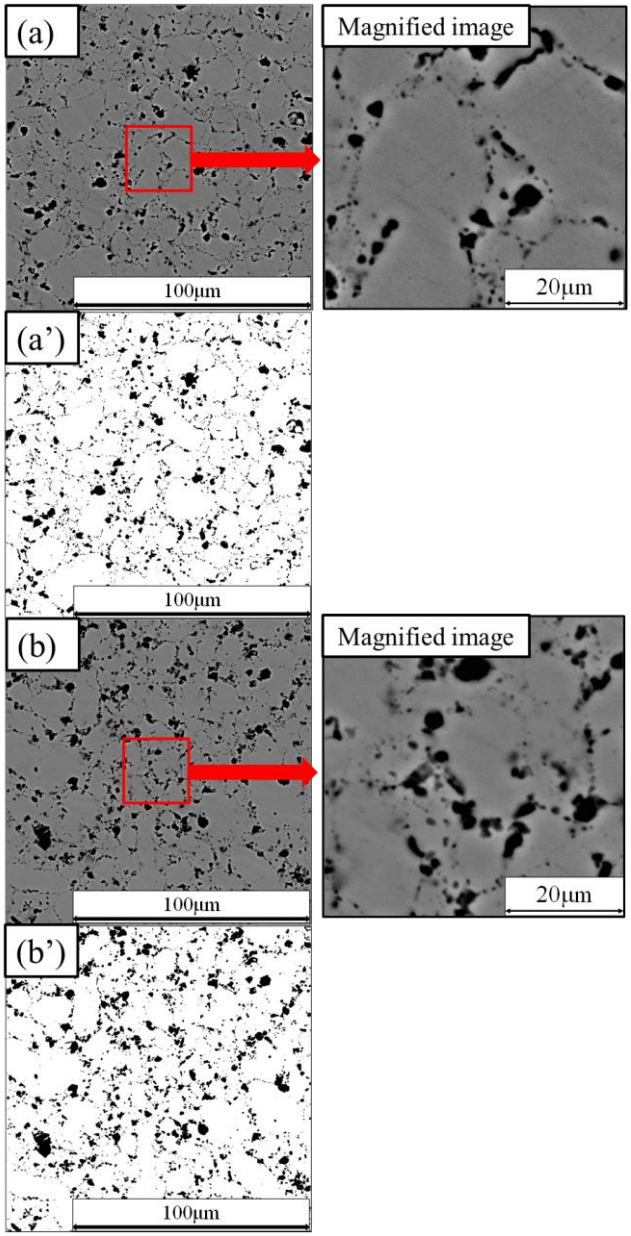

Fig. 3-9 Cross-sectional FE-SEM images (a and b) and image processing pictures (a'and b') of samples with 5 (a and a') and 10 (b and b') % volume fraction of SN with SN / SUS316L stainless steel composites (average particle diameter: 8μm).

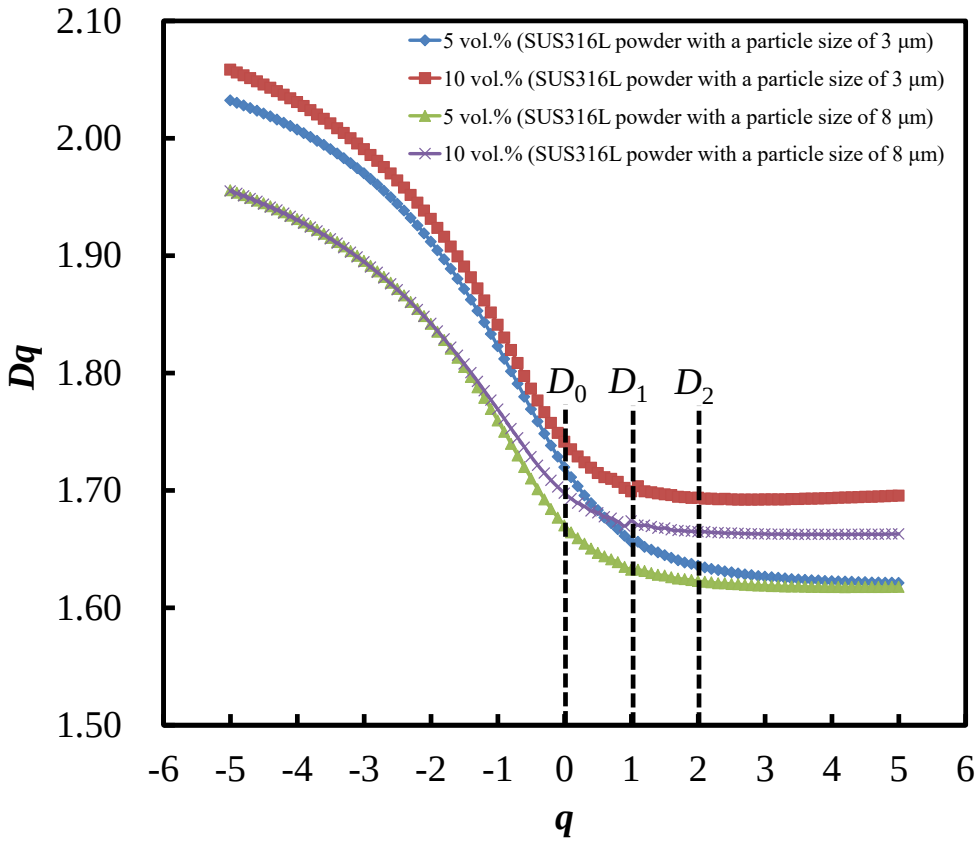

Fig.3-10 Relationship between D*q* and *q* of SN /SUS316L (3 μm and 8 μm).

μm, it was confirmed that the SN agglomerates were distributed relatively homogeneously in the SUS316L matrix, and the distance between the SN secondary particle groups was small. On the other hand, in the magnified images of the samples of the SUS316L powder with a particle size of 8 μm in Fig. 3-9 c, the self-assembled SN agglomerates deviated and the SN agglomerates were individual.

Previously, Sarika Jalan et al. [13] reported that the network was estimated by the generalized dimension of the multifractal analysis. They proposed that D_1 indicating the information entropy and D_2 indicating the correlation dimension were obtained from the generalized dimension [13]. In a previous report, D_0 was found to be related to the morphology of ceramics agglomerates, D_1 to the entropy of configuration affected by

Table 3-2 The multifractal dimension and characteristic of SN / SUS316L composites.

Average particle diameter of SUS316L powder / μm	SN Volume fraction / vol.%	Average particle area of SN fillers (S) / μm^2	Capacity dimension (D_0)	Entropy dimension (D_1)	Correlation dimension (D_2)	Relative density (ρ_{rel})/ %	Thermal Conductivity (λ_e) / $Wm^{-1}k^{-1}$
	0	0	-	-	-	92.1	13.65
3	5	1.40	1.72(4)	1.66(3)	1.63(9)	96.7	15.33
	10	1.93	1.73(5)	1.69(1)	1.68(0)	96.7	16.60
	0	0	-	-	-	97.1	14.13
8	5	1.31	1.69(1)	1.64(9)	1.63(5)	96.8	14.76
	10	1.66	1.70(7)	1.67(8)	1.67(2)	97.2	15.91

(The third decimal place in parenthesis contains an error.)

the dispersion of ceramic particles, and D_2 to the dispersibility among the particles [15]. The morphology, entropy of configuration, and dispersibility of self-assembled SN agglomerates in the SN / SUS316L stainless steel composites were investigated using D_0, D_1, and D_2, which were estimated via multifractal analysis. Fig.3-10 indicates the results for the generalization dimension of all samples, with D_0, D_1, and D_2 determined based on these results. In general, the relationship between D_0, D_1, and D_2 is reported to be $D_2 \leq D_1 \leq D_0$ [7]. However, equality $D_0 = D_1 = D_2$ occurs if the fractal is statistically or exactly self-similar and homogeneous [7]. The data related to the S, thermal conductivity (λ_e) , and D_0, D_1, and D_2 are shown in Table 3-2. According to the results of the samples of the SUS316L powders with a particle size of 3 μm and 8 μm in Table.1, the S was increased by adding SN particles. Comparing S the samples of the SUS316L powders with a particle size of 3 μm and 8 μm, the S of SUS316L (3 μm) was larger than that of SUS316L (8 μm). It was determined that SN particles in the SUS316L matrix with a particle size of 3 μm avoided being introduced to the vacant space more often than those in the SUS316L (8 μm) matrix due to the packing degree of the SUS316L powder with a particle size of 3 μm being higher than that of 8 μm.

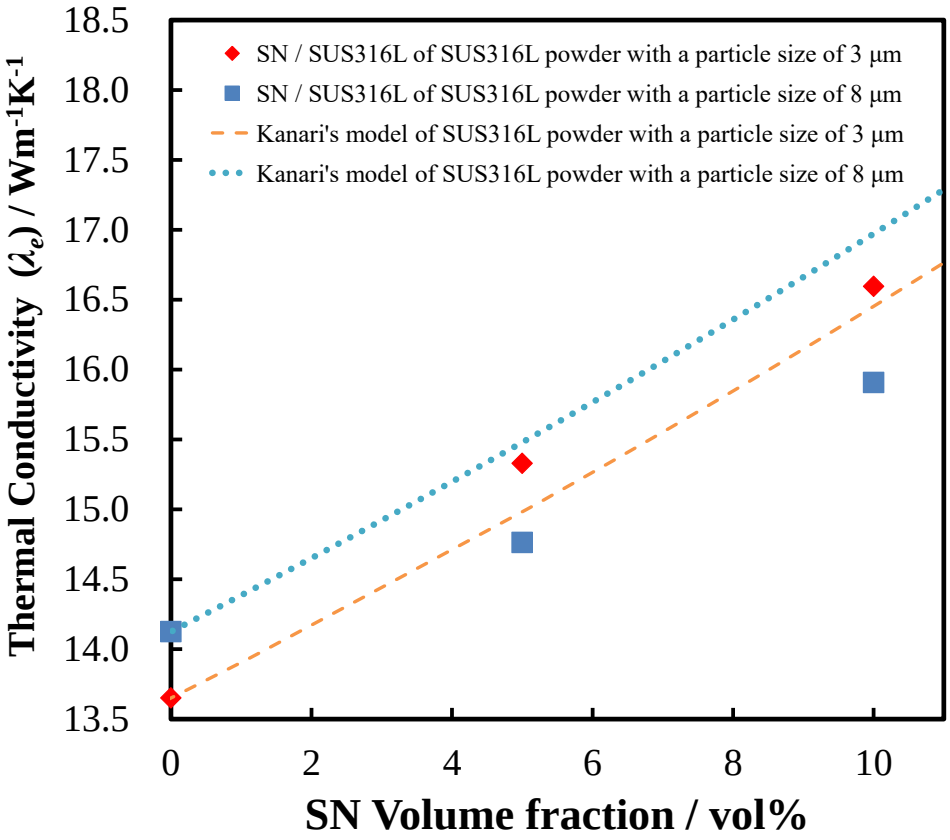

Fig. 3-11 Relationship between the volume fraction of SN and the thermal conductivity (λ_e) with 5% and 10% SN / SUS316L stainless steel.

3.2.4 Discussion

Fig.3-11 presents the results of the volume fraction of SN and the thermal conductivities of the samples. The results of the thermal conductivity estimated from Kanari's model are shown in Fig.3-11. The model can be described as [8], [9]:

$$1 - v = \frac{\lambda_e - \lambda_d}{\lambda_c - \lambda_d} \cdot \left(\frac{\lambda_c}{\lambda_e}\right)^{1/(x+1)} \tag{3-14}$$

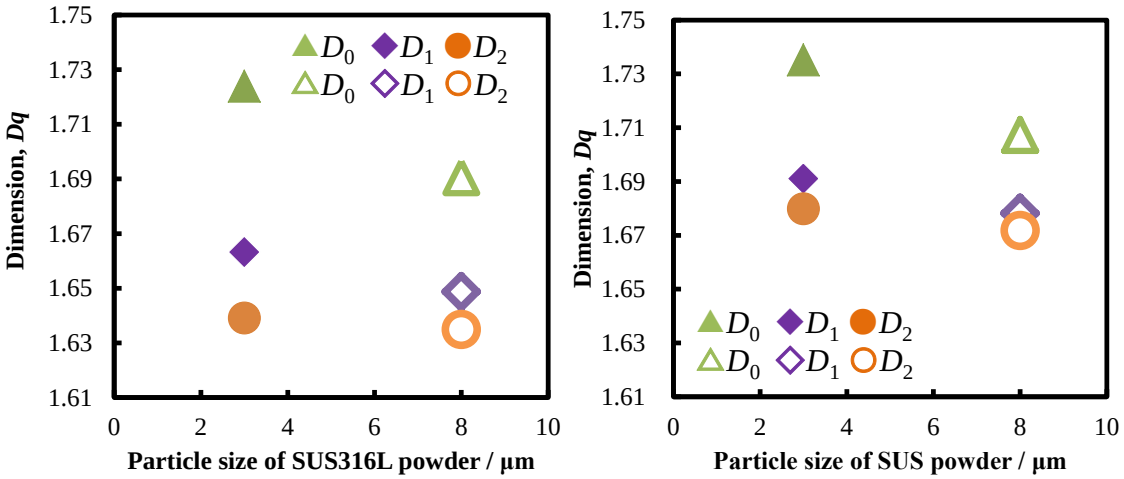

(a) SN volume fraction: 5 %　　(b) SN volume fraction: 10 %

Fig. 3-12 Relationship between particle size of SUS316L powder and the dimension.

where v is the volume fraction of the filler. λ_c, λ_d, and λ_e are the thermal conductivities of the matrix material (SUS316L), filler (SN), and composite material, respectively. x is determined by the particle shape of the additive and is 2 for a spherical shape. The thermal conductivity of the composite was calculated with λ_d of SN volume fraction 0 vol.% of each SUS316L particle size, assuming that λ_c of SN is 80 $Wm^{-1}K^{-1}$. The thermal conductivity of the samples of the SUS316L powder with a particle size of 3 μm was higher than that of Kanari's model. On the other hand, the thermal conductivity of the samples of the SUS316L powder with a particle size of 8 μm was lower than that of Kanari's model. In general, in order to improve thermal conductivity, it is important to form the thermal conduction network using filler particles [3]. In session 3.1, it was essential to form the thermal conductivity network by SN secondary particle groups to improve thermal conductivity [15]. Thus, a multifractal analysis was performed to

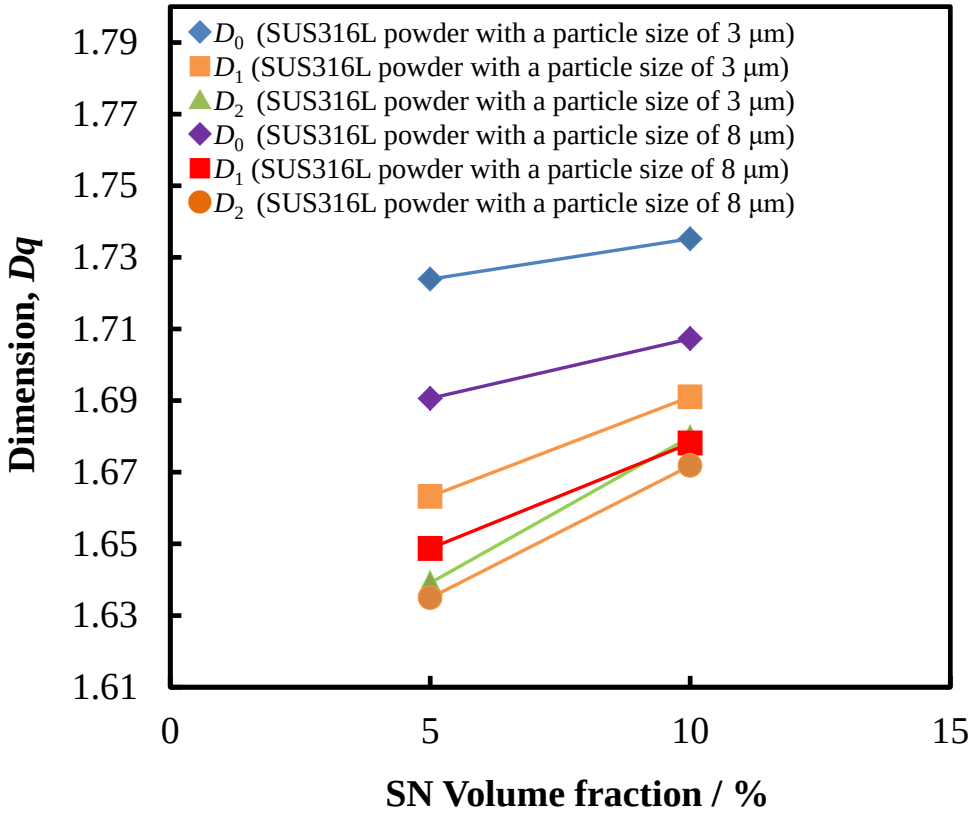

Fig.3-13 Relationship between the volume fraction of SN and the dimension.

discuss the formation of the thermal conductivity network by self-assembled SN secondary particle groups.

Fig.3-12a presents the results of the D_0, D_1, and D_2 of the samples of the SUS316L powder with a particle size of 3 μm and 8 μm for 5 vol.% of SN. The results of the D_0, D_1, and D_2 of the samples of the SUS316L powder with a particle size of 3 μm and 8 μm for 10 vol.% of SN are shown in Fig.3-12 b. Fig.3-13 shows the results of the D_0, D_1, and D_2 of the samples of the SUS316L powder with a particle size of 3 μm and 8 μm with the volume fraction of SN. Comparing the S of the SUS316L powder with a particle size of 3 μm and 8 μm of the volume fraction of 5 vol.% as shown in Fig.3-12a, the results of the D_0, D_1, and D_2 of the self-assembled SN / SUS316L stainless steel

composites of the SUS316L powder with a particle size of 3 μm were higher than those of 8 μm. In the D_0, it was found that the self-assembled SN agglomerates of the SN / SUS316L stainless steel composites of the SUS316L powder with a particle size of 8 μm were more anisotropic than that of 3 μm. In fact, according to the FE-SEM micrograph in Fig.3-8, it was confirmed that the SN agglomerates of the self-assembled SN / SUS316L composites of the SUS316L powder with a particle size of 8 μm were reflected by anisotropy. According to the results of the D_1 and D_2, the packing degree of the SUS316L powder with a particle size of 8 μm was lower than that of 3 μm, and the formation of the SN secondary particle group was limited. It was confirmed that the distribution of the SN secondary particle groups from the FE-SEM micrograph in Fig.3-8 and Fig.3-9. As the results for 10 vol.% of SN in Fig.3-12b, the D_0, D_1, and D_2 of the self-assembled SN / SUS316Lstainless steel composites of the SUS316L powder with a particle size of 3 μm were higher than those of 8 μm.

According to the results in Fig.3-12, the D_1 and D_2 of the SN / SUS316L stainless steel composites of the SUS316L powders with the particle sizes of 3 μm and 8 μm increased by adding SN fillers. Therefore, it was suggested that the configuration entropy and dispersibility of the self-assembled SN agglomerates were affected by the volume fraction of SN particles. Conversely, the D_0 was not changed by adding SN fillers. In general, the self-assembly (self-organization) process is observed in the reaction–diffusion system, which is assumed to occur due to a competitive reaction between an inhibitor and a promoter within the diffusion process., the formation of SN secondary particle groups is proposed in the kneading process of solid material.

$$\text{Agglomeration} \Leftrightarrow \text{Discomposition} + \text{Diffusion process} \tag{3-15}$$

The Van der Waals force acts as a cohesion force. The shear stress caused by the kneading speed contributes to decomposition. In this study, the subsequent sintering process was not contained for the diffusion process. It was reported that SN particles formed the secondary particle groups by the Van der Waals forces [12]. In the results of the samples of the SUS316L powder with a particle size of 3 μm and 8 μm, the D_0 was not changed by increasing the volume fraction of SN. This suggests that the packing degree of the SN agglomeration was controlled by the particle size of the SUS316L powder; however, the morphology of the SN secondary particle group was similar. In the results of the D_1 depending on the volume fraction of SN in Fig.3-13, the slope of the D_1 with the samples of the SUS316L powder with a particle size of 3 μm and 8 μm depending on the volume fraction of SN were the same. In the dependence of the volume fraction of SN in Fig.3-13, the slope of the D_2 with the samples of the SUS316L powder with a particle size of 3 μm was higher than those of 8 μm. From the FE-SEM micrographs as shown in Fig.3-8 and Fig.3-9, the location of the self-assembled SN agglomerates in which the samples were prepared with the SUS316L powder with a particle size of 3 μm was close. The self-assembled SN agglomerates of the samples of the SUS316L powder with a particle size of 8 μm were individual. In Fig. 3-13, the thermal conductivity of the samples of the SUS316L powder with a particle size of 3 μm was higher than Kanari's model. However, the thermal conductivity of the samples of the SUS316L powder with a particle size of 8 μm was lower than Kanari's model. From the results shown in Fig.3-13, the D_1 and D_2 of the samples of the SUS316L powder with a particle size of 8 μm were lower than that of 3 μm, and it was determined that the SN was agglomerated. According to the D_0 of the samples of the SUS316L

powder with a particle size of 8 μm as shown in Fig.3-13, the self-assembled SN agglomerates were anisotropic. Therefore, it was suggested that the self-assembled SN agglomerates of the samples of the SUS316L powder with a particle size of 8 μm were not connected for the formation of the thermal conductivity network.

Recently, it was proposed that global parameters $\tau(q)$ and D_q and local parameters $\alpha(q)$ and $f(\alpha)$ were determined by multifractal analysis to quantitatively evaluate the microstructural morphology of the texture of the self-assembled composite material. It was suggested that the D_0, D_1, D_2, and α (q) (related to internal energy) reflect the differences in morphology, arrangement (or configuration), dispersibility (or connectivity), and cohesion of the additive particle agglomeration composed of the self-assembly process under the solid-state reaction. In order to investigate the formation of the thermal conductivity network using SN particle groups, it is necessary to evaluate not only D_q but also the cohesion of the additive particle agglomeration composed of the self-assembly process of SN particles.

3.2.5 Conclusions

To investigate the morphology, entropy of configuration, and dispersibility of the self-assembled SN secondary particle groups and the formation of the thermal conductivity network by the SN secondary particle groups in relation to the SUS316L SUS316L powder with a particle size of 3 μm and 8 μm of 5vol.%–10 vol.% SN were prepared. The conclusions are as:

(1) According to the results of the FE-SEM micrograph, the self-assembled SN agglomerates of the SN / SUS316L stainless steel composites of the SUS316L

powder with a particle size of 3 μm were isotropic, and the location of the self-assembled SN secondary particle groups was close. On the other hand, the self-assembled SN agglomerates of the sample with the SUS316L powder with a particle size of 8 μm were reflected by anisotropy and the self-assembled SN agglomerates were individual.

(2) According to the results of the multifractal analysis, the D_0 of the samples of the SUS316L powders with particle sizes of 3 μm and 8 μm were not significantly changed with an increase in the volume fraction. Conversely, the D_1 and D_2 were increased by increasing the volume fraction of SN. It was suggested that the configuration entropy and dispersibility were affected by the SN volume fraction.

Hence, it was considered that the packing degree affected the morphology and distribution of the self-assembled SN secondary particle groups and affected the formation of the thermal conductivity network by the self-assembled SN secondary particle group. To investigate the formation of the thermal conductivity network using SN particle groups, it is necessary to evaluate not only D_q but also the cohesion of the additive particle agglomeration composed of the self-assembly process of SN particles with the multifractal analysis [$\alpha(q)$ and $f(\alpha)$].

3.3 Conclusions of chapter 3

In this chapter, the self-assembled SN / SUS316L stainless steel composite materials were prepared, and the relationship between the morphology, entropy of configuration, and dispersibility of the self-assembled SN agglomerated and the thermal conductivity of the composites was investigated by the multifractal analysis. The conclusions are as

follows:

(1) The secondary particle area of SN fillers was increased by increasing the thermal conductivity since it was considered that the self-assembled SN secondary particle group was formed and the thermal conductivity network using the self-assembled SN secondary particle group was formed in the SN / SUS316L stainless steel composite. The thermal conductivity of the SN / SUS316L composite of the SUS316L powders with particle sizes of 3 μm was improved by 1.22 times at 10 vol.% compared to the volume fraction of 0 vol.% for SN.

(2) It was suggested that the formation of the thermal conductivity network using the self-assembled SN secondary particle group was an important role in improving the thermal conductivity, and it was expected that the thermal conductivity was higher than Kanari's model.

(3) According to the results of the multifractal analysis, the D_0 of the samples of SUS316L powders with a particle size of 3 μm and 8 μm not were changed significantly with an increase of the volume fraction. On the other hand, the D_1 and D_2 were increased by increasing the volume fraction of SN. It was suggested that the configuration entropy and dispersibility were affected by the SN volume fraction.

Hence, it was considered that the packing degree affected the morphology and distribution of the self-assembled SN secondary particle groups and affected the formation of the thermal conductivity network by the self-assembled SN secondary particle groups.

References

[1] K. Furuya, F. Munakata, K. Matsuo, Y. Akimune, J. Ye, and A. Okada, "Microstructural control of β-silicon nitride ceramics to improve thermal conductivity," *J. Therm. Anal. Calorim.*, vol. 69, no. 3, pp. 873–879, 2002, doi: 10.1023/A:1020660006988.

[2] K. Komeya and F. Noda, "Aluminum nitride and silicon nitride for high temperature gas turbine engines," *SAE Pap.*, no. 40237, pp. 1030–1035, 1974.

[3] A. Shimamura, Y. Hotta, H. Hyuga, N. Kondo, and K. Hirao, "Effect of amounts and types of silicon nitride on thermal conductivity of Si3N4/epoxy resin composite," *J. Ceram. Soc. Japan*, vol. 123, no. 1441, pp. 908–912, 2015, doi: 10.2109/jcersj2.123.908.

[4] H. He, R. Fu, Y. Shen, Y. Han, and X. Song, "Preparation and properties of Si_3N_4/PS composites used for electronic packaging," *Compos. Sci. Technol.*, vol. 67, no. 11–12, pp. 2493–2499, 2007, doi: 10.1016/j.compscitech.2006.12.014.

[5] S. Mihcitaka, M. Yohikane, H. Mitsuaki, and O. Toshino, "Fractal dimensions of particle projecter shapes," vol. 25, pp. 11–15, 1988.

[6] S. Kobayashi, R. Kobayashi, and T. Watanabe, "Control of grain boundary connectivity based on fractal analysis for improvement of intergranular corrosion resistance in SUS316L austenitic stainless steel," *Acta Mater.*, vol. 102, pp. 397–405, 2016, doi: 10.1016/j.actamat.2015.08.075.

[7] A. Posadas, R. Quiroz, A. Tannús, S. Crestana, and C. M. Vaz, "Characterizing water fingering phenomena in soils using magnetic resonance imaging and multifractal theory," *Nonlinear Process. Geophys.*, vol. 16, no. 1, pp. 159–168, 2009, doi: 10.5194/npg-16-159-2009.

[8] K. Kanari and T. Ozawa, “充てん材配合エポキシ樹脂の熱伝導率,” 熱物性, vol. 3, no. 2, pp. 106–111, 1989.

[9] K. Kanari, “複合系の熱伝導率-充填剤を配合した高分子材料を中心に-,” vol. 26, pp. 557–561, 1977.

[10] L. Rolf, “The electrical resistane of binary metallic mixtures,” vol. 23, no. 779, pp. 779–784, 1952.

[11] F. Munakata *et al.*, “Multifractal characteristics of the self-assembly material texture of β-Si3N4/SUS316L austenitic stainless steel composites,” *J. Alloys Compd.*, vol. 853, p. 156570, 2021, doi: 10.1016/j.jallcom.2020.156570.

[12] T. Uchikoshi, Y. Fukada, T. S. Suzuki, and P. S. Nicholson, “Fabrication of silicon nitride ceramics by electrophoretic deposition,” *Funtai Oyobi Fummatsu Yakin/Journal Japan Soc. Powder Powder Metall.*, vol. 47, no. 9, pp. 1021–1025, 2000, doi: 10.2497/jjspm.47.1021.

[13] S. Jalan, A. Yadav, C. Sarkar, and S. Boccaletti, “Unveiling the multi-fractal structure of complex networks,” *Chaos, Solitons and Fractals*, vol. 97, pp. 11–14, 2017, doi: 10.1016/j.chaos.2017.01.021.

[14] M. Takeda *et al.*, “Fractal characters of material texture of self-assembled BaTiO $_3$ /poly-l-lactic-acid composites,” *Funtai Oyobi Fummatsu Yakin/Journal Japan Soc. Powder Powder Metall.*, vol. 66, no. 3, pp. 122–127, 2019, doi: 10.2497/jjspm.66.122.

[15] M. Takeda *et al.*, “Fractal characters and thermal conductive properties of self-assembled material texture of silicon nitride/stainless steel (SUS316L) composites,” *Funtai Oyobi Fummatsu Yakin/Journal Japan Soc. Powder Powder Metall.*, vol. 67, no. 6, pp. 307–312, 2020, doi: 10.2497/jjspm.67.307.

[16] R. Lopes and N. Betrouni, “Fractal and multifractal analysis: A review,” *Med. Image Anal.*, vol. 13, no. 4, pp. 634–649, 2009, doi: 10.1016/j.media.2009.05.003.

[17] E. Pérez, C. Bernal, and M. Piacquadio, “Multifractal analysis of tensile toughness and filler dispersion for polypropylene-$CaCO_3$ composites,” *Appl. Surf. Sci.*, vol. 258, no. 22, pp. 8940–8945, 2012, doi: 10.1016/j.apsusc.2012.05.124.

Chapter 4 Conclusions of this thesis and future works

4.1 Conclusions of this thesis

The targets applications of the ceramics / polymer and ceramics / stainless steel composite materials were the piezoelectric biosensor and the high thermal conductivity components in this study. In this study, the TB diagnostic method that combines the LAMP method and polymer piezoelectric material was proposed to solve the safety and cost problems. In order to achieve the final goal of TB diagnosis by combining the LAMP method and the polymer piezoelectric biosensor, it is necessary to improve the sensitivity and responsivity of the biosensor. Therefore, in this study, the ceramics / polymer composite materials were applied to biosensors to increase the dielectric properties related to the sensitivity and responsivity.

In high thermal conductivity components, the friction and abrasions of the engine generated cause energetic and material losses and decrease the efficiency of mechanical systems. However, the thermal conductivity of general iron alloys is low. Therefore, in order to improve the thermal conductivity, the ceramics/stainless steel composites were applied as high thermal conductivity components in this study.

In the general studies of composite materials, ceramic fillers are dispersed. However, the volume fraction of the filler is 50 vol.%, and it is not suitable for the applications. Therefore, the purpose of this study was to design composite materials in order to improve dielectric properties and thermal conductivity with a small amount of ceramic filler addition (0-20 vol.%). The dielectric properties and the thermal conductivity are affected by the material texture. Therefore, in this study, the material texture of the composite was controlled in order to improve the dielectric properties and thermal

conductivity. In particular, this thesis focused on the self-assembly process involving solids to control the material texture. The relationship between the dispersion states of self-assembled BT and SN secondary particle groups under the different manufacturing processes and the dielectric properties and the thermal conductivity of the BT / polymer and SN / SUS316L composites were investigated to design the materials. The multifractal analysis was performed to quantify the self-assembled material texture (the morphology, entropy of configuration, and dispersibility of the self-assembled BT and SN secondary particle groups). According to the results of this thesis, it was clarified that the morphology, the entropy of the configuration, and dispersibility of the BT and SN secondary particle groups and the interface state in the BT and SN secondary particle groups were able to be controlled by the self-assembly process. It was found that the dielectric properties and thermal conductivity were able to be improved by these morphologies, entropy of configuration, and dispersibility and interface states. Thus, the material designs that are able to improve dielectric properties and thermal conductivity with a small amount of filler were proposed. The conclusions of this thesis are as follows:

Chapter 1

The research background, problems, concepts and approach, and purpose were summarized in this chapter.

Chapter 2

In this thesis, in order to apply the BT / polymer composites to piezoelectric biosensors, the piezoelectric biosensors were prepared using polymeric piezoelectric

materials (β-PVDF), and the problems of the piezoelectric biosensors using polymeric piezoelectric material were presents. Based on the problems, the BT / polymer composite material was designed to improve the dielectric properties. In this study, the morphology, entropy of configuration, and dispersibility of the self-assembled BT secondary particle groups, and interfacial state in the BT secondary particle group were controlled using the self-assembly process involving solids. The relationship between these material textures and dielectric properties was discussed.

In the piezoelectric biosensors using β-PVDF, the biosensors were fabricated, and the sensor detection characteristics of the weight change with polymer tape and adsorption characteristics of fluorescently labeled avidin and biotin were investigated. The results are as follows.

(1) It was confirmed that the piezoelectric biosensor using β-PVDF detected with loading the weight of the polymer film (0 - 4.2 mg) by using the relaxation process of the complex permittivity.
(2) It was possible to detect biopolymers using the immobilization characteristics associated with the host-guest reaction at 100 kHz to 6 MHz.

The sensitivity of the piezoelectric biosensor using β-PVDF is 5 μg / ml and the response speed is 60 minutes. The problems of piezoelectric biosensors with β-PVDF are shown below.

(1) The shear vibration of β-PVDF was affected by the liquid viscosity since β-PVDF has a significantly lower elastic constant than quartz.

(2) In order to achieve the final goal of the sensitivity of less than 1 μg/ml and the reaction speed of 5 minutes, it is necessary to improve the sensitivity and responsivity of the polymer piezoelectric biosensor.

To solve the above problems, the ceramics / polymer composite materials were applied to the piezoelectric biosensors. The ceramics / polymer composite materials with high dielectric properties were designed to improve sensitivity and responsivity. In particular, the material textures of the BT / polymer composites were controlled using the self-assembly process. The relationship between the morphology, entropy of configuration, and dispersibility of the self-assembled BT secondary particle groups, and the interface state in the ceramic secondary particle groups and the dielectric properties of the BT / polymer composites were investigated using fractal analysis. BT filler (0-20 vol.%) was added to PLLA and PVDF, and BT / polymer composites were prepared by varying (1) the kneading conditions and (2) the viscosity of the dispersant to control the material textures. The self-assembled material textures were analyzed by fractal analysis using SEM images and binary images. The results are as follows.

(1) The manufacturing process affected the dispersion states and the interface states of the self-assembled BT secondary particle groups. In particular, BT agglomerate with the BT / BT interface was formed under high-speed kneading conditions (30 rpm) and high viscosity (10,000–15,000 cst) of PEG. On the other hand, the BT aggregates with the BT / polymer / BT heterointerface were formed under the low kneading conditions (10 rpm) and low viscosity (35–60 mPa・s) of PEG.

(2) It was suggested that it is possible that multifractal analyses were applied to evaluate

the morphology, configuration entropy, dispersibility and the formation of BT / polymer / BT heterointerfaces in self-assembled BT aggregates.

(3) It was suggested that it was an important role in improving the dielectric properties to form ceramics secondary particle groups having the ceramics / polymer / ceramics heterointerface by the self-assembling process since the electric dipole of a BT / polymer / BT heterointerface induced to improve the dielectric constant. In particular, the dielectric constant of the self-assembled BT aggregates with the BT/ PLLA / BT heterointerface depending on the average secondary particle area of BT fillers improved by 24.5 times compared to the BT / PLLA composite with BT / BT interface. Similarly, the dielectric constant of the self-assembled BT aggregates depending on the average secondary particle area of BT fillers improved by 1.16 times compared to the BT / PVDF composite with BT agglomerates.

Hence, it was suggested that the morphology, entropy of configuration, and dispersibility of the self-assembled BT secondary particle groups and the formation of BT / polymer / BT heterointerface in BT secondary particle group was controlled by using the self-assembly process. In addition, it was suggested that the dispersion states of BT secondary particle groups and the formation of BT / polymer / BT heterointerface were an important role in improving the dielectric properties of the BT / polymer composites. In the BT / PVDF composites, the materials with 2.22 times higher dielectric constant comparing 0 vol.% and 20 vol.% were designed. It was expected to improve the sensitivity by 2.1 times and responsivity by about 7 times compared to the conventional PVDF by applying the BT / PVDF composites to the piezoelectric biosensors. Hence, this study proposed the material design to solve problems that could

not be solved with conventional PVDF.

Chapter 3

In order to improve thermal conductivity, it is important to connect a thermal conductivity network using filler particles. Therefore, in this thesis, the formation of the thermal conductivity network using SN secondary particle groups was attempted by the self-assembly process. In particular, the purpose was that the thermal conductivity network of the self-assembled SN secondary particle group in the SN / SUS316L stainless steel composites was quantitatively evaluated with the multifractal analysis and the relationship between the morphology, entropy of configuration, and dispersibility of the self-assembled SN secondary particle group and the thermal conductivity was investigated.

(1) According to the results of the average secondary particle area of SN filler and thermal conductivity, the amount of SN / SN interfaces was increased and the thermal conductivity of the SN SUS316L composites was increased by forming the SN secondary particle groups. Thermal conductivity of the SN / SUS316L composites with 3μm SUS316L powder was improved by 1.22 times at 10 vol.% compared to the volume fraction of 0 vol.% for SN. That is, it was considered that the SN particle group acted as the thermal conductivity network with forming the SN secondary particle group, and the thermal conductivity was efficiently improved.

(2) It was suggested that the difference in packing within the self-assembly process affected the morphology, entropy of configuration, and dispersibility of the SN

secondary particle groups. Based on the FE-SEM images, the location of the self-assembled SN agglomerates with 3 μm SUS316L powder was close. The self-assembled SN agglomerates with 8 μm SUS316L powder were individual.

(3) According to the multifractal analysis, Comparing the SN/ SUS316L composites with 3 μm and 8 μm SUS316L powders at 5 vol.%, D_0 was 1.020 times higher, D_1 was 1.009 times higher, and D_2 was 1.003 times higher for 3 μm SUS316L powder than those of 8 μm SUS316L powder. At 10 vol.%, D_0 was 1.016 times higher, D_1 was 1.008 times higher, and D_2 was 1.005 times higher for 3 μm than those of 8 μm SUS316L powder. This is, it was possible to evaluate the character of the thermal conductivity network using the SN secondary particle group, and it was considered that the multifractal analysis could be used as an index.

Hence, it was suggested that the connection of the SN secondary particle group affected the formation of the thermal conductive network using the SN secondary particle groups and affected the thermal conductivity.

According to the material texture control in chapter 2 and chapter 3, it was suggested that the self-assembly process related to the solids was driven by the aggregation or agglomeration, decomposition, and diffusion processes. It was suggested that the dispersion states and the interface states of the BT / polymer and SN / SUS316L composites were controlled by the self-assembly process and improved the dielectric constant and thermal conductivity. The characters of the self-assembly process involving the solids with the fractal analysis are as follows:

< The self-assembly process of solids in the liquid>

(1) The morphology of the BT secondary particle group was changed by increasing the volume fraction of BT fillers. According to the result of D_0 of the BT / PLLA composites with Tegomer P121 using the box-counting method, the D_0 of the 20 vol.% sample was 1.16 times higher than that of the 5 vol.% sample.

(2) The configuration entropy and dispersibility were increased by increasing the volume fraction of BT fillers. This was the same as the process of self-assembly process of solids within solids. Based on the result of D_1 and D_2 of the BT / PVDF composites with PEG1000 using the multifractal analysis, The D_1 was 1.13 times higher and D_2 was 1.15 times higher for the samples of 20 vol.% than that of the samples of 5 vol.%.

(3) The results of the SEM images showed that the kneading speed affected the formation of BT aggregates having the BT / polymer / BT heterointerface and agglomerates having the BT / BT interface.

(4) It was considered that the viscosity of the dispersant affected the self-assembly process. In particular,

1. According to the SEM images, the BT aggregates having the BT / PVDF / BT heterointerfaces were formed with PEG1000. The BT agglomerates having the BT / BT interface were formed with PEG20000. It was proposed that the viscosity of the dispersant affected the formations of the self-assembled BT aggregates, the BT agglomerates, and the mixture of the BT aggregates and agglomerates.
2. It was proposed that the size, morphology, and distribution of the self-assembled BT secondary particle groups were depended on the viscosity of the dispersant based on the results of the relationship between the average secondary particle

area of BT fillers and the viscosity of PEG and the multifractal analysis. As one of the results, the average secondary particle area of the BT / PVDF composite with PEG2000 was 1.14 times larger than that of the sample with PEG1000.

Fig. 4-1 shows the self-assembly process of solids in liquid.

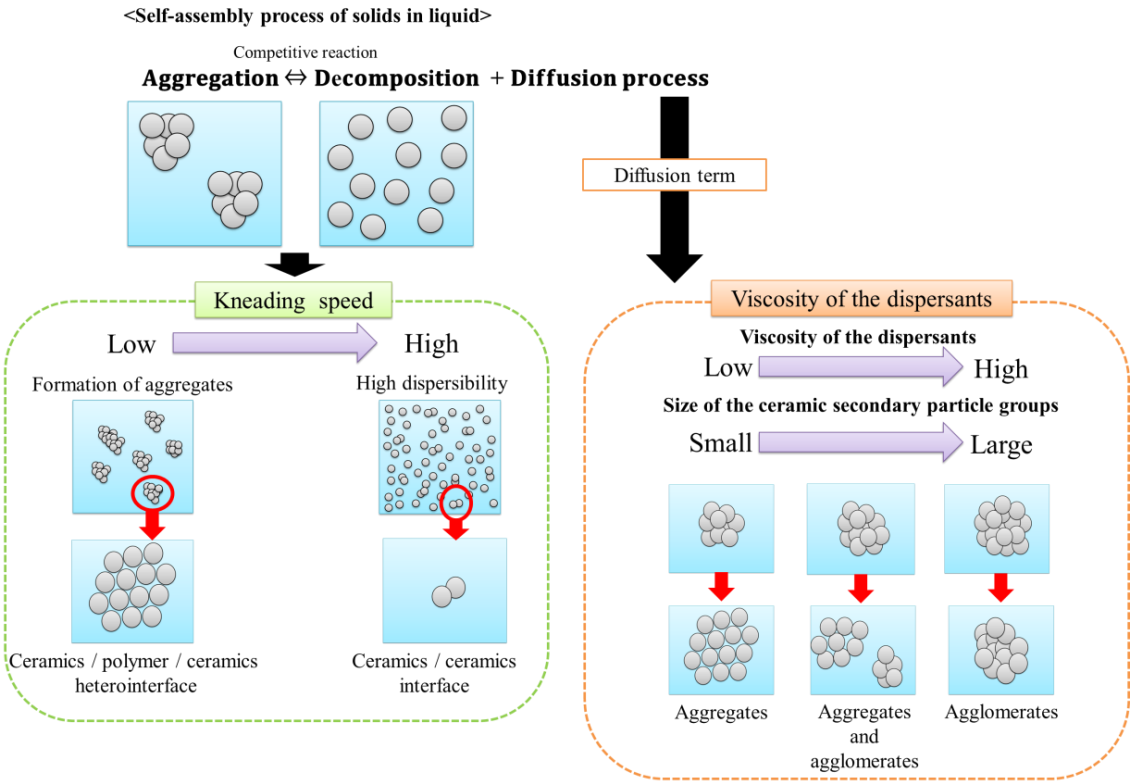

Fig. 4-1 The self-assembly process of solids in liquid in this study.

< The self-assembly process of solids in a solid >

(1) According to the results of the box-counting and multifractal analysis, the morphology of the SN secondary particle groups was not changed; however, the volume fraction of the SN fillers was increased. From the results of the box-counting method for the sample with 8 μm SUS316L powder, the D_0 of 5 vol.% and 10 vol.% was 1.68; however, the average secondary particle area of 10 vol.% was 1.27 times larger than that of 5 vol.%. In the self-assembly process of

solids in a solid, the van der Waals forces within mixing are the same, and it was considered that the morphology of the SN secondary particle group was not changed. This was different from the process of self-assembly process of solids in the liquid.

(2) It was suggested that the difference in packing within the self-assembly process affected the morphology, entropy of configuration, and dispersibility of the SN secondary particle groups based on the FE-SEM images and the multifractal analysis.

Fig. 4-2 shows the self-assembly process of solids in solid.

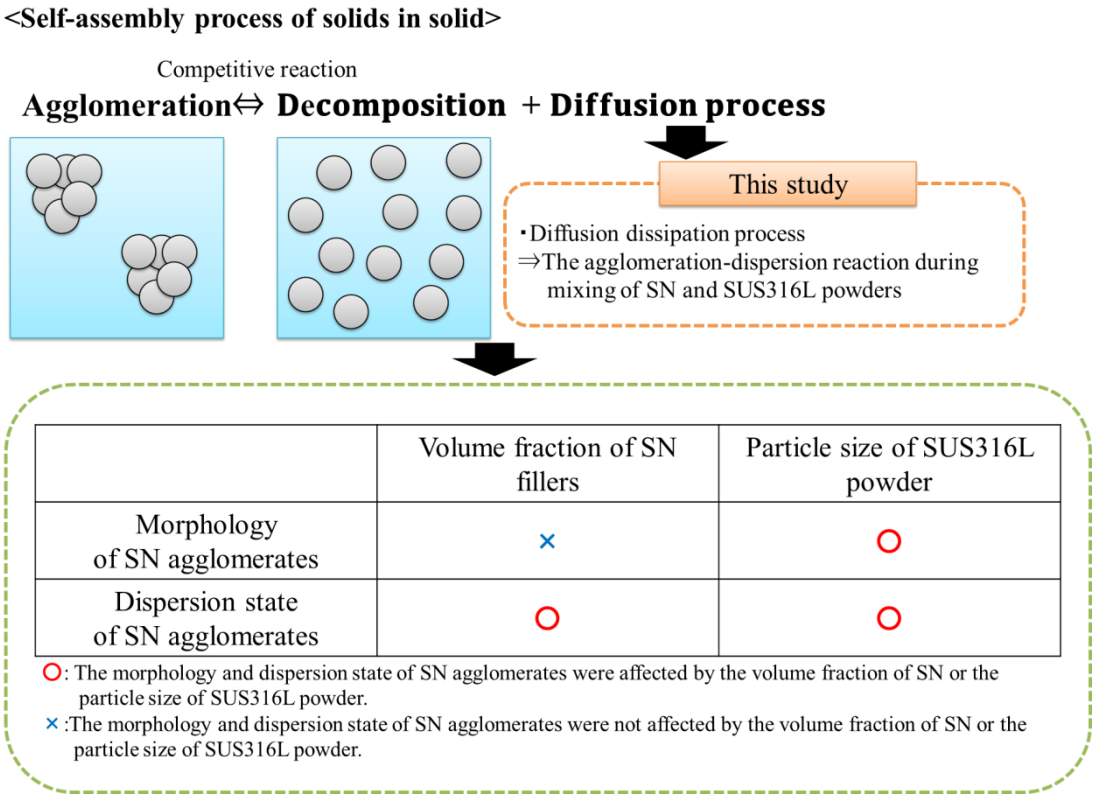

Fig. 4-2 The self-assembly process of solids in solid in this study.

The properties of ceramics / polymer composites and ceramics / stainless steel

composites were discussed with the material texture using the self-assembly process. In the dielectric material, it was suggested that the BT / polymer / BT heterointerface in the BT aggregates and the morphology and dispersion state of BT secondary particle groups were an important role in improving the dielectric constant. On the other hand, in high thermal conductivity components, it was proposed that self-assembly SN secondary particle groups were formed to reduce the SN / SUS316L interface, and the connectivity of SN secondary particle group was important for the formation of the thermal conductivity network using SN secondary particle groups. Hence, in this study, the material designs that were able to improve the dielectric properties and thermal conductivity by controlling the material texture with the self-assembly process were proposed.

4.2 **Future works**

The results of this thesis contributed to the material design for target applications for the piezoelectric biosensors and high thermal conductive components. In the future, the application of BT / polymer composites to piezoelectric biosensors for TB diagnosis requires improved selectivity and sensitivity. In the biorecepter of the piezoelectric biosensors, the target biomaterial can be selectively fixed by host-guest reactions on the sensor. For example, there is a method of detecting guest biopolymer by binding DNA-DNA and antigen-antibody. Based on the results of this study, it was found that fluorescently labeled avidin and biotin were immobilized on the sensor by the plasma ion irradiation method, which was expected to detect DNA, RNA, and proteins. By extending the results of this study, DNA, RNA, and proteins can be immobilized on the surface of the sensor, which is expected to improve the selectivity. As a specific method,

based on the results of this study, the plasma ion irradiation treatment is performed to fix avidin on the sensor, and biotinylated fluorescently labeled DNA, RNA, or protein is bound to the avidin. By measuring the fluorescence of DNA, RNA, and protein, the method of fixing biopolymer by plasma ion irradiation method will be investigated. In the QCM method, it is known that the detection characteristics of the sensor are different depending on the method of fixing DNA, RNA, and protein on the sensor and the structure of the biopolymer (shape, length of DNA, RNA, and protein). Therefore, it is necessary to consider the control of the fixation of DNA, RNA, and proteins. It is also necessary to investigate the sensor detection characteristics associated with the structure of biopolymers.

Based on the results of this study, it is expected that the sensitivity of the piezoelectric biosensors with the BT / PVDF composite materials is improved by 2.1 times. In the future, it will be necessary to fabricate piezoelectric biosensors using BT/PVDF composites and investigate the relationship between the material textures and sensor detection characteristics for TB diagnosis. β-PVDF has piezoelectric properties. To fabricate piezoelectric biosensors using BT / PVDF composites, electrical and mechanical polarization is required. For example, the treatment methods are the polarizations by applying an electric field or stretching. It is considered that the morphology of the BT secondary particle group is changed by stretching. For TB diagnosis, it is necessary to investigate the relationship between the morphology and dispersion state of BT secondary particle groups and sensor detection characteristics by multifractal analysis.

From this study, it was clarified that the morphology and dispersion state of the secondary particle groups of BT and SN fillers were controlled by the self-assembly

process. In order to improve the dielectric properties related to the sensitivity and thermal conductivity, the following methods are shown.

(1) Investigation of critical conditions for the formation of BT and SN secondary particle groups by the self-assembly process

In previous studies, changing the rotation speed of the ball milling resulted in the maximum size of the SN particle groups at 90 rpm. It was considered that there is a critical region for the formation of self-assembled secondary particle groups. Therefore, it is necessary to investigate the material textures and dielectric properties and thermal conductivity by changing the kneading conditions, time, and temperature related to the reaction-diffusion system.

(2) Investigation of the relationship between orientation and connectivity of ceramic secondary particle groups and dielectric properties and thermal conductivity

In order to improve the dielectric properties and thermal conductivity, it is necessary to control the orientation and connectivity of ceramic secondary particle groups by applying and stretching, electric and magnetic fields, and to investigate their material texture, dielectric properties and thermal conductivity.

(3) Chemical modification of ceramic filler surface

In our previous study, it was confirmed that the dispersant covered the BT secondary particle groups when the dispersant was not compatible with PVDF. The dielectric constant of the BT / PVDF composites was decreased by the dispersant. Therefore, it will be important to select a dispersant that is compatible.

According to the results of material texture control by the self-assembly process in this study, the material designs were able to be proposed to solve the problems of conventional PVDF and stainless steel. The material designs of this study can be applied to materials for other applications, as shown in Fig. 4-3, and the results of this study can contribute to the development of new materials. By combining the material design of the dielectric properties and thermal conductivity of the composite materials of this study, it is expected to contribute to the electronic substrate materials that are required low loss and high thermal conductivity.

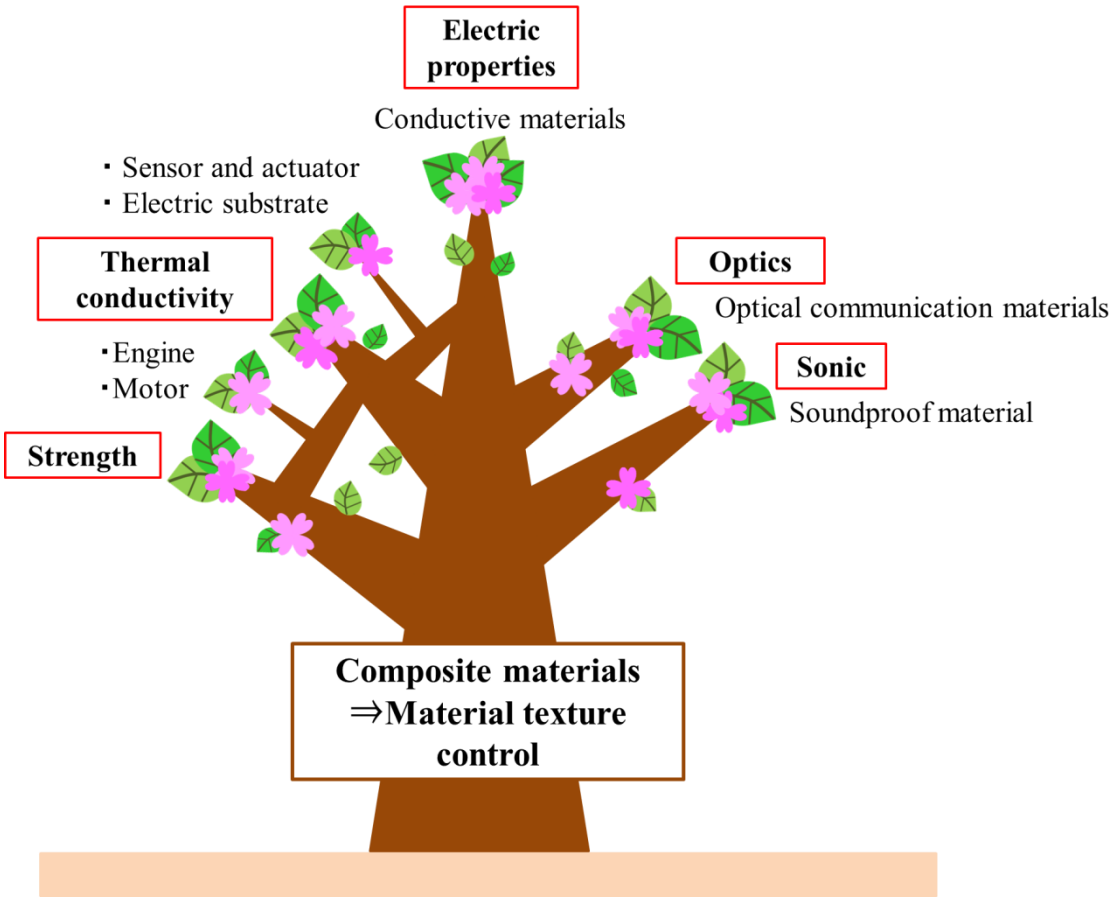

Fig. 4-3 Other applications with the material designs based on this study.

Appendix

(1) **Publications**：

1. Mariko TAKEDA, Kentaro YOSHINO, Akira ITO, Makoto TANIMURA, Yasuhide INOUE, Yasumasa KOYAMA and Fumio MUNAKATA" Effect of Ceramics / Polymer Heterointerface on Dielectric Property of Self-Assembled $BaTiO_3$ / Poly-L-Lactic Acid Composite Materials", Journal of the Ceramic Society of Japan, 129 [3], pp135-142, 2021. (Chapter 2)

2. Fumio Munakata, Mariko Takeda, Kazuhiro Nemoto, Kazuya Ookubo, Yoshihiro Sato, Yuka Mizukami, Masashi Koga, Satoko Abe, Yue Bao, Ryota Kobayashi, "Multifractal characteristics of the self-assembly material texture of β-Si_3N_4/SUS316L austenitic stainless steel composites", Journal of Alloys and Compounds, 15 August, 2020 (In Press, Journal Pre-proof)

3. 武田 真理子, 大久保 和也, 根本 一宏, 水上 侑香, 佐藤 圭浩, 阿部 聡子, 包 躍, 小林 亮太, 宗像 文男, "窒化ケイ素/ステンレス鋼(SUS316L)コンポジットにおける自己組織化材料組織のフラクタル特性と熱伝導特性 (Fractal Characters and Thermal Conductive Properties of Self-assembled Material Texture of Silicon Nitride/Stainless Steel (SUS316L) Composites)" , 粉体および粉末冶金, 一般社団法人粉体粉末冶金協会, Vol. 67, No. 6, pp307－312, 2020. (Chapter 3)

4. 武田 真理子, 矢萩 洸貴, 平田 孝道, 黒岩 崇, 中島 千絵, 鈴木 定彦, 宗像 文男, "緩和挙動を用いたポリマー圧電体バイオセンサにおける生体高分子検知特性 (Properties of Biopolymers Detection with Piezoelectric Polymer Biosensor in Relaxation Behavior Process)", 電気学会論文誌E(センサ・マイクロマシン部門誌), 一般社団法人電気学会, Vol. 140 , No. 2, pp43－49, 2020. (Chapter 2)

5. 武田 真理子, 吉野 謙太郎, 水上 侑香, 佐藤 圭浩, 伊東 顕, 包 躍, 宗像 文男, "自己組織化した$BaTiO_3$/ポリ-L-乳酸コンポジットの材料組織における

フラクタル特性 (Fractal Characters of Material Texture of Self-assembled $BaTiO_3$/Poly-L-Lactic-Acid Composites)”，粉体および粉末冶金，一般社団法人粉体粉末冶金協会，Vol. 66, No. 3，pp122－127，2019．(Chapter 2)

(2) Conference Proceedings (Not Peer-reviewed) :

1. 武田 真理子，平田 孝道，黒岩 崇 ，中島 千絵，鈴木 定彦，宗像 文男．“ポリマー圧電素子を用いた病原体特異的分子検出用バイオセンサの開発-分子識別素子の設計 (DEVELOPMENT OF BIOSENSOR USING PIEZOELECTRIC POLYMER FOR PATHOGEN SPECIFIC MOLECULAR DETECTION - BIORECEPTOR ELEMENT DESIGN -)”，Proceedings of the 61th Chemical Sensor Symposium ，Vol. 34， Supplement A ，電気化学会化学センサ研究会，pp37－39，2018.

2. 武田 真理子，矢萩 洸貴，杉山 龍男，平田 孝道，中島 千絵，鈴木 定彦，宗像 文男. “ポリマー圧電素子を用いた DNA 検出用バイオセンサの検知特性 (SENSING PROPERTIES OF BIOSENSOR WITH PIEZOELECTRIC POLYMER FOR DNA DETECTION)”，Proceedings of the Chemical Sensor Symposium 61，Vol. 33， Supplement A，電気化学会化学センサ研究会，pp 58－60，2017.

(3) Presentations at international conference：

< Peer-reviewed >

1. ○ Yuka Mizukami, Yoshihiro Sato, Mariko Takeda, Kazuya Okubo, Ryota Kobayashi, Fumio Munakata, Yue Bao, “QUANTITATIVE EVALUATION OF PARTICLE DISTRIBUTION USING MULTIFRACTAL ANALYSIS”, The 6th IIEEJ International Conference on Image Electronics and Visual Computing (IEVC 2019), 1P-15, Cebu Island, August (2019).

2. ○Yoshihiro Sato, Yuka Mizukami, Mariko Takeda, Kentaro Yoshino, Akira Ito, Fumio Munakata, Yue Bao, "VERIFICATION OF MATERIAL STRUCTURE FEATURES BY MULTIFRACTAL ANALYSIS", The 6th IIEEJ International Conference on Image Electronics and Visual Computing (IEVC 2019), 1P-13, Cebu Island, August (2019).

<Non-peer-reviewed >

3. ○Mariko TAKEDA, Kazuya OKUBO, Yuka MIZUKAMI, Yoshihiro SATO, Satoko ABE, Ryota KOBAYASHI, Yue BAO, Fumio MUNAKATA, " Self-assembly Material Texture of β-Si_3N_4 /Stainless Steel Composites (3)―Multifractal Analysis of the Aggregated Morphology Texture―", MATERIALS RESEARCH MEETING 2019 (MRM2019), A1-12-P12, Kanagawa, December (2019).

4. ○Mariko TAKEDA, Kazuya OKUBO, Yuka MIZUKAMI, Yoshihiro SATO, Satoko ABE, Ryota KOBAYASHI, Yue BAO, Fumio MUNAKATA, "Self-assembly Material Texture of β-Si_3N_4 /Stainless Steel Composites (2)―Effect of Kneading Process and Thermal Conductivity―", MATERIALS RESEARCH MEETING 2019 (MRM2019), A1-12-P11 , Kanagawa, December (2019).

5. ○Masashi KOGA, Mariko TAKEDA, Kazuya OKUBO, Yuka MIZUKAMI, Yoshihiro SATO, Satoko ABE, Ryota KOBAYASHI, Yue BAO, Fumio MUNAKATA , "Self-assembly Material Texture of β-Si_3N_4 /Stainless Steel Composites (1) ―Effect of Firing Process on the Formation of Agglomerated Texture―", MATERIALS RESEARCH MEETING 2019 (MRM2019), A1-12-P29, Kanagawa, December (2019).

6. ○Masashi KOGA, Mariko TAKEDA, Kazuya OKUBO, Yuka MIZUKAMI, Yoshihiro SATO Kazuhiro NEMOTO, Ryota KOBAYASHI, Yue BAO and Fumio MUNAKATA , "Thermal Conductivity and Self-assembly Material Texture of β-Si_3N_4/Stainless Steel Composites", The Seventh International Symposium on the

New Frontiers of Thermal Studies of Materials，p-07，Kanagawa，November (2019).

7. ○Mariko TAKEDA，Yuki NAKATA，Haruna YAMAZAKI，Kentaro YOSHINO，Yuka MIZUKAMI，Yoshihiro SATO，Akira ITO，Satoko ABE，Yue BAO，Makoto TANIMURA，Yasuhide INOUE，Yasumasa KOYAMA，Fumio MUNAKATA．“Self-assembly Material Texture of BaTiO3 / Piezo-Polymer Composites (2) ―Multifractal Analysis of Material Texture―”，The 13th Pacific Rim Conference of Ceramic Societies (PACRIM13)，28-P-S07-22，Okinawa，October (2019).

8. ○Mariko TAKEDA，Yuki NAKATA，Haruna YAMAZAKI，Kentaro YOSHINO，Yuka MIZUKAMI，Yoshihiro SATO，Akira ITO，Satoko ABE，Yue BAO，Makoto TANIMURA，Yasuhide INOUE，Yasumasa KOYAMA，Fumio MUNAKATA．“Self-assembly Material Texture of $BaTiO_3$ / Piezo-Polymer Composites (1) ―Composite Material Texture and Dielectric Property―”， The 13th Pacific Rim Conference of Ceramic Societies (PACRIM13)，28-P-S07-21，Okinawa，October (2019).

(4) Presentations at domestic conference：

【Oral presentation】

1. ○武田 真理子，吉野 謙太郎，水上 侑香，佐藤 圭浩，伊東 顕，包 躍，谷村 誠，井上 靖秀，小山 泰正，宗像 文男．“自己組織化した$BaTiO_3$/ポリ-L-乳酸コンポジットの材料組織におけるフラクタル特性(2) -マルチフラクタル解析による凝集体形態評価と誘電特性- (Fractal Characters of Material Texture of Self-assembled $BaTiO_3$/Poly-L-Lactic-Acid Composites (2) -Evaluation of aggregated morphology and dielectric properties using by multifractal analysis)”，日本セラミックス協会 2019年年会，3K01 ，東京，2019年3月．

2. ○武田 真理子，大久保 和也，水上 侑香，佐藤 圭浩，根本一 宏，小林 亮太，包 躍，宗像 文男．“β-Si_3N_4/ステンレス鋼コンポジット材料組織の熱伝

導特性とマルチフラクタル解析 (Thermal Conductivity and Multifractal Analysis of Material texture of β-Si_3N_4 /Stainless steel composites)", 第 54 回熱測定討論会，3A1140，神奈川，2018年11月.

【Poster】

3. ○山崎 陽菜，武田 真理子，井上 靖秀，小山 泰正，谷村 誠，宗像 文男，"自己組織化したチタン酸バリウム/圧電性ポリマー複合材料の誘電特性と分散剤効果 (The Dispersant effect on Dielectric Properties of Self-assembled Barium titanate/Piezoelectric Polymer Composites)"，日本セラミックス協会第33回秋季シンポジウム，1TH04，オンライン，2020年9月

4. ○武田 真理子，冨山 涼介，山崎 陽菜，仲田 勇貴，水上 侑香，佐藤 圭浩，伊東 顕，包 躍，谷村 誠，井上 靖秀，小山 泰正，宗像 文男，"自己組織化したセラミックス/PVDFコンポジット材料組織のマルチフラクタル特性 (Multifractal Characters of Material Texture of Self-assembled Ceramics/ PolyVinylidene DiFluoride (PVDF) Composites)"，日本セラミックス協会 2020年年会，1P011，東京，2020年3月.

5. ○冨山 涼介，武田 真理子，伊東 顕，気谷 卓，川路 均，谷村 誠，井上 靖秀，小山 泰正，宗像 文男，"自己組織化したBN/PVDFコンポジット材料の誘電特性と熱伝導特性の両立 (Compatibility of the dielectric properties and thermal conductivity of Self-assembled BN/PVDF Composite)"，日本セラミックス協会 2020年年会，1P006，東京，2020年3月.

6. ○武田 真理子，吉野 謙太郎，水上 侑香，佐藤 圭浩，伊東 顕，包 躍，宗像 文男，"自己組織化した$BaTiO_3$/ポリ-L-乳酸コンポジットの材料組織におけるフラクタル特性(1) -凝集体形態評価へのマルチフラクタル解析の適用- (Fractal Characters of Material Texture of Self-assembled $BaTiO_3$ / Poly-L-Lactic-Acid Composites (1) -Application of multifractal analysis to evaluation of aggregated morphology-)"，日本セラミックス協会 2019年年会，1P008，東京，2019年3月.

7. ○大久保 和也，武田 真理子，根本 一宏，水上 侑香，佐藤 圭浩，小林 亮太，包 躍，宗像 文男．“β-Si_3N_4/ステンレス鋼コンポジット材料の自己組織化と熱伝導特性 (Self-assembly and thermal conductivity of β-Si_3N_4/stainless composite material)”，第 54 回熱測定討論会，P35，神奈川，2018年10月．

8. ○武田 真理子，平田 孝道，黒岩 崇，中島 千絵，鈴木 定彦，宗像 文男．“ポリマー圧電素子を用いた病原体特異的分子検出用バイオセンサの開発-検知用バイオセンサの試作と評価- (Development of Biosensor using Piezoelectric Polymer for Pathogen specific molecular Detection -Development and Evaluation of Biosensor Element -)”，電気化学会第85回，PS-93，東京，2018年3月．

9. ○武田　真理子，矢萩　洸貴，杉山　龍男，黒岩　崇，平田　孝道，中島　千絵，鈴木　定彦，宗像文男．“高分子量を有する病原体特異的分子のポリマー圧電素子を用いた新規高感度検出素子の開発”，人獣共通感染症研究拠点シンポジウム，北海道，2018年2月．

(5) Award:

1. 日本セラミックス協会 2019年年会　優秀ポスター発表賞 (優秀賞)　受賞，2019年3月．

Acknowledgments

I would like to express my science gratitude to my supervisor, Professor Fumio Munakata for his encouragement, extensive discussions, and thoughtful guidance through the course of this thesis.

I would like to thank these thesis committee members Professor Chie Nakajima, Professor Takashi Kuroiwa, and Dr. Ryota Kobayashi for their valuable discussion and advice.

I would like to give my special thanks to Professor Takamichi Hirata (Tokyo City University), Professor Yasuhiko Suzuki (Hokkaido University), Professor Yue Bao (Tokyo City University), Yasumasa Koyama (Waseda University), Dr. Makoto Tanimura (Yokohama National University), Dr. Yasuhide Inoue (Waseda University), and Dr. Satoko Abe for their valuable discussion and carefully proofreading the manuscript.

I would like to thank Mr. Yoshihiro Sato, Ms. Yuka Mizukami for their supports of the multifractal analysis.

I am grateful to Professor Tetsuo Uchikoshi (National Institute for Materials Science) and Dr. Kento Ishii (National Institute for Materials Science) for useful discussions and comments.

I would like to thank preparing samples, Mr. Masahiko Ishikawa (Mitsubishi Gas Chemical Co., Inc), Mr. Akira Ito (Mitsubishi Gas Chemical Co., Inc), and Mr. Kentaro Yoshino.

I am grateful to Mr. Kouki Yahagi for his supports and useful advice on biosensors.

It is my great pleasure to my composites team, Ms. Haruna Yamazaki, Mr. Ryosuke Tomiyama, Mr. Yuki Nakata, Mr. Ryuji Iwasaki, and Ms. Miho Hamada for their supports.

I am grateful to SUS composite team, Mr. Kazuhiro Nemoto, Mr. Kazuya Okubo, and Mr. Masashi Koga for their supports.

I would like to thank Ms. Yasuko Kawai and my lab mates for their supports and for cheering me up.

I would like to thank the "Joint Research Center for Environmentally Conscious Technologies in Materials and Science" at Kagami Memorial Research Institute for Materials Science and Technology at Waseda University and Tokyo City University Interdisciplinary Research Center for Nano Science and Technology for instrumental analysis and their supports.

Finally, I would like to give the biggest thanks to my family for their understanding and support.

March, 2021
Mariko Takeda